Instituto Geológico
y Minero de España

Universidad de Salamanca
Departamento de Geología

Geología y evolución hidrotermal de los sulfuros masivos de la Faja Pirítica Ibérica, España

Geology and hydrothermal evolution of massive sulphides of the Iberian Pyrite Belt, Spain

Carmen Conde Rivas

2016

Universidad de Salamanca

Facultad de Ciencias

Departamento de Geología

Geología y evolución hidrotermal de los sulfuros masivos de la Faja Pirítica Ibérica, España

Geology and hydrothermal evolution of massive sulphides of the Iberian Pyrite Belt, Spain

Carmen Conde Rivas

Memoria presentada para optar al grado de Doctor en Ciencias Geológicas

Universidad de Salamanca, Febrero 2016

Tesis doctoral dirigida por el Dr. Fernando Tornos Arroyo, Científico Titular del Consejo Superior de Investigaciones Científicas y tutorizada por el Dr. José Ramón Martínez Catalán, Catedrático del Departamento de Geología de la Facultad de Ciencias de la Universidad de Salamanca.

VºBº VºBº

Fernando Tornos Arroyo José Ramón Martínez Catalán

A mi familia y
a mis dos grandes amigos.

La realización de este proyecto de tesis ha sido posible gracias a una beca de tesis doctoral del Instituto Geológico y Minero (2001-2004), y a las becas *"Hugh E. McKinstry Fellow"* (Society of Economic Geologist Foundation, Inc.) y *"Marie Curie Grant"* (European Commision's Improving Humana Potential Program Applications) para la formación y especialización de personal investigador. Los estudios estuvieron enmarcados dentro de los proyectos "Los sulfuros masivos de la Faja Pirítica Ibérica: modelo paleoambiental y geoquímica hidrotermal de los metales" (BTE 2000-0161-CO2-1), "Magmatismo, actividad hidrotermal y mineralizaciones en orógenos transpresivos: el SO de la Península Ibérica" (BTE 2003-0290) y "Tracking the formation of VMS deposits in extreme paleogeographic settings: anoxia, microbial activity and sulfide precipitation" (CGL2011-23207) de la Dirección General de Investigación (DGI) y coordinados por el Dr. Fernando Tornos. Este proyecto de investigación es una contribución a un amplio plan de investigación internacional que agrupa los proyectos GEODE (Geodynamics and Ore Deposit Evolution) de la European Science Foundation (ESF), y a "Global Comparison of Massive Sulfides" (Proyecto IGCP 502), dirigidos al estudio y comparación global de los principales yacimientos de sulfuros masivos.

No te rindas a los trabajos:
al contrario, procura vencerlos.

Virgilio

Resumen

La Faja Pirítica Ibérica (IPB) es una de mayores provincias metalogenéticas del mundo con más de 2500 Mt de sulfuros masivos volcanogénicos ricos en pirita. La mineralización se localiza en, al menos, dos niveles del Complejo Volcano-Sedimentario (Devónico Superior-Mississipiense Inferior) que rellena una cuenca marina continental.

Se diferencian dos tipos de mineralización: (1) En la zona septentrional, donde la secuencia está dominada por complejos de domo y cripto-domo de composición desde riodacita a andesita, con afinidad calcoalcalina, y con intercalaciones de basaltos toleíticos y pizarras, la mineralización es interpretada como de tipo remplazante y está preferentemente encajada en las facies más reactivas y permeables de las rocas volcanoclásticas ácidas ricas en pómez y vidrio situadas a techo de una unidad riodacítica específica – su edad más probable es Tournaisiense Inferior-. (2) En el dominio meridional, la secuencia encajante de la mineralización está dominada por pizarra intruida y recubierta por complejos de tipo domo con composiciones entre dacita y riolita con locales intrusiones y lavas de composición basáltica. La mineralización se localiza cerca del límite Devónico-Carbonífero, es de carácter exhalativo y encaja en niveles de pizarra oscura de marcado carácter anóxico.

Singularmente, en el distrito de Rio Tinto, localizado en la parte central de la FPI, se observan ambos tipos de mineralización, exhalativa y remplazante, asociadas a un domo félsico de edad Tournaisiense Inferior. En la zona de Filón Sur, la mineralización es (sub)-exhalativa y encaja en niveles de pizarra oscura de la *Unidad Sedimentaria Superior.* La mineralización remplazante se encuentra en la hialoclastita que forma las zonas apicales de un domo riodacítico infrayacente situado a techo de la *Unidad Félsica*.

El estudio geológico y geoquímico del sector septentrional de la Faja Pirítica ha permitido definir una secuencia estratigráfica que incluye una importante unidad basal de andesita seguida por coladas e intrusiones de basalto con intercalaciones sedimentarias y dos unidades de domos félsicos a techo. Esta secuencia está muy trastocada

tectónicamente pero es básicamente similar a la que se observa en la zona de Rio Tinto, aunque aquí la unidad andesítica está ausente. A escala regional, los sulfuros masivos están asociados a la unidad volcánica félsica más joven, una riodacita caracterizada por bajos contenidos en Zr, menores de 200 µg/g. Las rocas félsicas estériles tienen mayores contenidos en Zr y se interpretan como geoquímicamente más evolucionadas y emplazadas a mayor temperatura.

El estudio ha determinado una variabilidad en la geología, geoquímica y espesor de la secuencia volcánica, lo que sugiere una evolución espacial del vulcanismo, de norte a sur. En el sector septentrional hay una actividad volcánica continua que se caracteriza por la presencia de una potente unidad de andesita seguida de lavas basálticas, sedimentos y domos félsicos. En zona intermedia (Rio Tinto), la actividad volcánica es más discontinua, no está la andesita basal y hay varios niveles de pizarra. En la zona meridional hay mayor proporción de pizarra y no hay rocas máficas basales; es aquí donde se dan las condiciones anóxicas adecuadas para la formación de los grandes cuerpos exhalativos de sulfuros masivos.

El estudio detallado de la concentración y distribución de elementos traza en la pirita de los sulfuros masivos muestra que la geoquímica de la pirita puede ser de ayuda para diferenciar las zonas proximales y distales de los sulfuros masivos, así como para distinguir las zonas de stockwork de las venas de removilización tardía.

La formación de la mineralización está relacionada con la circulación convectiva de fluidos de cuenca originariamente contenidos y equilibrados con los sedimentos continentales infrayacentes, el Grupo PQ, tal y como demuestra la modelización numérica 2D. El modelo muestra que la formación de los sulfuros masivos en la zona sur de la Faja Pirítica pudo estar controlada por una circulación convectiva forzada asociada a un periodo extensional, sin que sea necesaria una fuente de calor procedente de intrusiones someras. Sin embargo, la salinidad de los fluidos y la presencia de estructuras tectónicas que canalizan los fluidos y compartimentan la cuenca fueran factores determinantes para

la formación de la mineralización. El modelo desarrollado muestra que los fluidos más salinos y calientes, y por lo tanto con mayor capacidad de transportar metales, fueron los primeros en ser exhalados en la cuenca marina anóxica; el modelo numérico sugiere que la duración de este evento fue inferior a 1 Ma algo que es consistente con la geocronología y con las características de la cuenca.

Abstract

The Iberian Pyrite Belt (IPB) is one of the largest and most important metallogenic provinces in the world, hosting more than 2500 Mt of pyrite-rich volcanogenic massive sulphides. The ore deposits are located in, at least, two different lithostratigraphic levels of the Volcanic Sedimentary Complex (Upper Devonian-Lower Mississippian), which fills a continental marine basin.

Two different mineralization types can be distinguished: (1) In the northern zone, the sequence is dominated by calc-alkaline dome and crypto-dome complexes of rhyodacitic to andesitic composition which are interlayered with tholeiitic basalts and shale. Here, the mineralization has been interpreted as of the replacement-type and is preferentially hosted in the most reactive and permeable facies of the glass- and pumice-rich acid volcaniclastic rocks situated on top of a specific rhyodacitic unit. The most probable age of this unit is Lower Tournaisian. (2) In the southern domain, the sequence hosting the mineralization is dominated by shale covering or intruded by dome-like complexes with dacitic to rhyolitic composition with local shallow intrusions and lava flows of basalt. These massive sulphide ores are located in a stratigraphic horizon close to the Devonian-Carboniferous limit. The mineralization is exhalative and hosted by anoxic black shale.

In the Rio Tinto mining district, located in the central part of the IPB, both types of mineralization, exhalative and replacement, coexist in close association with a felsic volcanic dome of Tournaisian age. In the Filón Sur area, the mineralization is (sub)-exhalative, being hosted by anoxic black shale of the *Upper Sedimentary Unit*. The replacement-type mineralization is hosted by glassy hyaloclastite located in the hanging wall of a rhyodacitic dome located in the top of the *Felsic Unit*.

The geological and geochemical study of the northernmost IPB has allowed proposing a new stratigraphic sequence. The footwall includes a large lower andesitic unit followed by extrusive and intrusive basalt intermixed with sediments and two units of felsic volcanic domes on the top of the sequence. This sequence is highly modified by later tectonics, but

it is basically similar to that observed in the Rio Tinto area, despite in the later case the andesitic unit is absent. The massive sulphides are spatially associated with the youngest felsic volcanic unit, a rhyodacite characterized by low Zr contents (i.e., below 200 µg/g). The underlying barren felsic rocks show higher Zr concentrations and have been interpreted as geochemically more evolved rocks which were likely emplaced at higher temperatures.

This study reveals a great variability in the geology, geochemistry and thickness of the volcanic sequence, something that suggests a spatial evolution of the volcanism from north to south. In the northern sector there is a continuous volcanic activity characterized by the presence of a basal thick unit of andesite followed by basaltic lavas, sediments and large felsic volcanic domes. In the intermediate zone (Rio Tinto area), the volcanic activity is more discontinuous, it lacks of the lower andesite level and there are several packages of shale. In the southern area there are large amounts of shale and there are no mafic rocks in the basal part of the sequence. It is in this zone where the anoxic conditions required for the formation of the large massive sulphide ore bodies are found.

The study of the concentration and distribution of trace elements in the pyrite of the massive sulphides by LA ICPMS shows that the geochemistry of this mineral may help to differentiate between distal and proximal zones in the massive sulphide deposits, as well as to distinguish between the stockwork or feeder zone and the veins product of the late remobilization.

The formation of the massive sulphides is related with the convective circulation of basinal fluids hosted and in equilibrium with the underlying continental sediments, the PQ Group, as the proposed 2D numerical model suggests. The model shows that the formation of the massive sulphides in the southern IPB was controlled by forced convective circulation associated to a period of tectonic extension. This model suggests that the heat could derive from an abnormal geothermal gradient without no involvement of a shallow magmatic heat source. Notwithstanding, the salinity of the fluid and the

existence of tectonic structures that channelize the fluids and compartmentalize the basins were key factors for the ore forming processes. The model shows that the denser and hotter fluids (i.e., those with the best capability for metal transport) were the first to upflow and vent in the seafloor. The model also predicts that the duration of this event was shorter than 1 Ma, something consistent with the geochronology and the evolution of the basin.

Contenido

CAPÍTULO II / CHAPTER II:

"Geology and geochemistry of the volcanic sequence hosting the giant Rio Tinto deposit (south of Spain)"

CAPÍTULO III / CHAPTER III:

"*Geology and geochemistry of the volcanic succession hosting the massive sulphides in the SE Iberian Pyrite Belt (Spain): the Aznalcóllar-Las Cruces zone"*

CAPÍTULO IV / CHAPTER IV:

"Laser Ablation-ICPMS analysis of trace elements in pyrite from the Tharsis massive sulphide deposit, Iberian Pyrite Belt (Spain)"

CAPÍTULO V / CHAPTER V:

"Modelización hidrodinámica y geoquímica de los sulfuros masivos de la zona sur de la Faja Pirítica Ibérica (España)"

Apéndices

Acknowledgements

(Agradecimientos)

En primer lugar, me gustaría agradecer de manera muy especial y por igual, a mi familia y a mi director de tesis, Fernando Tornos, por su paciencia y gran apoyo.

Fernando: gracias por enseñarme a disfrutar de la Geología. Gracias por enseñarme a cuestionar todo lo que veía en el campo, en el microscopio, en el laboratorio e incluso en la vida. Gracias por ayudarme a construir los cimientos que me han ayudado a conseguir los objetivos que nos propusimos al inicio de este largo viaje. Y finalmente, gracias por tu ayuda y paciencia en la revisión de los manuscritos de esta tesis.

También quiero tener un agradecimiento especial a mi tutor Juan Ramón Martínez Catalán por su ayuda y apoyo en la realización de mis estudios de doctorado en la Universidad de Salamanca.

Quiero agradecer al Instituto Geológico y Minero de España (IGME) por el soporte económico y material, sin los cuales no hubiera sido posible realizar la mayor parte de los trabajos de la tesis. También quisiera agradecer la ayuda y medios que me facilitaron en la Litoteca de Peñarroya.

No puedo olvidar a los que fueron mis compañeros en la oficina de proyectos de Salamanca: David, Ramón, Víctor y Pedro, ni a Manuel Lombardero y Rogelio Urbano, mis tutores en mi primer año en el IGME. También a mis compañeras, Silvia y Diana, y a Cecilio Quesada, Guillermo Ortiz, Pablo Gumiel, Juan Locutura y Alejandro Díez Montes por sus comentarios y consejos a lo largo de estos años.

Al CODES, por las facilidades y ayuda en la realización de los análisis de sulfuros y en especial, a mis tutores durante la estancia, Ross Large y Michael Solomon. Así como a Bruce Gemmel, Stuart Bull, Leonid Danyushevsky y Jocelyn McPhie, y a los compañeros y amigos que hicieron muy enriquecedora y grata mi estancia en Hobart: Fernando, Christine, Ben y Loreto.

Al “Natural History Museum” y al “Imperial College”, en concreto a mis tutores Richard Herrington y Stephan Matthäi, gracias a los cuales pude formarme y desarrollar los trabajos de modelización numérica hidrogeológica. Sin olvidar a Sebastian Geiger y Thomas Driesner, por las largas y enriquecedoras discusiones sobre los trabajos realizados. Y a mis compañeros, Robin Armstrong y Dionysia Antonakopoulou.

Del mismo modo, quisiera agradecer al Instituto de Ciencias de la Tierra “Jaume Almera” (CSIC), y en concreto a Carlos Ayora y Joaquín Salas, por introducirme en la modelización geoquímica e hidrodinámica de procesos geológicos.

No quiero olvidar a todos aquellos que durante los años de estudio en la Universidad de Salamanca me formaron y dieron las bases para poder realizar este trabajo. En especial, quisiera recordar a mis compañeros y amigos, Juan, Javier, Oscar, Ángel, Ana, Sole y Pepa, por las largas discusiones y tertulias en la biblioteca o tomando una cerveza.

Dar las gracias a todas las empresas mineras que han facilitado la realización de este trabajo, en especial a los Departamentos de Geología de: MATSA (Trafigura Mining Group), EMED-Tartessus (Emed Mining Company), Cobre Las Cruces (First Quantum), Cambriage Minerals y Boliden.

Y finalmente, recordar y agradecer enormemente a todos los amigos y compañeros que he encontrado durante este viaje y a lo largo de todos los países en los que he estudiado y trabajado: Åsa Edfelt, Baruch Spiro, Carmen Galindo, Cesar Casquet, Cesar Menor, Cornel de Ronde, Dave Lentz, Denis Martin, Enrique Lopez Pamo, Esther Santofimia, Gregor Borg, Jan Peter, Javier Sanchez España, Jesús M. Fernández, Jim Walker, Jorge Relvas, José Teixidor, Juan Carlos Videira, Kerr Anderson, Lorena Luceño, Massimo Chiaradia, Nick Badham, Paco Velasco, Raúl Hidalgo, Ricardo Amils, Rodney Allen, Sebastian G. Chioza, Steve McCutcheon, Tim Ireland, etc, por su apoyo y amistad.

Y por supuesto, a mi precioso tesoro, mi hija Valeria, y a mi amigo, compañero y marido, Julián.

INTRODUCCIÓN

Introducción

(Introduction)

La Faja Pirítica Ibérica (FPI) engloba la mayor concentración de sulfuros masivos volcanogénicos de la corteza terrestre y representa la mayor anomalía conocida de azufre. Está localizada en la parte central de la Zona Sudportuguesa (zona sur de Macizo Ibérico), dentro de una cuenca marina intracontinental tipo "pull apart" rellena por una secuencia de rocas volcánicas dominantemente félsicas con abundantes intercalaciones siliciclásticas y depositadas sobre una secuencia marina somera de plataforma.

A pesar de su alto interés científico e importancia económica, el encuadre volcanológico de muchos de los depósitos de la Faja Pirítica no está bien caracterizado, lo que hace difícil la correcta interpretación genética y definir pautas para su exploración. Esta tesis tiene como objetivo contribuir al conocimiento del encuadre geológico y la formación de estas mineralizaciones tomando como ejemplo un pequeño número de depósitos representativos del sector meridional, central y septentrional de la FPI, incluyendo los sectores de Aznalcóllar-Las Cruces, Rio Tinto y Aguas Teñidas-San Telmo. El trabajo realizado conjuga técnicas básicas tales como el estudio y cartografía geológica de detalle de las zonas seleccionadas, la testificación de sondeos de exploración, y la petrografía y la geoquímica con nuevas líneas de investigación no realizadas hasta el momento en la región, como el estudio de los elementos traza en la pirita por ablación láser y la modelización numérica de los procesos hidrodinámicos que intervienen en la formación de estos depósitos. Estos modelos incorporan gran número de variables y su integración requiere de una serie de herramientas numéricas que permitan reproducir de la manera más realista posible la variabilidad del medio natural. Mediante el desarrollo de modelos 2D, la modelización hidrogeológica plantea la simulación y predicción teórica del comportamiento de metales y fluidos, en unas condiciones fisicoquímicas tan peculiares como las que caracterizan a los sulfuros masivos volcanosedimentarios de la de la FPI.

Objetivos e interés del proyecto de investigación

(Objetives of thesis)

El proyecto de tesis se centra en el estudio de tres cuestiones fundamentales:

1) Estudio geológico y litogeoquímico de tres áreas mineras seleccionadas como zonas representativas de distintos dominios de la Faja Pirítica (Fig. 1).

2) Estudio geoquímico de elementos traza en pirita y evaluación del papel de los mismos en la identificación de las distintas facies de la mineralización.

3) Modelización numérica de los procesos hidrodinámicos que producen el transporte y precipitación de los metales durante la formación de los sulfuros masivos.

El ámbito de estas líneas de investigación se integra en el objetivo común de avanzar en el conocimiento del emplazamiento, identificación de los procesos, y ambiente de formación de los sulfuros masivos de la Faja Pirítica Ibérica.

La primera parte de la investigación está enfocada al estudio de la litoestratigrafía y litogeoquímica de la secuencia en la que encaja la mineralización para cada una de las tres áreas mineras (Fig. 1): (1) los yacimientos localizados desde la Mina de Aguas Teñidas a San Telmo, en el borde norte; (2) el distrito minero de Rio Tinto, situado en la parte central de la FPI, e históricamente el más importante; y (3) el distrito de Aznalcóllar (Aznalcóllar y Los Frailes) y la Mina de Las Cruces, en el borde sureste, junto a la cuenca terciaria del Guadalquivir.

Este estudio se ha estructurado en:

I. Descripción e interpretación geológica de las facies volcánicas y sedimentarias encajantes de la mineralización.

II. Estudio geológico y geoquímico de la pizarra directamente relacionada con la mineralización de la zona meridional, comparándola con otros niveles no mineralizados que aparecen a lo largo de la columna litoestratigráfica.

III. Caracterización petrográfica y geoquímica de las rocas volcánicas.

IV. Definición del ambiente y estilo de mineralización para cada uno de los sectores estudiados.

V. Estudio de las diferencias y similitudes en el emplazamiento y evolución de las rocas volcánicas en el sector meridional y septentrional de la Faja Pirítica.

VI. La caracterización geoquímica de la pirita con el fin de realizar un estudio piloto sobre el uso del análisis de elementos traza por LA-ICPMS para caracterizar mineralizaciones y como herramienta de exploración. El estudio se ha centrado en

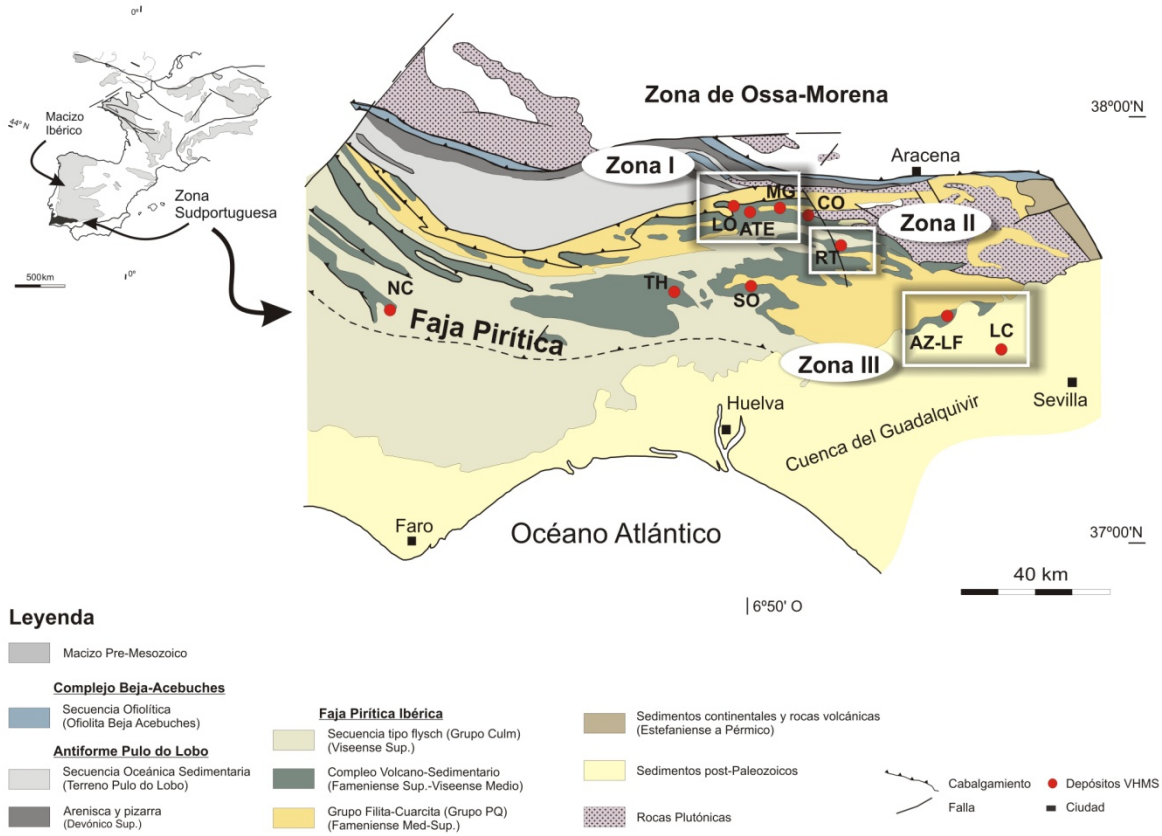

Figura 1. Mapa geológico general de la Faja Pirítica mostrando la localización de los principales depósitos minerales. Con un perímetro blanco se indican las tres zonas principales de estudio. Modificado de Oliveira & Quesada (1998) y Quesada (1998). Abreviaturas: AZ-LF, Aznalcóllar-Los Frailes; ATE, Aguas Teñidas; MG, Magdalena; CO, Concepción; LC, Las Cruces; LO, Lomero Poyatos; NC, Neves Corvo; RT, Rio Tinto, SO, Sotiel.

(1) caracterización y distribución de los elementos traza en pirita de cada una de las facies de la mineralización, y (2) identificación de los factores geoquímicos que controlan esta concentración

VII. Desarrollo de un modelo hidrodinámico conceptual para la formación de los sulfuros masivos volcanogénicos de la parte sur de la FPI.

Estructura de la memoria de tesis

(Structure of the thesis)

La memoria de esta tesis se presenta en formato compendio de publicaciones. Está formada por cinco capítulos que corresponden a manuscritos, enviados o pendiente de ser enviados a revistas internacionales especializadas en el campo de la geología y yacimientos minerales.

En la "*Introducción*" se presenta un amplio resumen en español del conjunto de los capítulos que forman la memoria de la tesis.

El "*Capítulo I*" incluye los resultados del estudio litológico, morfológico y estructural de las facies volcanoclásticas que dominan la secuencia estratigráfica en la parte norte de la FPI. Se presenta la síntesis de la cartografía y columnas geológicas, así como los resultados de la testificación de los sondeos representativos y el estudio petrográfico de las minas de Aguas Teñidas y Lomero Poyatos. Esta investigación esta complementada con la caracterización geoquímica de las unidades volcánicas definidas en el área. Sus resultados han permitido (1) correlacionar todas las unidades litológicas a escala regional, (2) definir el modo de emplazamiento de las rocas volcánicas, y, (3) proponer un modelo de reconstrucción paleogeográfica para la cuenca y los mecanismos de formación de los sulfuros masivos.

En el "*Capítulo II*" se presenta un estudio regional del área de Rio Tinto. El estudio incluye una cartografía general del distrito minero (especialmente de los depósitos de San

Dionisio, Salomón-Lago y Cerro Colorado), el estudio de la secuencia estratigráfica, y un estudio geoquímico de las rocas volcánicas. Debido a la intensa alteración hidrotermal de las rocas en las que encaja la mineralización, se han realizado correlaciones estratigráficas con zonas aledañas y fuera del campo de influencia de la alteración hidrotermal (Río Odiel y Zarandas). La compilación de todos los resultados ha permitido presentar una interpretación geológica y metalogenética para el distrito de Rio Tinto. Los datos generados evidencian que muchos de los estudios realizados son demasiado simplistas para describir la complejidad de los procesos que han tenido lugar en el área. En esta tesis se ha presentado una nueva perspectiva que propone un esquema geológico similar al descrito en otras zonas de la FPI. Además, se destaca que Rio Tinto incluye los dos estilos de mineralización principales descritos en la FPI (exhalativo y remplazante). El estudio sugiere que la mineralización exhalativa de Rio Tinto es la más moderna de la Faja Pirítica.

En el "*Capítulo III*" se describe las características geológicas y geoquímicas de la secuencia estratigráfica en la que encajan las mineralizaciones localizadas en el borde SE de la FPI. Se han estudiado dos zonas: el distrito de Aznalcóllar, con una cartografía detallada de los dos yacimientos principales (Aznalcóllar y Los Frailes), y la Mina de Las Cruces, actualmente en explotación, y localizada bajo una potente unidad de margas del Terciario. Además, se presentan los resultados y conclusiones más relevantes del estudio geoquímico de la pizarra encajante de la mineralización. La conclusión más relevante es que los tres depósitos se han formado en un ambiente geológico similar con la mineralización ligada a un horizonte específico.

El "*Capítulo IV*" recopila los resultados y las conclusiones de los análisis de sulfuros realizados mediante la técnica de ablación láser con plasma de acoplamiento inductivo (LA-ICPM). El estudio ha determinado los elementos traza en la pirita, calcopirita y esfalerita de ocho de los principales depósitos de la FPI. En la presente memoria se han presentado únicamente los resultados y conclusiones del estudio de la pirita en uno de

los yacimientos más importantes de la zona sur, Tharsis, por sus características geológicas y su peculiar mineralización. El estudio geoquímico revela un enriquecimiento sistemático y selectivo de algunos elementos traza, que parece estar controlado por la morfología de la pirita y las condiciones fisicoquímicas de precipitación de distintos tipos de mineralización.

En el "*Capítulo V*" se ha realizado un modelo hidrogeológico global para la circulación de fluidos durante la formación de los sulfuros masivos del sector meridional de la FPI. La modelización hidrológica incorpora simulaciones de flujo multi-fásico que reproducen la convección hidrodinámica y termohalina de las soluciones. Para ello se ha construido un modelo geológico simplificado que incluye las características estratigráficas, tectónicas y paleogeográficas generales de la zona de estudio durante la etapa metalogenética. Dicho modelo se implementó en dos modelos hidrodinámicos conceptuales: 1) circulación de agua pura; y 2) flujo de un fluido salino, representativo de los fluidos que circularon durante la formación de las mineralizaciones.

En el apéndice se han incluido tres apartados: dos de ellos con los datos analíticos utilizados en el estudio, y por último, una lista con las referencias de los trabajos publicados hasta el momento por el autor de la tesis.

I. Datos analíticos: litogeoquímica de las rocas volcánicas y pizarras.
II. Datos analíticos de la geoquímica de pirita del yacimiento de Tharsis.
III. Publicaciones y estudios en los que se ha participado.

RESUMEN DE LA TESIS

Capítulo I

"Litoestratigrafía, geoquímica y arquitectura volcánica de la secuencia que alberga los sulfuros masivos de la parte norte de la Faja Pirítica Ibérica (Huelva, España)"

La parte norte de la Faja Pirítica Ibérica alberga varios depósitos de sulfuros masivos volcanogénicos encajados en el Complejo Volcano-Sedimentario y alineados en una banda E-W situada al sur de un gran cabalgamiento regional que limita la Zona Sudportuguesa con la Unidad Pulo do Lobo. Por lo general estas mineralizaciones, excepto los depósitos de Aguas Teñidas y Magdalena (>45 Mt cada uno), tienen tonelajes relativamente pequeños pero son económicamente importantes por su alto contenido en metales base, oro y plata.

El análisis geológico detallado del Complejo Volcano-Sedimentario en la zona permite diferenciar seis unidades tectonoestratigráficas principales: (1) La Unidad Félsica de Muro (*Footwall Felsic Unit*) formada por un complejo tipo domo de composición riodacita con una textura porfídica (feldespato y cuarzo) que incluye facies masivas y brechas hialoclásticas asociadas e intrusiones equivalentes en forma de *sill* y dique. A techo y en los márgenes laterales del complejo alternan capas de rocas volcanoclásticas de grano fino y brechas félsicas ricas en pómez y vidrio. (2) La Unidad Volcano-Sedimentaria (*Volcano-Sedimentary Unit*) está formada por lavas submarinas vesiculares de composición basáltica y facies volcanoclásticas asociadas incluyendo arenisca máfica epiclástica con pequeñas intercalaciones de pizarra. La unidad se caracteriza por presentar drásticos cambios laterales de facies tanto verticales como horizontales. Una gran estructura tectónica – posiblemente un cabalgamiento- marca el contacto con la segunda unidad félsica suprayacente. (3) La Unidad Félsica de Techo (*Hanging wall Felsic Unit*) está formada también por un complejo de tipo domo de riolita masiva con texturas de flujo y rocas volcanoclásticas asociadas, con intercalaciones de rocas sedimentarias polimícticas; está cortada por intrusiones subvolcánicas félsicas y máficas.

(4) La Unidad Sedimentaria (*Sedimentary Unit*), compuesta por arenisca volcanoclástica (principalmente máficas) con intercalaciones de pizarra y roca epiclástica de grano fino. Esta Unidad está muy deformada y muestra frecuentes texturas miloníticas sugiriendo que las rocas sedimentarias canalizaron la deformación en contraste con las rocas félsicas adyacentes. (5) La Unidad Félsica Superior (*Upper Felsic Unit*), está formado por un complejo tipo domo de composición dacita-riolita con características morfológicas y composicionales similares a las de la Unidad Félsica de Muro. Los contactos superior e inferior de la unidad están marcados por una zona estrecha con intensa deformación. (6) La Unidad Andesítica (*Andesitic Unit*), ocupa la posición estructural superior de la secuencia. Está compuesta por la sucesión de varios domos de composición andesítica que alternan con hialoclastita, sedimentos volcanoclásticas y pequeños niveles piroclásticos de igual composición. Esta unidad está intruida por abundantes diques de composición félsica.

Geoquímicamente, el Complejo Volcano-Sedimentario está dominado por rocas magmáticas calcoalcalinas, desde andesita a riolita y, en menor proporción, basalto de afinidad toleítica. En general, el Complejo Volcano-Sedimentario incluye rocas desde basalto a riolita, con una gran proporción de dacita y andesita.

La Unidad Félsica de Muro y Unidad Félsica Superior son geoquímicamente iguales y probablemente representen partes desmembradas de un solo complejo volcánico félsico. De hecho, los sulfuros masivos están encajados principalmente en la Unidad Félsica de Muro, a excepción de Lomero Poyatos, San Telmo y El Carpio, asociados a la Unidad Félsica Superior. De ser esta hipótesis cierta, todos los depósitos de sulfuros masivos de la parte norte de la Faja Pirítica se encuentran encajados en rocas volcanoclásticas a techo de una única unidad cronoestratigráfica formada por un complejo de domo de composición dacita-riolita y con una composición geoquímica determinada. Esta unidad volcánica se caracteriza por un contenido en Zr menor de 200 µg/g, que es notablemente más bajo que el de las rocas de la Unidad Félsica de Techo (200-750 µg/g) y que serían

geoquímicamente más evolucionadas y emplazadas a mayor temperatura. En conjunto, ambas unidades se interpretan como producto de dos pulsos magmáticos diferentes a partir de una misma cámara magmática profunda.

Las relaciones de corte entre las rocas ígneas, el análisis estructural y la geoquímica de las rocas volcánicas sugieren que la secuencia estratigráfica original está modificada, estando generalmente las unidades más recientes en una posición estructural inferior. Por ello, se considera que la Unidad Andesítica es la más antigua de la zona norte de la Faja Pirítica y sobre ella se encuentran la Unidad Volcano-Sedimentaria, la Unidad Sedimentaria y los complejos ácidos de la Unidad Félsica de Techo y Unidad Félsica Superior. De ser esto cierto, los sulfuros masivos estarían ligados a las rocas félsicas más modernas de la Faja Pirítica.

Capítulo II

"Geología y geoquímica de la secuencia volcánica encajante del depósito de Rio Tinto (sur de España)

El distrito minero de Rio Tinto es la mayor concentración de sulfuros masivos encajados en rocas volcánicas de la corteza terrestre, con más de 1500 Mt de sulfuros masivos y un stockwork sub-económico asociado. El distrito minero alberga nueve cuerpos de sulfuros masivos que encajan en el Complejo Volcano-Sedimentario dentro de una zona fuertemente tectonizada y en ambos flancos de un antiforme Varisco.

La cartografía y el estudio geoquímico de las rocas volcánicas encajantes de la mineralización y de zonas adyacentes no afectadas por la alteración hidrotermal (Río Odiel y Zarandas) permiten diferenciar cuatro grandes unidades litológicas. De muro a techo estratigráfico se han definido: (1) la Unidad Máfico-Siliciclástica (*Mafic-Siliciclastic Unit*), compuesta por *sills* y lavas submarinas de composición basáltica que intruyen en una secuencia dominada por pizarra; hacia el techo, la pizarra presenta abundantes

intercalaciones de areniscas volcanoclásticas heredadas de las rocas anteriores; (2) Sobre esta unidad y de manera concordante se dispone la Unidad Sedimentaria Inferior (*Lower Sedimentary Unit*). Esta unidad está compuesta por pizarra oscura y a techo tiene un conglomerado polimíctico soportado por una matriz pizarrosa que incluye clastos de pizarra y roca félsica y, localmente, nódulos ricos en pirita de claro origen hidrotermal; (3) La Unidad Félsica *(Felsic Unit)* está formada por una potente secuencia volcánica constituida por domos y *sills* de dacita porfídica, rica en cuarzo y feldespato, y de riolita afírica, a los que se asocian autobrechas y brechas hialoclásticas interestratificadas con arenisca ricas en pómez, cristales y vidrio, ocasionalmente pizarra y con intrusiones de diques composicionalmente iguales a las rocas masivas. (4) La Unidad Sedimentaria Superior (*Upper Sedimentary Unit*) está compuesta por pizarras oscuras y sedimentos químicos (chert), que pasan lateralmente a areniscas volcanoclásticas. La intensa alteración hidrotermal que está Unidad presenta en algunas zonas, provoca un característico cambio de color de las pizarras a verde y moradas. A techo de la secuencia, y debido a una gran estructura de cabalgamiento, se encuentra el Grupo Culm.

La secuencia estratigráfica está afectada por una intensa e irregular alteración hidrotermal. La Unidad Félsica está intensamente sericitizada, y sólo localmente y cerca de las grandes fallas o de los sulfuros masivos, está alteración es remplazada por una paragénesis mineral de clorita y cuarzo. Por el contrario, la Unidad Sedimentaria Inferior y la Unidad Máfico-siliciclástica muestran una fuerte alteración clorítica produciendo un remplazamiento de la roca por clorita de grano fino y cuarzo.

El stockwork mineralizado está formado por una red de venas de cuarzo-sulfuros o sulfuros que cortan la roca alterada hidrotermalmente. La distribución de la alteración y el stockwork parece estar controlada por la porosidad y reactividad de las rocas encajantes, y está condicionada por fallas con dirección E-O y NO-SE que posiblemente correspondan a estructuras extensionales sinvolcánicas que han sido posteriormente

reactivadas durante la orogenia Varisca. En detalle, la mineralización está relacionada con los domos de dacita porfídica pero es anterior a la intrusión de la riolita.

Geoquímicamente, hay dos unidades volcánicas principales. La Unidad Máfico-Siliciclástica incluye rocas de composición entre basalto y andesita y afinidad toleítica. Los contenidos en los elementos inertes principales, Al_2O_3, TiO_2, y Zr, discriminan la existencia de dos grupos de rocas máficas, una unidad de basalto-andesita y otra de basalto rico en Ti-Zr que corresponde a intrusiones de dolerita y/o lavas localizadas en la zona sur del antiforme de Rio Tinto (El Campillo y al sur de Nerva). La Unidad Félsica, encajante de la mineralización y la volumétricamente predominante, está formada por rocas de composición dacítica a riodacítica. El contenido en tierras raras pesadas, Al, Y, Zr, Ti y Yb muestran dos grandes grupos que representan dos unidades volcánicas independientes: una riodacita con bajo contenido en Zr (50-200 µg/g) y localizada en Rio Odiel, Campillo y área de la mina, y un segundo grupo de riodacita con altos contenidos en Zr (>225 µg/g) y presente al norte del área de la mina. Es igual que en el sector septentrional de la Faja Pirítica, la geoquímica sugiere que ambos tipos provienen de una misma cámara magmática y la riodacita rica en Zr es el producto más evolucionado. Los sulfuros masivos se encuentran asociados a la riodacita con bajos contenidos en Zr, siendo rocas estériles las rocas félsicas más fraccionadas y evolucionadas.

Los sulfuros masivos se encuentran alineados según una dirección E-O en ambos lados del antiforme de Rio Tinto pero ocupan dos posiciones estratigráficas diferentes. La mineralización de la parte sur encaja en niveles de pizarra oscura de la Unidad Sedimentaria Superior y se interpreta como formada en un ambiente (sub-)exhalativo en una cuenca anóxica de tercer grado localizada a techo de un domo riodacítico. En el sector septentrional, la mineralización está formada por cuerpos estratoides de sulfuros masivos que han remplazado a las zonas apicales de los domos riodacíticos, sin que haya evidencias de depósitos formados por exhalación hidrotermal; estos cuerpos no están controlados por cuencas submarinas sino por las facies más permeables y

reactivas de los domos de la Unidad Félsica. El stockwork aflorante en la zona de Cerro Colorado correspondería a la zona de alimentación del sistema y corta a los cuerpos de remplazamiento.

Capítulo III

"Geología y geoquímica de la secuencia volcánica encajante de los sulfuros masivos del SE de la Faja Pirítica (España): La zona de Aznalcóllar-Las Cruces"

Los depósitos de sulfuros masivos del borde sureste de Faja Pirítica Ibérica (Aznalcóllar, Los Frailes y Las Cruces) se encuentran encajados en pizarra oscura y parcialmente cubiertos por los sedimentos del Terciario de la Cuenca del Guadalquivir. El distrito de Aznalcóllar alberga cinco cuerpos de sulfuros masivos y stockwork asociados, destacando por su tonelaje y riqueza los depósitos de Aznalcóllar y Los Frailes, con tonelajes iniciales de más de 120 Mt y con una leyes medias de 0.35% Cu, 1.95% Pb, 3.55% Zn y 64 gr/t Ag. El yacimiento de Las Cruces, situado 20 km al Este del distrito de Aznalcóllar, está formado un único cuerpo de morfología lentejonar con 20.7 Mt de reservas y unas leyes medias de 3.2% Cu, 0.4% Pb, 1.1% Zn, 28 gr/t Ag y 0.5 gr/t Au. Este depósito destaca por la intensa alteración secundaria de los sulfuros masivos primarios.

Las características estratigráficas y metalogenéticas de estos tres cuerpos de sulfuros masivos son muy similares. La mineralización encaja en pizarra oscura, ocasionalmente con niveles de argilita y/o arenisca, y justo a techo de un domo félsico que está, por lo general, intensamente alterado con cloritización y silicificación y en el que se encuentra el stockwork y la parte basal de los sulfuros masivos. Al igual que los otros depósitos del sector meridional de la Faja Pirítica, los cuerpos mineralizados se localizan en la parte inferior del Complejo Volcano-Sedimentario y suprayacente a la serie detrítica del Grupo PQ (pizarra y cuarcita).

La secuencia estratigráfica del CVS está formada por una serie sedimentaria con pizarra oscura, argilita y arenisca, en la que se emplazan (cripto-)domos y *sills* y rocas fragmentarias asociadas tales como depósitos de margen de domo, brechas autoclásticas, hialoclastitas y rocas epiclásticas. Se han diferenciado cuatro grandes unidades: (1) *La* Unidad Inferior (*Lower Unit*), formada por una complejo tipo domo de riodacita porfídica con fenocristales de cuarzo, plagioclasa y biotita y facies hialoclásticas asociadas situado bajo un nivel de pizarra oscura y arenisca volcanoclástica félsica, en los que encaja la mineralización. La riodacita y la pizarra basal presentan una intensa alteración irregular (cloritización ± silicificación ± sericitización) con un stockwork asociado. En Las Cruces se han observado rocas masivas (*sill* o lava) de carácter intermedio. A techo de la mineralización, y generalmente mediante un contacto mecánico, se pasa a; (2) La Unidad Intermedia *(Intermediate Unit)*, de carácter fundamentalmente félsico y en la que se diferencian dos subunidades: (A) una riodacita porfídica fragmentaria con fenocristales de feldespato, cuarzo y algo de biotita que se interpreta como un *mass flow* rico en pómez caracterizado por la presencia de un nivel guía de pizarra oscura con clastos de pómez alargados y asociado a niveles de ceniza. A techo, y separada por una secuencia poco potente de pizarras oscuras, verdes y hematíticas, y localmente, un *sill* basáltico (8-10 m) se encuentra la Unidad Intermedia (B). En Aznalcóllar, está formada por brechas polimícticas versicolores, con clastos de riodacita porfídica y afírica y que se interpretan como *debris-flows* distales a un domo félsico y que alternan con arenisca volcanoclástica y pizarra. En Los Frailes, es muy potente e incluye facies proximales de domo y consistentes en brecha félsica polimíctica, brecha riolítica monomictica estratificada, brecha riolítica in situ (hialoclastita), y riolítica porfídica masiva con textura de fino bandeado de flujo. En Las Cruces, la unidad tiene un mayor carácter volcanoclástico y está compuesta por una potente serie heterogénea de brecha y arenisca rica en cristales con características de *debris flow* y pizarras; localmente, lavas máficas; aquí se describe un nivel de pizarra rico en fragmentos de pómez con características similares a las observadas en el distrito de Aznalcóllar. (3) La Unidad

Superior *(Upper Unit)* en Aznalcóllar está formada por sedimentos siliciclásticos (pizarra y arenisca), niveles volcanoclásticos y brecha félsica, e intruidos por un complejo de *sills* félsicos con abundantes contacto peperíticos. En Las Cruces, esta unidad muestra características similares: está formada por pequeños cuerpos de composición dacítica en una secuencia donde alternan niveles volcanoclásticas de grano fino y pizarra. Aquí, las secuencia del CVS está cubierta por sedimentos del Neógono formado por marga y arena, y niveles de conglomerado polimíctico que incluye clastos siliciclástico, volcánicos y bioclastos.

La mineralización se interpreta como formada en una cuenca anóxica de tercer orden situada a techo de los domos de riodacita mas antiguos. La parte inferior de la mineralización parece remplazar a las facies apicales del domo y la superior es de carácter exhalativo.

La pizarra que es el encajante de la mineralización en el sector SE de la Faja Pirítica muestra un enriquecimiento en elementos típicamente presentes en ambientes anóxicos o reductores como el V, Cr, Mo y W, y consistentes con condiciones metalogénicas. Las relaciones Mn-Fe-V y V/(V+Ni) de las pizarras mineralizadas se proyectan en el campo de condiciones anóxicas (valores medios entre 0.69-0.92 V/V+Ni). Sin embargo, los niveles de pizarras estériles a techo de los sulfuros masivos muestran relaciones acordes a un ambiente de condiciones subóxicas a óxicas. Estos resultados confirman las conclusiones en otros depósitos de la parte meridional de la FPI, donde la mineralización está relacionada con condiciones anóxicas restringidas y locales.

Geoquímicamente, las unidades volcánicas de ambas zonas presentan algunas diferencias. Mientras que en el distrito de Aznalcóllar dominan las rocas de carácter ácido (riolita a dacita) y poco abundantes de composición basáltica, en Las Cruces son de carácter intermedio, variando de riodacita a andesita-basáltica. En ambos casos tienen una afinidad calcoalcalina. Los contenidos en elementos inmobiles tales como TiO_2, Zr y Nb discriminan claramente las unidades descritas en Aznalcóllar-Los Frailes, mientras

que en Las Cruces se proyecta en un único grupo sin grandes diferencias, aunque se puede diferenciar y correlacionar la Unidad Intermedia (A), unidad inmediatamente contigua a los sulfuros masivos en los tres depósitos. La geoquímica también remarcar una mayor e intensa alteración hidrotermal en Las Cruces donde toda la secuencia está afectada por una intensa cloritización con gran cantidad de sulfuros diseminados. Mientras, en Aznalcóllar y Los Frailes, esta queda restringida al muro de la mineralización, siendo nula o poco importante a techo.

Hay una importante deformación tangencial que hace que en todos los depósitos el stockwork se encuentre localmente cabalgando a los sulfuros masivos.

Capítulo IV

"Análisis de elementos traza por LA-ICPMS en pirita del depósito de Tharsis, Faja Pirítica (España)"

La pirita es el mineral principal en los sulfuros masivos volcanogénicos, algo que es especialmente relevante en la Faja Pirítica (FPI), donde la mayor parte de la mineralización (>90%) es pirita de grano fino. La pirita puede contener cantidades significativas de elementos traza, tanto en su estructura o como nanoinclusiones. El estudio de la concentración y distribución de estos elementos traza es un marcador que podría trazar la variación de los factores geoquímicos que controlan la precipitación de los sulfuros y podría ser hipotéticamente usado como guía de exploración. En este trabajo se presentan los resultados del estudio del análisis de los elementos traza mediante la técnica de ablación láser con plasma de acoplamiento inductivo (LA-ICPMS) en la pirita del cuerpo de Filón Norte, Tharsis, uno de los mayores yacimientos de la parte sur del la FPI.

En la mina de Tharsis, la mineralización está situada en la base del Complejo Volcano-Sedimentario (CVS), interestratificada con pizarra y en contacto directo con el Grupo PQ

infrayacente en el que se encuentra una grande e irregular zona de stockwork (>200m) fuertemente alterada a clorita. La mineralización está formada por varios lentejones apilados tectónicamente de pirita de grano fino con pequeños niveles de brecha con fragmentos de pirita y pizarra. En la zona basal, hay unas facies brechoides matriz-soportadas con fragmentos de sulfuros y siderita con texturas bandeadas (*mineralización cabonatada*) en una matriz de composición similar. En contacto con la pizarra de techo, alternan niveles de pirita y pizarra con abundantes estructuras sedimentarias (slump, brechas, laminaciones, etc.), probablemente relacionadas con actividad tectónica sinsedimentaria (mineralización bandeada).

Los análisis por LA-ICPMS muestran que los contenidos en Cu, Pb y Zn en la pirita de todas las facies son altos pero erráticos, destacando los elevados contenidos en Pb (1300-4900 µg/g). Estos valores se interpretan como debidos a la existencia de inclusiones nanométricas de calcopirita, galena y esfalerita, minerales muy abundantes en toda la mineralización. En general, hay una fuerte correlación de Pb:Ag (r=0.98), aunque en la mena brechoide esta es entre Ag y Cu (r=0,98). Estas relaciones sugieren la presencia de inclusiones de galena argentífera y tetraedrita, respectivamente. La pirita de la mineralización bandeada y carbonatada muestra una correlación entre Pb y Bi, posiblemente debida a la presencia de inclusiones de sulfosales de Pb-Bi, tales como wittichenita, común en las zonas del depósito ricas en Cu.

La textura de la pirita y la concentración de estos elementos están relacionadas con los mecanismos de cristalización de los sulfuros. En este sentido, podría establecerse un tipo de correlación entre ambos parámetros. Los valores más altos se registran en pirita espongiforme y/o agregados de pequeños cristales euhedrales de posible origen primario o diagenético temprano. Las concentraciones disminuyen gradualmente a medida que los granos de pirita se hacen más grandes.

Un segundo grupo de elementos, As, Mn, Tl, Mo, Ni, Co y Au, muestran una distribución más irregular que pudiera estar controlada por las condiciones de

precipitación. El As es la sustitución no estequiométrica más destacada. La pirita framboidal y coloforme de la zona de stockwork es la que tiene los valores más altos (1650-4730 µg/g); presenta una buena correlación con el contenido en Au, que aparece con valores entre 1 y 8 µg/g. El enriquecimiento de As se interpreta como relacionado con la precipitación rápida de la pirita en condiciones de alta temperatura y baja fS_2, lo que provoca el desequilibrio y rápida precipitación de la pirita coloforme incorporando As en su estructura.

La pirita de la mineralización carbonatada muestra los valores más altos de Mn (>300 µg/g). Este enriquecimiento estaría relacionado con la precipitación de pirita en condiciones de baja temperatura y condiciones de redox intermedias. Además, esta pirita también está enriquecida en Mo (2 µg/g) lo que podría estar asociado al cambio en las condiciones redox o a una recristalización hidrotermal tardía.

Los sulfuros masivos de la FPI muestran un contenido en Sn superior a otros distritos similares. En Tharsis, la mayor parte del Sn está como inclusiones de casiterita en la esfalerita y probablemente en la pirita. Aunque la estannita es un mineral accesorio, no siempre hay correlación positiva entre Cu y Sn. La casiterita submicroscópica precipitaría junto a la pirita en condiciones de fS_2 intermedia.

El Co y Ni son los elementos traza más utilizados en el estudio geoquímico de la pirita. Ambos elementos suelen presentarse como sustitución estequiométrica ya que por sus características isomorfas y su carácter calcófilo se incorporan en la estructura de la pirita remplazando al Fe. En Tharsis, las concentraciones más altas de Co se encuentran en la pirita que forma agregados cristalinos de las facies de stockwork (<330 µg/g) y en la mineralización bandeada (<730 µg/g). La mineralización bandeada presenta los valores medios más bajos (<50 µg/g). En general, la pirita de todos los tipos de mineralización tiene contenidos muy bajos de Ni, por debajo de 8 µg/g. La variabilidad de Co y Ni parece estar asociada a la alta temperatura de precipitación, que desestabiliza la estructura de la pirita y aumenta la solubilidad del Co.

Por lo tanto, el estudio geoquímico de la pirita de los sulfuros masivos de Tharsis sugiere que el contenido en elementos traza está controlado por tres factores: (a) el grado de madurez textural, con la pirita más temprana y menos ordenada siendo más proclive a la captura de los metales; (b) la temperatura de formación, que facilitaría la entrada de metales en la estructura; y, (c) las condiciones fisicoquímicas que favorecerían la precipitación de determinados tipos de nanoinclusiones.

Estos resultados preliminares muestran que la concentración y distribución de elementos traza en la pirita podrían ser de ayuda en la definición de campañas de exploración minera. Sería de utilidad para diferenciar las zonas proximales y distales de los sulfuros masivos, así como las zonas de stockwork y removilizaciones tardías.

Capítulo V

"Modelización hidrodinámica de los sulfuros masivos de la zona sur de la Faja Pirítica Ibérica (España)"

En la parte sur de la Faja Pirítica Ibérica (FPI) se encuentran algunos de los cuerpos de sulfuros masivos volcanogénicos más grandes de esta provincia metalogenética. Son cuerpos estratiformes ricos en pirita que se encuentran en niveles de pizarra oscura depositados en condiciones sub-óxicas a anóxicas en cuencas restringidas de tercer orden con circulación restringida; la edad de todos estos depósitos coincide con el límite Devónico-Carbonífero. En la mayor parte de los casos - excepto Tharsis - se encuentran a techo de una unidad de (cripto-domos) de riodacita félsica con rocas masivas flanqueadas por rocas volcanoclásticas asociadas. La formación de estos sulfuros masivos es producto de la mezcla de fluidos hidrotermales profundos y calientes que se mezclaron con agua marina en la que el sulfato ha sido reducido biogénicamente a H_2S.

En este trabajo se presentan los resultados de dos modelos bidimensionales (2D) de alta resolución que simulan la formación de este tipo de sulfuros masivos en una cuenca

marina durante los primeros estadios de extensión e intrusión de rocas ígneas durante el límite Devónico-Carbonífero. Se han supuesto dos casos extremos de composición de fluidos hidrotermales. El primer modelo fue testado para un supuesto en el que el basamento - una secuencia siliciclástica con arenisca y pizarra equivalente al grupo PQ - está saturado en agua “pura” con una salinidad 0% peso NaCl; el segundo modelo supone que el basamento está saturado en un fluido de salinidad y densidad intermedia, similar al detectado en los sulfuros masivos de la Faja Pirítica. El modelo tiene como objetivo verificar si es posible generar un campo de flujo suficiente para generar los depósitos gigantes de sulfuros masivos por convección térmica y cómo influye la salinidad del fluido connato en el sistema.

Los modelos han sido desarrollados mediante un programa denominado CSP, “Complex System Platform” que resuelve simultáneamente las ecuaciones físicas que controlan el flujo de fluido y el transporte de calor en un medio poroso. Las condiciones geológicas del sistema están basadas en un modelo ideal de la Faja Pirítica con un gradiente geotérmico típico de cuencas similares y bajo la superficie del mar.

El modelo basado en la circulación de “agua pura” muestra, ya en los primeros estadios, el desarrollo de una circulación convectiva capaz de conducir grandes cantidades de fluidos calientes y moderadamente salinos al fondo oceánico. Los fluidos ascienden principalmente a lo largo de grandes fallas y pueden producir eventualmente la precipitación de los sulfuros masivos en sistemas ricos en H_2S y condiciones reductoras. Los resultados de la simulación en un ambiente en el que los fluidos connatos son más salinos (Caso 2) muestran que el campo de flujo convectivo generado, es muy sensible a la salinidad de la solución. La dinámica de los fluidos, la velocidad de la convección termohalina y la transferencia de solutos cambia significativamente. El flujo de fluido termohalino requiere más tiempo para que el gradiente geotérmico anómalo desarrolle la circulación convectiva (el triple de tiempo de modelización que para el modelo con “agua

pura") y nunca llega a generar un campo de temperaturas elevadas y velocidades de flujo anómalas en el fondo oceánico.

Los resultados también sugieren que la formación de los sulfuros masivos en la zona sur de la Faja Pirítica puede ser controlada por una circulación convectiva forzada asociada a un periodo extensional pero sin que sea necesaria una fuente de calor procedente de intrusiones someras. Una intrusión ígnea no es un factor condicionante para que se formen las grandes células convectivas en el sistema. Por el contrario, la salinidad y estructuras tectónicas sí que son elementos críticos. La salinidad condiciona la temporalidad y tamaño de las células convectivas, mientras que la distribución de las fallas determina la distribución de las celdas y controlando la compartimentación del flujo.

En ambos casos, los modelos numéricos muestran que los fluidos más salinos y de mayor temperatura son los primeros en ascender y ser exhalados en el fondo marino. Estos procesos tienen lugar tan pronto como se desarrollan las primeras células hidrotermales convectivas, alcanzándose salinidades de 4-5% peso NaCl y temperaturas de hasta 150-250ºC, condiciones consistentes con las de formación de muchos de los depósitos de la zona meridional de la Faja Pirítica. Teniendo en cuenta la relación directa entre la salinidad, la temperatura y la solubilidad de los metales transportados como complejos clorurados, sería lógico pensar que estos flujos convectivos serían los que dieron lugar a la formación de los sulfuros masivos en la zona sur. Los resultados también son coherentes con la edad de los sulfuros masivos; la palinología sugiere que se formaron en un lapso de tiempo muy corto, de menos de 1 Ma. El modelo muestra que solo durante los primeros estadios el campo de flujo generado es capaz de transportar fluidos salinos y calientes hacia el fondo marino, declinando la temperatura y salinidad rápidamente. Si se excluye una anomalía térmica de origen magmático en la base del sistema, los fluidos tardíos son demasiado fríos y poco salinos como para transportar cantidades significativas de metales.

CAPITULO I

Lithostratigraphy, geochemistry and architecture of the volcanic host sequence of the massive sulphides in the northern Iberian Pyrite Belt (Huelva, Spain)

Litoestratigrafía, geoquímica y arquitectura volcánica de la secuencia que alberga los sulfuros masivos en la parte norte de la Faja Pirítica Ibérica (Huelva, España)

Abstract

The northernmost Iberian Pyrite Belt hosts several massive sulphide orebodies aligned in a major E-W belt located just south of the regional thrust that limits the South Portuguese Zone with the Pulo do Lobo Unit. Except for Aguas Teñidas and Magdalena (ca. 45 Mt of massive sulphides each one), these massive sulphide bodies have small tonnages (< 15 Mt) but they are economically important because of their high base and precious metal grades.

A detailed geological study of the hosting Volcanic Sedimentary Complex allows differentiation of six principal tectonostratigraphic units: (1) The *Footwall Felsic Unit*, that is composed of feldspar-quartz-phyric rhyodacite (crypto)-dome complexes including coherent facies and associated hyaloclastite breccia, also intruded by sills and dykes of similar composition. Alternating volcaniclastic siltstone and pumice and glass-rich breccia beds occur at the top and on the lateral margins of the dome complexes. A major shear zone separates the Footwall Felsic Unit from the overlying Volcano-Sedimentary Unit. (2) The *Volcano-Sedimentary Unit*, composed of vesicular basaltic lava and associated mafic epiclastic sandstone and siltstone, intercalated with thin beds of shale. This Unit is characterized by striking lateral and vertical facies changes. Another major tectonic contact marks the boundary between this unit and a second felsic-dominated unit. (3) The *Hanging wall Felsic Unit,* a series of intercalated coherent rhyolite domes and associated volcaniclastic rocks, and polymictic epiclastic sedimentary rocks, cut by numerous felsic and mafic volcanic and geochemically equivalent sub-volcanic intrusions. (4) The *Sedimentary Unit*, a highly deformed package of grey siltstone with interlayered shale and fine-grained epiclastic sedimentary rocks. Mylonitic fabrics are common in this unit, recording greater strain accommodation relative to the rest of the complex. (5) The *Upper Felsic Unit,* a package of dacitic to rhyolitic dome complexes with similar characteristics to the Footwall Felsic Unit. Both the basal and upper contacts of this unit are narrow and

high-strain tectonized zones. (6) The uppermost unit, the *Andesite Unit*, comprises andesitic dome complexes rich in hyaloclastite breccias and andesitic volcaniclastic sedimentary rocks. Massive sulphides are hosted dominantly by the Footwall Felsic Unit with only some orebodies related spatially to the Upper Felsic Unit (Lomero Poyatos, San Telmo and El Carpio).

Geochemically, the Volcanic Sedimentary Complex is dominated by andesitic to rhyolitic calc-alkaline magmatic rocks with subordinate tholeiitic basalt. Overall, the Volcanic Sedimentary Complex includes rocks defining a continuum of silica content ranging from basalt to rhyolite, with a significant proportion of dacite and andesite. The Footwall Felsic and Upper Felsic Units are geochemically identical and probably represent dismembered parts of a single volcanic felsic complex. If that holds true, massive sulphide deposits of the northern IPB are hosted in volcaniclastic rocks located in the hanging wall of a single unit dominated by dacite-rhyolite dome complexes. This volcanic unit is characterized by Zr contents below 200 µg/g, that are significantly lower than those of the more evolved Hanging wall Felsic Unit (200-750 µg/g); they are interpreted as two independent batches of magma of the same deep magma chamber.

Cross-cutting relationships, structural analysis and the geochemical data suggest that the volcanic sequence is tectonically inverted, with the youngest units located at the lowest structural position. The proposed reconstructed stratigraphic sequence comprises an andesitic footwall, overlain by the felsic complexes of the Hanging wall Felsic and Footwall-Upper Felsic Units. Mafic rocks and related sediments occurred interbedded with the felsic rocks right above Andesitic Unit. Thus, the massive sulphide deposits formed toward the top of the felsic package and associated with the youngest felsic rocks.

Keywords: Northern Iberian Pyrite Belt; volcanogenic massive sulphides; geochemistry; volcanic architecture; hydrothermal alteration.

1. Introduction

The northern Iberian Pyrite Belt (IPB) hosts several large and well known massive sulphide orebodies such as Rio Tinto (Rambaud, 1969; Williams et al., 1975; Solomon et al., 1980; Badham, 1982, 2001; García Palomero, 1992; Boulter, 1993a, 1993b; Mellado et al., 2006; González Clavijo et al., 2010; Valenzuela et al., 2011a, 2011b; Martín Izard et al., 2015), La Zarza (Strauss et al., 1981), Concepción (Sánchez España, 2000), San Platón, or San Miguel (Fig. 1). However, near its margin with the adjacent terrane of the Pulo de Lobo Zone there is a significant group of deposits that has deserved significantly less attention. Despite being poorly known, these deposits define one of the most interesting exploration targets of the IPB because of their high base and precious metal contents in contrast with the dominance of pyrite in other zones of the belt. From west to east, the area includes the mines of El Carpio, San Telmo, Lomero Poyatos, Confesionarios, Aguas Teñidas, Magdalena, Castillejito, Cueva de la Mora and Monte Romero (IGME, 1982; www.trafigura.com). The total tonnage of the Aguas Teñidas deposit is about 41.4 Mt of massive sulphides and ca. 21.2 Mt of mineralized stockwork (pers. comm., 2015), including a large barren pyrite zone, while the recently discovered deposit of Magdalena has more than 41.5 Mt of massive sulphides (Pons, pers. comm., 2015). The other deposits are relatively small if compared to the giant deposits of the southern IPB (Table 1). Aguas Teñidas and Magdalena are the only deposits currently in production, being mined by MATSA, a subsidiary of Trafigura Mining Group (www.trafigura.com).

All these mines are aligned along a 15 km E-W trending band. In general, the deposits are located near zones of high strain and spatially associated with regional thrusts or shear zones that probably represent early extensional syn-depositional structures that were later inverted during the Variscan orogeny (Quesada, 1998) (see Figs. 1 and 2).

The massive sulphides of the northern IPB are hosted by a deformed sequence of

Figure 1. Simplified geological map of the northern zone of the Iberian Pyrite Belt, showing the location of the major massive sulphide deposits (modified from IGME 1982; ITGE 2000; Junta de Andalucía, 2004; Oliveira, 1990; Quesada 1991, 1996, 1998). The study area (Fig. 2) is indicated by a rectangle. The inset shows the map of the South Portuguese Zone (modified from Quesada 1998) and its localization in the Variscan Belt of the Europe (adapted from Oliveira and Quesada, 1998). Ore deposit abbreviations: AZ-LF: Aznalcóllar-Los Frailes; ATE: Aguas Teñidas; MA: Magdalena; CO: Concepción; LC: Las Cruces; LO: Lomero Poyatos; NC: Neves Corvo; RT: Río Tinto; SO: Sotiel; TH: Tharsis

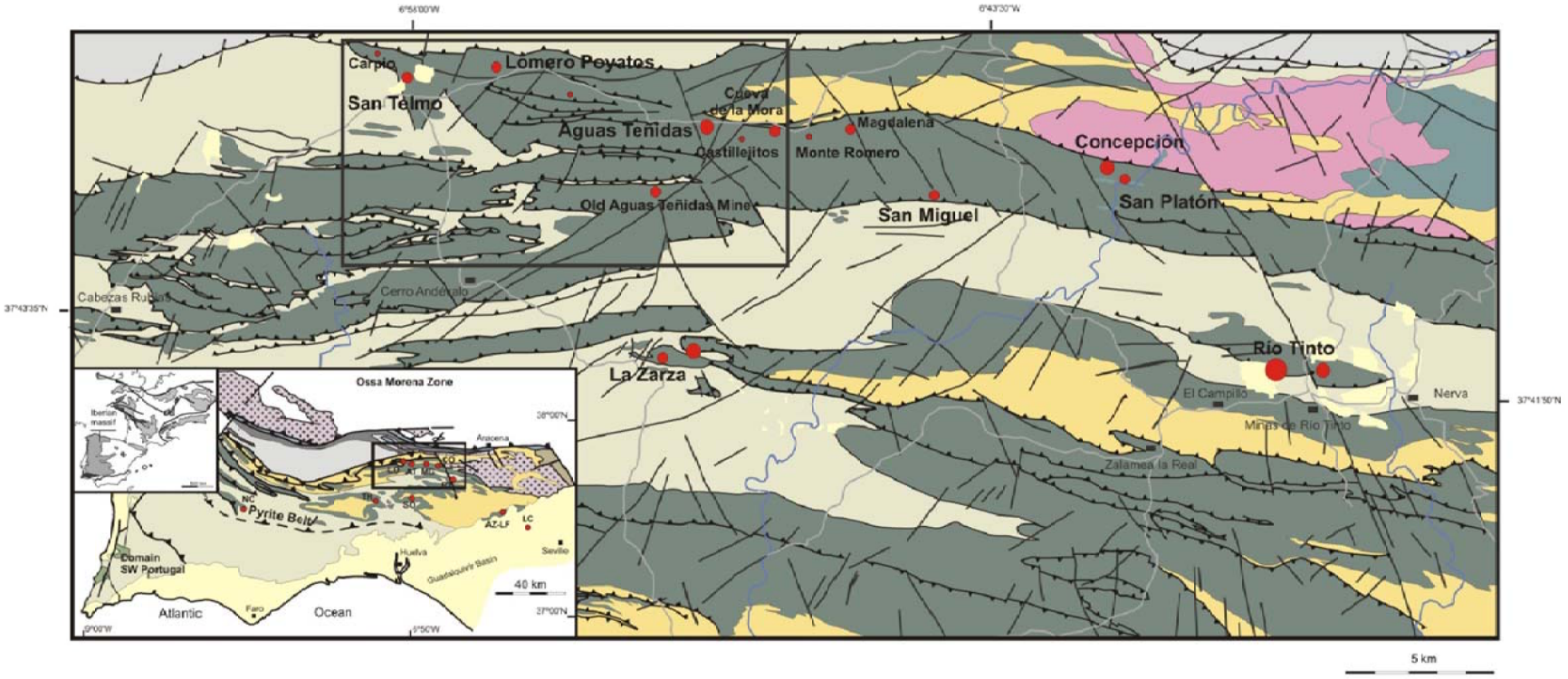

Pre-Mesozoic Massif

Beja-Acebuches Complex

Ophilitic Sequence (Beja Acebuches Ophiolite)

Pulo do Lobo Antiform

Oceanic Sedimentary Sequence (Pulo do Lobo Terrane)

Sandstone and shale (late Devonian)

Iberian Pyrite Belt

Flysch sequence (Culm Group) (late Visean)

Volcanic Sedimentary Complex (late Fammenian-M. Visean)

Phyllite-Quartzite Group (PQ Group) (middle-late Fammenian)

SW Portuguese Domain

Pre-orogenic sequence (late Devonian-late Carboniferous)

Continental sediments and volcanic rocks (Stephanian to Permian)

Post-Paleozoic Cover

Plutonic rocks

Granite & granodiorite

Gabbro & diorite

Thurst

Fault

VHMS deposits

Township

volcanic and sedimentary rocks (Volcanic Sedimentary Complex, VS Complex) dominated by felsic volcanic rocks (approximately 60%; Tornos, 2006). Mafic volcanic rocks are scarcer and occur in tectonostratigraphic units apparently unrelated to the massive sulphides. Primary stratigraphic relationships of the VS Complex are poorly known because of the abundance of tectonic contacts, the wide variety of volcanic rocks displaying rapid lateral and vertical facies changes, and the presence of widespread overprinted deformation and hydrothermal alteration.

Table 1. Tonnages and ore grades of the most important massive sulphide deposits of the northern zone of Iberian Pyrite Belt.

Deposit	Mt	%Cu	%Pb	%Zn	Ag g/t	Au g/t	Reference
Old Aguas Teñidas [1]	0.42	5.66					Pinedo (1963)
Aguas Teñidas Mine [1]							
cupriferous	9.43	2.40	0.20	0.90	28.30	0.40	Iberian Minerals Corp
pollymetalic	10.12	1.10	2.50	8.20	77.80	0.90	(2009)
stockwork	1.36	2.25	0.06	0.25	7.1	0.06	
Carpio	3.35	0.50	0.12	2.77			Leistel et al. (1998)
Concepción	55.85	0.57	0.19	0.48	6.68	0.21	Leistel et al. (1998)
Cueva de la Mora	4.2	1.45	0.26	0.73			Pinedo (1963)
La Zarza	171.6	1.24	1.09	2.49	45	1.79	Tornos (2006)
Lomero Poyatos	15.45	1.35	1.12	3.76	83.48	3.25	Tornos (2006)
Monte Romero	0.8	2.0	2.5	5.0			IGME (1982)
Río Tinto [2]	707.2	0.39	0.12	0.34	22	0.36	Tornos (2006)
San Platón	2.5	1.5	0.2	5.6	31	0.9	Tornos (2006)
San Miguel	1.3	3.0					Pinedo (1963)
San Telmo	4	1.2	0.4	12	60	0.8	IGME (1982)

[1] Aguas Teñidas Mine and old Aguas Teñidas are nowadays a single ore deposit. Tonnage here is that of the minable ore (cupriferous + polymetallic Zn-Pb) but the pyrite-rich massive sulphides exceed 100 Mt.

[2] Primary+secondary ore

Facies analysis of volcanic rocks is critical and has been successfully employed elsewhere as a tool to aid in the interpretation of the environment of formation of massive sulphide mineralization and, thus, for exploration (e.g., Allen et al., 1996a, 1996b; Lentz, 1999; Doyle and McPhie, 2000; Lafrance et al., 2000; Montelius, 2005; Schlatter, 2007).

This is because massive sulphides are usually spatially related to specific volcanic facies (i.e., above felsic domes or within or near crystal/pumice-rich volcaniclastic strata) or in third order basins.

Most studies of the volcanology in the IPB focused on the southern and central Iberian Pyrite Belt. In the Portuguese sector, the most significant volcanological studies are those of Rosa (2007) and Rosa et al. (2008, 2010) in Neves Corvo (Portugal). However, several studies have been done in the Spanish part of the IPB, including the Rio Tinto district (e.g., Boulter, 1993a, 1993b, 2001), the Odiel River and the Paymogo area (e.g., Valenzuela et al., 2001, 2002, 2003; Donaire et al., 2006), the Aznalcóllar-Los Frailes deposits (Sierra, 1984a, b; Almodóvar et al., 1998; Allen, 2001; Donaire et al., 2002; Conde et al., 2003) Las Cruces Mine (Bobrowicz, 1995; Knight, 2000; Conde et al., 2007), and the more general studies of Soriano (1997), Soriano and Martí (1999), Boulter et al. (2001, 2004), Tornos (2006) and Valenzuela et al, (2011 a, b).

Soriano (1997) and Soriano and Martí (1999) presented the first systematic and detailed study of the volcanic and sedimentary rocks of the central IPB. They discriminated between different types of volcanic facies, including coherent silicic and mafic volcanic, siliciclastic, transported volcaniclastic, and hydrothermal facies. Their facies analysis indicated a submarine and below-wave base environment for the volcanism, with most of the coherent rocks interpreted as sub-volcanic sills. These rocks are associated with syn-eruptive and volcaniclastic mass flows, in a scheme similar to that proposed by Boulter (1993b, 2004). In these models, up to 90 percent of the volcanic rocks are high level sills intruded into water-saturated sediments, leading to abundant peperitic intrusions in a sediment-sill complex similar to that developed in the Guaymas basin. These models highlight the importance of these sills in the volcanic architecture of the IPB, in contrast with more recent and detailed studies that show that sills, despite being present, form only a small portion of the VS Complex (Donaire et al., 2002; Valenzuela et al., 2002; Tornos, 2006; Rosa et al., 2008). These latter authors suggest

that the VS Complex is comprised of variable proportions of dome-sill complexes, associated breccia and sandstone, pumice- and crystal-rich volcaniclastic rocks, and locally abundant shale, all deposited in a submarine environment.

The comprehensive studies of the volcanic and sedimentary facies of the VS Complex in the Neves Corvo area and other selected zones of the IPB (Rosa, 2007; Rosa et al., 2008, 2010) show that the volcanic rocks were deposited in a submarine, below wave base setting, comprised of felsic volcanic rocks (rhyolitic and dacitic coherent rocks and breccia, fiamme-rich volcanic rocks, and volcaniclastic rocks), minor mafic rocks (intrusions and lava flows) and mudstone. The analysis of the architecture of the volcanic facies indicates that most of them represent the classic dome complex scheme with three different environmental and depositional styles relative to the centres of volcanism: proximal, dominated by lava flows, domes and intrusions; intermediate, with autoclastic and pyroclastic deposits lateral and above the proximal facies; and, distal facies composed by interbedded crystal-rich sandstone and mudstone. A similar scheme was described by Conde et al. (2003, 2007) for the felsic volcanic sequence of the southeastern Iberian Pyrite Belt, including the massive sulphide deposits of Aznalcóllar-Los Frailes and Las Cruces (see Chapter III).

These volcanological studies have been accompanied by systematic detailed studies of the geology, structure and geochemistry of the major ore deposits, in some with special emphasis on the genesis of the massive sulphides and their relationships with the hosting sedimentary and volcanic rocks (Barriga, 1990; Oliveira, 1990; Munhá et al., 1997; Almodóvar et al., 1998; Leistel et al., 1998; Tornos et al., 1998, 2005; Carvalho et al., 1999; Sáez et al., 1999; Relvas, 2000; Relvas et al., 2006; Tornos, 2006; Rosa, 2007; Rosa et al., 2010; Valenzuela et al., 2011a, b).

However, there are no detailed studies of the regional geology of the northernmost IPB; the few descriptions are based on the volcanic rocks directly related to the ore deposits

(Bobrowicz, 1995; Hidalgo et al., 1996, 2003; Sánchez España, 2000; McKee et al., 2001, 2003; Tornos, 2006). Sánchez España (2000) focused his work on the massive sulphide deposits of the northwestern area of the IPB (San Telmo, San Miguel and Peña del Hierro). That study dealt with the mineralogy and geochemistry, and using fluid inclusion and isotope analyses of the massive sulphides concluded that they formed due to the circulation of modified seawater with a significant magmatic component. This study only briefly examined the geology and the lithogeochemistry of the volcanic rocks and their hydrothermal alteration. Bobrowicz (1995), McKee et al. (2001; 2003) and Hidalgo et al. (2003) confined their studies to the Aguas Teñidas deposit and surrounding areas. Only, Bobrowicz (1995) undertook a detailed study of the geology, mineralogy and geochemistry of the Aguas Teñidas massive sulphides and their host rocks.

This contribution presents the results of a comprehensive study of the structure and lithology of the volcanic units that dominate in the northern IPB. It is a synthesis of detailed field mapping, using cross sections and lithological columns, systematic logging of selected drill cores from the Aguas Teñidas and the Lomero Poyatos mines, and detailed petrography. This has been complemented by the geochemistry of the volcanic units. These data permit the characterization of the volcanic facies, the mode of emplacement of each unit, and a proposed stratigraphic sequence and the reconstruction of the volcanic and ore-depositional environment.

2. Geological setting

The Iberian Pyrite Belt is arguably the largest volcanogenic massive sulphide province in the world. It contains more than 2,500 Mt of massive sulphides mainly hosted in nine “giant” (> 100 Mt) deposits and more than 80 smaller mines (Leistel et al., 1998; Tornos, 2006), making it the largest sulphur anomaly in the Earth’s crust (Laznicka, 1999). The IPB is interpreted as having formed within a late Devonian to early Carboniferous intracontinental pull-apart basin on the South Portuguese Zone. This basin formed during

the Variscan Orogeny above a subducting plate as a forearc trench basin during oblique collision with the autochthonous Iberian Massif terrane (Silva et al., 1990; Quesada et al., 1998). This somewhat unusual geotectonic setting provided the environment for the development of major volcanic and hydrothermal activity that were critical to the ore forming processes (Fig. 1).

The lower part of the stratigraphic sequence is composed of interbedded quartz sandstone and shale. These rocks were deposited in a stable and shallow continental platform during the Fammenian and are included in the Phyllite-Quartzite Group (PQ Group); the total thickness of this footwall succession is unknown but probably exceeds 2000 m (Tornos, 2006). They are conformably overlain by a complex sequence of volcanic rocks and intercalated mudstone and chemical sediments. The magmatic sequence ranges in composition from basaltic to rhyolitic and includes massive volcanic rocks, subvolcanic intrusions and volcaniclastic rocks (Munhá, 1983; Boulter, 1993a, 1993b; Sáez et al., 1996; Mitjavila et al., 1997; Leistel et al., 1998; Soriano and Marti 1999; Tornos, 2006; Rosa, 2007; Valenzuela et al., 2011b). This volcano-sedimentary unit formed from late Fammenian to early Visean times (Oliveira, 1990) and is included in the VS Complex with a thickness of up to 1300 m (Tornos, 2006). The VS Complex is overlain by the thick and monotonous turbidite-like sediments of the Baixo Alentejo Flysch Group, an up to 3000 m thick synorogenic sequence deposited in the foreland basin of the growing orogeny (Moreno and Sáez, 1990; Moreno, 1993).

Large scale folds and thrusts with south to southwest vergence deformed the sequence during the late Visean, in response to the final collision of the South Portuguese Zone with the autochthonous Iberian Terrane (Onézime et al., 2003; Simancas et al., 2006; Azor et al., 2008). Further, during late Carboniferous a second tectonic episode (D_2) developed a deformation event dominated by NW-SE to E-W trending structures (Silva et al., 1990; Quesada, 1998; Onézime et al., 2002). The regional metamorphic grade varies from prehnite-pumpellyite to greenschist facies (Schermerhorn, 1975; Munhá, 1979, 1990).

Both the deformation and the metamorphic increase to the north and with proximity high strain zones (Sánchez España, 2000).

The VS Complex shows major lithological differences along the IPB. The southern IPB is characterized by the abundance of sedimentary rocks, mostly shale, whereas the northern part is characterized by the predominance of volcanic rocks which show a deformation and metamorphic grade more intensive that on the south part. These geological parameters –lithology and deformation- seem to affect greatly to the style of mineralization.

The massive sulphides are traditionally interpreted as located in the hanging wall of felsic dome complexes (Barriga, 1990; Sáez et al., 1996), in a situation similar to that described by Ohmoto (1996) in the Hokuroko district or Barrie et al. (1993) for some of the deposits in the Abitibi Belt. This is not true for the deposits in the southern part of the belt (e.g., Tornos et al., 2008), but is typical of the deposits in the northern part. Thus, massive sulphide deposits of the IPB can be grouped in two broad categories (Tornos, 2006). In the northern zone, where volcanic rocks predominate, massive sulphide mineralization is hosted by volcaniclastic and epiclastic breccia and sandstone rich in pumice and glass-shards, and is interpreted to have formed primarily by replacement of these rocks. In contrast, massive sulphide deposits of the southern zone are hosted by shale and appear to have formed by hydrothermal exhalation into third order anoxic marine basins.

3. Geology of the Volcanic Sedimentary Complex in the northernmost IPB

The northern IPB is characterized by a complex Variscan structure in which several tectonostratigraphic units crop out in narrow and elongated domains of ca. 10-15 km long and up to 1-3 km thick, dipping steeply to the north or moderately to the NNE. These are limited by major NW-SE to WNW-ESE south-verging thrusts and shear zones. Laterally, these tectonostratigraphic units wedge between adjacent units, reflecting the overall ramp

Figure 2. Geological map of the San Telmo-Aguas Teñidas area showing the distribution of the main lithofacies, structures and ore deposits. The studied areas are marked by rectangles.

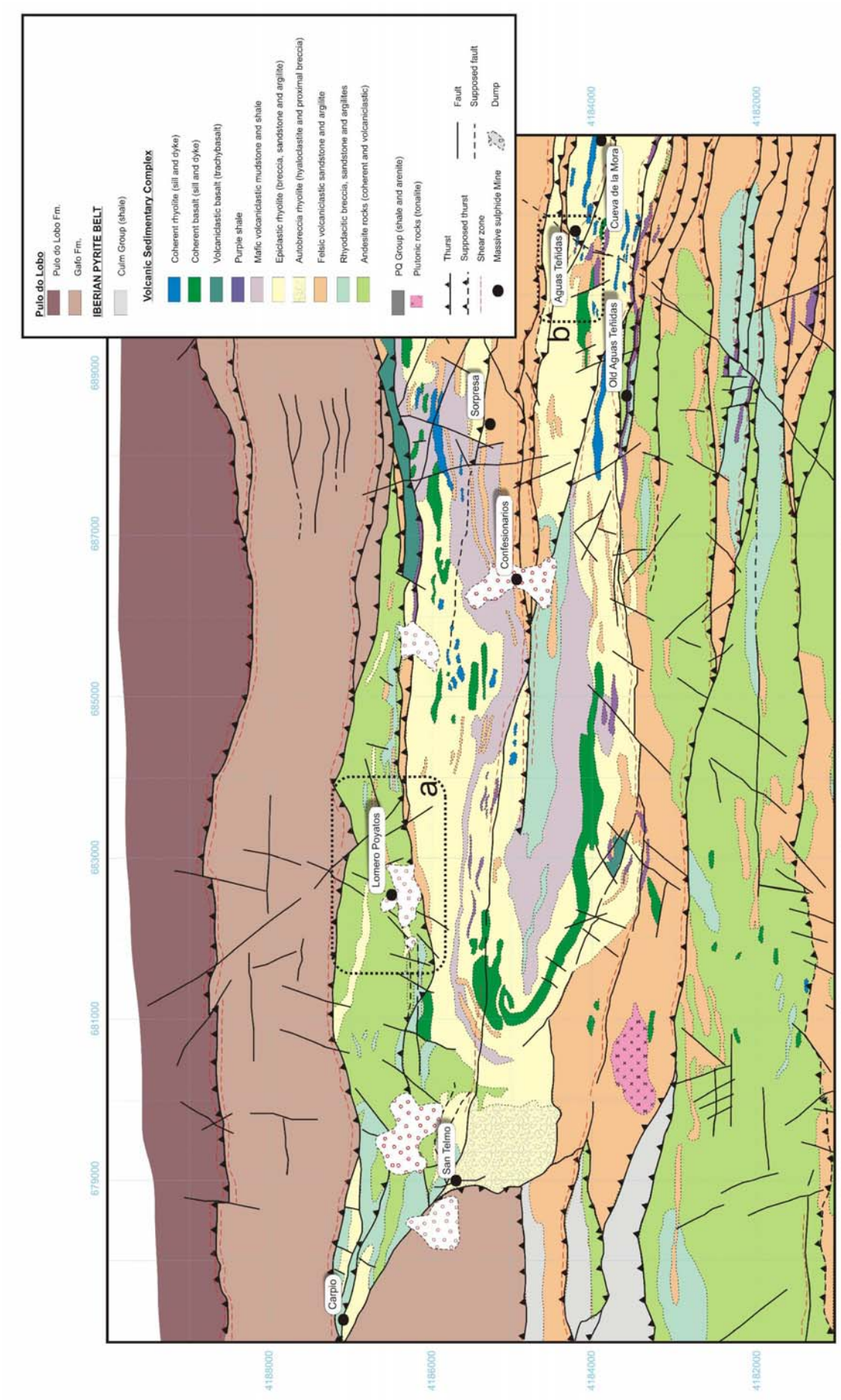
Pulo do Lobo
Pulo do Lobo Fm.
Gafo Fm.
IBERIAN PYRITE BELT
Culm Group (shale)
Volcanic Sedimentary Complex
Coherent rhyolite (sill and dyke)
Coherent basalt (sill and dyke)
Volcaniclastic basalt (trachybasalt)
Purple shale
Mafic volcaniclastic mudstone and shale
Epiclastic rhyolite (breccia, sandstone and argilite)
Autobreccia rhyolite (hyaloclastite and proximal breccia)
Felsic volcaniclastic sandstone and argilite
Rhyodacitic breccia, sandstone and argilites
Andesite rocks (coherent and volcaniclastic)
PQ Group (shale and arenite)
Plutonic rocks (tonalite)
Thrust
Supposed thrust
Shear zone
Massive sulphide Mine
Fault
Supposed fault
Dump
Carpio
San Telmo
Lomero Poyatos
Sorpresa
Confesionarios
Aguas Teñidas
Old Aguas Teñidas
Cueva de la Mora
a
b
679000
681000
683000
685000
687000
689000
691000
4188000
4186000
4184000
4182000

and flat structure of the IPB (Quesada, 1999). In detail, these units represent structurally dismembered parts of the VS Complex. Internally, they also reproduce the regional ramp and flat structures that are developed synchronously with cleavage and give rise to spindle-like morphologies at all scales. The area was affected by major deformation with almost all the lithologies showing conspicuous cleavage and widespread thrusting. The development of foliation is controlled by rock competency. Massive and coherent rocks have little or no foliation, whereas volcaniclastic rocks, fine grained siliciclastic rocks, and hydrothermally altered rocks commonly have conspicuous foliation. There is a main cleavage (S_1) formed synchronously with major shearing that is locally overprinted by a younger crenulation cleavage (S_2). In general, major shear bands are channelized along the more ductile rocks.

Many of these structures are latterly reactivated with a sinistral strike-slip component. Finally, late NE-SW faults offset the volcanic sequence. Most massive sulphide deposit in this sector of the IPB are located close to some of these major structures and are themselves strongly deformed (Fig. 2).

The northern limit of the study area is a major Variscan thrust zone that delineates the contact between the IPB with the southern limb of the Pulo do Lobo Antiform that in this area comprises the Pulo do Lobo Fm and the overlaying Gafo Fm (Fig. 2), which it is made up of a turbiditic unit (greywacke and shale) with minor intercalations of acid and/or basic volcanic rocks and dykes (Lake et al., 1988; Oliveira et al., 1990), of the early Frasnian (late Devonian) (Pereira et al., 2007). The adjacent Pulo do Lobo Terrane includes highly tectonized quartzite and phyllite interbedded with basalt and is interpreted as a sequence deposited in a passive continental margin that developed in the boundary between the Ossa-Morena Zone and the South Portuguese Zone (Silva et al., 1990; Oliveira 1990; Quesada 1998). The VS Complex crops out widely across the central and eastern parts of the study area (Fig. 2). Here, it is composed of intercalated felsic and mafic volcaniclastic rocks (mainly hyaloclastite and mass flows), coherent volcanic and

subvolcanic rocks, and minor thin shale beds. Felsic and microgabbro dykes intrude the sequence. The western sector is dominated by turbiditic sandstone and shale of the Culm Group.

3.1. **Lithostratigraphic analysis of the volcanic sequence**

More than 95% of the VS Complex that crops out in the study area consists of volcanic rocks; shale accounts for less than 5%. The most common volcanic rocks are felsic, and include well variegated facies, including: (a) coherent facies such as domes, crypto-domes and sills, autoclastic breccia (hyaloclastite) generated during quenching of the margins of massive bodies; (b) volcaniclastic rocks produced by resedimentation of the autoclastic facies, volcaniclastic rocks of possible pyroclastic origin that are rich in pumice, glass and glassy shards; and, (c) epiclastic facies such as breccia, sandstone and siltstone that are the products of resedimentation of the primary volcanic deposits (Fig 3a). The intermediate rocks show the same physical features. Mafic rocks occur in minor proportions as coherent lavas that laterally grade into monomictic and polymictic breccia (Fig 3b), sometimes with hyaloclastic features.

Detailed mapping and drillcore logging show that the VS Complex sequence comprises the following tectonostratigraphic units (Fig. 4) from the base to top (Table 2):

- *Footwall Felsic Unit* (FFU; 200-400 m thick), that is composed of domes, crypto-domes and lesser sills and dykes of quartz-feldspar porphyritic rhyodacite to rhyolite with related hyaloclastite breccia facies. The hanging wall of the FFU includes abundant intercalated alternating bedded pumice and glass-bearing volcaniclastic breccia and fine to medium grained volcaniclastic sandstone.
- *Volcano-Sedimentary Unit* (VSU; <300m thick), made up by a sequence composed of basaltic lava flows, mafic volcaniclastic rocks, epiclastic sediments (polymictic breccias, sandstone and siltstone) derived from the erosion of volcanic

edifice of dominant mafic composition. All the volcanic and volcaniclastic units exhibit frequent lateral facies changes, and are intercalated with thin dark shale beds. The footwall of this unit shows major deformation with a dominant mylonitic fabric.

- *Hanging wall Felsic Unit* (HFU; 250-300m thick), consisting of alternating flows and monomictic to polymictic (clast of rhyolite, dacite, basalt and lithic fragments) breccia of overall felsic composition, intercalated with some mafic flows, coarse- to fine grained volcaniclastic rocks of felsic and minor mafic composition and minor shale. This heterogeneous pile is interstratified with felsic coherent sills (dacite and rhyolite) and crosscut by mafic dykes.

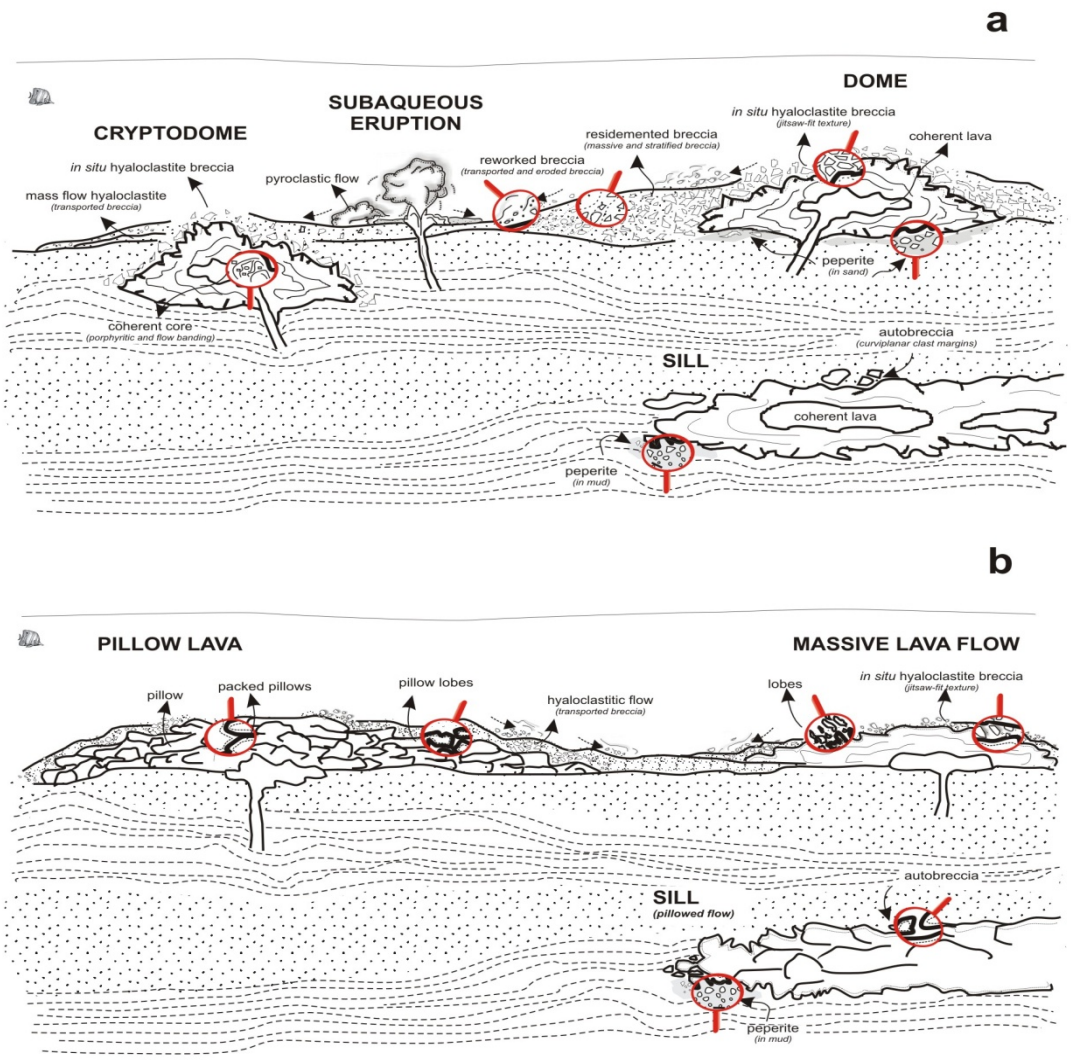

Figure 3 Schematic representation of the architecture and morphology of the main volcanic facies of the IPB, showing (a) the common emplacement of the felsic facies and (b) the mafic facies (modified from McPhie et al., 1993). The magnifying glasses show the details of the facies disposition.

- *Sedimentary Unit* (SU; <150m thick), composed of grey siltstone interstratified with shale and fine grained felsic volcaniclastic sandstone. This unit shows a widespread penetrative mylonitic foliation suggesting that it is probably a tectonic mélange between major units.
- *Upper Felsic Unit* (UFU; <100m thick), including dome complexes of rhyodacitic composition with related autoclastic facies.
- *Andesite Unit* (AU; 100-200m thick), consisting of several dome complexes of andesitic composition and locally intruded by felsic and mafic dykes.

3.1.1. Footwall Felsic Unit (FFU)

The Footwall Felsic Unit is the only unit that does not crop out in the study area. However, it dominates in the underground workings and in drillcore of the Aguas Teñidas mine. It is dominated by coherent felsic rocks and associated hyaloclastite, and pumice and glass mass flows, which, as a whole, seem to form a classic dome complex (Cas et al., 1990; Allen, 1992; McPhie and Allen, 1992; Allen et al., 1996a).

The coherent facies are interpreted as the internal parts of a dome or crypto-dome, but perhaps some could correspond to coeval dykes and sills of similar composition. They consist of a porphyritic rhyodacite to rhyolite with 5-10% phenocrysts of quartz and feldspar in a groundmass of microcrystalline quartz and feldspar, and rarely biotite ghosts replacived by chlorite. Phenocrysts are primarily subhedral feldspar crystals <5 mm, with lesser and smaller quartz crystals 1-2 mm (Fig. 5a). The feldspars are usually replaced by polycrystalline aggregates of albite and only locally preserve residual primary orthoclase. Occasionally, myrmekitic textures have been observed. Other accessory (zircon, apatite and rutile) and secondary minerals (chlorite, sericite, epidote and calcite) occur in this mineral assemblage. In several samples, this massive facies display magmatic flow

Table 2. Synthesis of the lithostratigraphic characteristics of the tectonostratigraphic units of the Volcanic Sedimentary Complex in the northern IPB.

Unit	A	B	Thickness	Characteristics	Interpretation
Andesite Unit	UD	UA	100-200 m	Massive andesite and andesitic breccias intercalated with epiclastic sedimentary rocks of the same composition. Lesser felsic dykes and breccias, and intercalated shale.	Flow-dome complex of andesitic composition cut by felsic and microgabbro dykes.
Upper Felsic Unit		UFU	100-150 m	Felsic epiclastic breccias and sandstones intruded by dacitic sills. Local felsic domes with associated pumice-rich breccia.	Dome complex with abundant re-sedimented felsic fragmental deposits.
Sedimentary Unit	US	SU	< 150m	Intensely deformed sequence of finely interbedded shale, siltstone and epiclastic sandstone.	Turbiditic and suspension sedimentation distal to volcanism.
Hanging wall Felsic Unit	URT	HFU	250-300 m	Felsic volcaniclastic rocks, intercalated with polymictic breccia, shale and sandstone. Rare mafic intrusions and common felsic sills.	Lateral facies of felsic domes interbedded by sediments from an external system.
Volcano-Sedimentary Unit	UVS	VSU	< 300m	Basaltic lava flows and interbedded epiclastic rocks	Basaltic lava flows and sedimentary deposits related to their erosion.
Footwall Felsic Unit	URD	FFU	200- 400 m	Felsic dome complex systems with coherent rhyolite-dacite with associated hyaloclastite and epiclastic sedimentary equivalents among which mass flow deposits rich in pumice and glass are common.	System of domes and cryptodomes with genetically related pyroclastic and epiclastic sedimentary deposits.

[1]Column A indicates the nomenclature used in the Aguas Teñidas mine by Bobrowicz (1995) and internal reports. URD: Rhyodacite Unit (Unidad Riodacítica); UVS: Volcano-Sedimentary Unit (Unidad Volcanosedimentaria); URT: Hanging wall Rhyolite Unit (Unidad Riolítica de Techo); US: Sedimentary Unit (Unidad Sedimentaria); UD: Dacitic Unit (Unidad Dacítica).

[2]Column B shows the new nomenclature proposed on the basis of lithostratigraphy presented in this study.

banding and evidences of devitrification. These late ones include sub-millimeter and concentric fine fractures of accurate shape as relicts of perlitic textures, which are caused by changes of volume due to rapid cooling, possibly in the step from melts to glass (Ross and Smith, 1955; Davis and McPhie, 1996). They coexist with radial crystal intergrowth within pore space or spherulites that characterize the devitrification textures.

Autoclastic in situ quench-fragmented breccia (hyaloclastite) and allochthonous breccia dominated by transported fragments of the same composition are intercalated with the massive facies. The hyaloclastite includes clasts with curviplanar edges and usual jigsaw contacts of porphyritic rhyolite with sharp margins encased in a dark-coloured fine-grained clastic material groundmass of the same bulk composition but with pervasive alteration to quartz, sericite and minor chlorite. In general, they are overlain by bedded breccia of transported quench-fragmented rhyolite. These rocks are interpreted as in-situ hyaloclastite formed during quenching in the carapace of a growing submarine dome; the proportion of the groundmass increases with the percolation of seawater and related alteration.

Epiclastic rocks occur in lateral and vertical distal positions with respect to the coherent facies. They are composed of subrounded blocks (5-25 cm) of rhyolite in a fine grained, commonly strongly altered, volcaniclastic matrix of equivalent composition. These rocks have crude banding and irregular sorting suggesting limited transport in an aqueous environment. They are interpreted to have been formed by transportation over a short distance and resedimentation of the hyaloclastite (transported hyaloclastite).

The uppermost part of the Footwall Felsic Unit is dominated by irregular breccia bodies rich in flattened and altered fragments of pumice and volcanic glass (Fig. 5b). These clasts have irregular sizes (2-10 cm) and a lens-shaped morphology, aligned parallel to the regional foliation. The groundmass is comprised of fine-grained chlorite and sericite

Figure 4. Simplified stratigraphic column of the submarine volcanic sequence in the northern area of the IPB (San Telmo-Aguas Teñidas area).

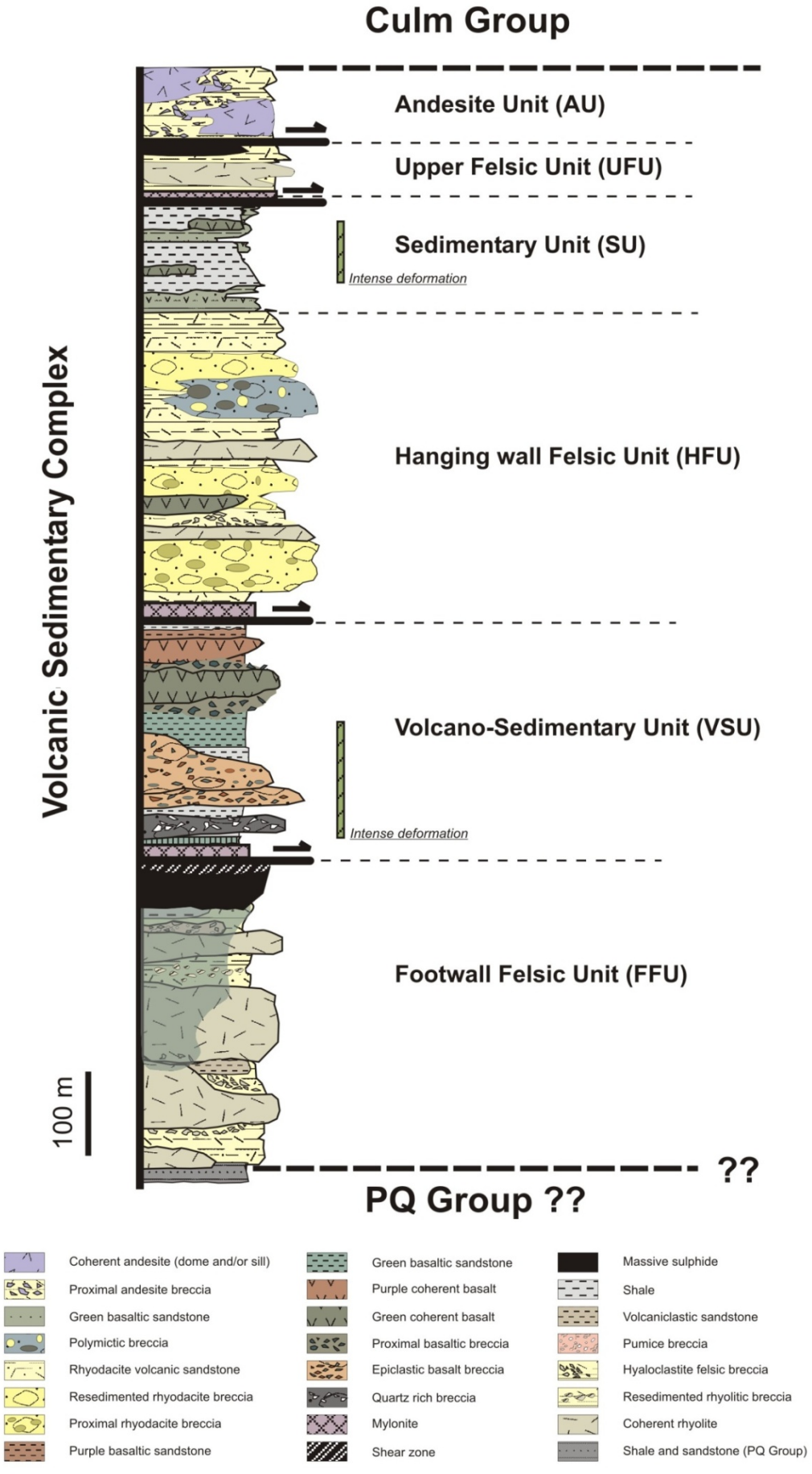
Culm Group
Andesite Unit (AU)
Upper Felsic Unit (UFU)
Sedimentary Unit (SU)
Intense deformation
Hanging wall Felsic Unit (HFU)
Volcanic Sedimentary Complex
Volcano-Sedimentary Unit (VSU)
Intense deformation
Footwall Felsic Unit (FFU)
100 m
??
PQ Group ??
Coherent andesite (dome and/or sill)
Proximal andesite breccia
Green basaltic sandstone
Polymictic breccia
Rhyodacite volcanic sandstone
Resedimented rhyodacite breccia
Proximal rhyodacite breccia
Purple basaltic sandstone
Green basaltic sandstone
Purple coherent basalt
Green coherent basalt
Proximal basaltic breccia
Epiclastic basalt breccia
Quartz rich breccia
Mylonite
Shear zone
Massive sulphide
Shale
Volcaniclastic sandstone
Pumice breccia
Hyaloclastite felsic breccia
Resedimented rhyolitic breccia
Coherent rhyolite
Shale and sandstone (PQ Group)

and contains a high proportion of euhedral and subhedral feldspar and quartz crystals. Laterally, the breccia grades into fine-grained volcaniclastic sandstone layers with intercalated thin beds of shale that is rich in fragments of glass shards; these fragments are interpreted as flattened and compacted highly porous pumice. Originally, the pumice-rich fragments were dominated by glass, they are nowadays systematically altered to an aggregate of quartz and sericite, with lesser chlorite, epidote and disseminated sulphides. These deposits are typical of the uppermost part of thick subaqueous mass flows of pumiceous debris flows and are interpreted as gas-rich volcanic fragments that floated and travelled away from the vent till they saturated in water and sank, being deposited distal to the source and interbedded with low energy fine-grained sediments.

The physical and textural properties of the coherent volcanic and volcaniclastic facies contained in the lower part of the Footwall Felsic Unit reflect an environment typical of a subaqueous felsic dome or cryptodome and proximal associated facies (e.g., Allen, 1992; Cas, 1992; McPhie et al., 1993). These volcanic bodies are characterized by an aphanitic or porphyritic massive core, locally with flow banding. Their external surfaces, where in contact with cool water experienced quench fragmentation causing *in situ* hyaloclastite that passes lateral and gradationally outward to stratified hyaloclastite breccia, and resedimented breccia, occasionally interbedded with fine grained shard and pumice-bearing volcaniclastic rocks. This pyroclastic facies has lateral and thickness variations, and are volumetrically minor. This facies usually contain welding textures that would be result of compaction and alteration of pumice clasts produced by the submarine explosive eruptions or caldera collapse. Similar volcanic rocks have been described in other areas of IPB as the hosting volcaniclastic package of massive sulphides (Tornos, 2006; Rosa, 2007; Rosa et al., 2010; Valenzuela et al., 2011a).

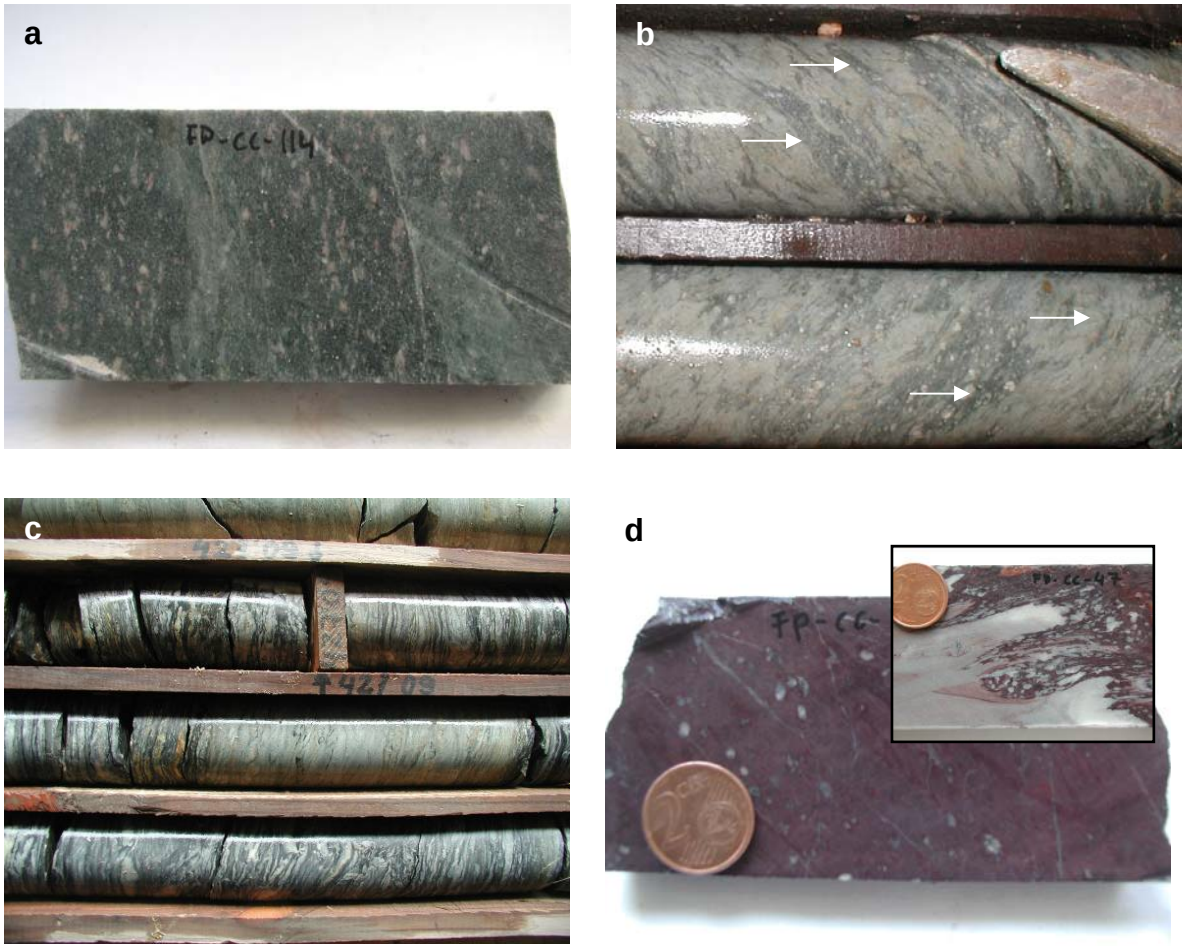

Figure 5. Representative photographs of the main lithofacies of the Footwall Felsic Unit (FFU) and Volcano-Sedimentary Unit (VSU). (a) Drill core slab of the porphyritic rhyodacite of the Footwall Felsic Unit (FFU) (width of core: 4.5 cm). (b) Quartz-feldspar-phyric pumice clast from the upper part of the Footwall Felsic Unit (width of core: 4.5 cm). (c) Green-grey and purple fine-grained and foliated siltstone interbedded with highly deformed coarse epiclastic breccia (width of core: 4.5 cm) (VSU). (d) Purple mafic lava rich in quartz vesicles (VSU). The inset shows a peperitic contact between the mafic lava and the underlying pale-coloured silty volcaniclastic rocks (coin for scale: 1.8 cm).

3.1.2. Volcano-Sedimentary Unit (VSU)

This heterogeneous unit is primarily composed of interdigitated epiclastic breccia, sandstone and shale, all of which have important lateral facies variations. Within these sedimentary rocks there is a thick (1-100 m) and characteristic intercalation of aphyric basalt. The contact between this unit and the underlying Footwall Felsic Unit is marked by a shear zone, <5-25 m thick, that affects the footwall of this unit, made up of volcaniclastic

rocks, and the uppermost part of the Footwall Felsic Unit, including the massive sulphides. Rocks of the Volcano-Sedimentary Unit crop out widely in the central part of the study area (Fig. 2), always in close association with the overlying Hanging wall Felsic Unit. The lowermost part of the VSU is dominated by mafic epiclastic breccia and sandstone interbedded with variably-coloured (green, purple and grey) shale. The breccia includes elongated and subrounded clasts of basalt in a fine grained groundmass of quartz, sericite, chlorite and epidote (Fig. 5c), with abundant disseminated small (μm) grains of magnetite. Frequently, there are intercalations of crystal-rich sandstone with normal graded bedding and shale beds of from mm to meter thickness. This volcaniclastic sequence grades laterally into the aphyric massive basalt.

The aphyric basalt is dominantly massive and has abundant amygdales filled with quartz, chlorite, epidote, zeolites and calcite (Fig. 5d). Only locally shows subtle indicators of the presence of pillow lavas or their hyaloclastic equivalents as well as some peperites locally developed at its footwall contacts, indicating that these rocks were submarine lava flows. The flows are interbedded with layers of epiclastic breccia composed of multicoloured mafic clasts. As for the epiclastic facies, the colour of this rock varies from dark green to purple. These deposits are interpreted as reworked fragments of hyaloclastite related to quenching of the margins and footwall of the basaltic lava flows.

The uppermost part of the Volcano-Sedimentary Unit is dominated by fine-grained volcaniclastic rocks intercalated with well-bedded grey shale. As noted above, the basalt and related breccia and the shale in both the footwall and hanging wall of this unit are multicoloured, with common purple and green zones that are clearly epigenetic in origin.

3.1.3. Hanging wall Felsic Unit (HFU)

This unit concordantly overlies the Volcano-Sedimentary Unit and, together, these two units occupy the central part of the study area, outcropping in a large area between the

San Telmo deposit in the west and the Cueva de la Mora Mine in the east (Fig. 2). The Hanging wall Felsic Unit is dominated by felsic volcanic rocks with a minor proportion of mafic epiclastic rocks. Broadly, the unit may be divided in two parts: (1) a lower subunit dominated by felsic volcaniclastic rocks, breccia and volcaniclastic sandstone, with lesser bodies of coherent felsic facies; and, (2) an upper subunit dominated by a polymictic breccia intercalated with sandstone and siltstone.

The lower part of the unit includes characteristic lensoidal bodies of aphanitic magnetite-rich black rhyolite that outcrop near the Cueva de la Mora mine and in the abandoned railway. The aphyric rhyolite has abundant devitrification textures, perlite and spherulites, as well as porphyritic dacite with 1-3 mm phenocrysts of quartz, plagioclase and orthoclase set in a microcrystalline quartz-feldspar groundmass with common devitrification textures (Figs. 6a and 6b) and rare some ferromagnesian phenocrystals replaced by chlorite. Coherent dacite is associated with abundant in situ hyaloclastite and related hyaloclastic breccia with also devitrification textures (Fig. 6c). The hyaloclastite is interbedded with resedimented facies in which subrounded clasts occur in a fine grained volcaniclastic matrix (Fig. 6d). The subunit also includes beds of felsic, and rarely mafic, sandstone and siltstone suggesting that, as a whole, they form dome complexes similar to those found in the Footwall Felsic Unit. There is no unequivocal evidence for the origin of the black rhyolite but it likely correspond to shallow subvolcanic aphyric sills or dykes cutting sedimentary rocks, with the black colour inherited from an original glassy texture.

The upper part of the Hanging wall Felsic Unit comprises a complex sequence of mass flow deposits including polymictic breccia with poorly sorted subrounded clasts of aphyric rhyolite, quartz-feldspar porphyritic dacite, vesicular basalt, dolerite and other lithic fragments. The irregular clasts, which are 3 to 6 cm long, are encased and supported by a fine-grained volcaniclastic matrix of phyllosilicates and microcrystalline quartz irregularly affected by chlorite and/or sericite alteration. These breccia facies are interbedded with thin layers of polymictic volcaniclastic sandstone, siltstone and shale. These clastic beds

Figure 6. Photographs of outcrops and drill core samples of the volcanic facies from the Hanging wall Felsic Unit. (a) Sill of dark quartz-feldspar phyric rhyolite showing a groundmass with perlitic texture. (b) Dacitic sill with flow banding hosted by the volcaniclastic quartz-rich sandstone and argillite. (c) Devitrification textures in coherent dacite (coin for scale: 1.8 cm). (d) Foliated coarse breccia made up of porphyritic pink clasts of rhyolite composition within a groundmass of equivalent composition but with widespread chloritic alteration; (e) Volcaniclastic rock with alternating fine grained breccia, sandstone and argillite, showing sedimentary structures such as laminations, normal graded bedding and slumps (coin for scale: 2.2 cm); (f) Coherent rhyolite with abundant quartz-filled vesicles (v) and subrounded heterogeneous fragments (xenoliths?) (coin for scale: 2.1 cm).

are normally graded, with local cross bedding and syn-depositional slumping (Fig. 6e). Locally, this sedimentary sequence was intruded by small bodies of vesicular mafic rocks (Fig. 6f).

3.1.4. Sedimentary Unit (SU)

The Sedimentary Unit is dominated by fine-grained volcaniclastic rocks, shale and vitriclastic siltstone, and contains only minor beds of mafic rocks that are very similar to those found in the underlying unit.

Shale is interbedded with thin quartz-rich sandstone, with structures equivalent to those found in turbidite (Bouma 1962; Lowe, 1982). These alternations are themselves interbedded with fine to medium-grained epiclastic rocks, commonly multicoloured, similar to those found in the Hanging wall Felsic Unit and the Volcano-Sedimentary Unit. The sandstone is composed of small grains of quartz, chlorite and opaque minerals in a microcrystalline matrix of quartz, chlorite and sericite. They are interpreted to be the reworked product of coarser-grained epiclastic rocks of felsic composition. Laterally, they grade to fine grained quartz siltstones with a quartz-sericite matrix. Rarely, these beds contain clasts of volcanic fiamme that are interpreted as resedimented pyroclast rocks.

All rocks in this unit have major deformation features, with common tectonic thinning, development of a SC cleavage, and presence of sheath folds and quartz veining. This suggests that this unit hosts a major shear zone of the area.

3.1.5. Upper Felsic Unit (UFU)

This relatively thin unit crops out irregularly along the faulted contact between the Sedimentary and the Andesitic Units (Fig. 2). It also occurs as isolated, tectonically-bound, discontinuous lenses within the latter, as is the case in the Lomero Poyatos mine (Fig. 7). This unit includes dominantly felsic rocks. Here, the rhyodacite is usually massive

Figure 7. Geological map of the Lomero Poyatos Mine. (a) Detailed surface geology in the Poyatos area showing the distribution of the volcanic rocks and hydrothermal alteration. (b) Geological cross section of the Lomero area. (c) Simplified lithostratigraphic column. Map modified from internal reports of Cambridge Mineral Resources.

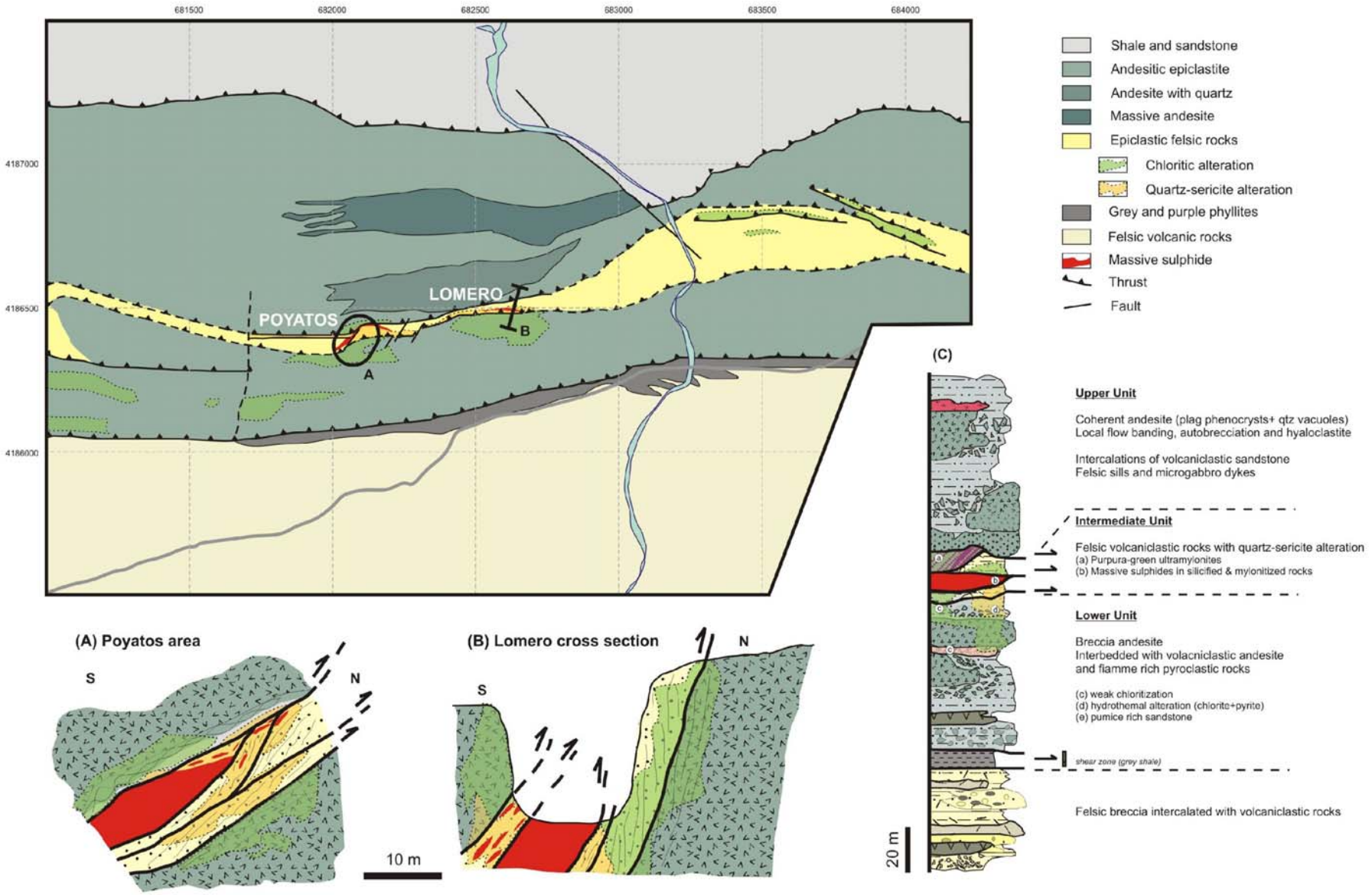
681500
682000
682500
683000
683500
684000
4187000
4186500
4186000
LOMERO
POYATOS
A
B
Shale and sandstone
Andesitic epiclastite
Andesite with quartz
Massive andesite
Epiclastic felsic rocks
Chloritic alteration
Quartz-sericite alteration
Grey and purple phyllites
Felsic volcanic rocks
Massive sulphide
Thrust
Fault
(A) Poyatos area
S
N
10 m
(B) Lomero cross section
S
N
(C)
Upper Unit
Coherent andesite (plag phenocrysts+ qtz vacuoles)
Local flow banding, autobrecciation and hyaloclastite
Intercalations of volcaniclastic sandstone
Felsic sills and microgabbro dykes
Intermediate Unit
Felsic volcaniclastic rocks with quartz-sericite alteration
(a) Purpura-green ultramylonites
(b) Massive sulphides in silicified & mylonitized rocks
Lower Unit
Breccia andesite
Interbedded with volacniclastic andesite
and fiamme rich pyroclastic rocks
(c) weak chloritization
(d) hydrothemal alteration (chlorite+pyrite)
(e) pumice rich sandstone
shear zone (grey shale)
Felsic breccia intercalated with volcaniclastic rocks
20 m

It has only some interbedded layers, between 1 and 4 m thick, of autoclastic or hyaloclastic breccia, typical of dome complexes (McPhie et al., 1993) (Fig. 8b). The rhyodacite is stratigraphically overlain by a package of epiclastic breccia and quartz crystal-rich sandstone, suggesting an environment of formation similar to the Footwall and Hanging wall Felsic units. The epiclastic breccia is composed of 1-6 cm sized fragments of quartz- and feldspar-phyric rhyodacite in a fine-grained chloritized matrix; locally, pumice and volcanic glass-bearing fragments are preserved. Felsic to mafic polymictic volcaniclastic sandstone occurs at the top of the unit, locally intercalated with the breccia. Where strongly altered and deformed, this Unit consists of quartz-sericite-rich rocks with a pervasive tectonic foliation with only a few quartz phenocrysts and locally flattened, cm-sized, lenses of massive sulphides (Fig. 8a); the alteration and deformation precludes the characterization of protolith. The deformation was less intense where the outcrops are thicker and coherent (e.g., footwall of the San Telmo mine). These rocks are commonly associated with minor amounts of shale that is also locally intensely sericitized and chloritized.

3.1.6. Andesite Unit (AU)

The uppermost exposed tectonic unit of the VS Complex includes volcanic rocks that are very different from those of the underlying units, and are dominated by coherent and volcaniclastic andesite. The Andesite Unit crops out along the northern part of the study area and throughout a large belt across its southern part (Fig. 2).

The Andesite Unit is composed of tectonic slivers of alternately massive and volcaniclastic andesite localized in several superimposed dome complexes in which porphyritic and vesicular andesite are capped with fragmental rocks, mostly transported hyaloclastic breccia. Generally, they are associated with different bedded deposits of reworked andesite fragments, lesser felsic epiclastic deposits and minor shale. In previous

regional maps studies, this andesite has been mapped as a dacite, being considered part of the Upper Felsic Unit (Ruiz, 1984; Cambridge Minerals Resource, 2006).

The mine workings at the Lomero Poyatos mine show the best outcrops (Fig. 7). Here, the lower part of the Unit is formed by monotonous transported hyaloclastic breccia comprised of andesite fragments with some intercalated epiclastic layers of similar composition; there are also thin layers of fragmental rocks of equivalent composition and with abundant glass shards. These late rocks are interpreted as proximal pyroclastic facies related to a locally explosive dome complex of andesitic composition. Andesite tectonically overlying the mineralization (Fig. 7) shows a wide variety of facies ranging from coherent through *in situ* hyaloclastic breccia, transported and resedimented hyaloclastite to epiclastite (Fig. 8c). As a whole, this sequence has at least three monotonous and superimposed dome-complexes. The massive andesite is dark and contains phenocrysts of plagioclase and clinopyroxene, the latter commonly replaced by chlorite and clinoamphibole; it contains irregularly distributed but sometimes abundant vesicles. Flow and devitrification textures are common, and peperitic breccia has been observed at the margins and footwall of the massive rocks. Locally, andesite is crosscut by dykes of microgabbro and fine-grained felsic rocks. A common feature of these rocks is the presence of large amygdales which are typically filled with quartz, and less commonly with chlorite, epidote, chalcedony, zeolite and calcite (Fig. 8d). The unit shows pervasive devitrification and the irregular hydrothermal alteration that is characterized by an enrichment of sericite, chlorite and epidote. However, this alteration is interpreted as due to regional spilitization and unrelated to the massive sulphides.

Detailed field work shows that andesitic volcaniclastic units are much more abundant in the southern part of the study area than in the northern part. This is interpreted to indicate that the southern zone represents a more distal position relative to the dome complexes, which are mostly located in the northern part.

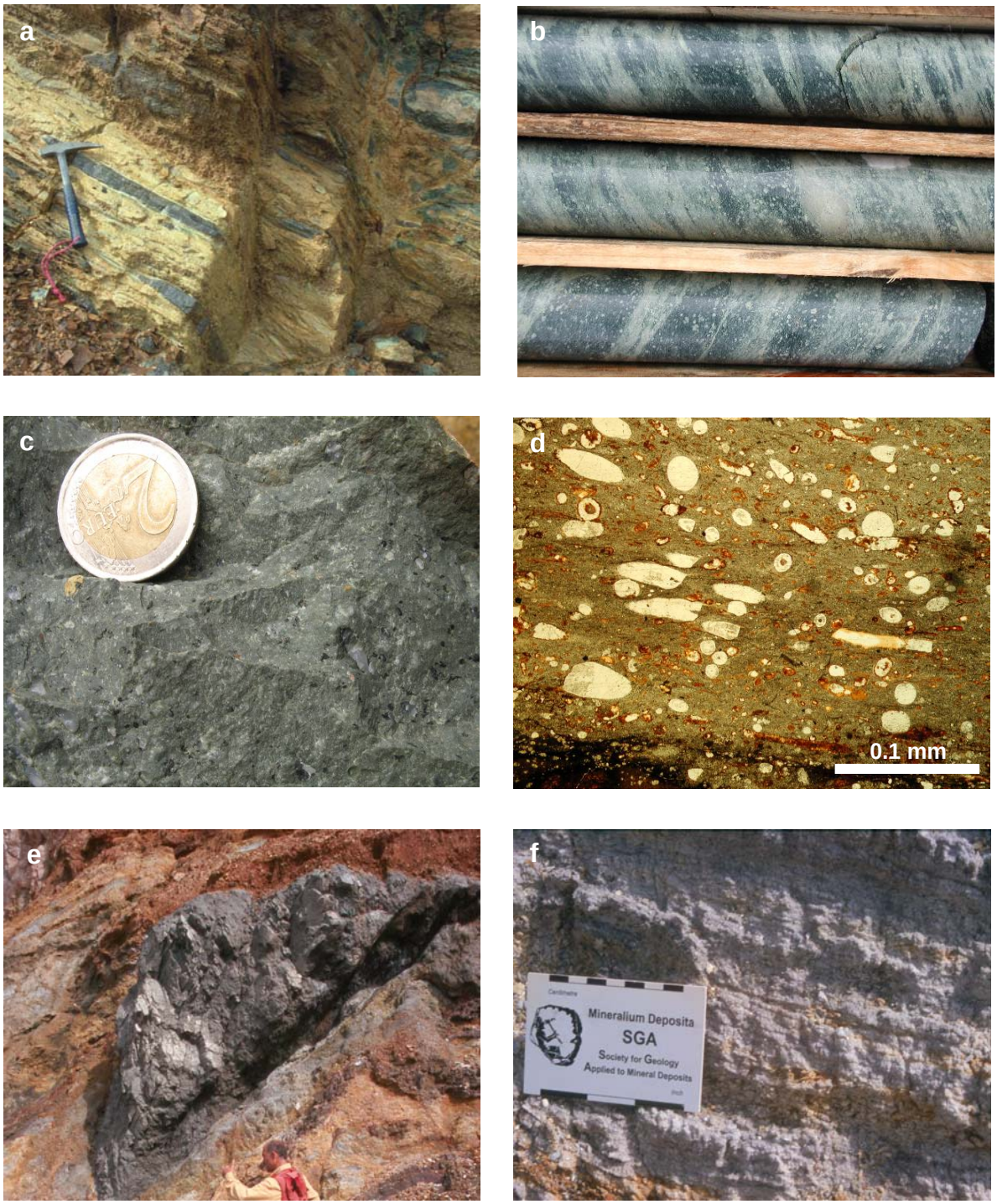

Figure. 8 Photographs of representative outcrops and drill core slabs of the Lomero Poyatos and San Telmo mines. (a) Small tectonic lenses of highly deformed massive sulphides hosted by sericitized and mylonitized felsic volcanic rocks of the Upper Felsic Unit; Poyatos open pit. (b) Strongly altered and highly deformed coarse breccia containing pumice clasts, belonging to the Upper Felsic Unit (width of core: 4.5 cm), Lomero Poyatos Mine (LO-3). (c) Typical outcrop of the porphyritic andesite with quartz-rich vesicles (coin for scale: 2.6 cm). (d) Photomicrographs of coherent andesite, locally showing vesicles filled with quartz in a chloritized groundmass. (e) Dismembered sulphide lens in sericitized dacite, San Telmo Mine; (f) Thin interlayered gypsum (former anhydrite) and pyrite that originally capped the San Telmo orebody.

4. Hydrothermal alteration

Most of the rocks of the VS Complex have undergone some hydrothermal alteration. Two principal groups of alteration assemblages can be described: a primary hypogene assemblage directly associated with the formation of the massive sulphides (Bobrowicz, 1995; Sánchez España et al., 2003), and a late alteration related to oxidation caused by ground water penetration along Variscan structures (Tornos, 2006; Velasco and Tornos, 2006).

The hypogene alteration is irregular and of variable intensity, being especially pronounced in the felsic footwall of the massive sulphide deposits where related to the stockwork or feeder zones (Bobrowicz, 1995; Tornos, 2006). Here, the felsic rocks show large alteration zones that are interpreted to reflect widespread fluid flow associated with the formation of the massive sulphides. Due to the intense superimposed deformation, original contacts with the footwall sequence are not commonly observed. However, where preserved, the alteration pattern show an asymmetric cone-shaped zonation with a central core of quartz and chlorite, an intermediate zone of chlorite-carbonate-sericite-quartz and an external margin composed of sericite and quartz (Brobrowicz, 1995; Mckee, 2003). Generally, disseminated pyrite occurs throughout all the alteration halo while the stockwork is usually associated with the chlorite-quartz alteration. Locally, there are some minor stockwork zones unrelated to the massive sulphides, a feature interpreted to be related to tectonic dismembering of the ore forming systems. Alteration is less important in the hanging wall, but its exact extent is unknown due to the widespread presence of shear zones.

Alteration dominated by epidote, chlorite and hematite is typical of mafic and intermediate volcanic rocks and grade inwards into massive chloritization. However, these rocks are usually not so intensely altered as felsic ones. As noted above, hydrothermal alteration is dominated by phyllosilicates and thus altered rocks are the preferred loci for

channelizing deformation and major shearing. This is perhaps why most massive sulphides are adjacent to major structures that have been interpreted as reactivated extensional syndepositional faults (Quesada, 1998).

The second style of alteration includes the widespread oxidation of the volcanic and sedimentary rocks. It is typical of iron-rich rocks such as basalt and shale that are intensely deformed. This alteration is responsible for the formation of purple shale and a characteristic reddening of the mafic volcanic rocks. The spatial relationship with major zones of deformation strongly suggests that this episode of hydrothermal alteration took place during the Variscan orogeny and caused by the inflow of exotic oxidized waters, of likely surficial origin, into the system. In fact, the uppermost part of the Aguas Teñidas deposit shows abundant lenses of magnetite that are also interpreted as formed during the syn-orogenic desulphurization of pyrite (see below).

5. The massive sulphide deposits

The most significant deposits in the area are San Telmo, Lomero Poyatos, Magdalena and Aguas Teñidas. The San Telmo mine is the westernmost massive sulphide deposit of those studied here (Fig. 2). The ore is hosted by three lenses: San German, Cruzadillo and Santa Barbara. The deposit has been worked since Roman times, and more intensely in the last two centuries, mainly by Sociedad Minera La Hispalense (Pinedo, 1963). The mineralization is hosted by a felsic dome complex of the Upper Felsic Unit including a coherent core and marginal hyaloclastite, transported breccia and volcaniclastic apron rocks. In detail, the ore lenses are interbedded with minor pumice and/or vitriclast-rich volcaniclastic sandstone and thin shale beds. Locally, jasper zones occur related to grey and purple mudstone above the aforementioned rocks. The massive sulphides are highly deformed and tectonically dismembered (Fig. 8e). The mineralization, dominated by massive pyrite, shows a marked Cu zonation. The upper part has a high grade banded Cu+Zn ore (Tornos, 2006), overlain by a characteristic cap of interlayered pyrite and

gypsum (formerly anhydrite; Tornos, 2006) (Fig. 8f). Besides, as in many other VMS deposits, there is a pyrite-rich core and a basal Cu-rich zone (Pinedo, 1963; Sánchez España, 2000) that grades downwards into the stockwork zone, which is hosted by the chlorite and sericitic alteration zones.

The Lomero-Poyatos mine is one of the most peculiar ore deposits of the northern IPB (Fig. 7) because of its geological setting and the high grade in precious metals. It has been worked as a pyrite mine since 1859 by Compagnie des Mines de Cuivre d'Huelva and Sociedad Francesa de Piritas de Huelva (Pinedo, 1963) until its closure in 1991. During the last decade it has been re-evaluated due to its high-grade precious and base metal contents by Cambridge Mineral Resources (www.cambmin.co.uk) (Table 1), Corporación de Recursos Iberia and Kimberley Diamonds.

The orebody is hosted by a thin, up to 20 m thick, slice of highly deformed dacite probably belonging to the Upper Felsic Unit, and tectonically sandwiched in the Andesite Unit (Tornos, 2006; Tornos and Velasco, 2006) (Figs 7a to 7c). Host rocks show a pervasive quartz-sericite alteration with abundant disseminated pyrite and only minor chloritization. Despite the widespread hydrothermal overprinting and tectonic deformation of the original rock, the presence of some remnants of pumice and fiamme-rich breccia suggests that it was originally a volcaniclastic felsic breccia. This rock is partially replaced by the massive sulphide, which shows an external aureole of stockwork-like mineralization and a massive core.

The Lomero Poyatos deposit includes two sulphide lenses (Lomero and Poyatos) that converge at depth and are interpreted as tectonically dismembered parts of the same orebody. Regional mapping shows that the massive sulphides and the host rocks have a pinch and swell shape due to a ramp and flat geometry developed during thrusting (Fig. 7). Massive sulphides are thicker and less deformed between flats, whereas deformation is concentrated in the ramp zones; here, the massive sulphides form only cm-sized

flattened and dismembered lenses in a strongly foliated felsic rock (Fig. 8a). The mineralization consists of coarse-grained semi-massive to massive sulphides intergrown with variable quantities of quartz, siderite, sericite, barite and minor chlorite. The metallic assemblage includes pyrite and variable proportions of chalcopyrite, sphalerite, galena and tetrahedrite-tennantite group minerals; there are minor amounts of arsenopyrite, pyrrhotite, magnetite and some native gold (5.76 g/t Au; Cambridge, 2004). The mineralization is dominated by massive barren pyrite and shows only a weak zonation with Cu-enrichment in the central area and polymetallic (Zn-Pb) enrichment towards the eastern and western margins. The formation of these types of ore is directly related with the Variscan deformation, with the more ductile phases enriched –in gold- along shear zones. Gold, mostly as electrum or as invisible gold (Velasco et al., 2000, 2003; Velasco and Tornos, 2006), and is irregularly distributed in the chalcopyrite and falhore minerals of the cupriferous ore and the polymetallic ore as well as in quartz-rich zones developed in the more deformed zones (Cambridge Minerals Resources, Int. Report, 2004; Velasco and Tornos, 2006).

The Aguas Teñidas deposit is the largest massive sulphide deposit in the northern Iberian Pyrite Belt. Although the other deposits (except Castillejito and Magdalena) crop out and have been mined since ancient times, this deposit was discovered following a deep electromagnetic/gravimetric anomaly was detected during the joint venture between Promotora de Recursos Naturales S.A. and Billiton Española S.A. during the 1980's. In 1995, Navan Resources Huelva S.A. continued with the exploration and started an intermittent mining operation until early 2004. Since 2007, Iberian Minerals Corp. and its Spanish subsidiary company (Minas de Aguas Teñidas SA) have developed the mine and produced ore since 2008 (www.iberianminerals.com). Presently, the mine is in underground production by Trafigura Minerals Group (www.trafigura.com) but exploration continues for increasing reserves and for delineating the potential of the chalcopyrite and magnetite-rich stockwork (Table 1).

The orebody is located in the hanging wall of coherent rhyodacite belonging to the Felsic Footwall Unit, showing pervasive sericitic and chlorite plus quartz and magnetite hydrothermal alteration. The most altered rocks include zones of disseminated pyrite and stockwork veins of quartz, chlorite pyrite, and chalcopyrite. The inner and uppermost zones of the stockwork include large zones of rich in magnetite and chalcopyrite that locally grade into irregular stratabound masses of magnetite and chlorite with abundant veins of chalcopyrite and quartz that are located directly below the massive sulphides.

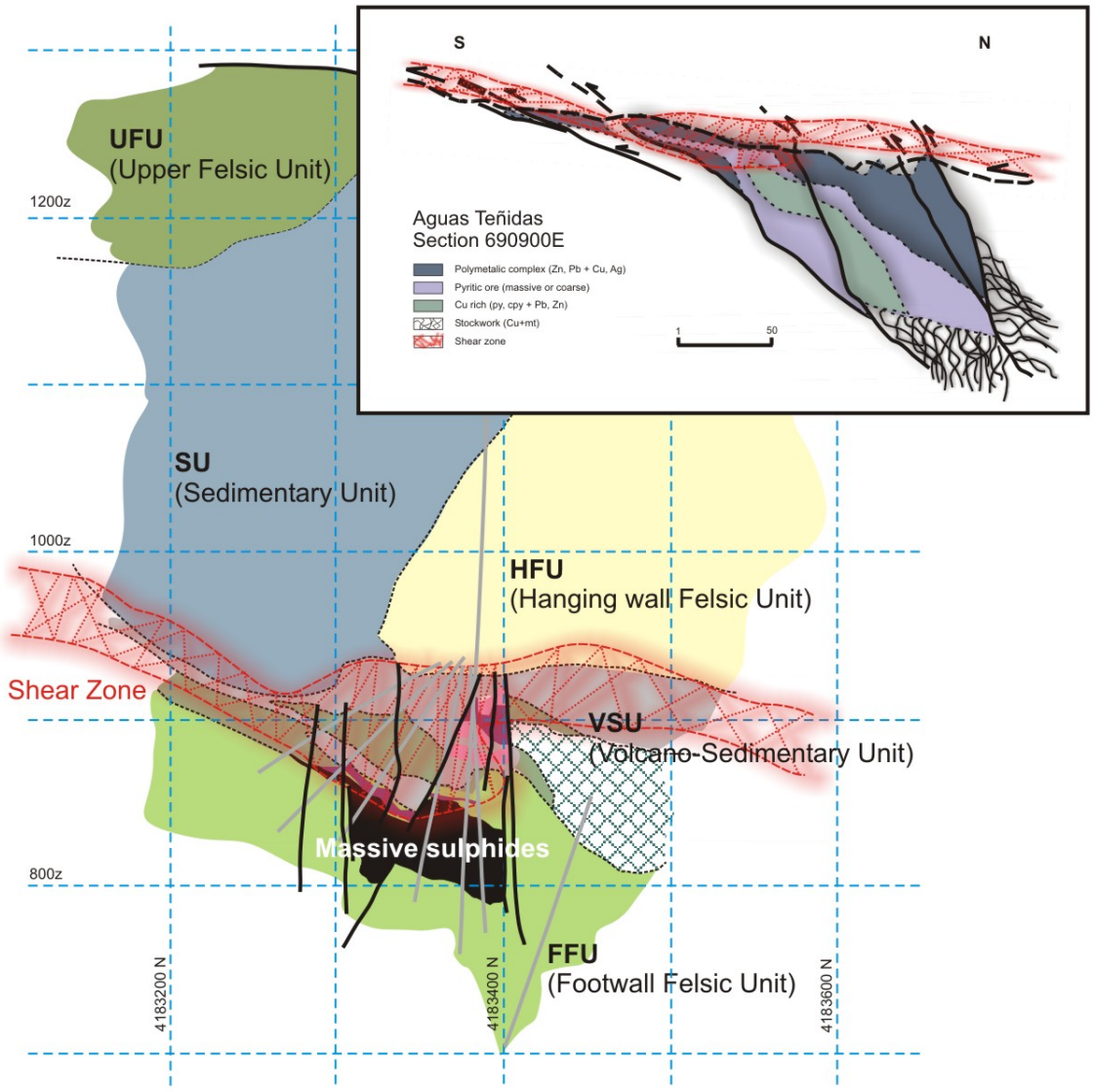

Figure 9. Cross-section through the Aguas Teñidas Mine area showing a simplified geology of the host volcanic sequence and the zonation of orebody (modified from Aguas Teñidas internal report, 2009).

The massive sulphide orebody is wedge-shaped and between 150 and 300 m wide, with a maximum thickness about 80-90 m (Fig. 9). It is laterally limited abruptly by three major faults with strike-slip component (McKee et al., 2001; McKee, 2003; Hidalgo, 2003), probably representing reactivated syn-hydrothermal faults. However, the orebody is open towards the east (Luceño, pers. comm., 2009). The massive sulphides show an irregular zonation similar to the other nearby deposits. There is a banded fine-grained Zn-Pb-Ag rich massive ore in the upper part of the sulphide lens (Fig. 10a) overlying a coarse-grained barren pyrite zone that close to the footwall shows a Cu-rich zone that grades downward into the stockwork (Fig. 10b).

The massive sulphide includes pyrite, sphalerite, chalcopyrite and galena, and minor magnetite, arsenopyrite and tetrahedrite-tennantite group minerals. Locally, pyrrhotite, bournonite, stannite group minerals, Cu-Pb-Bi sulphosalts and bismuthinite occur (Bobrowicz, 1995). Metamorphism and deformation caused several changes in the primary mineralization, including formation of a widespread tectonic banding, grain coarsening and a gold enrichment (> 6 g/t) in the copper-rich and polymetallic ore (Bobrowicz, 1995; McKee et al., 2001; McKee, 2003).

The hanging wall of the massive sulphides is marked by a major shear zone that limit the overlying Volcano Sedimentary Unit (Fig. 9). Both the massive sulphides and host rocks show widespread deformation (Fig. 10c). Locally, in the southern end of the orebody there are remnants of a, fragmental layer of jasper that is replaced by fine-grained pyrite (Fig. 10d). Here, in contrast, in the northern part of the orebody, semi-massive sulphides and stockwork were thrust above the massive sulphides.

In detail, all the studied deposits show a direct spatial association with pumice-rich breccia and green fine-grained felsic sandstone. Despite being masked by intense deformation, the massive sulphides show replacive contacts with the host volcanic rocks and have an underlying stockwork or feeder zone. No direct relationship with black shale

nor rocks indicative of anoxic and quiescence environment of deposition have been found. This markedly contrasts with the geologic setting of the VMS deposits of the southern Iberian Pyrite Belt, which are mostly shale-hosted and interpreted as being exhalative (Tornos, 2006; Tornos et al., 2008).

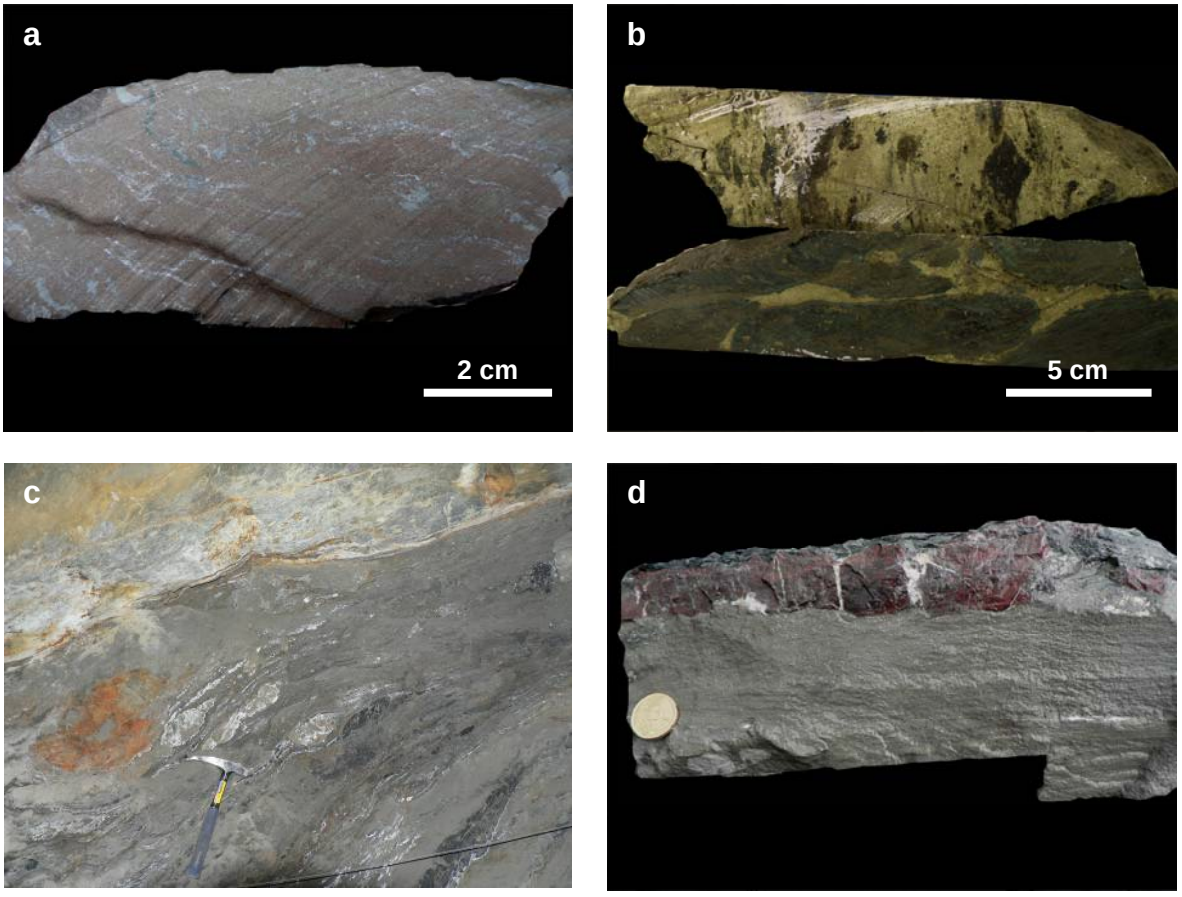

Figure 10. Mineralization of the Aguas Teñidas deposit. (a) Polymetallic ore, rich in sphalerite and galena. Banding is interpreted as of tectonic origin. (b) Deep stockwork-related mineralization with chalcopyrite veins in a chlorite + magnetite rock. (c) Complex folding and boudinage of the contact between the massive sulphides and the overlying hydrothermally altered felsic volcanic rocks. Aguas Teñidas deposit (952 Chamber). (d) Fine grained pyrite-rich massive sulphide in contact with capping jasper (coin for scale: 2.2 cm).

6. Geochemistry of the volcanic rocks

The geochemistry of volcanic rocks is a basic tool for lithological discrimination, especially in zones where major hydrothermal alteration, deformation or metamorphism occurred. During these processes many elements can be gained or lost; only elements that are virtually immobile during hydrothermal processes are usually reliable for

characterization of their petrological signature (Whitford et al., 1989; MacLean and Barrett, 1993; Barrett and MacLean, 1994, 1999; Lentz, 1996).

Plots including the least mobile elements ratios (i.e., Zr/Al_2O_3, Al_2O_3/TiO_2 and Zr/TiO_2), high field strength elements (HFSE), such as Al, Ti, Zr, Y, Th, Nb and rare earth elements (REE) are particularly effective for lithogeochemical discrimination. They also help to quantify the degree of hydrothermal alteration. However, some authors have shown that the immobile elements, such as Y, Nb and, in general, light REE should be used with caution in hydrothermal rocks formed at very high fluid/rock ratios or in presence of volatile-rich fluids because in these conditions they can be mobile; this is particularly true in the case of light REE, particularly Eu (Ewart, 1979; Campbell et al., 1984; Barrett and MacLean, 1994).

This geochemical approach has been used elsewhere in the study of massive sulphide deposits such as in the Skellefte district (Sweden), Bathurst Camp and Kidd Creek (Canada), or in the Mount Read Volcanics (Tasmania) (Allen 1992; Allen et al., 1996a, b; Lentz et al., 1997; Lentz, 1999; Gemmell and Fulton, 2001; Schlatter, 2007; Barrett et al., 2005; Montelius, 2005) with excellent results in the exploration of VHMS deposits; they provide key information in the stratigraphy and discrimination of volcanic units and define vectors to ore.

6.1. Methodology and analytical methods

Selected rock samples from outcrops and drill core, belonging to the already defined tectonostratigraphic units were selected for characterization and geochemical discrimination. They were analyzed for major and trace elements by X-ray fluorescence (XRF) and ICP-MS at the Laboratorios Generales of the IGME (Appendix I.I). Prior to analyses, petrographic studies were performed in order to characterize the rocks and determine the degree and type of superimposed alteration. The geochemical compilation

also includes unpublished analyses belonging to the database of the Aguas Teñidas mine and Bobrowick (1995).

Most of the studied samples are affected by variable hydrothermal alteration. Only a small number of samples of the coherent nuclei of lava domes, flows and sills appear to preserve their primary geochemical composition.

6.2. Lithogeochemical results

As a first approach, the data have been plotted on the AFM diagram of Irvine and Baragar (1971) and the FeO/MgO vs. SiO_2 plot of Miyashiro (1974) to determine the bulk magmatic affinity. However, these diagrams are only tentative because all elements involved are highly mobile during hydrothermal alteration. The majority of the samples of felsic and intermediate composition (Footwall Felsic Unit, Hanging wall Felsic Unit, Upper Felsic Unit, and Andesite Unit), which are the volumetrically dominant units in the study area, plot in the calc-alkaline field. Only basalt from the Volcano-Sedimentary Unit and the small basaltic intrusions in the Hanging wall Felsic Unit have a tholeiitic affinity (Fig. 11a). These magmatic affinities can be also deduced from the elemental ratios of the mobile elements such as Zr/Y, $[La/Yb]_n$ and Th/Yb, which have been used by Barrett and MacLean (1994). The rhyolite, dacite and andesite typically have ratios of Zr/Y > 7 and $[La/Yb]_n$ of less than 5.5, consistent with their interpreted calc-alkaline affiliation. The basalt is consistently tholeiitic with Zr/Y ratios less than 4.5. These findings are similar to those found elsewhere in the Iberian Pyrite Belt (Munhá, 1983; Mitjavila et al., 1997; Thieblemont et al., 1998; Sánchez España, 2000; Rosa et al., 2004; Barrett et al., 2008).

Overall, the volcanic rocks range widely in composition. The majority have compositions between dacite and rhyolite (SiO_2 > 63%), something evident if the data for unaltered samples are plotted on the TAS (total alkali-silica) diagram (Fig. 10b; Le Bas et

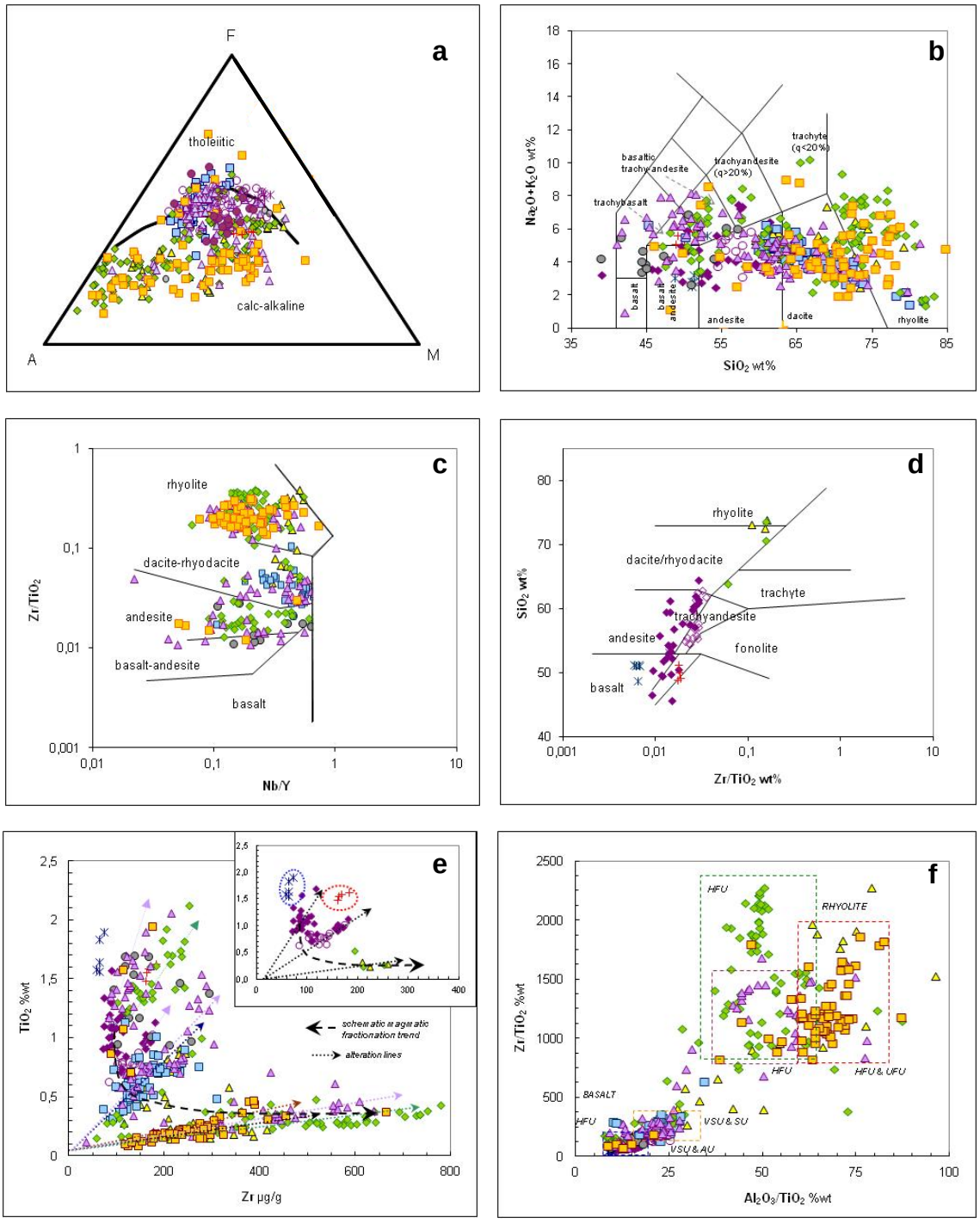

Aquas Teñidas

- Andesitic Unit (AU)
- Upper Felsic Unit (UFU)
- Sedimentary Unit (SU)
- Hanging wall Felsic Unit (HFU)
- Volcano Sedimentary Unit (VSU)
- Footwall Felsic Unit (FFU)

Lomero Poyatos

- Microgabbro (hanging wall)
- AU (hanging wall)
- Microgabbro (footwall)
- Felsic dyke (footwall)
- AU (footwall)
- HFU

al., 1986: Na_2O+K_2O vs. SiO_2). A significant proportion (~20%) of the samples have mafic and intermediate compositions ($47 < SiO_2 < 63\%$) and total alkalis in the range 2-5% (Fig. 11b). As previously stated, as both silica and the alkalis are mobile during hydrothermal alteration, these results are not necessarily a direct reflection of the primary compositions. This is especially true when dealing with rocks belonging to the Andesite Unit or Volcano-Sedimentary Unit, where the abundance of quartz-rich vesicles increases significantly the SiO_2 content of the rocks. In fact, rocks of the Andesite Unit have silica contents between 54 to 66% SiO_2 that are significantly higher than those of rocks having trace element and petrographic features of andesite. This is probably why andesitic rocks have been overlooked in the Iberian Pyrite Belt and systematically classified as dacite.

The classification based on the immobile element diagrams Zr/TiO_2 vs. Nb/Y and SiO_2 vs. Zr/TiO_2 (Figs. 11c and 11d) characterize more accurately the different units. The felsic rocks of the Footwall Felsic Unit, Hanging wall Felsic Unit and Upper Felsic Unit can be chemically classified as rhyodacite-rhyolite. Among the other units, only a small number of sills and volcaniclastic rocks of the Volcano-Sedimentary Unit and Sedimentary Unit have dacitic to rhyolitic compositions. As described along the work, andesite is a common constituent of the volcanic pile. Thus, the aforementioned results show that the volcanism in the IPB is not bimodal as has been previously proposed by Routhier et al. (1980), Soriano (1997), Mitjavila et al. (1997), Leistel et al. (1998) and Thieblemont et al. (1998) which consider the rocks of intermediate composition irrelevant in comparison with felsic and basaltic volcanic rocks. The existence of a voluminous basalt-andesitic and andesitic volcanism indicates that there is a continuous sequence between basalt and rhyolite with silica contents between 44.3 and 84.6 $\%SiO_2$. However, there are two major groups of magmatic rocks: one including tholeiitic basalt; and a calc-alkaline trend comprising from basaltic andesite to rhyolite. The first likely represent small amounts of primitive melts of mantle derivation that arrived to the upper crust while the second ones, volumetrically much more significant, are probably product of the partial melting of continental crust

induced by juvenile magma underplating and later fractional crystallization (Silva et al., 1990; Quesada,1998; Tornos et al., 2005).

6.2.1. Felsic rocks (dacite and rhyolite)

The relationships between immobile elements (i.e., Zr vs. TiO_2 or Al_2O_3 vs. TiO_2) help in the interpretation of the magmatic evolution because of their different behaviour during fractional crystallization, magma mixing, assimilation or contamination (MacLean, 1990; MacLean and Barrett, 1993; Lentz, 1996). Thus, different elemental ratios can help to discriminate igneous units or geochemically different batches of magma derived from the same magma chamber intruding sequentially in the crust. The TiO_2 vs. Zr diagram (Fig. 11e) allows discriminating two distinct groups of felsic rocks: (a) rhyodacite-rhyolite with high Zr contents between 300 and 750 µg/g, which belong to the Hanging wall Felsic Unit (HFU) and minor fine grained volcaniclastic rocks from the Volcano-Sedimentary Unit (VSU); and, (b) a group of samples with Zr content <200 µg/g that belong primarily to the Footwall Felsic Unit (FFU) and the Upper Felsic Unit (UFU). A small number of these late samples are from dykes that cut the upper part of the Volcano-Sedimentary Unit (VSU). This separation in two groups of the felsic rocks is also evident, albeit with more overlap, in terms of Zr/TiO_2 vs. Al_2O_3/TiO_2 ratios. As a whole, the data suggest that the Upper Felsic Unit is geochemically identical to the Footwall Felsic Unit. The two units are not only geochemically similar but also are composed of felsic dome complexes with similar lithofacies, share similar hydrothermal alteration assemblages and, above all, host all of the massive sulphide deposits in the zone. These similarities lead to the conclusion that they very likely represent tectonically dismembered parts of the same magmatic unit, the Footwall Felsic Unit being more massive and the Upper Felsic Unit being dominated by volcaniclastic sediments, corresponding to distal parts of a subaqueous dome-flow complex.

However, the most significant difference between the Footwall Felsic Unit and the Upper Felsic Unit is the intensity of the hydrothermal alteration. The Footwall Felsic Unit at Aguas Teñidas and the Upper Felsic Unit in the northernmost part of the studied zone both exhibit widespread sericitization with more localized zones of chloritization-silicification in the vicinity of massive sulphides. However, the rocks of the Upper Felsic Unit in the central part of the study area have little or no hydrothermal alteration and do not host massive sulphides.

The felsic rocks of the Footwall Felsic Unit and the Upper Felsic Unit have generally higher Zr/TiO_2 and Al_2O_3/TiO_2 ratios than the other volcanic units, Hanging wall Felsic Unit, Andesite Unit and Volcano-Sedimentary Unit. This clearly suggests that the host felsic sequence to the ore (Upper Felsic Unit and Footwall Felsic Unit) is comparatively less fractionated. This observation, as well as the presence of dykes or sills of similar evolved composition cutting the Volcano-Sedimentary Unit and Hanging wall Felsic Unit, indicates that the ore-bearing, less fractionated, felsic units (UFU and FFU) are the youngest of the northern IPB and younger than those that currently occur in the tectonic hanging wall to mineralization (Volcano-Sedimentary Unit, Andesite Unit and Hanging wall Felsic Unit). It is probably, as suggest other authors for similar host felsic rocks in other areas, that these rocks showed a low to medium degrees of partial melting previously to fractionation processes (Hart et al., 2004).

In the Sedimentary Unit, fine- to medium-grained volcaniclastic rocks of felsic composition are intercalated with shale. These rocks have Zr/TiO_2 similar to the sills present in the Volcano-Sedimentary Unit, suggesting a common origin. It is likely that some of these sedimentary rocks are the result of the transport and resedimentation of proximal facies of a volcanic centre being genetically related to these sills and the Footwall and Upper Felsic Units.

The results show a low Zr content in the ore-hosted rocks in contrast with the previous works which the volcanogenic massive sulphide are related to high Zr saturation and high temperature felsic rocks (Barrie, 1995). That means that the ore-felsic rocks in the northern IPB have a zircon subsaturation of magmatic source or a less temperature -in comparison with other district- in a zircon saturated system which contained significant amounts of volatiles which could contribute to develop of volcanic hydrothermal systems (Piercey 2011).

The ore-hosted felsic rocks are plotted on the discrimination diagrams proposed by Lesher et al. (1986) and Hart et al. (2004). They show chemical parameters similar to FII group, dacite-rhyolite rocks with calc-alkaline affinity, associated to Phanerozoic and Proterozoic, as in the IPB and showing a HFSE and REE enriched.

6.2.2. Intermediate and mafic rocks (andesite and basalt)

Rocks of mafic and intermediate mineralogy and geochemical composition ranging from basalt to andesite occur in three of the tectonostratigraphic units, the Volcano-Sedimentary Unit, the Sedimentary Unit and the Andesite Unit (Figs 11b and 11c).

The relationships between immobile elements Zr/Y, TiO_2/Zr and Al_2O_3/TiO_2 permit the discrimination of two groups of mafic rocks. The first group includes vesicular basalt to basaltic-andesite lavas at the base of the Volcano-Sedimentary Unit, small intrusions that cut the Hanging wall Felsic Unit (HFU), and the microgabbro dykes that cut the Andesite Unit. These rocks have low Al_2O_3/TiO_2 and TiO_2/Zr ratios, and Zr/Y values lower than 4.5. The second group, including primarily rocks of andesitic composition, includes the rocks that dominate the Andesite Unit as well as fine-grained volcaniclastic rocks interbedded in the Sedimentary Unit and the andesitic breccia and sandstone of the Volcano-Sedimentary Unit. As noted above, this group has a calc-alkaline affinity and Zr/Y ratios

typically above 7. Such a major geochemical difference between the two groups suggests different origins and genetic processes (Fig. 11e).

6.3. Chemostratigraphy (Lomero Poyatos and Aguas Teñidas)

The chemical variations in the previously described volcanic units are highlighted when using downhole plots of immobile elements ratios. In two sampled sections of the Lomero Poyatos and the Aguas Teñidas deposits, the limits between the main units are marked by notable chemical variations (Figs. 12 and 13), reflecting both changes in the lithology and the hydrothermal alteration. The degree of hydrothermal alteration is highlighted by variations in two multi-component ratio indexes, the Alteration Index (AI) of Ishikawa et al. (1976) and the CCPI (Chlorite-Carbonate-Pyrite index) of Large et al. (2001). The alteration index (AI) (see below, Figs 12 and 13) was developed initially by Ishikawa et al. (1976) for chemically tracking chlorite and sericite-rich alteration in the Hokuroko district. However, this AI does not take into account the carbonate alteration and is unable discriminate chlorite from sericite alteration which is the relevant to VHMS exploration. Assuming these limitations of the AI, Large et al. (2001) developed the CCPI index, including FeO contents, in addition to MgO, Na_2O, and K_2O previously considered by Ishikawa et al. (1976). The combination of these parameters in a bivariant plot, the AI-CCPI-Alteration Box Plot, affords an effective method for discriminating the different trends relate to hydrothermal and diagenetic alteration (Large et al., 2001).

The chemical composition of rocks from drillcore from drillholes LP-9, LP-7 and LP-2 of the Lomero Poyatos deposit indicates that there are two different sub-units within the Andesite Unit (Fig. 12) as based on immobile element ratios. In holes LP-7 and LP-2, the uppermost part of the Andesite Unit shows an enrichment in Zr, with Zr/TiO_2 ratios above 50 and Zr/Al_2O_3 ratios above 10; there is a second andesitic sub-unit with ratios <175 and <12, respectively (Figs 12a to c). Hole LP-9 show Zr/TiO_2 ratios between 90 to 210 and

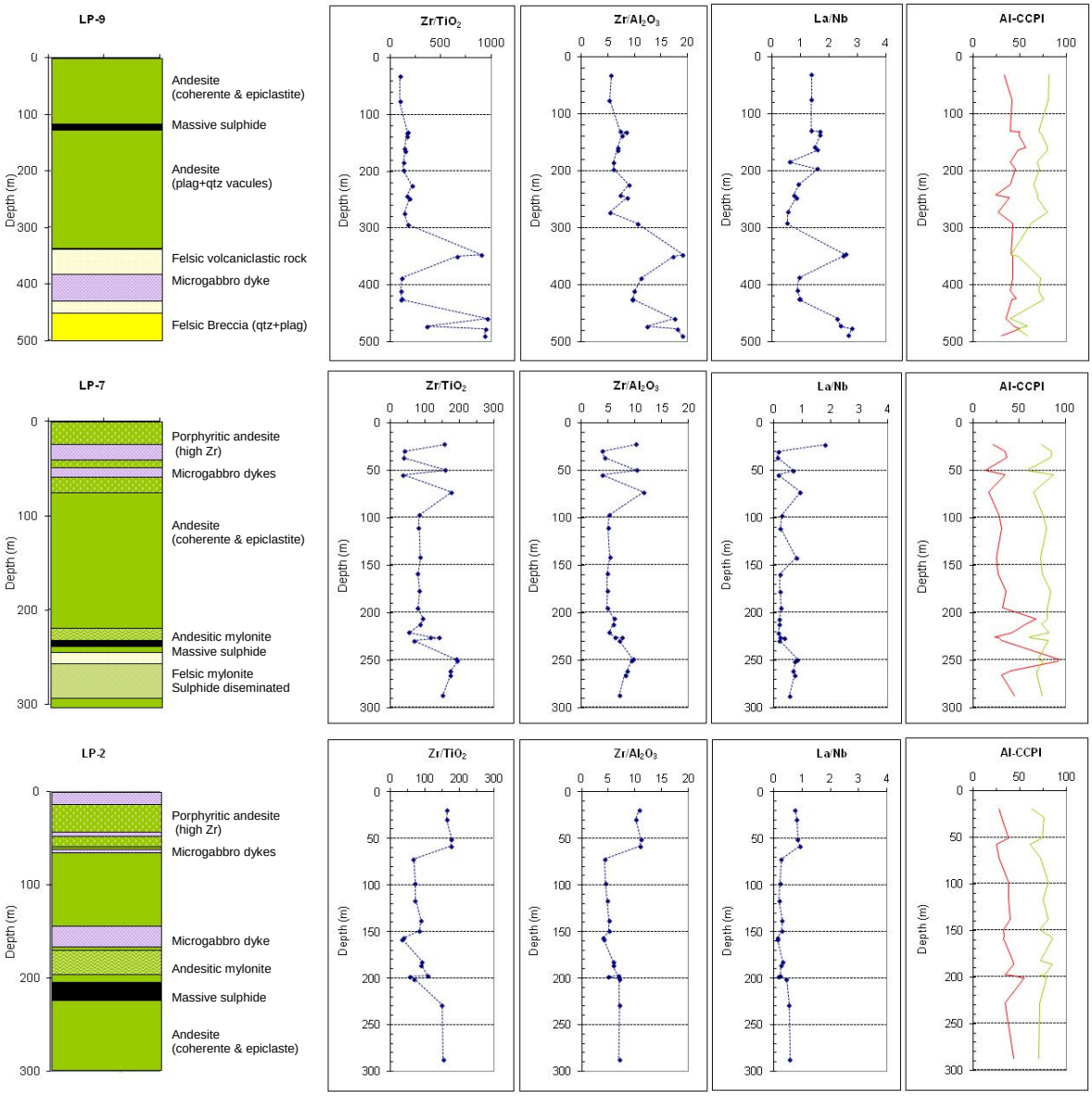

Figure 12. Downhole plots of rock types and chemical composition for drillcore from holes LP-9, LP-7 and LP-2 of the Lomero Poyatos Mine. The Zr/TiO2, Zr/Al2O3 and La/Nb ratios monitor the rock type. The ratio of alteration indexes AI/CCPI is a measure of the hydrothermal alteration affecting the sequence (AI=100(K2O+MgO)/(K2O+MgO+Na2O+CaO) and CCPI=100(Mg+FeO)/(MgO+FeO+Na2O+K2O); Large et al., 2001).

Zr/Al_2O_3 ratios below 9 being very homogeneous throughout the whole log. Microgabbro dykes and felsic rocks have high (above 200) Zr/TiO_2 ratios in the felsic rocks belonging to the Upper Felsic Unit and low values in the microgabbro (<40).The alteration indices are very irregular through the volcanic sequence, but they show a change close to the sulphide lenses and tectonic contacts (Fig. 12d).

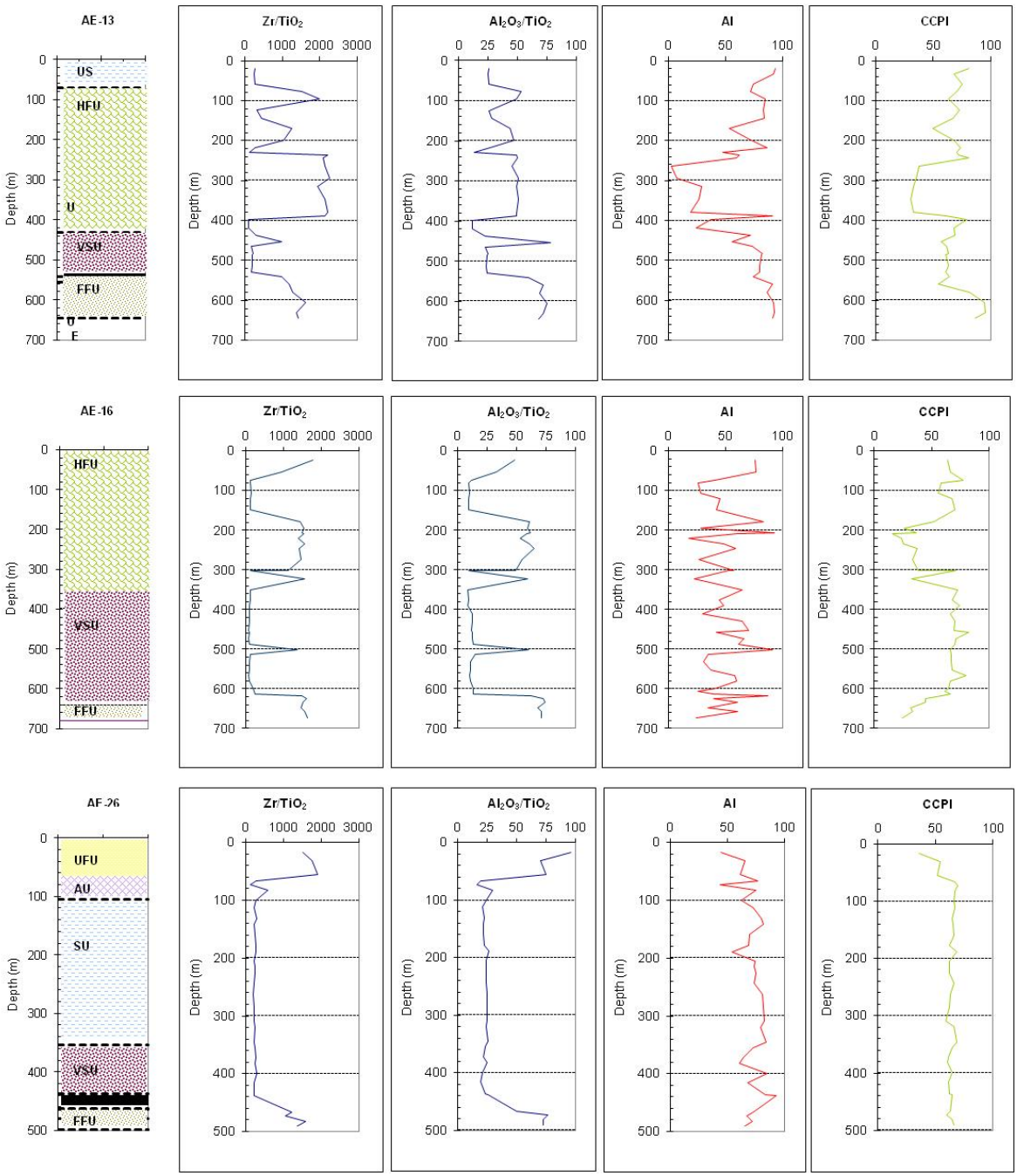

Figure 13. Downhole plots of logged rock types versus immobile-elements and alteration index for drillholes AE-13, AE-16 and AE-26 from section 903E of the Aguas Teñidas Mine. The two plots on the right show the Zr*1000/TiO2 and Al2O3/TiO2 ratios, both of which permit a clear chemical discrimination of the main volcanic lithotypes. The AI and CCPI highlight the irregular distribution of the hydrothermal alteration.

Regarding the Aguas Teñidas mine, the study was based on section 903E that includes drillholes AE-16, 14 and 26 (Fig. 13). Plots based on immobile elements ratios (Zr/TiO_2 and Al_2O_3/ TiO_2) show similar and parallel trends, with high ratios (>1500 and

>50, respectively) in the felsic rocks from Upper Felsic Unit, Hanging wall Felsic Unit and Footwall Felsic Unit. The basaltic rocks of the Volcano-Sedimentary Unit and the Sedimentary Unit have lower values (<500). However, AI and CCPI indexes show an irregular variation. Rarely, the alteration indexes range above 50. Except in massive coherent rocks of the Volcano Sedimentary Unit and Hanging wall Felsic Unit (see, Fig. 13) where the values are low, the alteration indices have a saw-tooth line, ranging from strong to moderate alteration. Plots show large variation in the mass change due to compositional diversity of host volcanic facies, but also there are intense variations associated with large tectonic structures (e.g., thrusts, falls and shear zones), which are very numerous in the study area.

7. Discussion: The volcanic architecture

The geology of the Aguas Teñidas-San Telmo area is complex but the combined mapping, and definition of volcanic facies and geochemistry suggest a rather consistent picture that is probably representative of the whole northern Iberian Pyrite Belt. Previous studies (Bobrowicz, 1995; NAVAN S.A., 1996; Rodriguez, 1996; Sánchez España, 2000; McKee et al., 2001) have defined broadly equivalent units in the Aguas Teñidas mine area but have not integrated them into a more regional study.

The absolute chronology of these units is unknown. Most of the major contacts are tectonic and, thus it has not been possible to determine the stratigraphic relations between the units. However, the comparison between the different lithofacies, the crosscutting relationships and the geochemistry allows rebuilding a general stratigraphic column for the area to be determined. Dykes of felsic composition with immobile element chemistry similar to the Hanging Wall Unit cross-cut the Andesite Unit, and dykes similar to the Footwall Felsic Unit intruded the Hanging wall Felsic Unit. The Volcano-Sedimentary Unit includes volcaniclastic sediments of andesitic composition whereas both the Footwall-Upper Felsic Units and the Hanging wall Felsic Unit have intercalations of

mafic rocks similar to those of the Volcano-Sedimentary Unit. Furthermore, dykes of basaltic composition cross-cut the Andesite Unit.

These cross-cutting relationships indicate that the Andesite Unit must be older than the Hanging Wall Rhyolite Unit, which is in turn older than the Footwall Felsic Unit (Fig 14a). The Footwall and Hanging Wall Rhyolite units are geochemically similar and probably represent two discrete broadly contemporaneous magma batches. The basalt and related sedimentary rocks of the Volcano-Sedimentary and Sedimentary Units are interpreted as broadly contemporaneous with the felsic rocks. The existence of epiclastic mafic rocks interbedded with the felsic strata in the Volcano-Sedimentary Unit suggest that mafic edifices were dominant in areas lateral to the basin and were emplaced and eroded during the extrusion of the felsic rocks.

In general, the characteristics of the volcanic facies, and especially of the units underlying the massive sulphides, suggest a below storm wave base marine environment of eruption and deposition. The presence of explosive volcanism is interpreted as characteristic of shallow environments of deposition. However, studies work by Kokelaar and Busby (1992) and Gibson et al. (1999) have shown that this is not true, and explosive volcanism can occur even at more than 1.5 km depth. There are no precise markers of the depth of deposition of the VS Complex in this area, but the few sedimentary and depositional structures are all consistent with a deposition below base wave level in a subaqueous environment (e.g., McPhie and Allen, 2003). This is also consistent with the conclusions of previous studies (Tornos, 2006; Rosa, 2008; Rosa et al., 2010) and probably defines another major difference with the VS Complex of the southern IPB, where locally there are evidences of shallow or even to subaerial deposition (Moreno and Sáez, 1990; Moreno et al., 1996; Quesada, 1996; Sáez et al., 1996).

a

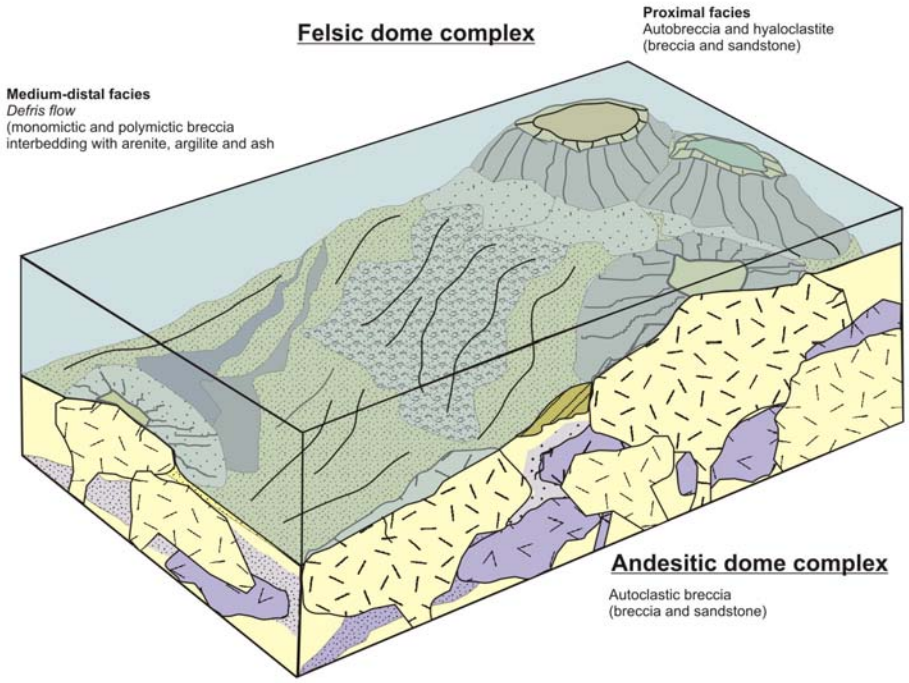

b

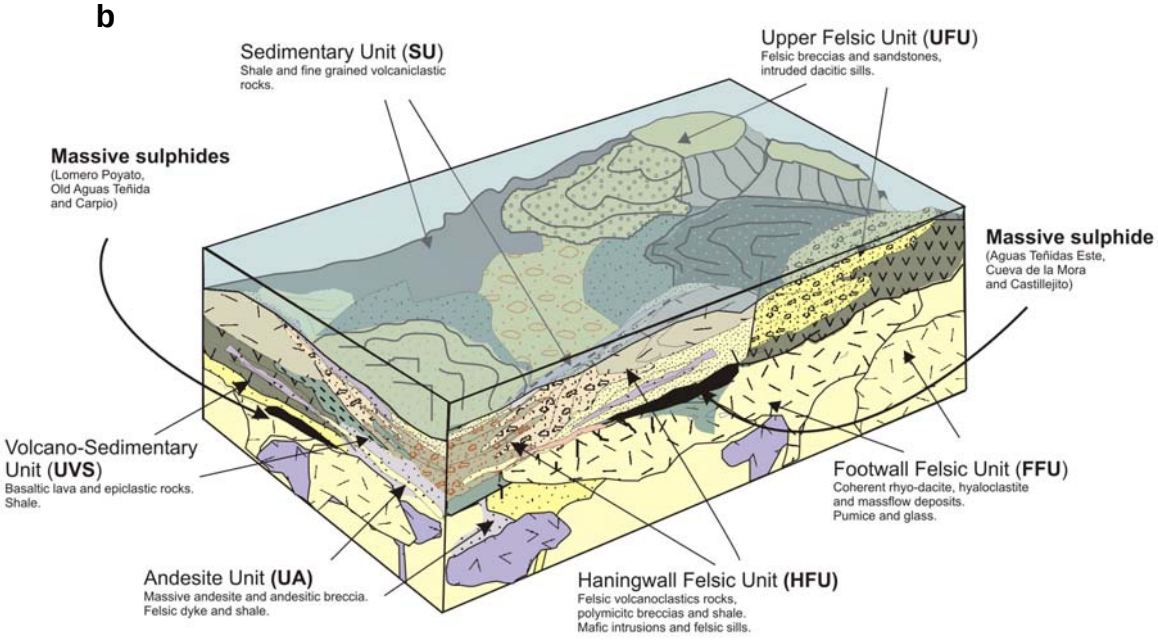

Figure 14. Schematic diagram showing the hypothetical stratigraphic evolution of the VS Complex in the northern of Iberian Pyrite Belt.

The geology of the Aguas Teñidas-San Telmo area is dominated by abundant bodies of early massive intermediate (Andesite Unit) and later felsic (Hanging wall Felsic Unit, and Footwall Felsic Unit-Upper Felsic Unit) rocks that formed large dome and crypto-dome complexes and related sills that were emplaced at or just below the seafloor. Proximal autoclastic breccia and hyaloclastite formed contemporaneously with the extrusion of the coherent facies and dome growth. Disaggregation and reworking of the proximal facies gave rise to bedded, matrix-rich volcaniclastic breccia, and siltstone with subrounded clast components. Also, outboard and above the domes, there are large pumice- and glass-rich breccia bodies. These are interpreted to be contemporaneous valley-fill deposits associated with explosive eruptions and pyroclastic flows; the geochemistry consistent with that of the massive rocks indicate that they are not allochthonous deposits transported from nearby subaerial environments. Distal to the domes, the sequence is dominated by alternating sandstone, siltstone and shard-rich siltstone all of which are intercalated with polymictic breccia that include clasts from multiple eruption centres. Mafic volcanic centres occurred lateral and synchronous with the felsic domes but the exact timing has not been determined (Fig. 14b).

Clay-rich sediments accumulated locally, and the proportion of shale in the sequence is broadly inverse to the abundance or proximity to volcanic activity in a given location. During local volcanic quiescence, sequences composed exclusively of shale and fine grained volcaniclastic sedimentary rocks were deposited. However, these fine-grained sediments are scarce and significantly volumetrically less important than in the southern Iberian Pyrite Belt, indicating that volcanism was more active in the northern IPB with volcanic rocks forming the bulk of the sequence.

It is proposed here that the sequence represents a tectonically reversed stratigraphic succession with the younger units on top of the actual sequence. However, this simplified sequence is probably distorted by out of sequence thrusts and internal tectonic subunits but the lack of outcrops does not allow for a more precisely defined structure.

At a regional scale, the sequence proposed here is somewhat similar to that deduced by Tornos (2006), and Mellado et al. (2006) in the Río Tinto area, some 40 km SE. There, the PQ Group is overlain by a thick basaltic unit, including submarine flows and sills interbedded with shale and a felsic unit comprising dacitic domes and related pumice-bearing rich mass flows. What is missing in Río Tinto is the Andesite Unit that probably corresponds to a volcanic centre of significance only in the northernmost IPB (Fig. 15).

In synthesis, the massive sulphide deposits of the northernmost Iberian Pyrite Belt show a well defined lithologic relationship. The Aguas Teñidas, Castillejito and Cueva de la Mora deposits occur at the top of the Footwall Felsic Unit. The massive sulphide orebodies of the old Aguas Teñidas and El Carpio deposits occur either in the Upper Felsic Unit or along its tectonized footwall contact with the Sedimentary Unit. The mineralization at San Telmo is also interpreted to have formed in one of the upper, isolated domes of the Upper Felsic Unit. The Lomero Poyatos deposit occurs in volcaniclastic rocks of the Upper Felsic Unit, but is sandwiched in a small tectonic window within the overlying Andesite Unit. If the Upper Felsic Unit correlates with the Footwall Felsic Unit, then all the massive sulphides are contemporaneous and formed on top of domes that are the youngest volcanic rocks of the area. These orebodies are hosted in hyaloclastite or pumice-and-glass-rich breccia that exhibit intense hydrothermal alteration and are interpreted as replacive, formed below the seafloor by replacement of permeable and reactive units such as the pumice-and-glass-rich breccias (Tornos, 2006). However, the chemical analyses show that the ore-bearing domes are not the most “fractionated” of the northern IPB, which is the barren Hanging wall Felsic Unit. Maybe, the variations of these felsic rocks could be explained by the participation of partial melting of mafic sources material at a variable range of depths, P-T conditions and time, and subsequent fractionation processes. This unit is characterized by high Zr contents that may be the result of a unique history of magmatic assimilation of previous primitive rocks. This could support the hypothesis that the igneous rocks are only heat engines to hydrothermal flow

and are not the main source of the metals related to ore-forming fluids of the IPB, which could be of basinal derivation (Tornos and Heinrich, 2008). If there is a genetic relationship between domes and ore forming fluids then the IPB does not follow the pattern observed in the Abitibi Belt and in Skellefte district (Barrie et al. 1993; Lentz 1999; Barrett et al., 2005), in which the mineralization is genetically related to the more fractionated and hot magmatic rocks. However, Gaboury and Pearson (2008) suggest that there are no an absolutely favourable type of rhyolite which host Volcanic Massive Sulphide deposits. The depth where occur the magma chamber and source of the rhyolite (shallow, <5 km; and depth, > 30 km), is considered the key parameter.

This setting of formation of massive sulphides at the top of felsic domes has been quoted in many VMS districts such as Skellefte area (Allen, 1992; Allen et al., 1996a, 1996b), the Kuroko district (Ohmoto, 1996), the Bathurst Mining Camp (Goodfellow, 1975;

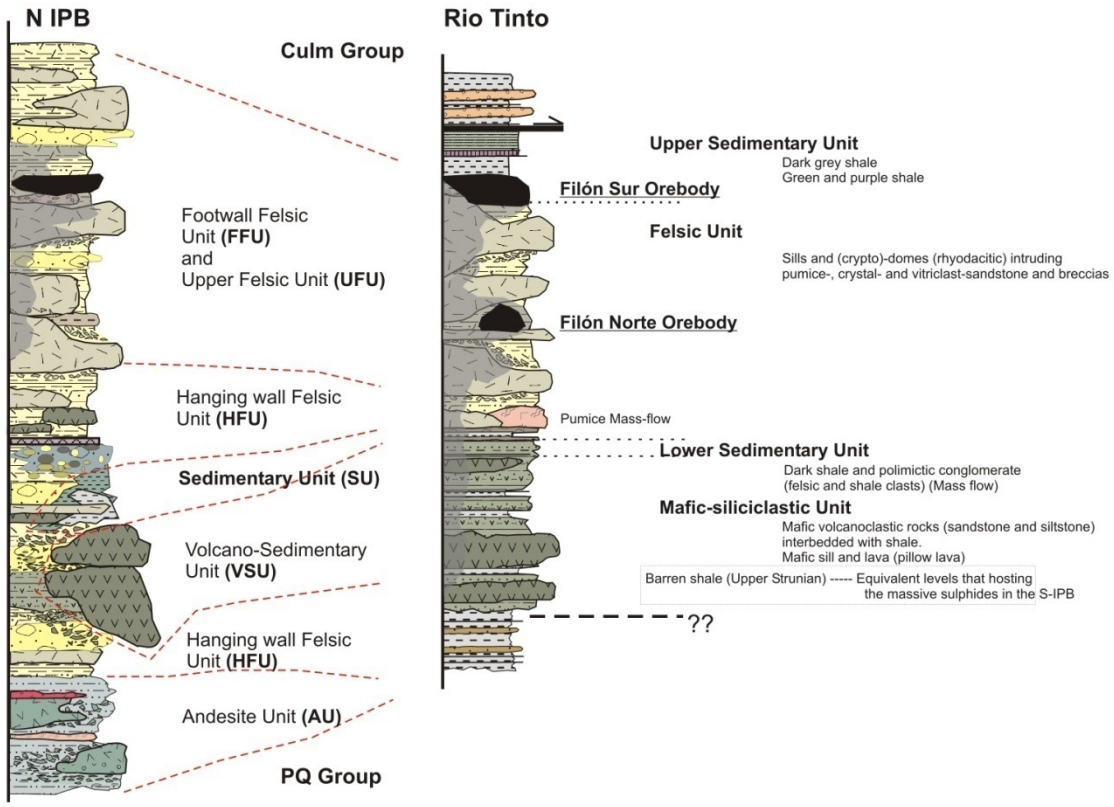

Figure 15. Proposed reconstruction of the original relationships of lithostratigraphic units of the northern sector of IPB and its correlation with the equivalent sequence in the Río Tinto Mine (modified from Mellado et al., 2006).

Goodfellow and McCutcheon, 2003; Lentz, 1996, 1999; Lentz and McCutcheon, 2006; McCutcheon et al., 1997, 2003) or the Abitibi greenstone belt (Lafrance et al., 2000) and it is strictly associated to a paleo heat-flow that provide an extra and maximum drive for convective circulation, high temperature leaching reactions developing the formation of VMS deposit. In the IPB, spatial relationships of VMS deposits with the uppermost part of domes was originally suggested by Strauss et al. (1981) in La Zarza and Barriga (1990) and later described in detail in Neves Corvo (Rosa et al., 2004, 2008, 2010; Rosa, 2007), in Sotiel-Migollas (Tornos, 2006) and in the Aznalcóllar area (Conde et al., 2003).

8. Conclusions

The VS Complex of the northern Iberian Pyrite Belt is dominated by felsic volcanic rocks with minor amounts of andesite, basalt and shale. These rocks are grouped in six tectonostratigraphic units, of which five have distinctive geological and geochemical characteristics. Two of the tectonostratigraphic units (Footwall Felsic Unit and Upper Felsic Unit) are probably dismembered parts of the same volcanic complex with the underlying and less fractionated Upper Felsic Unit forming a large sequence of subaqueous volcanic dome complexes of dacitic to rhyolitic composition. They exhibit many the typical lithofacies variations of a classic volcanic centre, from massive flow and dome-dominated facies at the centre outward to increasingly fine-grained epiclastic sediments in more distal positions. This felsic volcanism is younger than a regionally extensive andesitic volcanism (Andesite Unit) that also forms dome complexes and represents the largest accumulation of intermediate volcanism in the entire Iberian Pyrite Belt. As a whole, the intermediate to felsic volcanic rocks define a single calc-alkaline trend without major geochemical breaks and related by fractional crystallization.

The area also includes tholeiitic basalt and related sediments. Coherent and fragmental basaltic rocks intercalated with shale dominate in the Volcano-Sedimentary Unit. The Sedimentary Unit is dominated by bedded sedimentary rocks, which nonetheless have

very important volcanogenic components. The relative timing of the deposition of these units is unknown but they were likely synchronous with the felsic volcanism. The basalt is probably the extrusive equivalent of the juvenile melts that were responsible of crustal melting and generation of the calc-alkaline melts at depth due to their underplating.

The massive sulphide deposits appear to have formed in concert with the emplacement of a regionally continuous unit of dacite and rhyolite. There is every indication that they are located near the top of the same volcanic unit, specifically in the pumice- and glass-rich rocks capping the more evolved and youngest felsic domes. However, the most fractionated felsic rocks are apparently barren and possibility they mean the lowest amount of partial melting, and thus a poor and insufficient heat source to develop and drive a convective system.

The shale-rich units (Volcano-Sedimentary Unit and Sedimentary Unit) have absorbed much of the deformation that has affected the area, and a large part of their constituent rocks have been mylonitized. Among the rock types that were strongly affected by deformation (basalt, shale and massive sulphides) there is a direct relationship between the bulk strain and certain types of alteration; green-purple colouration of shale, hematitization of basalt, and oxidation of massive sulphides. This relationship is interpreted to reflect syn-tectonic oxidation mediated by circulation of oxidized groundwater during the Variscan deformation.

Acknowledgements

This study falls within the broader project entitled “Geologic and Structural Research of the Massive Sulphide Deposits of the Northern Iberian Pyrite Belt”, partially financed by the Spanish CICYT-FEDER 2003-0290 and DGI 2011-23207 Projects. This work has been possible due to the collaboration of MATSA SA and Cambridge Minerals SA that allowed land and mine access, sampling of drill core and provided information. We would like to thank Juan Manuel Pons, Juan Carlos Videira, Lorena Luceño, Raul Hidalgo, Victor Guerrero, Bill Sheppard and Colin Andrew for their help and Francisco Velasco for his valuable comments and suggestions. In addition, we would like to thank the staff at the Laboratorios Generales del IGME, especially J.A. Martín Rubí for their assistance with the geochemical analyses. We would like to extend our thanks to David Mellado for his help in the sampling and GIS mapping, and to Ruben García for his help with field work.

References

Allen, R.L., 1992. Reconstruction of the tectonic, volcanic and sedimentary setting of strongly deformed Zn-Cu massive sulfide deposits at Benambra, Victoria. Economic Geology 87, 825-854.

Allen, R.L., 2001. Volcanic facies in VHMS districts and their use in reconstructing stratigraphy: an example from Los Frailes-Aznalcóllar, Iberian Pyrite Belt. GEODE workshop “Massive sulphide deposits in the Iberian: New advances and comparisons with equivalent systems”. Aracena (Huelva, Spain), 1-3.

Allen, R.L., Lundström, I., Ripa, M., Simeonov, A., Christofferson, H., 1996a. Facies analysis of a 1.9 Ga, continental margin, back-arc, felsic, caldera province with diverse Zn-Pb-Ag- (Cu-Au) sulphide and Fe oxide deposits, Bergslagen region, Sweden. Economic Geology 91, 979-1008.

Allen, R.L., Weihed, P., Svenson, S.-Å., 1996b. Setting of Zn-Cu-Au-Ag massive sulphide deposits in the evolution and facies architecture of a 1.9 Ga marine volcanic arc, Skellefte district, Sweden. Economic Geology 91, 1022-1053.

Almodóvar, G.R., Sáez, R., Pons, J.M., Maestre, A., Toscano, M., Pascual, E., 1998. Geology and genesis of the Aznalcóllar massive sulphide deposits. Iberian Pyrite Belt, Spain. Mineralium Deposita 33, 111-136.

Azor, A., Rubatto, D., Simancas, J. F., González Lodeiro, F., Martínez Poyatos, D., Martín Parra, L. M., Matas, J., 2008. Rheic Ocean ophiolitic remnants in southern Iberia questioned by SHRIMP U-Pb zircon ages on the Beja-Acebuches amphibolites. Tectonics 27.

Badham, J.P.N., 1982. Further data on the formation of ores at Rio Tinto, Spain. Transactions-Institution of Mining and Metallurgy. Section B. Applied Earth Science 91, 26-32.

Badham, J.P.N., 2001. Physical and chemical paleogeography of the Rio Tinto area during ore deposition. GEODE workshop “Massive sulphide deposits in the Iberian: New advances and comparisons with equivalent systems”, Aracena (Huelva, Spain), 4.

Barrett T.J., MacLean W.H., 1994. Chemostratigraphy and hydrothermal alteration in exploration for VHMS deposits in greenstones and younger volcanic rocks. In: Lentz DR (eds.) Alteration and alteration processes associated with ore-forming systems. Geological Association of Canada, Short Course Notes 11, 433-467.

Barrett, T.J., MacLean, W.H., 1999. Volcanic sequences, lithogeochemistry, and hydrothermal alteration in some bimodal volcanic-associated massive sulphide systems. In: Barrie, C.T., Hannington, M.D. (Eds.) Volcanic-associated massive sulphide deposits: processes and examples in modern and ancient settings. Reviews in Economic Geology 8, 101-131.

Barrett, T.J., MacLean, W.H., Årebäck, H., 2005. The Palaeoproterozoic Kristineberg VMS deposit, Skellefte district, northern Sweden. Part II: Chemostratigraphy and alteration. Mineralium Deposita 40, 368-395.

Barrett, T.J., Dawson, G.L., MacLean, W.H., 2008. Volcanic stratigraphy, alteration, and sea-floor setting of the Paleozoic Feitais massive sulfide deposit, Aljustrel, Portugal. Economic Geology 103, 215-239.

Barrie, C.T., Ludden, J.N., Green, T.H., 1993. Geochemistry of volcanic rocks associated with Cu-Zn and Ni-Cu deposits in the Abitibi subprovince. Economic Geology 88, 1341-1358.

Barrie, C.T. 1995. Zircon thermometry of high temperature rhyolites near volcanic-associated massive sulfide deposits, Abitibi Province, Canada. Geology 23, 169-172.

Barriga, F.J.A.S., 1990. Metallogenesis in the Iberian Pyrite Belt. In: Dallmeyer, R.D., and Martínez Barcía, E. (Eds), Pre-Mesozoic Geology of Iberia. Springer-Verlag, Berlin, 369-379.

Bobrowicz, G.L., 1995. Mineralogy, geochemistry and alteration as exploration guides at Aguas Teñidas Este, Pyrite Belt, Spain. Unpublished PhD Thesis, Birmingham University, 424 pp.

Boulter, C.A., 1993a. Comparison of Río Tinto, Spain, and Guaymas Basin, Gulf of California: An explanation of a supergiant massive sulphide deposit in an ancient sill-sediment complex. Geology 21, 801-804.

Boulter, C.A., 1993b. High level peperitic sills at Rio Tinto, Spain: implications for stratigraphy and mineralization. Transactions Institution of Mining and Metallurgy. Section B. Applied Earth Science 102, 30-38.

Boulter, C.A., 1999. Comment on “Geological constraints on massive sulphide genesis in the Iberian Pyrite Belt” by Sáez, R., Almodóvas, G.R., Pascual, E. Ore Geology Reviews 14, 147-150.

Boulter, C.A., Hopkinson L.J., Ineson M.G., Bronckwell, J.S., 2004. Provenance and geochemistry of sedimentary components in the Volcano-Sedimentary Complex, Iberian Pyrite Belt: discrimination between the sill-sediment-complex and volcanic-pile models. Journal of the Geological Society, London 161, 103-115.

Boulter, C.A., Soriano, C., Zimman, P., 2001. The Iberian Pyrite Belt: a mineralized system dismembered by voluminous high-level sills. Terra Nova 13, 103-115.

Bouma, A.H., 1962. Sedimentology of some flysch deposits. Elsevier, Amsterdam 168 pp.

Cambridge Mineral Resources, 2006. The Geology of the Lomero-Poyatos VHMS Deposit, Iberian Pyrite Belt, Spain.

Campbell, I.H., Lesher, C.M., Coad, P., Franklin, J.M., Gorton, M.O., Thurston, P.C., 1984. Rare-earth element mobility in alteration pipes below massive sulphide deposits. Chemical Geology 45, 181-202.

Carvalho, D., Barriga, F., Munhá, J., 1999. Bimodal siliciclastic systems: the case of the Iberian Pyrite Belt. Reviews in Economic Geology 8, 375-408.

Cas, R.A.F., 1992. Submarine volcanism; eruption styles, products, and relevance to understanding the host-rock successions to volcanic-hosted massive sulfide deposits. Economic Geology 87, 511-541.

Cas, R.A.F., Allen, R.L., Bull, S.W., Clifford, B.A., Wright, J.V., 1990. Subaqueous, rhyolitic come-top tuff cones: a model based on the Devonian Bunga Beds, southeastern Australia and a modern analogue. Bulletin of Volcanology 52, 156-174.

Conde, C., Tornos, F., Doyle, M., 2007. Geology and lithogeochemistry of the unique Las Cruces VMS deposit, Iberian Pyrite Belt. In: Andrew, C.J. et al. (Eds.) Digging Deeper, Biennial SGA Meeting, Dublin, (Ireland), 1101-1104.

Conde. C., Tornos, F., Fernández, J. Doyle, M., 2003. Encuadre estratigráfico de los sulfuros masivos de la parte suroriental de la Faja Pirítica: Aznalcóllar-Los Frailes, y Las Cruces. Boletín Sociedad Española de Mineralogía 26, 161-162.

Davis, B.K., McPhie, J., 1996. Spherulites, quench fractures and relict perlite in a Late Devonian rhyolite dyke, Queensland, Australia. Journal of Volcanology and Geothermal Research 71, 1-11.

Donaire, T., Pascual, E., Valenzuela, A., 2002. Review and proposal for igneous rock nomenclature in the volcano-sedimentary complex of the Spanish Pyrite Belt. In Tornos, F., Pacual, R., Sáez, R., Hidalgo, R. (Eds.), GEODE Workshop Massive Sulphide Deposits in the Iberian Pyrite Belt: New advances and comparison with equivalent systems, 16-17.

Donaire, T., Pascual, E., Valenzuela, A., González Roldán, M.J., Toscano, M., 2006. Sucesión de secuencias volcánicas félsicas en el Complejo Vulcanosedimentario de la Faja Pirítica Ibérica: discriminación entre modelos volcánicos y subvolcánicos. Geogaceta 40, 119-122.

Doyle, M.G., McPhie, J., 2000. Facies architecture of a silicic intrusion-dominated volcanic centre at Highway-Reward, Queensland, Australia. Journal of Volcanology and Geothermal Research 99, 79-96.

Ewart, A., 1979. A review of the mineralogy and chemistry of Tertiary-Recent deictic, latitic, rhyolitic, and related salic volcanic rocks. In: Barker, F. (Eds), Trondhjemites, dacites, and related rocks: Amsterdam, Netherlands, Elsevier Scientific Publications, 13-121.

Gaboury, D., Pearson, V., 2008. Rhyolite geochemical signatures and association with volcanogenic massive sulphide deposits: Examples from the Abitibi Belt, Canada. Economic Geology 1003, 1531-1562.

García Palomero, F., 1992. Mineralizaciones de Riotinto (Huelva): geología, génesis y modelos geológicos para su explotación y evaluación de reservas minerales. In: Recursos Minerales de España, Textos Univ., 15, CSIC, 1325-1352.

Gemmell, J.B, Fulton, R., 2001. Geology, genesis and exploration implications of the footwall and hanging-wall alteration associated with the Hellyer volcanic-hosted massive sulphide deposit, Tasmania, Australia. Economic Geology 96, 1003-1035.

Gibson, H.L., Morton, R.L., Hudak, G.J., 1999. Submarine volcanic processes, deposits, and environments favourable for the location of volcanic-associated massive sulphide deposits. In: Barrie CT, Hannington MD (Eds.) Volcanic-associated massive sulphide deposits: processes and examples in modern and ancient settings. Reviews in Economic Geology 8, 13-51.

González Clavijo E., Díez Montes, A., 2010. Propuesta de estructura geológica para el depósito gigante de sulfuros masivos volcanogénicos de Río Tinto, Faja Pirítica Ibérica. Geogaceta 48, 210-214.

Goodfellow, W.D., 1975. Rock geochemical exploration and ore genesis at Brunswick No 12 deposit: Unpublished Ph.D. thesis, Fredericton, University of New Brunswick, 411 p.

Goodfellow, W.D. McCutcheon, S.R., 2003. Geologic and genetic attributes of volcanic hediment-Hosted massive sulfide deposits of the Bathurst mining camp, northern New Brunswick—A synthesis. Economic Geology Monograph 11, 245-301.

Hart, T.R., Gibson, H.L., Lesher, C.M., 2004. Trace element geochemistry and petrogenesis of felsic volcanic rocks associated with volcanogenic massive Cu-Zn-Pb sulfide deposits

Hidalgo, R., Rodríguez, P., Anderson K., 1996. Yacimiento de Sulfuros Polimetálicos Aguas Teñidas. Boletín geológico y minero 107 (5-6), 193-200.

Hidalgo, R., Guerrero, V., Pons, J.M., Anderson, I.K., 2003. The Aguas Teñidas Este mine, Huelva Province, SW Spain. In: Kelly, J.C., Andrew, C.J., Ashton, J.H., Boland, M.B., Earls, G., Fusciardi, L. and Stanley, G. (Eds), Europe's Major Base Metal Deposits. Irish Association for Economic Geology, 367–379.

IGME, 1982. Síntesis Geológica de la Faja Pirítica del SO de España. Instituto Geológico y Minero de España, Madrid, 106.

Irvine, T.N., Baragar, W.R.A., 1971. A guide to chemical classification of the common volcanic rocks. Canadian Journal of Earth Sciences 8, 523-548.

Ishikawa, Y., Sawaguchi, T., Iwaya, S., Horiuchi, M., 1976. Delineation of prospecting targets for Kuroko deposits based on modes of volcanism of underlying dacite and alteration halos. Mining Geology 26, 105-117.

ITGE, 2000. Mapa de Síntesis geológica y situación de yacimientos e indicios minerales en la Faja Pirítica Española.

Junta de Andalucía, 2004. Mapa Litológico de Andalucía: Unidades Litológicas. Consejería de Medio Ambiente. Junta de Andalucía. Escala 1:400.000.

Knight, F. 2000. The mineralogy, geochemistry and genesis of the secondary sulphide mineralization of the Las Cruces deposit,Spain. PhD thesis, University of Cardiff.

Kokelaar P., Busby, C., 1992. Subaqueous explosive eruption and welding of pyroclastic deposits. Science 257, 196-201.

Lafrance, B., Mueller, W.U., Daigneault R., Dupras, N., 2000. Evolution of a submerged composite arc volcano: volcanology and geochemistry of the Normétal volcanic complex, Abitibi greenstone belt, Quebec, Canada. Precambrian Research 101, 277-311.

Lake, P.A., Oswin, W.M., Marshall, J.E., 1988. A palynological approach to terrene analysis in the South Portuguese Zone. Trabajos de Geología 17, 125-131.

Large, R.R., Gemmell, J.B., Paulick, H., 2001. The alteration box plot –a simple approach to understanding the relationship between alteration mineralogy and lithogeochemistry associated with volcanic-hosted massive sulphide deposits. Economic Geology 96, 957-971

Laznicka, P., 1999. Quantitative relationships among giant deposits of metals. Economic Geology 94, 455-473.

Le Bas M.J., Le Maitre R.W., Streckeisen A., Zanettin B.A., 1986. Chemical classification of volcanic rocks based on the total alkali-silica diagram. Journal of Petrology 27, 745-750.

Leistel, J.M., Marcoux, E., Thieblemont, D., Quesada, C., Sánchez, A., Almodóvar, G.R., Pascual, E., Sáez, R., 1998. The volcanic-hosted massive sulphide deposits of the Iberian Pyrite Belt. Review and preface to the special issue. Mineralium Deposita 33, 2-30.

Lentz, D.R., 1996. Trace-element systematics of felsic volcanic rocks associated with massive sulphide deposits in the Bathurst mining camp; petrogenetic, tectonic and chemostratigraphic implications for VMS exploration. In: Wyman, D.A. (Ed.) Trace element geochemistry of volcanic rocks; applications for massive sulphide exploration. Geological Association of Canada, Short Course Notes 12, 359-402.

Lentz, D.R., 1999. Petrology, geochemistry, and oxygen isotope interpretation of felsic volcanic and related rocks hosting the Brunswick 6 and 12 massive sulfide deposits (Brunswick Belt), Bathurst mining camp, New Brunswick, Canada. Economic Geology 94, 57-86.

Lentz, D.R., Hall, D.C., Hoy, L.D., 1997. Chemostratigraphic, alteration, and oxygen isotopic trends in a profile through the stratigraphic sequence hosting the Health Steele B zone massive sulphide deposit, New Brunswick. Canadian Mineralogist 35, 841-874.

Lentz, D.R., McCutcheon S.R., 2006. The Brunswick No. 6 massive sulphide deposit, Bathurst Mining Camp, Northern New Brunswick, Canada: A synopsis of the geology and hydrothermal alteration system. Exploration and Mining Geology 15, 1-34.

Lesher, C.M. Goodwin, A.M., Campbell, I.B., Gorton, M.P., 1986. Trace element geochemistry of ore-associated and barren, felsic metavolcanic rocks in the Superior Province, Canada. Canadian Journal of Earth Sciences 23, 222-237.

Lowe, D.R., 1982. Sediment gravity flows: II. Depositional models with special reference to the deposits of high density turbidity currents. Journal of Sedimentary Petrology 52, 279-297.

MacLean, W.H., 1990. Mass change calculations in altered rock series. Mineralium Deposita 25, 44-49.

MacLean, W.H., Barrett, T.J., 1993. Lithogeochemical techniques using immobile elements. Journal of Geochemical Exploration 48, 109-133.

Martin-Izard, A., Arias, D., Arias, M., Gumiel, P., Sanderson, D.J., Castañon, C., Lavandeira, A., Sanchez, J., 2015. A new 3D geological model and interpretation of structural evolution of the world-class Rio Tinto VMS deposit, Iberian Pyrite Belt (Spain). Ore Geology Reviews 71, 457-476.

McCutcheon, S.R., Fyffe, L.R., Gower, S.J., Langton, J.P., Wilson, R.A, 1997. The Bathurst Mining Camp: stratigraphic and structural synthesis: New Brunswick Department of Natural Resources and Energy, Minerals and Energy Division, Mineral Resource Report 97-4, 129-148.

McCutcheon, S.R., Luff, W.M., Boyle, R.W., 2003. The Bathurst Mining Camp, New Brunswick, Canada: History of discovery and evolution of geologic models, In: Goodfellow, W., McCutcheon, S.R., Peter, J. (Eds), Massive Sulphide Deposits in the Bathurst Mining Camp, New Brunswick, and Northern Maine. Economic Geology Monograph 11, 17-35.

McKee, G.S., 2003. Genesis and deformation of the Aguas Teñidas Este massive sulphide deposit and implications for the formation, structural evolution and exploration of the Iberian Pyrite Belt: D. thesis, University of Birmingham, 413 pp.

McKee, G.S., Hidalgo, R., Ixer, R.A., Boyce, A., Guerrero, V., Pons, J.M., 2001. Deposit formation and structural evolution at Aguas Teñidas Este. In: Tornos, F., Pascual, E., Sáez, R., Hidalgo, R. (Eds.), GEODE Workshop Massive Sulphide Deposits in the Iberian Pyrite Belt: New Advances and Comparison with Equivalent Systems, 38– 89.

McPhie, J., Allen, R.L., 1992. Facies architecture of mineralised submarine volcanic sequences: Cambrian Mount Read Volcanic, western Tasmania. Economic Geology 87, 587-596.

McPhie, J., Allen, R.L., 2003. Submarine, silicic, syn-eruptive pyroclastic units in the Mount Read Volcanics, Western Tasmania: Influences of vent setting and proximity on lothofacies characteristics. In: White, J.D.L., Smellie, J.L., and Clague, D.A. (Eds), Explosive subaqueous volcanism. Geophysical Monograph Series 140, 245-258

McPhie, J., Doyle, M., Allen, R., 1993. Volcanic textures: A guide to the interpretation of textures in volcanic rocks. Centre for Ore Deposit and Exploration Studies, University of Tasmania, Hobart (Tasmania),198 pp.

McPhie, J., Hunns, S.R., 1995. Secondary welding of submarine, pumice.lithic breccia at Mount Chalmers, Queensland, Australia. Bulletin of Volcanology 57, 170-178.

Mellado, D. González Clavijo, E., Tornos, F. Conde, C., 2006. Geología y estructura de la Mina de Río Tinto (Faja Pirítica Ibérica, España). Geogaceta 40, 231-234.

Mitjavila, J., Marti, J., Soriano, C., 1997. Magmatic evolution and tectonic setting of the Iberian Pyrite Belt volcanism. Journal of Petrology 38, 727– 755.

Miyashiro, A., 1974. Volcanic rocks series in Island arcs and active continental margins. American of Journal Science 274, 321-355.

Montelius, C. (2005) The genetic relationship between rhyolitic volcanism and Zn-Cu-Au deposits in the Maurliden volcanic centre, Skellefteå district, Sweden: Volcanic facies, lithogeochemistry and geochronology. Ph.D. thesis, Luleå University of Technology, Sweden, ISSN: 1402-1544.

Moreno, C., 1993. Post-volcanic Paleozoic of the Iberian Pyrite Belt: an example of basin morphologic control on sediment distribution in a turbidite basin. Journal of Sedimentary Petrology 63, 1118- 1128.

Moreno, C., Saez, R., 1990. Sedimentación marina somera en el Devónico del anticlinorio de Puebla de Guzmán, Faja Pirítica Ibérica. Geogaceta 8, 62-64.

Moreno, C., Sierra, S., Sáez, R., 1996. Evidence for catastrophism at the Famenian-Dinantian boundary in the Iberian Pyrite Belt. Recent Advences. In: Strogen P., Somerville D., and Jones G. Ll. (Eds.) Lower Carboniferous geology. Geological Society, London, Special Publication, 107, 153-162.

Munhá, J., 1979. Blue amphiboles, metamorphic regime and plate tectonic modelling in the Iberian Pyrite Belt. Contribution to Mineral and Petrology 107, 153-162.

Munhá, J., 1983. Hercynian magmatism in the Iberian Pyrite Belt. Memorias Servicio Geológico Portugal 29, 39–81.

Munhá, J., 1990. Metamorphic evolution of the South Portuguese/Pulo do Lobo Zone. In: Dallmeyer R.D. and Marínez García E. (Eds.) PreMesozoic Geology of Iberia. SpringerVerlag, Berlín, 363-368.

Munhá, J., Pacheco, N., Beliz, A., Relvas, J.M.R.S., Hodder, R.W., 1997. Physical and geochemical characterisation of the Neves Corvo felsic volcanism. Neves Corvo Field Conference Abstracts, Lisbon, 89.

NAVAN,S.A., 1996. Aguas Teñidas deposit. Faja Pirítica en Simposio Sulfuros metálicos de la Faja Pirítica Ibérica. Huelva, 21-23.

Ohmoto, H., 1996. Formation of volcanogenic massive sulphide deposits: the Kuroko perspective. Ore Geology Reviews 10, 135– 177.

Oliveira, J.T., 1990. South Portuguese Sone: introduciton. Stratigraphy and synsedimentary tectonism. In: Dallmeyer, R.D., Martínez García, E. (Eds.) PreMesozoic Geology of Iberia. Springer Verlag, pp. 333-347.

Oliveira, J.T., Quesada, C., 1998. A comparison of stratigraphy, structure and paleogeography of the South Portuguese Zone and Southwest England, European Variscides Geoscience in south-west England (The Scott Simpson Lecture, Annual Conference of the Ussher Society 1998, 141-159.

Onézime, J., Charvet, J., Faure, M., Bourdier, J. L., and Chauvet, A., 2003. A new geodynamic interpretation for the South Portuguese Zone (SW Iberia) and the Iberian Pyrite Belt genesis: Tectonics 22, 1–17.

Onézime, J., Charvet, J., Faure, M., Chauvet, A., Panis, D., 2002. Structural evolution of the southernmost segment of the West European Variscides: the South Portuguese zone (SW Iberia): Journal of Structural Geology 24, 451–468.

Pereira, Z., Matos, J., Fernandes, P., Oliveria, J.T., 2007. Devonian and Cargoniferous palynostratigraphy of the South Portuguese Zone, Portugal – An overview. Comunicaçoes Geológicas 94, 52-79.

Piercey, S.J., 2011, The setting, style, and role of magmatism in the formation of volcanogenic massive sulfide deposits. Mineralium Deposita 46, 449-471.

Pinedo, I., 1963. Piritas de Huelva. Su historia, minería y aprovechamiento. Summa Editorial, Madrid. 1003 pp.

Quesada, C., 1991. Geological constraints on the Paleozoic tectonic evolution of tectonostratigraphic terranes in the Iberian Massif. Tectonophysics 185, 225-145

Quesada, C., 1996. Estructura del sector español de la Faja Pirítica Ibérica: implicaciones para la exploración de yacimientos. Boletín Geológico y Minero 107, 265-278.

Quesada, C., 1998. A reappraisal of the structure of the Spanish segment of the Iberian Pyrite Belt. Mineralium Deposita 33, 31-44.

Quesada, C., 1999. Tectnostratigraphic evolution of the Iberian Pyrite Belt. In: Gamez, J.A., Eguiluz, L., Palacios, T. (Eds.). Post-conference Field Trip guide book: XV Reunión de Geología del Oeste Peninsular. Diputación de Badajoz, Badajoz, Spain. 30 pp.

Rambaud, F., 1969. El sinclinal Carbonífero de Río Tinto (Huelva) y sus mineralizaciones asociadas. IGME, Memorias 71.

Relvas, J.M.R.S., 2000. Geology and metallogeny at the Neves Corvo deposit, Portugal. Unpublished Doctoral Thesis. University of Lisbon, 319 pp.

Relvas, J.M.R.S., Barriga, F.J.A.S., Longstaffe, F.J., 2006. Hydrothermal alteration and mineralization in the Neves-Corvo volcanic-hosted massive sulfide deposit, Portugal; II, Oxygen, hydrogen, and carbon isotopes. Economic Geology 101, 791-804.

Rodríguez, P., 1996. Aguas Teñidas Deposit, Faja Pirítica, Cu-Pb-Zn-Ag. In: Simposio Sulfuros Polimetálicos de la Faja Pirítica, Huelva 21-23 Feb. 1996, Spain, 6 pp.

Rosa, C.J.P., 2007. Facies architecture of the Volcanic Sedimentary Complex of the Iberian Pyrite Belt, Portugal and Spain. Ph.D. thesis, University of Tasmania, 357 pp.

Rosa, C.J.P., McPhie, J., Relvas, J.M.R.S., 2010. Type of volcanoes hosting the massive sulphide deposits of the Iberian Pyrite Belt. Journal of Volcanology and Geothermal Research 194, 107-126.

Rosa, C.J.P., McPhie, J., Relvas, J.M.R.S, Pereira, Z., Oliveira, T., and Pacheco, N., 2008. Facies analyses and volcanic setting of the giant Neves Corvo massive sulphide deposit, Iberian Pyrite Belt, Portugal. Mineralium Deposita 43, 449-466.

Rosa, D.R.N., Invierno, C.M., Oliveira, V.M.J., Rosa, C.J.P., 2004. Geochemistry of volcanic rocks, Albernoa Area, Iberian Pyrite Belt, Portugal. International Geology Review 46, 366-383.

Ross, C.S., Smith, R.L., 1955. Water and other volatiles in volcanic glass. American Mineralogist 40, 1071-1089.

Routhier P., Aye, F., Boyer, C., Lecolle, M., Moliere, P., Roger, G., Picot. P., 1980. La ceinure sud-ibérique à amass sulfurés dans sa partie espagnole medine. Bureau Recherches Géologique Miniers Memoires 94, 1-265.

Ruiz García, C., 1984. Estudio de la mineralización y rocas encajantes den la mina Lomero-Poyatos (Huelva) Boletín Geológico y Minero XCV-II, 151-164.

Sáez, R., Almodovar, G. R., Pascual, E., 1996. Geological constraints on massive sulphide genesis in the Iberian Pyrite Belt. Ore Geology Reviews 11, 429-451.

Sáez, R., Pascual, E., Toscano, M., Almodóvar, G.R., 1999. The Iberian type of volcano-sedimentary massive sulphide deposits. Mineralium Deposita 34, 549– 570.

Sánchez España, F.J., 2000. Mineralogía y geoquímica de los yacimientos de sulfuros masivos en el área Nor-Oriental de la Faja Pirítica Ibérica, San Telmo–San Miguel–Peña del Hierro, Norte de Huelva, España. Unpublished Ph.D. thesis. Universidad del País Vasco, 307 pp.

Sánchez España, F.J. Velasco, F., Boyce, A.J., Fallick, AE., 2003. Source and evolution of ore-forming hydrothermal fluids in the northern Iberian Pyrite Belt massive sulphide deposits (SW Spain) evidence form fluid inclusions and stable isotopes. Mineralium Deposita 38, 519-537.

Sánchez España, F.J., Velasco, F., Yusta, I., 2000. Hydrothermal alteration of felsic volcanic rocks associated with massive sulphide deposition in the Northern Iberian Pyrite Belt (SW Spain). Applied Geochemistry 15, 1265– 1290.

Schlatter, D.M., 2007. Volcanic strarigraphy and hydrothermal alteration of the Petiknäs South Zn-Pb-Cu-Au-Ag Volcanic-hosted Massive. Ph.D. thesis, Luleå University of Technology, Sweden, ISSN: 1402-1544.

Shermerhorn, L.J.G., 1975. Spilites, regional metamorphism and subduction in the Iberian Pyrite Belt: some comments. Geologie en Mijnbouw 54, 23-35.

Sierra, J., 1984. Geología, Mineralogía y Metalogenia del Yacimiento de Aznalcóllar. (Primera parte: Litoestratigrafía yTectónica). Boletín Geológico y Minero 95, 440-455.

Sierra, J., 1984. Geología, Mineralogía y Metalogenia del Yacimiento de Aznalcóllar. (Segunda parte: Mineralogía y sucesión mineral). Boletín Geológico y Minero 95, 553-568.

Silva, J.B., Oliveira, J.T. Ribeiro, A., 1990. Structural outline of the South Portuguese Zone. In: Dallmeyer, R.D., Martínez García, E. (Eds.) Pre-Mesozoic Geology of Iberia. Springer-Verlag, Verlin, 348-362.

Simancas, J.F., Carbonell, R., González Lodeiro, F., Pérez Estaún, A., Juhlin, C., Ayarza, P., Kashubin, A., Azor, A., Martínez Poyatos, D., Sáez, R., Almodóvar, G.R., Pascual, E., Flecha, I., Martí, D., 2006. Transpressional collision tectonics and mantle plume dynamics: the Variscides of southwestern Iberia. In: Gee, D.G. and Stephenson, R.A. (Eds.) 2006. European Lithosphere Dynamics. Geological Society London, Memoirs 32, 345-354.

Solomon, M., Walshe, J.L., García Palomero, F., 1980. Formation of massive sulphide deposits at Río Tinto, Spain. Transactions of the Institution of Mining and Metallurgy. Section B. Applied Earth Science 89, 16-24.

Soriano, C., 1997. Vulcanisme i estructura de la Faja Piritica Iberica. Zona Sud Portuguesa Tesis Doctoral. Universitat de Barcelona (Spain), 265 pp.

Soriano, D., Martí, J., 1999. Facies analysis of volcano-sedimentary successions hosting massive sulfide deposits in the Iberian Pyrite Belt, Spain. Economic Geology 94, 867-882.

Strauss, G. K., Roger, G., Lecolle, M., and Lopera, E., 1981. Geochemical and geologic study of the volcano-sedimentary sulfide orebody of La Zarza, Huelva Province, Spain. Economic Geology 76, 1975–2000.

Thiéblemont, D., Pascual, E., Stein, F., 1998. Magmatism in the Iberian Pyrite Belt: petrological constrains on a metallogenic model. Mineralium Deposita 33, 259-307.

Tornos, F., 2006. Environment of formation and styles of volcanogenic massive sulphides: The Iberian Pyrite Belt. Ore Geology Reviews 28, 259-307.

Tornos, F., González Clavijo, E., Spiro, B. F., 1998. The Filón Norte orebody (Tharsis, Iberian Pyrite Belt): a proximal low-temperature shale-hosted massive sulphide in a thin-skinned tectonic belt. Mineralium Deposita 33, 150-169.

Tornos , F., Casquet, C., Relvas, J.M.R.S., 2005. 4: Transpressional tectonics, lower crust decoupling and intrusión of deep mafic sills: A model for the unusual metallogenesis of SW Iberia. Ore Geology Reviews 27, 133-163.

Tornos, F., Heinrich, C.A., 2008, Shale basins, sulfur-deficient ore brines, and the formation of exhalative base metal deposits. Chemical Geology, 247, 195-207.

Tornos, F., Solomon, M., Conde, C., Spiro, B.F., 2008. Formation of the Tharsis massive sulphide deposit, Iberian Pyrite Belt: geological, lithogeochemical, and stable isotope evidence for deposition in a brine pool. Economic Geology 103, 185-214.

Valenzuela, A., Donaire, T., Pascual, E., 2001. The Odiel Rives section: an example of complexities in volcanic evolution of the Volcano Sedimentary Complex in the Iberian

Pyrite Belt, Spain. In: GEODE Workshop “Massive sulphide deposits in the Iberian Pyrite Belt: New Advances and comparison with equivalent systems”, Tornos, F. Sáez, R., Hudalgo, R., (eds.), Aracena, Huelva (Spain), 61-62.

Valenzuela, A., Donaire, R., Pascual, E., 2002. Secuencia de facies volcánicas en el área del río Odiel (Faja Pirítica Ibérica, España). Geogaceta 32, 131-134.

Valenzuela, A., Donaire, M., Pascual, E., 2003. The Villanueva de los Castillejos section: The geology of volcanic-hosted massive sulphides of the Iberian Pyrite Bel. Geode-Global Comparison Massive Sulphide project. Field Trip Guide, 40-42.

Valenzuela, A., Donaire, T., Gonzalez-Roldan, M.J., Toscano, M., Pascual, E., 2011a. Volcanic architecture in the Odiel river area and the volcanic environment in the Riotinto-Nerva Unit, Iberian Pyrite Belt, Spain. Journal of Volcanology and Geothermal Research 202: 29-46.

Valenzuela, A., Donaire, T., Pin, C., Toscano, M., Hamilton, M.A., Pascual, E., 2011 b. Geochemistry and U-Pb dating of felsic volcanic rocks in the Riotinto-Nerva unit, Iberian Pyrite Belt, Spain: crustal thinning, progressive crustal melting and massive sulphide genesis. Journal of the Geological Society 168, 717-731.

Velasco, F., Sánchez España, J., Yanguas, A., Tornos, F., 2000. The occurrence of gold in the sulfide deposits of the Iberian Pyrite Belt: evidence of precious metal remobilisation In: Gemmell J.B., Pongratz J. (eds) Volcanic environments and massive sulfide deposits, Program and Abstracts. CODES, Hobart, Tasmania (Australia), 221-223.

Velasco, F., Tornos, F., 2006. Los sulfuros masivos (Cu-Zn-Au) de Lomero Poyatos (Faja Pirítica Ibérica): encuadre geológico, alteración hidrotermal y removilización. Macla 6, 489-492.

Velasco, F., Tornos, F., Herrero, J.M., 2003. Gold remobilization in metamorphosed VMS deposits, Iberian Pyrite Belt, Spain 105th Annual General Meeting. Canadian Institution Mining Metallurgy, Halifax (Canada), pp 153.

Whitford, D.J., McPherson, W.P.A., Wallace, D.B., 1989. Geochemistry of the host rocks of the volcanogenic massive sulphide deposit at Que River, Tasmania. Economic Geology 84, 1-21.

Williams, D., Stanton, R.L., Rambaud, F., 1975. The Planes-San Antonio pyritic deposit of Rio Tinto, Spain: its nature, environment and genesis. Transactions of the Institution Mining Metallurgy 84, B73-B82.

Winchester, J.A., Floyd, P.A., 1977 Geochemical discrimination of different magma series and their differentiation products using immobile elements. Chemical Geology 20, 325-343.

CAPITULO II

Geology and geochemistry of the volcanic sequence hosting the giant Rio Tinto deposit (south of Spain)

Geología y geoquímica de la secuencia volcánica encajante del depósito de Rio Tinto (sur de España)

Abstract

The Rio Tinto district is the most important volcanic-hosted massive sulphide district in the earth's crust, containing more than 1500 Mt of pyrite-rich massive sulphide and more than 2 Gt of mineralized stockwork. The mining district consists of nine ore deposits hosted by a strongly hydrothermally altered volcanic-sedimentary sequence of Late Devonian-Early Carboniferous age.

Systematic mapping and geochemical studies have allowed distinguish four major lithologic units. From bottom to top, they include: (1) the *Mafic-Siliciclastic Unit*, that comprises mafic sills and submarine lava flows interbedded and intruding a sequence dominated by dark shale intercalated with mafic volcaniclastic rocks (sandstone and siltstone). This volcanic unit is conformably overlain by, (2) the *Lower Sedimentary Unit*, made up of dark shale and a characteristic layer of polymictic conglomerate. This conglomerate is shale-supported and includes fragments of shale, and felsic rocks; locally, there are some pyrite rich nodules that are of likely hydrothermal replacive origin. (3) The thick *Felsic Unit,* that is an heterogeneous and usually hydrothermally altered volcanic sequence that includes quartz-feldspar porphyritic dacite to rhyodacite domes and sills with associated autobreccias and hyaloclastite. The domes are interbedded with pumice-, crystal- and vitriclast-rich sandstone and breccia with only some minor shale. This unit forms the bulk of the outcrops of the Rio Tinto area. (4) The *Upper Sedimentary Unit,* which caps the Felsic Unit, is formed by dark shale, green and red siltstone and chemical sediments (chert) and laterally grades into volcanic sandstone. Finally, the Baixo Alentejo Flysch Group is thrusted above the VS Complex.

Most of this sequence is affected by an irregular and intense hydrothermal alteration. The Felsic Unit is pervasively sericitized and only locally, near major faults or close to the massive sulphides, the sericite + quartz ± pyrite alteration is replaced by a chlorite + quartz ± pyrite assemblage. By contrast, both the Lower Sedimentary Unit and the Mafic-Siliciclastic Unit have a pervasive chloritic ± quartz ± pyrite alteration.

The sulphide-bearing stockwork consists of an anastomosed network of quartz-sulphide or sulphide veins that crosscut rocks affected by both sericitic and chloritic alteration. The type and distribution of the alteration and the presence of stockwork seem to be controlled by the reactivity and porosity of the host rocks and the presence of E-W and NW-SE trending faults, which probably correspond to inverted synsedimentary extensional structures. As a whole, the structure of the Rio Tinto area is an antiformal stack formed by several sheets that formed during the thin skinned tectonics of the Variscan orogeny.

The massive sulphide orebodies occur aligned E-W in both limbs of the Rio Tinto antiform and within different imbricated sheets. The uppermost lenses (Filon Sur and Corta Atalaya) are hosted by dark shale in the Upper Sedimentary Unit capping the Felsic Unit; they are interpreted as exhalative on the seafloor and formed on a small local anoxic basin. A second mineralization, hosted by Filón Norte, Salomón, Lago, Dehesa and Quebrantahuesos orebodies), occurs as replacive bodies within the rhyodacite of the Felsic Unit.

The lithogeochemistry of immobile element tracks the existence of the two main volcanic units. The coherent volcanic rocks of the lower Mafic-Siliciclastic Unit have a composition of basalt to andesite. The contents in Al_2O_3, TiO_2, and Zr suggest that there are two different types of mafic rocks, a basaltic-andesite and a high Ti-Zr basalt, both of tholeiitic affinity. They are likely derived from deep juvenile magmas of mantle derivation that underplatted continental crust during crustal thinning and the basin formation. The overlying Felsic Unit is formed by massive and volcaniclastic rocks of dacitic to rhyodacitic composition. The HREE, Al, Y, Zr, Ti and Yb contents show the existence of two main subtypes: a rhyodacite group with Zr values between 50 to 200 µg/g that is found in the Odiel river, Campillo and the mine (Corta Atalaya) areas, and a second one formed by high Zr rhyodacite (225-300 µg/g Zr) located in the north of the mine area. As a whole, they are interpreted as formed in an unique magma chamber where they interacted with

previous primitive rocks; the high-Zr rocks represents the most fractionated batch. The mineralization is related to the Zr-poor felsic rocks while the high-Zr ones are always barren.

Keywords: Rio Tinto district; lithostratigraphy; geochemistry; massive sulphide; hydrothermal alteration.

1. Introduction

The Rio Tinto mining district is the largest and the most emblematic of the several giant volcanogenic massive sulphide mines of the Iberian Pyrite Belt (IPB) (Fig. 1) and arguably the largest massive sulphide concentration on Earth, with more than 1500 Mt of massive sulphides and more than 2000 Mt tons of low grade ore in the underlying stockwork (Leistel et al., 1998; Tornos, 2005, 2006) (Table 1).

Rio Tinto is a significant milestone in the history of mining and one of the most charismatic mine districts worldwide. It has been actively worked for more than 5000 years and is the origin of one of the largest mining companies, Rio Tinto plc.

The area has been mined successively by Tartessians, Phoenicians, Romans, Arabs and, during the XIX and XX century, by British and Spanish mining companies. A detailed overview of the mining history can be found in Avery (1974), Pinedo (1963), Blanco and Rothenberg et al. (1981), Rothenberg et al. (1987) and Gonzalo and Tarín (1988). In brief, there are evidences of old mining from the V millennium BC to V. century AD. The oldest archaeological remnants are of the second half of the IV millennium BC but there are evidences of permanent settlings during the II m. BC. The smelters near the Lago open pit started during the late Bronze Age (XII-IX c. BC) and were active till the Iron Age (Blanco and Rothenberg, 1981). Major mining activity, mostly oriented to the extraction of silver, was between the IX-VIII c. BC and it slowly declined till the VI c. BC due to the end of trading with Phoenicians and Greeks.

Renewed mining activity occurred under the Roman Empire (III c. BC to V c. AC). This mining was especially active between the third and first c. BC (Rothenberg et al., 1987) and targeted to the extraction of gold and silver-bearing "*jarositic sands*" located in the contact between the gossan and the underlying massive sulphides, as well as the copper-rich ores within the cementation zone. The "*jarositic sands*" consist of alternating ochre

Figure 1. Simplified geological map of the intermediate and northern part of the Iberian Pyrite Belt, showing the location of the major massive sulphide deposits (modified from IGME, 1982; ITGE, 2000; Junta de Andalucía, 2004; Oliveira, 1990; Quesada, 1991, 1996, 1998). The main study areas, Rio Tinto district (Fig. 2), Río Odiel and Zarandas are indicated by rectangles. The inset shows the map of the South Portuguese Zone (modified from Quesada, 1998) and its localization in the Variscan belt of the Europe (adapted from Oliveira and Quesada, 1998). Ore deposits: AZ-LF: Aznalcóllar-Los Frailes; ATE: Aguas Teñidas; CO: Concepción; LC: Las Cruces; LO: Lomero Poyatos; NC: Neves Corvo; RT: Rio Tinto; SO: Sotiel; TH: Tharsis.

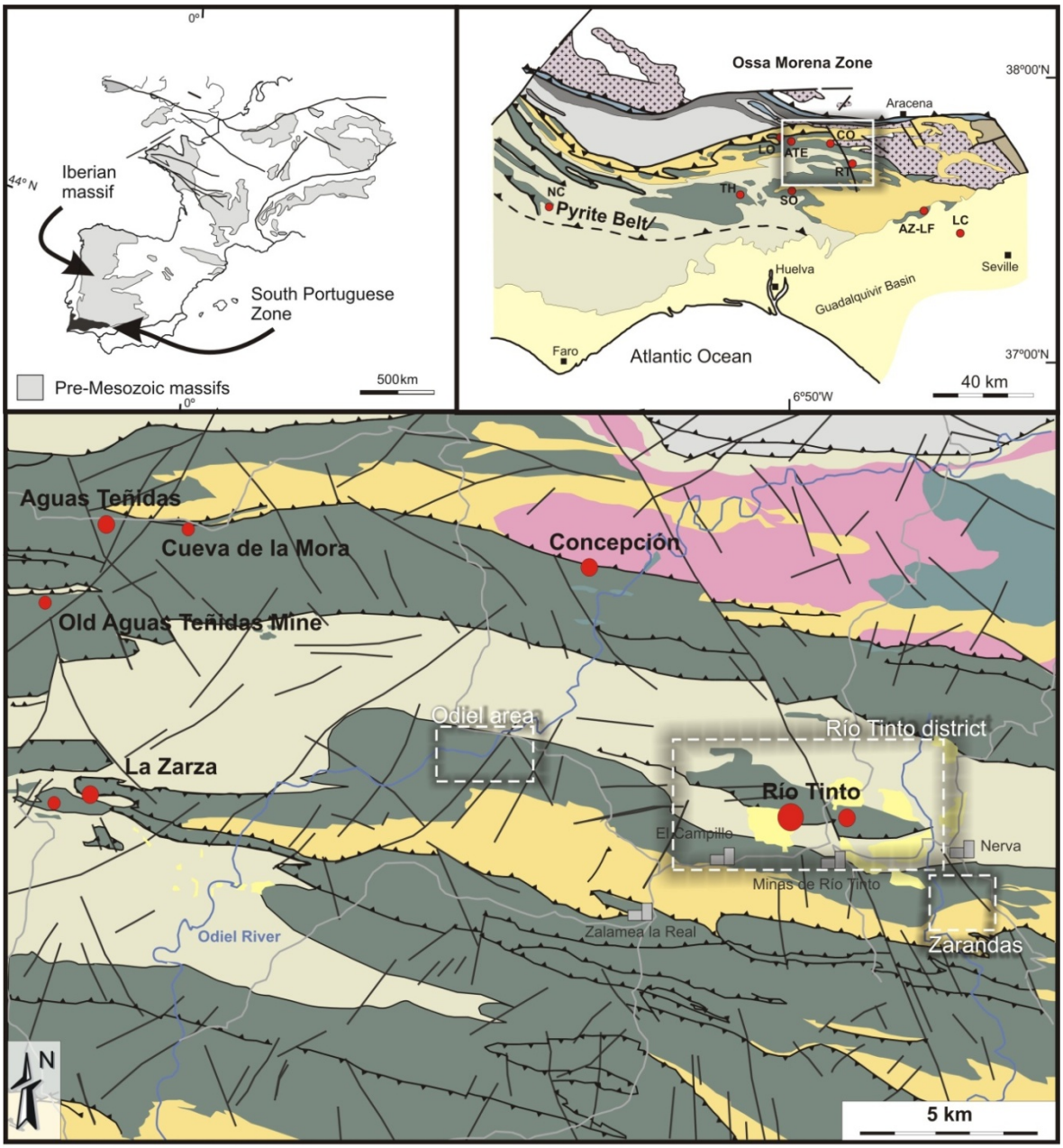

Pre-Mesozoic Massif

Beja-Acebuches Complex

Ophilitic Sequence (Beja Acebuches Ophiolite)

Pulo do Lobo Antiform

Oceanic Sedimentary Sequence (Pulo do Lobo Terrane)

Sandstone and shale (late Devonian)

Iberian Pyrite Belt

Flysch sequence (Culm Group) (late Visean)

Volcanic Sedimentary Complex (late Fammenian-M. Visean)

Phyllite-Quartzite Group (PQ Group) (middle-late Fammenian)

Continental sediments and volcanic rocks (Stephanian to Permian)

Post-Paleozoic Cover

Plutonic rocks

Granite & granodiorite

Gabbro & diorite

Thurst

Fault

VHMS deposits

Township

and yellow sandstone layers, up to 5m in thickness, composed of jarosite, plumbojarosite, argentojarosite and beaudantite and have up to 25 g/t Au and 2100 g/t Ag (Williams, 1990). Roman operations were at large scale and incorporated new technologies imported from other mines, mainly in Greece. The discovery of new deposits in Brittany and the decline of the empire finished with mining during the V c. AC. Roman remnants include about 16 Mt of slag, abundant adits and shafts, the ruins of smelters and a graveyard.

As other nearby mines, Rio Tinto was only sporadically worked until the XIX c. There is little evidence of Visigoth- and Arab-period mining. During the early XVII c., an expedition was sent to the area to locate the fabulous Tharsis mines described in the Bible. Despite they found the old roman mines, mining was not economic until the XVIII c. In 1724, the Swedish Lieberto Wolters started to mine copper at a small scale. The mine was acquired by the Spanish government in 1783 and operated until 1828. In 1873, the Rio Tinto mine and the neighbouring land were sold to the British Hugo Matheson that created the Rio Tinto Company Ltd (Avery, 1958). This company mined the area until 1954, when it started to be operated by the Compañía Española de Minas de Rio Tinto S.A. During that time, Rio Tinto was the largest company in Spain and had a dramatic influence in the social and economic habits of the area. Up to 40.000 people were contracted by the company in the early XX c. Mining was first orientated to the copper-rich ores and after the 1950's decade to the pyritic massive sulphides for the production of hydrosulphuric acid, becoming one of the major world producers of such commodity. In more recent times and after the almost complete exhaustion of the massive sulphides, the mining was focused in the expansion of the Cerro Colorado open pit and the Alfredo shaft (Fig. 2), that mined the Cu-bearing stockwork (1973-1986). When the copper prices felt in 1987, the mining was oriented to the gold and silver-bearing gossan (1987-2002). After, the acquisition of the mine and the smelter by Atlantic Copper in 1995, the mine was symbolically sold to the miners (Minas de Riotinto S.A.L.) that have tried to rationalize the

mining operations, and intermittently mined some remaining gold-bearing gossans as well as some high grade zones of the stockwork.

Table 1. Tonnages and metal grades of the main massive sulphide orebodies of Rio Tinto district and adjacent deposits (Iberian Pyrite Belt).

Deposit	Mt	%Cu	%Pb	%Zn	Ag g/t	Au g/t	Reference
Aguas Teñidas Mine [1]							
cupriferous	9.43	2.40	0.20	0.90	28.30	0.40	Iberian Minerals Corp (2009)
pollymetalic	10.12	1.10	2.50	8.20	77.80	0.90	
stockwork	1.36	2.25	0.06	0.25	7.1	0.06	
Concepción	55.85	0.57	0.19	0.48	6.68	0.21	Leistel et al. (1998)
La Zarza	171.6	1.24	1.09	2.49	45	1.79	Tornos (2006)
Lomero Poyatos	15.45	1.35	1.12	3.76	83.48	3.25	Tornos (2006)
Rio Tinto [2]	707.2	0.39	0.12	0.34	22	0.36	Tornos (2006)
Filón Sur + San Dionisio	268	2.0	0.7	1.4			
Filón Norte	25.7	1.5					
Cerro Colorado [3]	200	0.4	0.1	0.2	7	0.1	
Planes + San Antonio	19.5	1.4	0.9	1.6			
Valle	0.19	1.50					
San Platón	2.5	1.5	0.2	5.6	31	0.9	Tornos (2006)
San Miguel	1.3	3.0					Pinedo (1963)
Tharsis	115	0.5	0.6	2.7	22	0.7	Tornos et al. (1998)

[1] Aguas Teñidas Mine and old Aguas Teñidas are nowadays a single ore deposit. Tonnage here is that of the minable ore (cupriferous + polymetallic Zn-Pb) but the pyrite-rich massive sulphides exceed 100 Mt.

[2] Primary+secondary ore

[3] Stockwork

In 2004, the company was acquired by Mantesur Andévalo, S.L. that scheduled to restart the operation in some selected areas such as Quebrantahuesos (Fig. 2). In 2007, EMED-Tartessus (subsidiary of EMED Mining Company, Cyprus; www.emed-tartessus.com) acquired the exploitation and focused its interest in the Quebrantahuesos and Filón Sur orebodies. The company has been arranging the permitting process and institutional negotiations during 2013 and 2014 and the mine operations have restarted again in mid 2015.

The total extracted ore is unknown but the compilations of Pinedo (1963) and later data indicate that until 2001 it was approximately 241 Mt, being more than 50% taken out in the

last middle XX c. Currently, the new evaluation made by EMED-Tartessus reveals reserves of 123 Mt with a 0.46 % Cu, and a potential mine life upper than 10 years (www.emed-tartessus.com).

Despite its major historical and mining significance, relatively few recent papers have been published on the geology and ore deposits of the district. Most of the general geology is based on the pioneer works of Williams (1934, 1966) and Williams et al. (1975), that have been only partially modified by the later studies of Rambaud (1969) and García Palomero (1980, 1992). These authors have defined the basic geology of the area, proposing that the mine area consists of a syncline-anticline structure with a continuous sequence in which a lower mafic unit is overlain by felsic volcaniclastic rocks and shale and conformably capped by the synorogenic flysch-like Culm Group. The massive sulphides occur in the shale above the felsic volcanics. The studies of Boulter (1993a, 1993b, 1996) and Boulter et al. (2001) have proposed a different model, in which the volcanic complex postdated the overlying mineralization and the hosting shale, intruding mainly as a post-ore sediment-sill complex in wet sediments. Costa (1996) has dealt on the geochemistry of the hydrothermal alteration and Pereira and González Clavijo et al. (2007) have made a detailed geochronological study. Ore forming processes have been widely discussed by Solomon et al. (1980), Badham (1982), Eastoe et al. (1986), Hallsall and Sawkins (1989) and Adamides (2013) whereas fluid inclusion data have been presented by Nehlig et al. (1998). The structural geology of the area has been discussed by Quesada (1999), González Clavijo & Díez Montes (2010) and Arias et al. (2012) and recently there are two studies that have dealt with the 3D modelling of the deposit (Díez Montes et al., 2015; Martín Izard et al., 2015). Further information on Rio Tinto has also been published in Badham (2001) and in field trip guides (Sobol et al., 1997; Pascual et al., 2001; Sáez et al., 2001; Tornos 2001; Tornos et al., 2003; Mellado et al., 2006) and in general studies on the Iberian Pyrite Belt (Tornos, 2006).

This study synthesizes our regional studies carried out in the Rio Tinto area. The study includes a general mapping of the mining lease, together with that of key ore bodies such as San Dionisio, Salomón-Lago and Cerro Colorado, and a systematic geochemical study of the volcanic rocks. Rocks in Rio Tinto are sometimes so altered that the original features needed inferred by correlation with sequences outside of the district, notably in the Odiel and Zarandas areas (Fig. 1), are not always easy to observe. However, the data have allowed us to present an advanced geological, structural and metallogenic interpretation of the Rio Tinto district. Summarizing, our data show that some previous models were fairly simplistic (e.g., Boulter, 1993). The Rio Tinto area shows a complex structure, in a scheme similar to that of other many areas in the IPB (Tornos et al., 1998) with a first extensional and later compressive events developed a thin-skinned thrust belt with imbrication of structural units (González-Clavijo & Díez-Montes, 2010). Furthermore, the massive sulphides include both exhalative ores hosted by shale and replacive mineralization hosted by underlying felsic domes. Thus, Rio Tinto includes the two styles of mineralization quoted in the Iberian Pyrite Belt, being the hosting sequence equivalent to that of the northern IPB (see Chapter I).

2. Geological setting

2.1. Geological background of Iberian Pyrite Belt

The Rio Tinto district is located in the South Portuguese Zone (SPZ), the southernmost domain of the Iberian segment in the Variscan Massif (Fig. 1). It is an exotic terrain that collided during Variscan times (late Devonian to late Visean) with the Iberian Autochthonous Terrane, producing a south verging, thin-skinned fold and thrust belt that propagated southwards over a mid-crustal basal detachment (Silva et al., 1990). The Iberian Pyrite Belt (IPB) is the northernmost unit of the SPZ and consists a 250 km long and 25 to 75 km wide belt dominated by volcanic and sedimentary rocks of late Devonian-

Figure 2. Geological map of the Río Tinto area, modified after Mellado et al. (2006) and González-Clavijo & Díez-Montes (2010), showing the distribution of the main lithofacies, structures and orebodies.

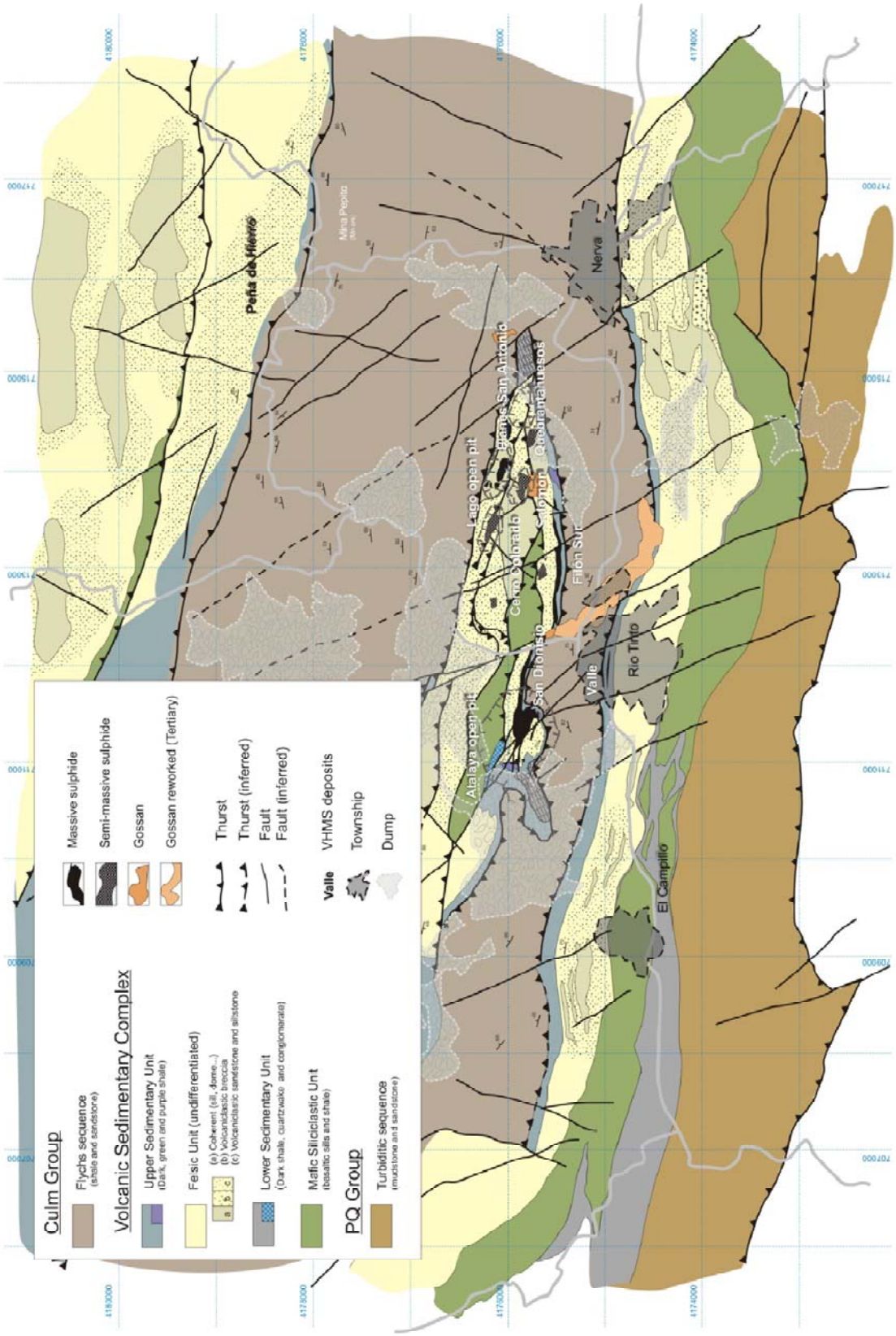
Culm Group
Flychs secuence
(basic and sandstone)
Volcanic Sedimentary Complex
Upper Sedimentary Unit
(Dark, green and purple shale)
Felsic Unit (undifferentiated)
(a) Coherent (all, dome, ...)
(b) Volcaniclastic breccia
(c) Volcaniclastic sandstone and siltstone
Lower Sedimentary Unit
(Dark shale, quartzwake and conglomerate)
Mafic Siliciastic Unit
(basaltic sills and shale)
PQ Group
Turbiditic sequence
(mudstone and sandstone)
Massive sulphide
Semi-massive sulphide
Gossan
Gossan reworked (Tertiary)
Thurst
Thurst (inferred)
Fault
Fault (inferred)
Valle
VHMS deposits
Township
Dump
Peña de Hierro
Nerva
Lago open pit
Cerro Colorado
Filon Sur
San Dionisio
Atalaya open pit
Valle
Rio Tinto
El Campillo

Pennsylvanian age hosting about 80 massive sulphide orebodies (Leistel et al., 1998; Tornos, 2006).

Historically, there have been defined three major lithostratigraphic units within the IPB (Schermerhorn, 1971). They include, from footwall to hanging wall, the Phyllite-Quartzite (PQ) Group, the Volcanic Sedimentary (VS) Complex and the Baixo Alentejo Flysch Group. The depositional environment evolved from a stable platform during the sedimentation of the PQ Group to the deposition in pull-apart basins during oblique collision (VS Complex) and a syn-orogenic foreland basin with flysch sedimentation (Baixo Alentejo Flysch Group) in a ridge that propagated southward as the Variscan orogeny progressed (Silva et al., 1990; Quesada, 1998).

The PQ group consists of a detrital sequence dominated by shale and quartzite of more than 2000 m thick (Tornos, 2006) and of late Devonian (Givetian-Famennian) age. It has been interpreted to record deposition in a storm-dominated shallow continental platform, evolving to progressively higher energy facies near the top, where sand bars, debris-flows, limestone lenses and near-shore sediments are common (Moreno et al.,1996). These late features are plausibly related with the basin instability related to the launching of the Variscan orogeny. The overlying VS Complex (0-1300 m thick) has been dated as of late Famennian to middle Visean age. It is a highly heterogeneous unit with abrupt lateral and vertical changes of facies. Both massive and fragmental volcanic rocks (basalt to rhyolite) are interbedded with shale, epiclastic sediments and chemical precipitates such as chert, manganese-rich exhalites and massive sulphides. The magmatism is essentially rhyodacitic, although the composition ranges the whole sequence from basalt to rhyolite (Mitjavila et al., 1997; Thieblemont et al., 1998; Valenzuela et al., 2011a, b). The formation of this volcaniclastic unit seems to be triggered by the development of pull apart continental basins, underplatting of mafic magmas and decompression-related melting of the crust. The Baixo Alentejo Flysch Group is a monotonous turbidite-like sequence of siliceous and carbonaceous shale, greywacke and

conglomerate of late Visean age, up to three kilometres thick. It records an extensive accumulation of synorogenic flysch deposited in a foreland basin (Oliveira, 1983; Moreno, 1993).

The regional metamorphism is always of low grade, prehnite-pumpellyite to greenschist facies, decreasing in intensity from north to south (Schermerhorn, 1975; Munhá, 1983, 1990) but being more intense near major thrust zones and/or in the northernmost part of the belt (Sánchez España et al., 1999). Tectonic structures in the IPB have been traditionally related to three major tectonic phases of folding and faulting episodes (Silva et al., 1990; Onézime et al., 2002; Soriano et al., 2002). During the first one (E-W trending), thrusts and associated south-verging folds formed synchronously with the regional metamorphism. The structures belonging to the second phase are the prevailing ones and consist also of south-verging thrusts and folds that are subparallel to earlier ones. Interfering with D_1 folds led to the development of E-W trending regional lineations. The dominant structure related to the third phase is a major thrust that was emplaced southward emplaced during of the synorogenic Culm Group.

2.2. **Geological characterization of Rio Tinto volcanic-bearing sequences**

The sequence hosting the massive sulphides at Rio Tinto is a thick volcano-sedimentary package broadly similar to the VS Complex located in other areas of the IPB (Schemerhorn, 1971; Routhier et al., 1980; Thieblemont et al., 1998; Soriano & Martí, 1999; Rosa et al., 2010; Valenzuela et al., 2011b). In brief, the structure consists of a major southward verging E-W trending antiform (Rio Tinto anticline) in which the core is formed by felsic and mafic volcanism showing hydrothermal alteration and stockwork type mineralization (Williams, 1934; Garcia Palomero, 1980). In its southern limb it includes a small subvertical tight synform (Corta Atalaya syncline). In detail, these structures fold several tectonically stacked units (see, Fig. 3). These results are consistent with the observations of Quesada (1999) that interpret the general structure of the area as related

to a large antiformal stack associated to a mostly blind out of sequence thrust (Quesada, 1999) with inversion of the previous synvolcanic structures and formation of large folds crosscut by later thrust. This thin-skinned deformation developed three main imbricated sheets forming an antiformal stack structure (González Clavijo & Díez Montes, 2010). The major Variscan structures are crosscut by late E-W and NW-SE normal and strike-slip faults.

In general, igneous rocks at Rio Tinto have been considered to be pyroclastic or extrusive lava (Rambaud, 1969; Lecolle, 1977; García Palomero, 1980, 1992). Nevertheless, Boulter (1993, 1996) has shown that abundant hydroclastic rocks occur in this area suggesting that the VS Complex in the Rio Tinto area is a shallow sill-sediment complex, in which the lower part is dominated by dolerite whereas the upper one would correspond to a quartz-feldspar porphyry; however, Tornos (2006) proposed that the Felic Unit is composed by superimposed felsic domes. Only recently, Valenzuela et al. (2011a, b) have studied in detail the volcanic sequence east of the mine, also proposing that there are two major felsic dome complexes which occur in the same stratigraphic position that in the Rio Tinto mine, and a dacite intrusive sill at the base of the Volcanic Sedimentary Complex – only cropping out in the Odiel river-.

2.2.1. *Lithostratigraphy*

The VS Complex is up to 1000 m thick but this fairly simple stratigraphy is complicated by the presence of several large thrusts and faults and a pervasive hydrothermal alteration that usually masks the original features. Thus, the composite section presented in this work has been supported with data from Atalaya open pit, the Zarandas and Odiel River areas.

The general lithologic sequence of the area includes the three major units that are found at a regional scale. The PQ Group does not crop out in the Rio Tinto area but can

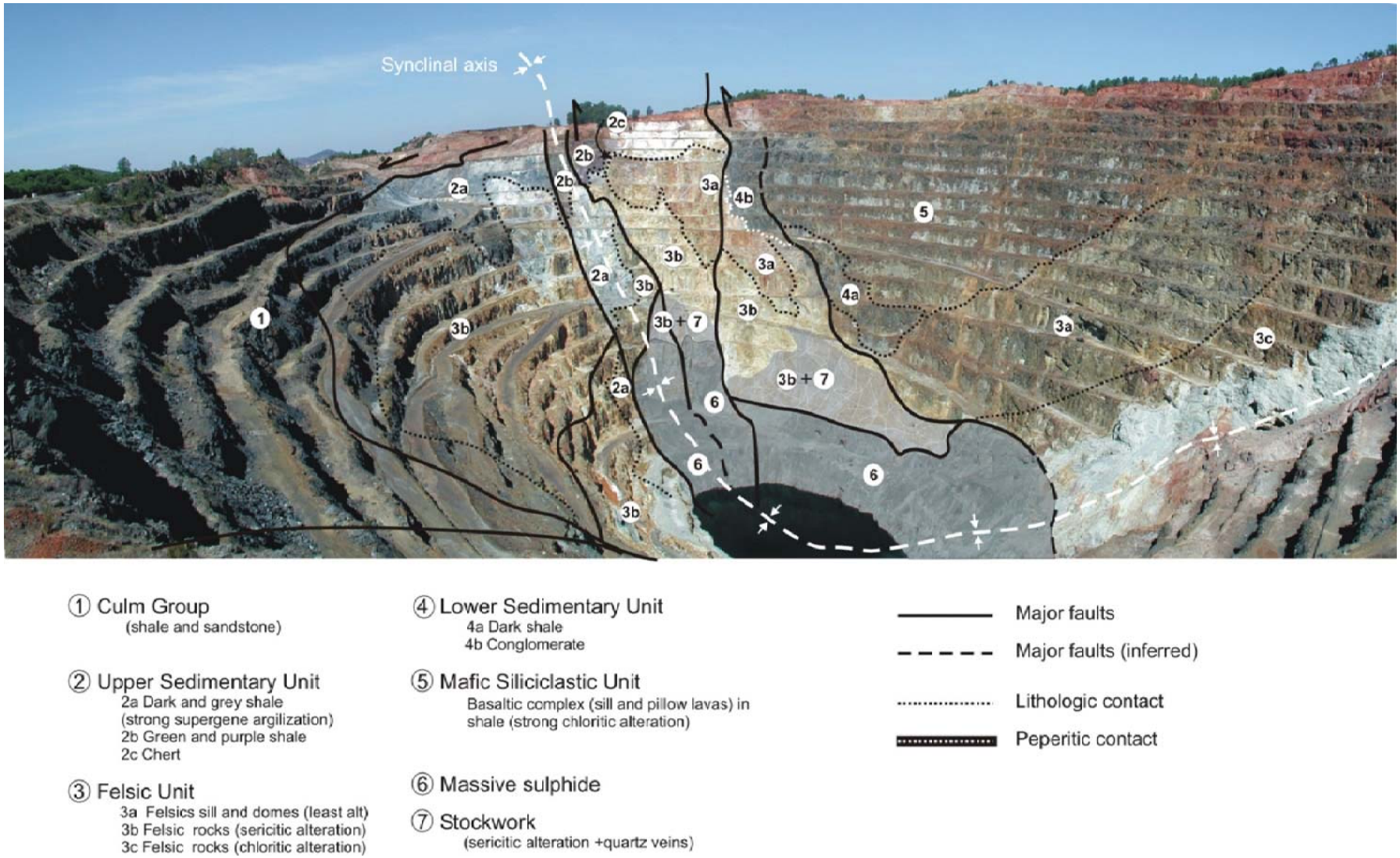

Figure 3. Panoramic view of the Corta Atalaya showing the tectonic structures and outcropping stratigraphic units.

be found in the adjacent areas north and south of the Rio Tinto structure (Fig. 2). In the Zarandas area the contact of the PQ Group and the VS Complex is defined by a few metres of shale hosting 10-20 cm thick sills of aphyric glassy rhyodacite overlain by mafic rocks that, in turn, are capped by the volumetrically dominant felsic rocks.

From bottom to top, four units have been differentiated in the lithostratigraphic sequence; field observations and mapping are supported by the petrography and geochemistry (Fig. 4) and the results summarized in the Table 2:

(1) The *Mafic-Siliciclastic Unit* comprises up to 450 m of interbedded shale, siltstone and basalt, with basalt dominating in the lower part of the Unit. This Unit outcrops in a continuous E-W band in the core of the Rio Tinto antiform, on the south of the Rio Tinto mine and the Zarandas area (Fig. 5). The shale, predominately located above mafic package (see Fig. 5a), is late Strunian in age (Rodríguez et al., 2002). It is therefore chronologically equivalent to shale that hosts the massive sulphides in the southern part of the Iberian Pyrite Belt (Pereira et al., 1996; Oliveira et al., 1997; González et al., 2002) but here is barren and lacks of hydrothermal alteration suggesting that no exhalative hydrothermal processes took place in the area.

Coherent basalt occurs mostly as flows characterized by the presence of sedimentary contacts with the interbedded sediments (shale and volcanic siltstone), and a conspicuous layering with irregularly alternating facies. Occasionally, the least altered basalt that outcrops on the southern area develops columnar jointing. Lower contacts include common peperites as well as breccias formed by shale fragments supported by basalt with resembling hyaloclastic breccias typically formed in the footwall of lava flows, as consequence of quenching and autobrecciation in the contact of the basalt and sediments. They occur also pillowed with the typically inter-pillow spaces, confirming a locally extrusive volcanic episode on the seafloor (Fig. 6a). The basalt is massive in the lower part of the flows, but near the hanging wall there are abundant banded, vesicular, or

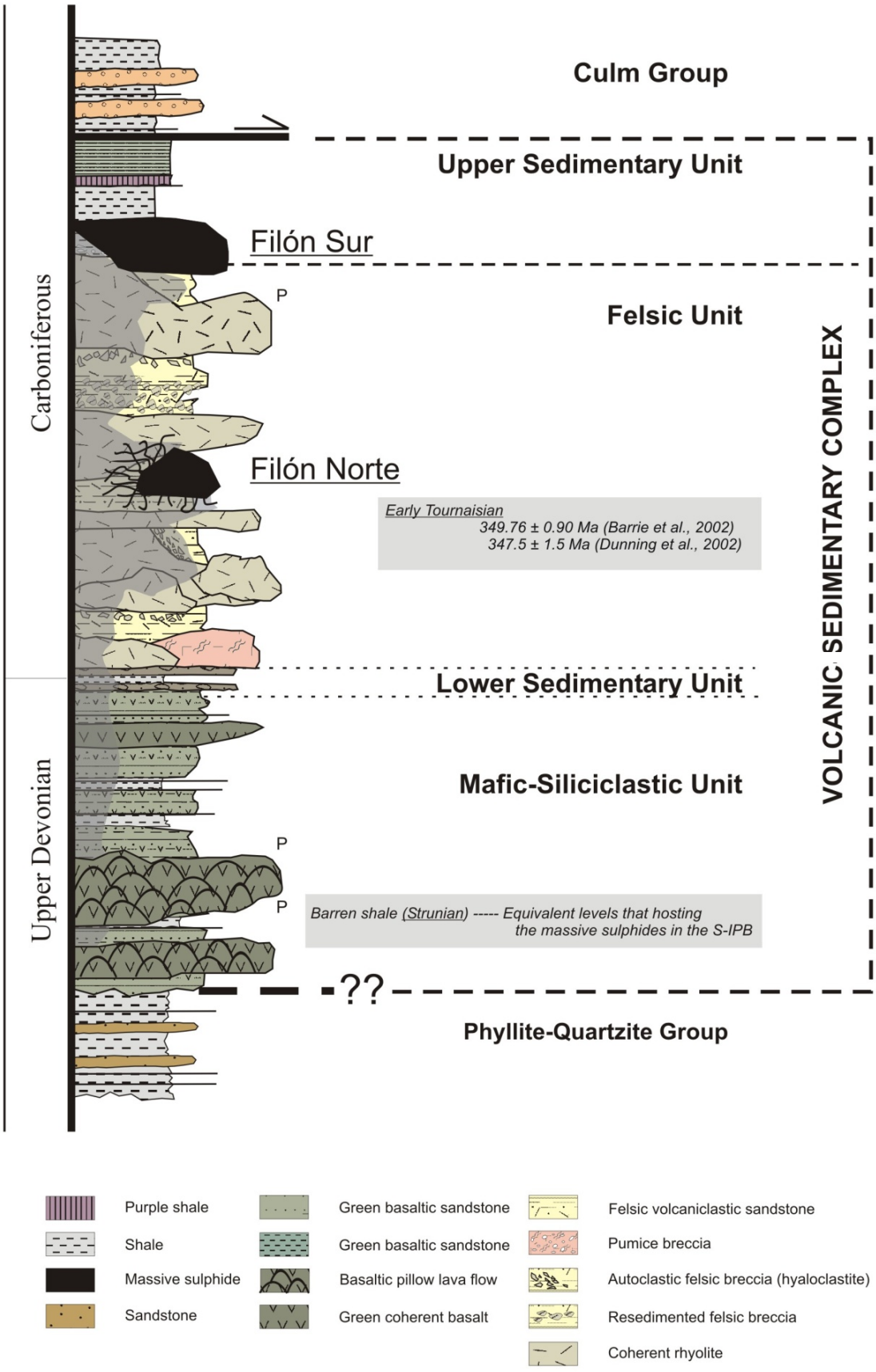

Figure 4. Simplified stratigraphic column of the volcano-sedimentary sequence in the Rio Tinto area.

plagioclase-phyric rich facies. The basalt consists of rarely preserved pyroxene phenocrysts (5-10%), enclosed in plagioclase (albite) laths and chlorite + quartz ± epidote groundmass. The basalt is usually fine grained and massive, ophitic to slightly porphyritic and rarely exhibit flow banding. It has abundant randomly located enclaves of the host rocks or even previous basalt. Vesicles are 0.2-1 cm in size, usually flattened and filled with carbonate-chlorite and zeolites, and occasionally zoned (Fig. 6b). Quartz and sulphides also occur infilling the vesicles (Halsall, 1989).

However, some of the basalt has intrusive contacts with the associated sediments or earlier basalt, and therefore correspond to shallowly emplaced sills and dykes. Some show peperitic contacts on both edges, suggesting that they correspond to shallow-intruded sills and dykes of coherent lava in unconsolidated water-rich sediments (Boulter, 1993a). Even so, a minor group of dykes of the Zarandas area show associated contact metamorphism, suggesting that they intruded at higher depths. These microgabbro dykes are probably equivalent to those that crosscut the overlying felsic rocks suggesting that some mafic magmatism is late in the VS Complex evolution.

Despite shale and minor siltstone are present in the Mafic-Siliciclastic Unit, they clearly dominate in the upper part of the sequence, where occur interbedded with mafic volcaniclastic epiclastites (breccias and sandstone), probably derived from the erosion of the underlying coherent basalt and related breccias (Fig. 6c). Although the mafic rocks have been recognized in Rio Tinto since the first mapping of Williams (1934), recent maps (Junta de Andalucia, 2004) do not include this unit. Mafic rocks were not identified in the core of Rio Tinto Synclinal, assuming that they were part of the upper Felsic Unit and interpreted as highly chloritized rocks.

In the Odiel River and bellow the Mafic-Siliciclastic Unit, Valenzuela el al. (2011a, b) describe a porphyritic dacite intrusive interpreted as a subvolcanic sill. It shows tectonic contacts with the over and under-lying rocks of the Mafic-Siliciclastic Unit and PQ Group,

Table 2 Summary of the main units of the Volcanic Sedimentary Complex in the Río Tinto district, Iberian Pyrite Belt.

Unit	Thickness	Facies		Alteration
Upper Sedimentary Unit	40-50 m	(1) Chert: thin white chert beds capped the massive sulphide orebody (2) Mudstone and volcanic sandstone: irregular thin interlayers of mudstone and qtz-rich volcaniclastic rocks (3) Green and purple shale (4) Dark shale: shale interbedded with thin layers of felsic volcaniclastic rocks. Shale layers host the mineralization.		chloritic ± chloritic +
Felsic Unit *Early Tournaisian* 349.76±0.90 Ma (Barrie et al., 2002) 347.5 ± 1.5 Ma (Dunning et al., 2002)	10-500 m	DOME COMPLEX	(5) Coherent aphyric rhyodacite: massive, aphyric, rarely <0.5mm fd + qtz microphenocrists, in a cryptopcrystalline silicious matrix (qtz+fd) (6) Coherent fd-qtz prophyritic rhyodacite: massive, evenly porphyritic, 10-15%, 1-2 mm euhedral to subhedral phenocrysts of fd (albite) + subrounded qtz phenocryst, few broken. In a microcrytalline matrix of qtz+fd±ser±chl±ep±cab. Some occurrence of flow banding and perlitic textures. (7) In situ autoclastite and/or hyaloclastite: massive, monomictic clast-supported, heterometric angular-curviplanar clast in a fine to medium-grained matrix. Often small pumice clast. Compositionally and textural to adjacent coherent facies. (8) Mass flow breccia: monomictic to polymictic, unsorted or poorly graded, irregular to subrounded felsic and porphyric pumice clast in a chlorite-rich fine-grained matrix. (9) Sandstone to siltstone rhyodacite: succession of crystal-rich sandstone with disseminated pyrite interbedded with siltstone, locally convolute lamination and synsedimentary tectonic structures.	sericitic ++ chloritic + sericitic ++ chloritic ± sericitic ++++ chloritic +
		(10) Shale: grey to dark barren shale.		sericitic ++++ chloritic + carbonate ±
Lower Sedimentary Unit	< 90 m	(12) Sediment-matrix conglomerate: polymictic conglomerate, unsorted, shale matrix supported, and/or locally clast supported, with pebbles of shale, qtz-rich sandstone, greywacke and volcanic rock locally derived and mainly mafic and rhyolityic. (13) Shale: grey to dark barren shale		chloritic + sericitic +
Mafic Siliciclastic Unit *Strunian (shale)* Rodriguez et al. (2002)	< 450m	FLOWS	(14) Coherent basalt: massive, ophitic to slightly porphyritic (5-10%, px+ab, chl+qtz+ep matrix), at margins frequent peperitic, rarely occurrence of flow banding. And frequently occurrence as pillowed or with vesicles. (15) Epiclastic basalt (breccia and sandstone): monomictic breccia moderately sorted and clast supported, and interbedded graded sandstone. Basaltic rounded and/or angular clast, derived to coherent basalt. (16) Basaltic sill and/or dyke: massive and/or intrusive autobreccia or peperitic hyaloclastite by emplaced into wet sediment. (17) Basaltic sandstone to siltstone: interbedded green and grey tuffaceous silt with sandstone, normal graded.	chloritic + chloritic ++++ sericitic + silicic + carbonate + chloritic ++++ sericitic +
		(18) Shale: grey to dark barren shale		

[1]Abbreviations: px=pyroxene, qtz=quartz, ab=albite, fd=feldspar, ser=sericite, chl=chlorite, ep=epidote, cab=carbonate. Intensity of alteration: intense ++++, strong +++, moderate ++, weak +, occasionally ±.

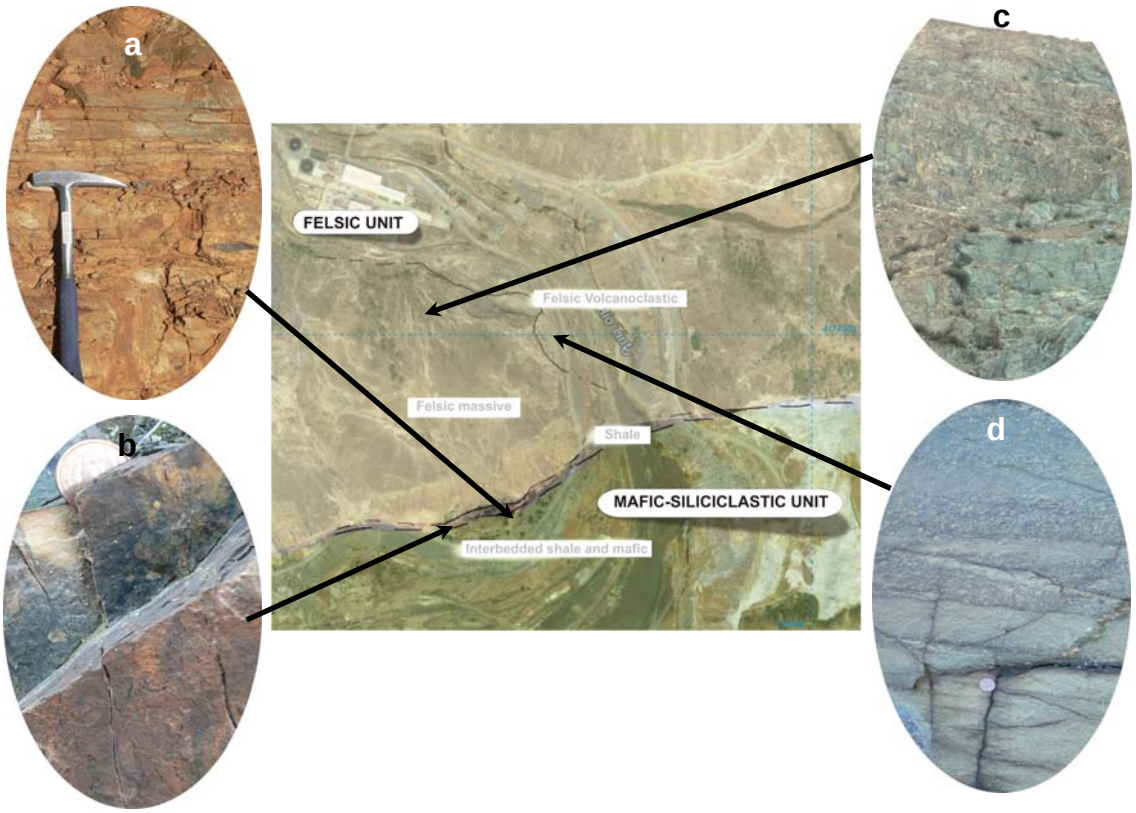

Figure 5. Aerial photograph of the Zarandas area (Fig. 1) showing a simplified geological mapping. The shaded green area represents the Mafic-Siliciclastic Unit and the yellow one the Felsic Unit. Photographs from outcrops of Zarandas area: (a) interbedded shale and fine-mafic volcaniclastic rocks; (b) level of shale that occasionally contains exotic clasts of 1-5 cm; (c) coherent felsic rocks (dome) of the Felsic Unit; (d) pumice-rich layers interbebbed with felsic volcaniclastic rocks of the Felsic Unit.

respectively. The dyke has been dated by zircon U-Pb as of 351.5±0.4 Ma and is older than the overlying Felsic Unit (349.5±0.4 Ma) (Valenzuela et al., 2011b). These rocks are not present in the rest of the Rio Tinto district.

(2) The *Lower Sedimentary Unit*, is conformable above the Mafic Siliciclastic Unit and consists of alternating sequence, up to 90 m thick, of dark shale, siltstone and quartzwacke with a characteristic conglomerate level in the upper part (García, Palomero, 1980). This Unit is only found in the Atalaya open cut and eastwards (Figs. 2 and 3), although in the Cerro Colorado area it does not crop out probably due to the tectonic lamination between the felsic and mafic-rich units. The conglomerate forms 5-25 m thick

Figure 6. Photographs of representative outcrops of the Mafic Siliciclastic Unit and Lower Sedimentary Unit. (a) Basaltic pillow lava showing multiple-rind structures exposed in a wall-section of Cerro Colorado open cut. (b) Detailed photography of massive vesicular basalt. Vesicles have a variable size (0.2-1cm) and here are infilled with carbonate. (c) Sequence of the shale interbedded with mafic volcaniclastic rocks (Cerro Colorado). (d) Shale-supported conglomerate with polymictic pebbles that only is present in the Corta Atalaya open cut.

lenses of shale-supported unsorted and subrounded pebbles of shale, greywacke, quartz-rich sandstone and felsic glassy volcanic rocks (dacite-rhyolite) as well as some mafic fragments. These volcanic clasts probably are derived from volcanic bodies marginal to the third order basin where these conglomerates formed (Fig. 6d). The quartzwacke has more or less equivalent composition. The conglomerate includes some pyrite-rich nodules and the quartzwacke hosts some lensoidal bodies of massive sulphides that we interpret as due to the sub-seafloor selective replacement of fragments and favourable layers; in fact, the sulphide-rich rocks are only found in places with major hydrothermal alteration, mainly chloritization. This conglomerate is coarser and more polymictic towards the west, with the presence of both mafic and felsic volcaniclastic rocks, dark shale and peculiar

quartzitic clasts. Boulter (1993b) quotes blocks as big as 1 m^3 near Campillo. The granulometry, shape and distribution of the pebbles imply formation of a clast supported conglomerate adjacent to a fault scarp, such as the growth margin of a half graben. Previous works have interpreted this unit as debris flows related to the intrusion of the sills (Boulter, 1993b).

(3) The *Felsic Unit* forms a thick sequence of 10 to 500 m thick and is made up of dacitic-rhyodacitic volcanic rocks; the unit includes only minor and thin shale levels.

The Felsic Unit is the predominant lithology in the Rio Tinto area. Primary features are mostly masked by superimposed hydrothermal alteration and deformation but in the Odiel River and Zarandas areas (Fig 5), primary structures are preserved and more evident. In the first area, major mass flows with pumice (Fig. 7a) and coherent rhyodacite are intruded by geochemically equivalent sills (Valenzuela et al., 2002; Valenzuela et al., 2011a). However, the sequence at the Zarandas area is dominated by major domes intruding vitriclast-rich breccia and felsic volcaniclastic sandstone with alternating crystal- and glass-rich layers, being probably distal to earlier and lateral domes (Fig. 5 and 7b). Such features are difficult to observe in Rio Tinto. Locally is possible to confirm that the sequence consists of a dome complex that includes small (crypto-) domes (Fig. 7c) and juvenile, usually monomictic, volcaniclastic breccias intruded by sills with extensive autobrecciation and marginal peperites (Fig. 7d). However, most of the textures interpreted as peperites by Boulter (1993) are here explained in a different way, as described below.

Coherent rhyodacite is highly monotonous and show a rather homogeneous porphyritic texture with a 10-15% of quartz and plagioclase (albite) phenocrysts (1-2 mm) within a quartz-feldspar (minor sericite and epidote) microcrystalline groundmass (Fig. 8a). Hydrothermal alteration has enhanced the presence of extensive autobrecciation as columnar joints and/or autofragments 3-10 cm in size with more altered joints. Only the

cores of the sills and domes are massive and show flow banding and perlitic textures; however, these structures are not seen in Rio Tinto and only found in the Odiel River area. Occasionally, in the Odiel River this felsic rocks contains vesicle-rich basaltic enclaves, mostly located near the hanging wall of the intrusive units (Fig. 8b). In detail, there are two different facies, one dominated by aphyric or poor-phyric rhyodacite and another with 2-4 cm-sized phenocrysts of quartz and plagioclase. The first seems to younger and is usually less altered.

The fragmental facies include breccias, some of them having features of being originally pumiceous (Odiel River; see Valenzuela et al., 2011a). Pumiceous-rich rocks

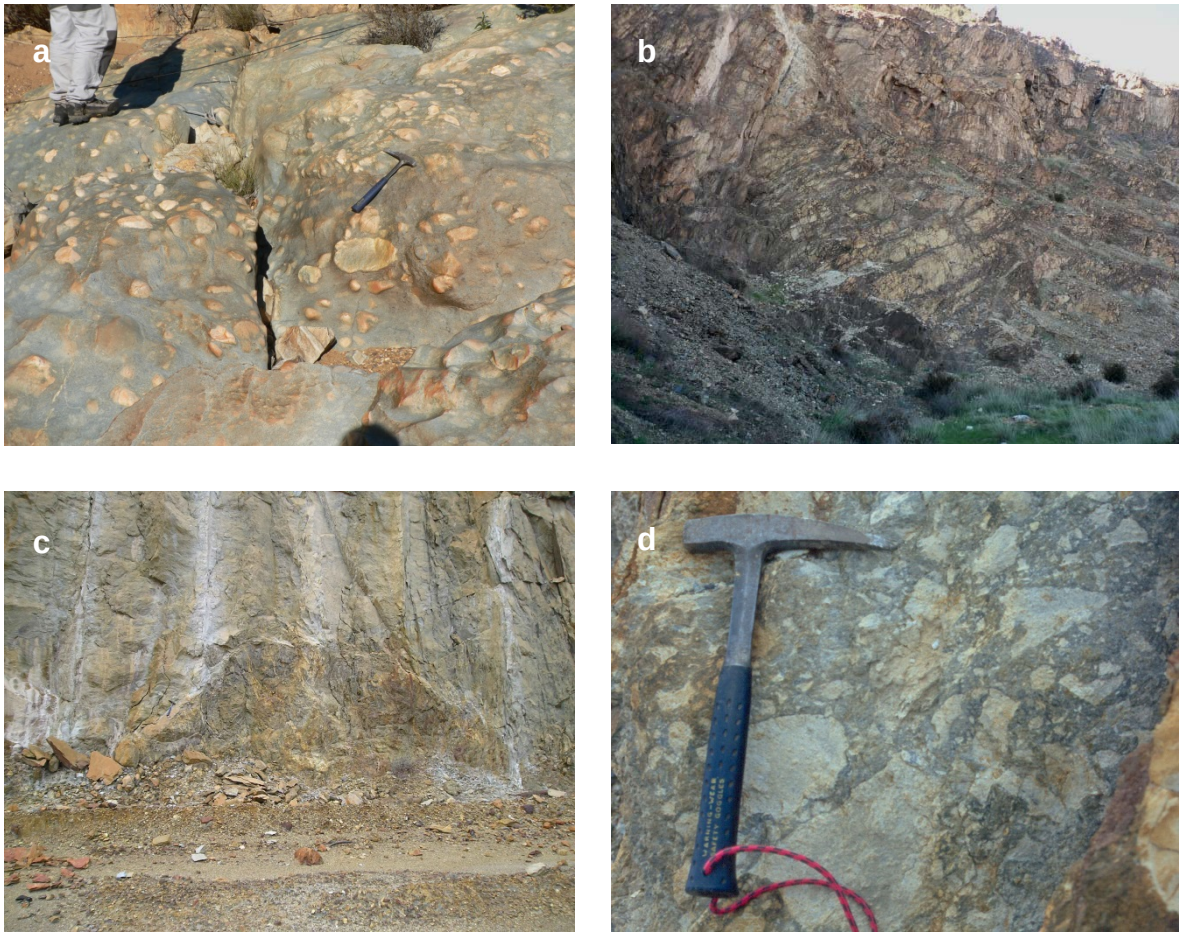

Figure 7. Photographs of representative outcrops of the Felsic Unit. (a) Felsic mass flow with rounded clasts of porphyritic coherent rhyodacite and pumice, showing poorly defined graded bedding (Río Odiel). (b) Felsic dome intruding volcaniclastic felsic rocks from lateral domes (Zarandas). (c) Small crypto-dome of rhyodacite intruding coetaneous felsic volcaniclastic rocks (Corta Atalaya). (d) Autobreccia or hyaloclastite of the upper part of a dome with jigsaw-fit blocks of coherent rhyodacite supported by a groundmass with the same composition.

occur as breccia and sandstone, and are composed by clast of *fiamme*, quartz and feldspar fragments in a fine groundmass and variable volume of rhyolite, dacite and quartz clasts. These facies are similar to described by Rosa (2007) and Rosa et al (2010) in Neves Corvo and Serra Branca. Most of the fragments are made of coherent rhyodacite, very similar to that found in the sills and internal facies of the domes. However, locally there are sparse fragments of rocks having a different proportion of phenocrysts that highlight the clastic nature of these rocks. No glass-rich rocks have been found but probably they have been pervasively replaced. The volcanic breccias commonly exhibit a wide range of clast/groundmass proportion which is interpreted to reveal their proximity to related coherent volcanic rocks. They appear from likely mass-flow deposits - common in the Odiel River area - made up of monomictic and/or polymictic -porphyritic felsite, dark mudstone, chert and quartz-clasts (>25%) in a fine grained chloritic volcanic matrix with clear evidences of subaqueous deposition and soft-sediment deformation (Fig. 8c) to autoclastic and/or hyaloclastic breccia that contains juvenile clasts (>60%), heterometric and monomictic within of a matrix that consists of a medium-fine grained, glassy and small sharp particles (Fig. 8d). Thus, the Felsic Unit forms a rather heterogeneous, variable and large felsic dome complex in which massive dacitic-rhyodacitic (crypto)-domes and cogenetic dykes and related hyaloclastite coexist with pumice-, crystal- and vitriclast-rich breccias. Absolute dating of these rocks have yielded early Tournaisian ages of 349.8 ± 0.9 Ma (Barrie et al., 2002), 347.5 ± 1.5 Ma (Dunning et al., 2002) and 349.5 ± 0.6 Ma (Valenzuela et al., 2011b).

These rocks include several lenses of massive sulphides, always hosted by highly altered rocks that correspond to the most glassy members of the Felsic Unit, perhaps the carapace or hyaloclastite that cap the different dome units (e.g., Filón Norte). These felsic rocks underlying the massive sulphides at Rio Tinto have the same position (but not age) than other located below many other massive sulphides of the IPB such as Aznalcóllar-Los Frailes, Las Cruces or Aguas Teñidas (Almodovar et al., 1998; Tornos, 2006; Conde

& Tornos, 2014) and Neves Corvo (Rosa et al., 2008, 2010). The massive sulphides are coarse grained and show always replacive contacts with the overlying and underlying felsic volcanic rocks, which sometimes host a well developed stockwork. The massive sulphides include large amounts of interstitial silicates, dominantly quartz, sericite and chlorite and lack of sedimentary structures. In detail, they seem to be formed on a previous stockwork and due to the gradual replacement of the altered volcanic rocks, leading to a massive sulphide that inherits the brecciated nature of the former stockwork.

The origin and interpretation of these rocks has been controversial. Traditionally, they have been interpreted as acid lava flows and related pyroclastic rocks (Rambaud, 1969; Lecolle, 1977; García Palomero, 1980, 1992; Halsall 1989). Occasionally, they have been described with ignimbritic features (Costa, 1996), but Boulter (1993a, 1993b) interpreted them as homogeneous sills intruding wet sediments. He distinguishes two generations of felsic rocks, the first one predating the massive sulphides and with an extensive hydrothermal alteration and a second one postdating the ore and with negligible alteration. Sediments are accessory in this Unit and occur as metre sized screens of gray and dark shale, siltstone and minor sandstone intruded or interbedded with the rhyodacite. In the lower part of the Unit, sediments are mostly monotonous shale. However near the hanging wall shale and siltstone exhibit parallel bedding and are interbedded with crystal rich volcaniclastic sandstones which host disseminated pyrite and are highly altered to sericite and supergene but subordinate kaolinite and montmorillonite (García Palomero, 1980). Locally there are some evidences of synsedimentary tectonics, including the presence of convolute lamination and intraformational breccias (Fig. 9a).

The intrusive emplacement of the felsic rocks into sedimentary sequences led to the local formation of well-developed peperite textures in the edge of dykes and coherent intrusions (Fig. 9b). The morphology of the peperites is highly variable, their features depending on the water content and size grain of the host sediment, the volume and temperature of the intrusive unit, and the external confining pressure of the water column

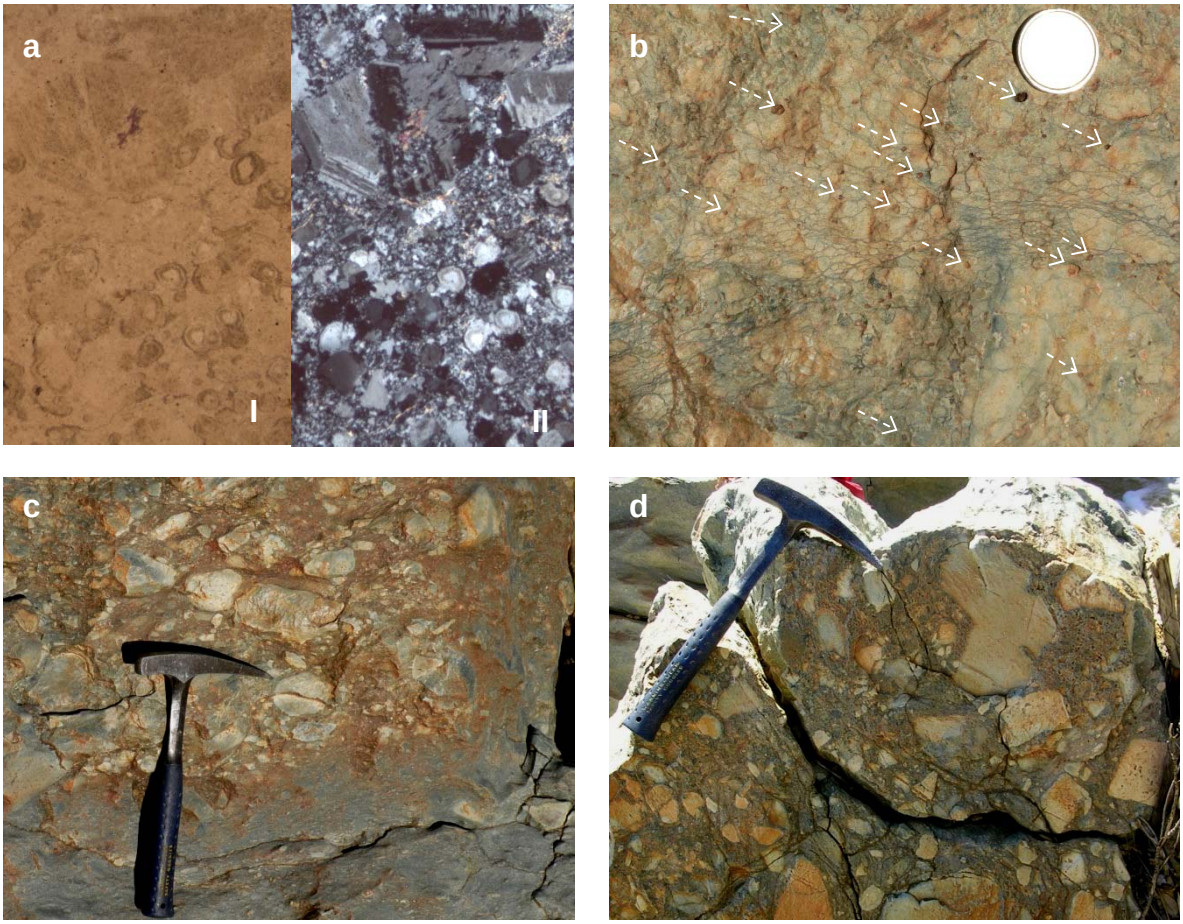

Figure 8. Photographs of the main facies of the Felsic Unit. (a) Photomicrographs of the coherent porphyritic rhyolite composed by quartz and plagioclase in a groundmass the comprises a microporphyritic matrix of quartz+feldspar±sericite±chlorite; under normal and polarized light, size of the field 1 mm. (b) Basaltic enclaves with vesicules filled by plagioclase. (c) Coarse-grained mass flow of felsic composition with fragments of porphyritic rhyodacite in a fine-grained groundmass showing clear structures sedimentary. (d) Autobreccia or hyaloclastic breccia with angular clasts into a medium-fine monomictic groundmass.

or/and overlaying sediment (Kokelaar, 1982; Busby-Spear & White, 1987). Peperites mostly include up to cm-sized fragments of rhyodacite into the shale, which can be found up to a metre away from the contact. There are also common individual phenocrysts of quartz floating in a shale groundmass (Fig 9c). Within the rhyodacite, injected shale occurs as veinlets, isolated or forming a stockwork, or filling vesicles (Fig 9d).

There is a late intrusive rhyolite that crosscuts the hydrothermally altered rhyodacite and the related stockwork. Crosscutting contacts are observed in the Filon Norte area. This rhyolite is fine grained and almost aphyric, with only sparse phenocrysts of albite-

plagioclase in a fine grained quartz-rich groundmass. It is similar to other rhyolite found elsewhere in the Iberian Pyrite Belt and regionally interpreted as related to the one lattermost felsic pulses.

The contact between the Lower Sedimentary Unit and the Felsic Unit is usually tectonic and marks one of the major tectonic discontinuities in the area due to the coexistence of rocks with very different contrasting rheology. When the contact is visible, the Felsic Unit is always intrusive within shale. For example, in the eastern Corta Atalaya, the rhyodacite shows a 6-8 m thick phenocryst-poor (quartz>plagioclase), glassy but partially devitrified edge, and locally, peperitic textures (Boulter 1993; Conde et al. 2007). The few observed non-tectonic contacts with the Mafic-Siliciclastic Unit are always intrusive.

(4) In the Corta Atalaya and Filón Sur area, the Felsic Unit occurs tectonically below a second sedimentary sequence, the *Upper Sedimentary Unit* (or Transition Series of García Palomero, 1980). It is formed by a 40-50 m thick sedimentary package of grey shale with some minor intercalations of felsic volcaniclastic sandstone, multicolour argillite and dark shale. The volcaniclastic rocks are matrix supported and show a poor sorting suggesting a local derivation. The massive sulphides of Filón Sur (San Dionisio and Filón Sur) are located in the lowermost shale (Fig. 4). They are capped by a 1-3 thick layer of white chert probably equivalent to the capping chert-rich sedimentary rock described in the Hokuroko district (Ohmoto, 1996) and has also been found in other deposits of the IPB.

The green and purple shale found in this unit has been interpreted as equivalent to the purple shale located in the uppermost VS Complex that forms the more extensive marker level in the southern part of the IPB (García Palomero, 1980; Routhier et al., 1980; Boulter et al., 1996). This versicolour facies contains a fine-grained phyllosilicate matrix and locally includes Mn-oxides, jasper layers and chert clasts. This horizon, also enriched in radiolarian, could be a condensed sequence formed during the deepening of the basin

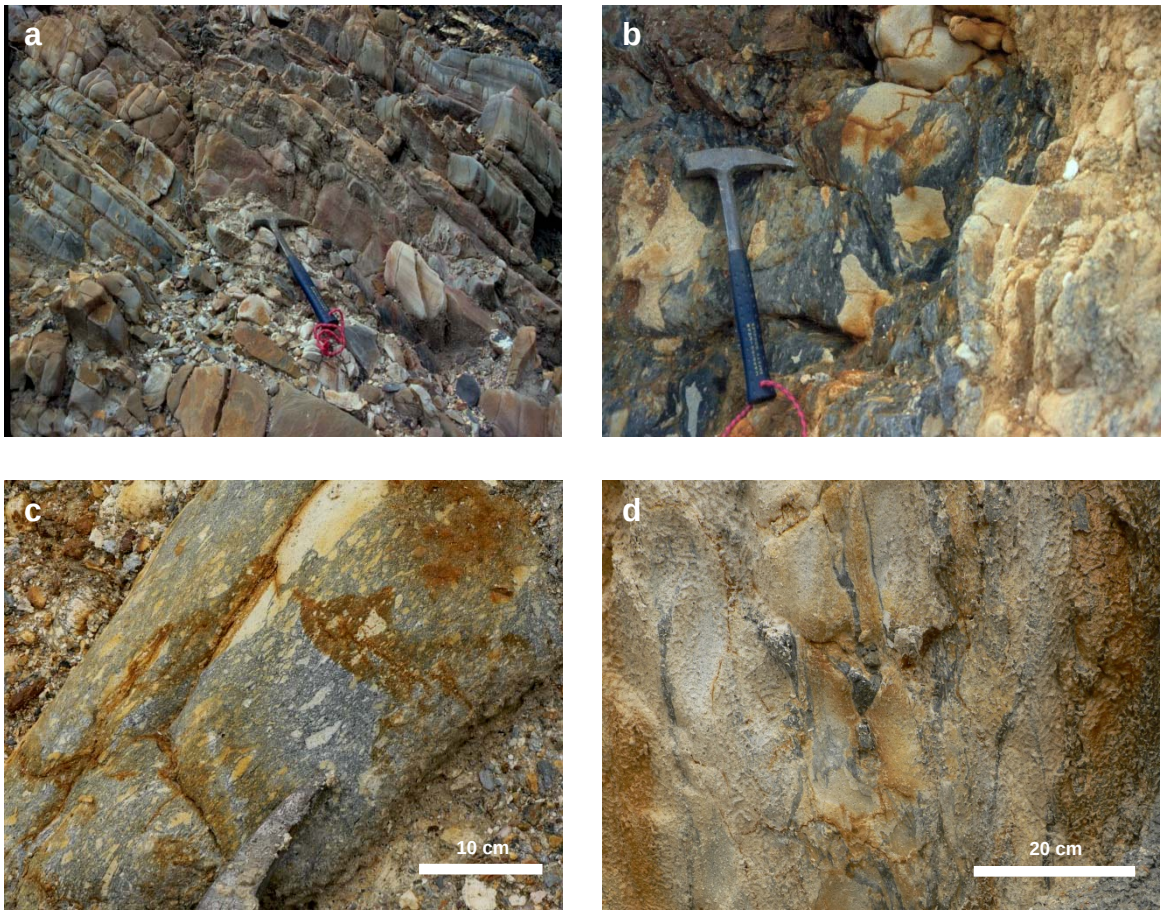

Figure 9. Selected photographs of the sedimentary rocks interbedded in the Felsic Unit. (a) Rhyodacitic volcaniclastic sandstone interbedded with shale with convolute lamination and layers of breccia. (b) Peperite formed during the interaction of a felsic melt with shale. (c) Detailed photograph of the peperite showing fragments of rhyodacite and and individual phenocrysts of quartz within the shale. (d) Peperite: shale forcefully injected into cracks or infilling vesicles within the rhyodacite.

(Quesada 1998; Oliveira and Quesada, 1998). Therefore, these rocks are of sedimentary origin and not tectonic as in the northernmost Iberian Pyrite Belt where is associated to the flow of oxidized fluids through major shear zones (Conde & Tornos, 2014).

The Upper Sedimentary Unit has been dated as early Tournaisian (Rodríguez et al., 2002), but has only a local extent and is characteristic of the Rio Tinto area, perhaps suggesting that it was deposited in a small third order basin.

The Upper Sedimentary Unit hosts a second group of massive sulphides that are hosted by shale but directly overlying the Felsic Unit and only some meters below the

purple shale. As quoted above, they were originally capped by a large some meters thick layer of pyrite-bearing white and grey chert.

The Baixo Alentejo Flysch Group, formed by dark shale and sandstone with turbidite facies, occur tectonically overlying the previous volcanic sedimentary sequence (Fig. 3) along an out of sequence thrust (González Clavijo et al., 2010). The minimum thickness in the Rio Tinto area is 500 m. Its origin is likely a synorogenic through located north of the area (Moreno, 1993).

2.2.2. *The hydrothermal alteration*

The main evidence of widespread fluid circulation in Rio Tinto is found in the core of the antiformal structure, which is affected by a pervasive and irregular hydrothermal alteration developed over an area of about 8 km^2 (García Palomero, 1980; Costa, 1996) (Fig. 10). The alteration has affected both the Mafic-Siliciclastic and Felsic units and can been traced down at least to about 600 m depth. Intimately associated with this alteration there is an extensive but irregularly distributed sulphide-rich stockwork. This hydrothermally altered zone has been traditionally interpreted as the feeder system that channelized the upflow of the ore forming hydrothermal fluids that mixed with seawater and formed the massive sulphides (Williams, 1962; García Palomero, 1980). These feeder systems are characteristic of volcanic-hosted massive sulphides (e.g., Franklin et al., 1981; Lydon, 1984; Large et al., 1992; Humphris et al., 1995). However at Rio Tinto, this zone does not show the typical conical shape of the stockwork zones with a chloritic core and an outer sericitic halo (Franklin et al., 1981); here the alteration is highly irregular and is mainly controlled by syn-hydrothermal structures, lithologic contacts and the composition of the protolith (Solomon et al., 1980; Gumiel et al., 2001; Tornos 2006). Solomon et al. (1980) and Badham (1982) defined two WNW-ESE trending fractures located north and south of the Cerro Colorado area that controlled the chloritic alteration and the venting of hydrothermal fluids.

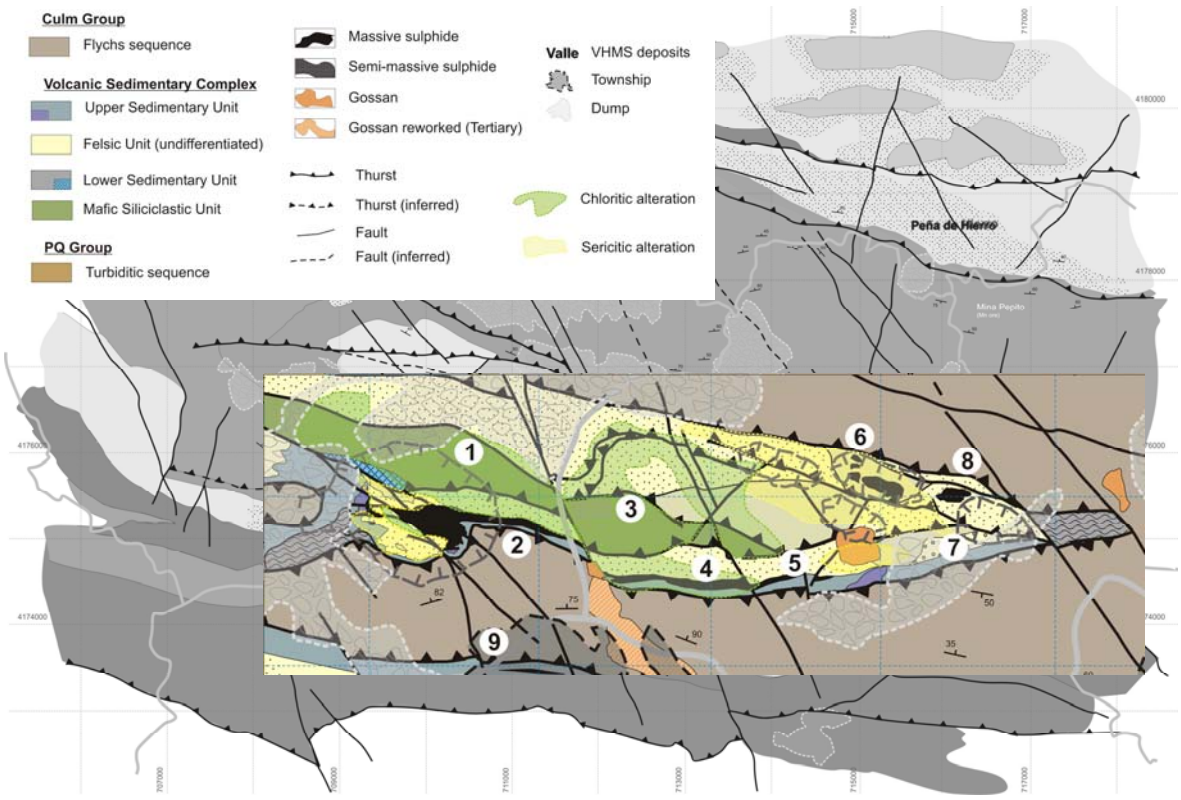

Figure 10. Geological map of the Río Tinto area showing the different types of hydrothermal alteration. The area is dominated by a sericitic alteration restricted to the felsic rocks and a chloritic alteration that affect affects both the mafic and felsic rocks. (1) Corta Atalaya, (2) San Dionisio, (3) Cerro Colorado, (4) Filón Sur, (5) Salomón, (6) Lago, (7) Quebrantahuesos, (8) Planes-San Antonio, (9) Valle.

Three major alteration zones are found in Rio Tinto, sericitization, chloritization, and silicification (Fig. 10). The last one is rather accessory and only related to the main upflow channels and adjacent to highly mineralized zones (Fig. 11a) despite in some areas such as the stockwork zones in Quebrantahuesos or Corta Atalaya it predates sericitization, chloritization and sulphide replacement (Fig. 11b). Evidences of silicification have been also observed in the felsic rocks north of Rio Tinto (Halsall, 1989). These pervasive and sometimes destructive types of hydrothermal alteration are superimposed to more regional, texturally conservative and subtle ones. The felsic rocks have an irregular albitization while the mafic rocks show widespread spilitization with replacement of the primary mineralogy by albite, clinoamphibole, quartz, chlorite, epidote and minor apatite, zircon and ilmenite (Barriga, 1983).

As quoted above, there seems to be a major lithological control on the style of alteration. The chloritization is dominant in the mafic rocks and shale, where no hypogene sericitic alteration has been found; in general, the shale is more pervasively replaced by the chloritite than the volcanic rocks. The felsic rocks show widespread sericitic alteration and chloritization only dominates near the feeder structures or when adjacent to the massive sulphides, as occurs below the San Dionisio orebody. Here, the chloritic alteration clearly postdated the sericitic one (Fig. 11c).

The Lower Sedimentary Unit, formed mainly by shale, and despite being located between the two volcanic units with pervasive alteration, shows only minor replacement because of its impermeable character; only the conglomerate and the quartz-wacke levels show widespread replacement of the groundmass and some specific clasts. Pervasive chloritic alteration of the shale is restricted to the lowermost 20-40 cm and to minor irregular stratabound zones suggesting that these rocks were originally impermeable or non-reactive with the hydrothermal fluids.

The sericitic alteration is the main one and responsible of the large zones with yellowish colour that dominate in the area (Fig 3). Sericitized rocks are systematically cleavaged, while rocks affected by chloritic alteration are green and more massive. Sericitization consists of a replacement of the original rock by quartz, Ba-rich illite (Costa, 1996) and, sometimes, ankerite as fine veins. Chloritic alteration is dominated by ripidolite-picnochlorite, quartz, and some illite. Both rocks have significant amounts of disseminated pyrite as well as hydrothermal zircon, apatite and other opaque minerals as ilmenite and/or magnetite. The silica-rich alteration is restricted to the faults or lithologic contacts where there is a major fluid flow. Here, the rocks are replaced by quartz with accessory chlorite or sericite with a large amount of pyrite.

Pervasively chloritized shale, rhyodacite and basalt are difficult to distinguish during field work, especially if the mafic rocks are rich is vesicles and the igneous rocks are fine

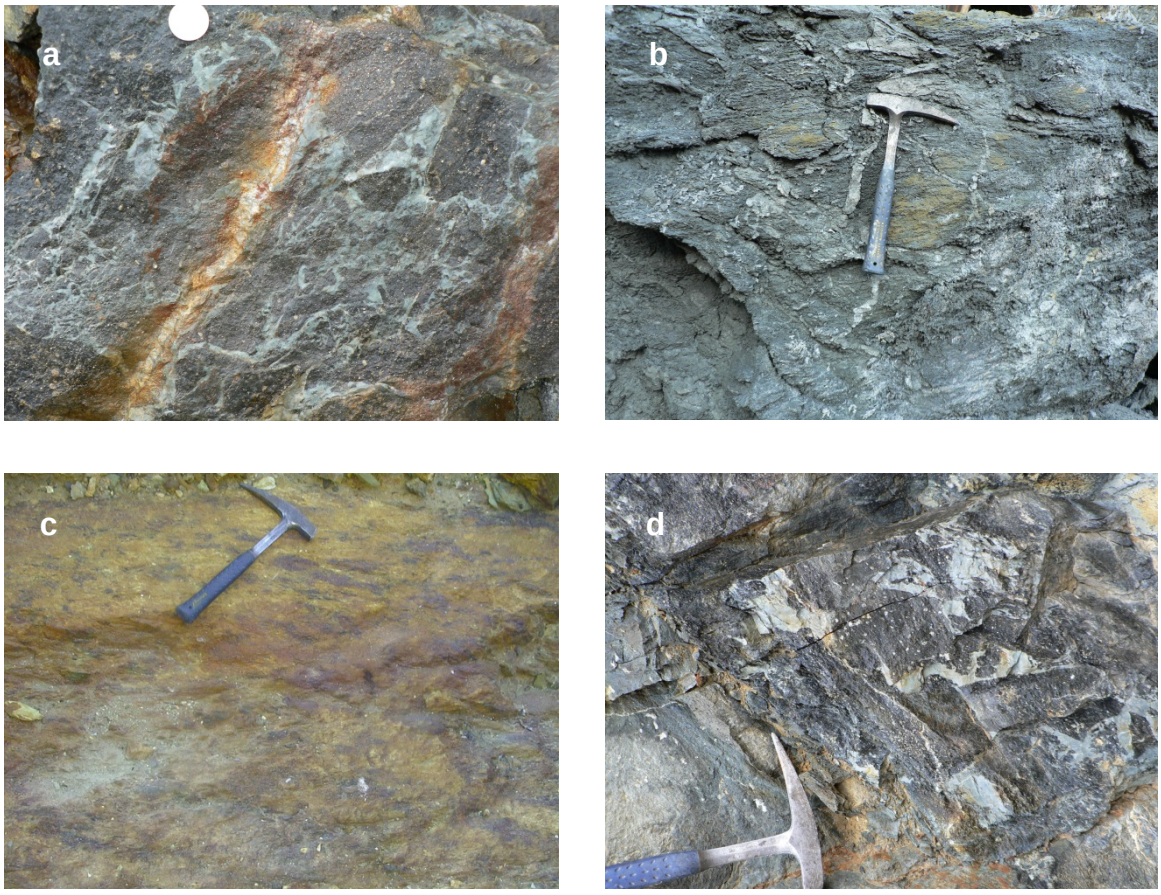

Figure 11. Representative photographs of outcrops showing hydrothermal alteration in the Río Tinto district. (a) Shale with pervasive chloritic alteration and laminated sulphides cut and replaced by the stockwork. (b) Outcrop of felsic rocks showing a pervasive sericitic alteration with superimposed chloritization (Corta Atalaya). (c) Silicification of the shale and the mafic volcaniclastic rocks. (d) Shale with pervasive silicification cut by a stockwork vein infilled by pyrite

grained. The shale and the mafic siltstone are usually fine grained and its replacement produced masses of fine grained chlorite with intergrown quartz (Fig. 11d). This is probably why in the recent times some studies have neglected the presence of mafic rocks in the Rio Tinto mine (Junta de Andalucia, 2004; González Clavijo et al., 2010).

Williams et al. (1975) in Planes-San Antonio and García Palomero (1980) in San Dionisio have described ample zones of altered volcanic rock with disseminated sulphides that grade into zones with stockwork-like veins and a core with a discordant pipe of massive sulphides that grade upwards into the overlying stratiform exhalative ore. In Planes, the pipe has a diameter of about 0.7 km and its core is made of brecciated pyrite

with some chalcopyrite with increasing sphalerite and galena towards the top and the edges. Downwards, it seems to grade into quartz-chlorite-magnetite-rich rocks (Williams et al., 1975). The estimated original reserves in the stockwork are ca. 1900-2000 Mt of low grade mineralization with 0.15%Cu with 0.07 g/t Au and 7 g/t Ag (García Palomero, 1990).

The stockwork hosts different types of ore. In the large Cerro Colorado open pit, shale, basalt and rhyodacite show large zones of chloritic alteration with Cu-rich zones. In the Quebrantahuesos area, the sericitized rhyodacite has disseminated sphalerite and chalcopyrite in a stockwork later replaced by massive sulphides. The San Dionisio orebody, north of the Filon Sur massive sulphides in the Atalaya open cut, consists of a dense stockwork hosted by chloritized rhyodacite, basalt and shale and includes pyrite along with chalcopyrite, sphalerite, galena, and magnetite with significant amounts of quartz and chlorite; ankerite is specially abundant near the contact with the massive sulphides while the magnetite content of this stockwork increases downwards (García Palomero, 1980; Solomon et al., 1982). Grades within this stockwork are locally high, the San Dionisio orebody averaging 1.7% Cu (Solomon et al., 1980). In general, the stockwork seems to be enriched in Sn (Badham, 1982) and Cu and Bi (Marcoux et al., 1998) if compared with the overlying massive sulphides. This late enrichment seems to be rather common in the IPB (Marcoux et al., 1998) and is probably related with the upflow of reduced sulphur-depleted fluids (Tornos and Heinrich, 2009).

The host rock also controls the style of the stockwork mineralization. Stockwork mineralization in the chloritized shale is characterized by the presence of thin sulphide veins (<2 cm) while the chloritite replacing basalt has most of the sulphides as disseminations. The sericitic alteration has lesser amounts of disseminated sulphides and the stockwork veins, where present, are more continuous and thicker, between 1 and 5 cm (Fig. 12a) and sometimes as thick as 1 meter (Fig. 12b). In the massive rocks, the veins tend to follow the columnar joining or highlight the limits of the fragments in autobreccias. In general, copper grades are higher in the chloritite – especially when

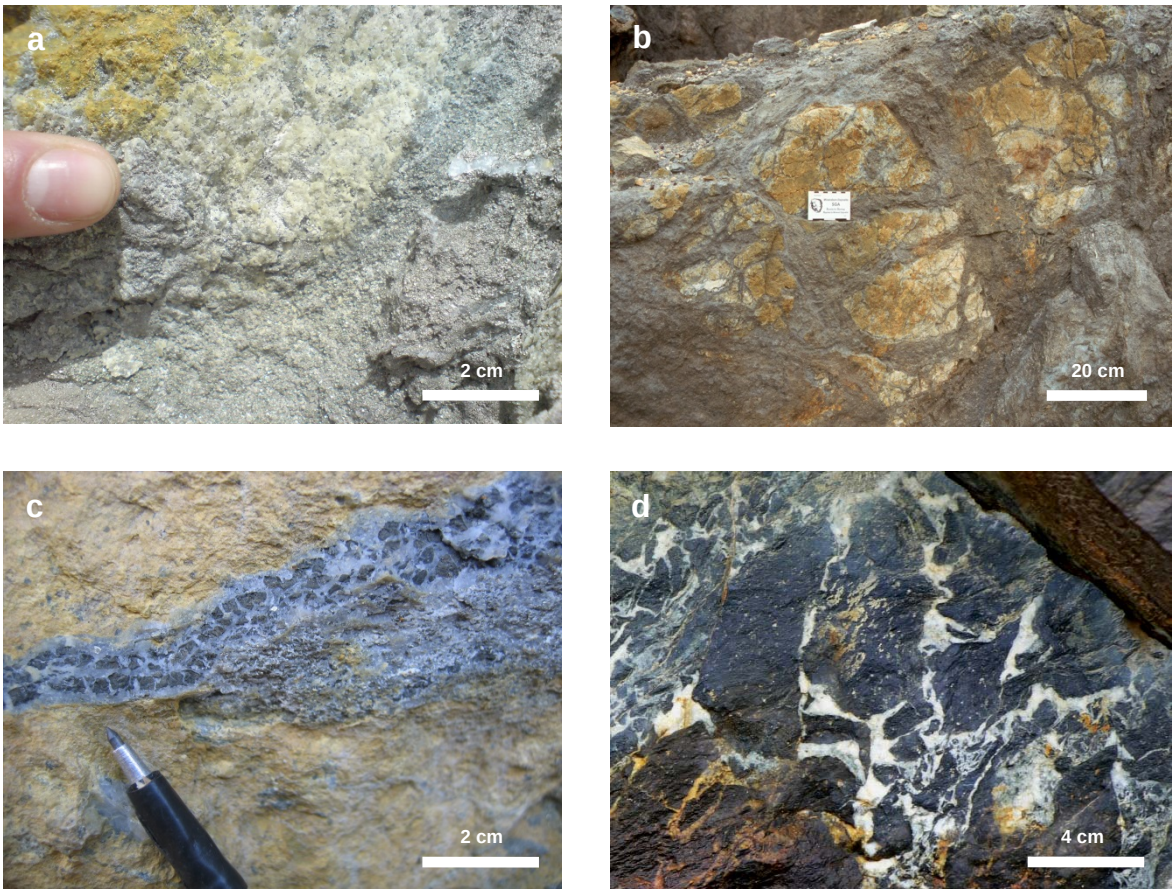

Figure 12. Selected photographs of the stockwork. (a) Detailed photograph of the stockwork in a pervasively sericitized felsic rock (Quebrantahuesos) (b) Stockwork developed on felsic rocks, showing 1-5 cm thick veins of pyrite (Quebrantahuesos). (c) Detailed photograph of the stockwork veins with hive texture filled by pyrite, quartz, and minor ankerite. (d) Outcrop of a pervasively silicified shale with hydrafracturing breccia (Cerro Colorado).

replacing shale - while the Pb and Ag are enriched in the sericitic alteration. Zn shows a rather erratic behaviour.

The thickest veins are made up of quartz, pyrite and more accessory ankerite, chlorite and sericite and show textural evidences of being formed by pure extension and crack and seal processes. When both pyrite and quartz are present in the same vein, banded structures are common, with quartz in the edge and pyrite in the centre, a feature indicating the early precipitation of quartz (Nehlig et al., 1992). However, the smaller veins are formed by replacement. In both cases, the veins have a selvage of alteration and sometimes leading to breccia-like textures (Fig. 12c). Excluding the syntectonic veins (see below), the veins do not show offsets nor crosscutting relationships suggesting that they

likely belong to a long lived extensional event of hydrofracturing (Fig. 12d) in a system with high fluid pressures (Solomon et al., 1980; Nehlig et al., 1992). Hydrothermal breccias are fairly abundant in the mafic rocks and consist of fragments of chloritized basalt pulled apart by a network of veins related with pervasive silicic alteration.

It seems that the frequency and size of the veins diminishes downwards and away from the major faults and there is a rather homogeneous distribution with most of the dips to the north, suggesting that the veins originally had subvertical dips (Nehlig et al., 1992). The originally high dips are only in the deepest part of the system. Solomon et al. (1980) and Nehlig et al. (1982) have also shown that about 100 m below the paleosurface the veins tend to be sub-parallel to the massive sulphide-footwall contact, something that interpret as reflecting fluid flow subparallel to the seafloor. However, perhaps this feature is more likely due to the existing superimposed penetrative deformation that is usually channelized along the highly altered rocks that follow this contact. However, based on fractal methods, Gumiel et al. (2010) have proposed that the morphology of the stockwork is independent of the composition and the hydrothermal alteration of the host rock. They distinguish two systems of connected fractures - something typical of mineralized and fragmented systems - which enhanced fluid flow and caused the mineralized stockwork.

Despite most of the stockwork has evidences of being formed synchronously with the massive sulphides, there are abundant evidences of a second generation of veins formed during the Variscan deformation, as was noted by Williams et al. (1975). These veins are usually larger than the predeformation ones and enriched in quartz, coarse grained pyrite, chalcopyrite and sometimes barite; locally, this stockwork has economic copper grades. This late quartz is not deformed and occurs as large crystals rich in two-phase fluid inclusions (Nehlig, 1998). These veins do not show related hydrothermal alteration and cut the regional cleavage. In fact, mapping and structural analysis have shown that there are two types of stockwork (Gumiel, 1988). The early veins are oriented, have a homogenous lognormal distribution and are impoverished in Au (<0.5 g/t) while the syn-

Variscan veins are enriched in copper and gold and do not have a preferential orientation but a fractal distribution (Gumiel et al., 2001).

2.2.3. Geochemistry of the igneous rocks

The entire suite of 43 samples from outcrops within the major open pits, were analyzed out in the General Laboratory of the Instituto Geológico y Minero de España (IGME), using X-ray flourescence (XRF) for major elements, and ICP-MS for REE and trace elements (Appendix I.I). The study also includes 115 analyses from the previous study of Costa (1996), and Hallsal (1980), and 15 previous analyses from internal reports of the IGME. Of these samples, 58 are from Mafic-Siliciclastic Unit, and 99 from the Felsic Unit.

More than a half of the analyzed mafic and felsic rocks show a major hydrothermal alteration, having alteration indexes higher than 50 (see below). They are characterized by an almost complete replacement of the original mineralogy by variable proportions of sericite, chlorite and sulphides. For this reason, interpretation the geochemistry of the mobile components (SiO_2, MgO, MnO, Na_2O, and K_2O) has been only performed in the least altered samples. However, the ratios between immobile elements, mainly high field strength elements (HFSE), such as Zr, Ti, Nb and Y, have been used in all the samples, as essential parameters for the lithogeochemical discrimination and the determination of the magmatic affinity and the fractionation trend.

In the fresh and least altered rocks, the magmatic affinity has been determinate using major elements. The samples were plotted in the AFM diagram (Irvine & Baragar, 1971) (see Fig 13a). Porphyritic coherent felsic rocks and related volcaniclastic rocks plot in the field of the calc-alkaline series, whereas mafic rocks fall on the transitional to tholeiitic field. Singularly, a few of the felsic rocks (Halsall sampling) that correspond to sulphide-rich and altered samples plot towards the Fe_2O_3+FeO field.

In the highly altered samples, the incompatible trace element ratios such as Zr/Y, La/Yb and Th/Yb should inherit the original geochemical characteristics (MacLean et al., 1993). The felsic samples have values of Th/Yb >0.65, confirming that they are calc-alkaline, while the mafic rocks are also classified as transitional to tholeiitic (Th/Yb rates between 0.1 and 0.65) (Munhá, 1983; Mitjavila et al., 1997; Thieblemont et al., 1998).

The different rocks from Rio Tinto can be clearly discriminated in the TAS (total alkali-silica) diagram (Fig. 13b). The rocks from the Felsic Unit have compositions of dacite to rhyolite; here, the massive rocks forming the sills and domes have an ample SiO_2 content ($60 < SiO_2 < 84$ wt%) that includes the dacite-rhyolite field while the volcaniclastic rocks show more restricted silica compositions ($61 < SiO_2 < 77$ wt%) within the dacitic field. When these volcanic samples are plotted in the immobile-element diagrams, such as SiO_2 vs. Zr/TiO_2 (Fig. 13c), both coherent and volcaniclastic rocks are identified as dacite-rhyodacite, more according to the petrography.

The high SiO_2 contents (>80%) are from the late massive rhyolite intrusions of the northern part of the Rio Tinto district. Thieblemont et al. (1998) linked the high SiO_2 and low MgO and TiO_2 contents of these rocks with a high degree of magmatic fractionation.

The projection of the samples in the binary diagrams that involve the ratios of immobile elements (Zr/Al_2O_3 vs. Al_2O_3/TiO_2; Fig. 13d) indicates that the rocks belonging to the Felsic Unit are probably derived from different magmatic units that separated from a single magma chamber. The pumice and glass-rich sandstone and the breccia plot above the massive rocks but define an alteration line that suggests a common origin but a higher degree of alteration. This also shows that the volcaniclastic rocks are lateral aprons product of the dismantling of evolving domes and not exotic mass flows derived from the erosion of distal, or even subaerial, domes with no geochemical link to the adjacent domes. A similar situation has been described in the northern Iberian Pyrite Belt (Conde & Tornos, 2014). An interesting feature of these rocks is the wide variation in the Al_2O_3, TiO_2

Figure 13. Geochemical diagrams of igneous rocks of the Río Tinto district. (a) AFM diagram for the magmatic affinity discrimination, based on the relationships between FeOt + MgO (M), K_2O + Na_2O (A) and SiO_2 (F) (Irvine & Baragar, 1971). (b) Compositional discrimination plot for the fresh and least-altered volcanic rocks from Río Tinto area, based on major elements (Na_2O+K_2O vs. SiO_2; Le Bas et al.,1986). (c) Zr/TiO_2 vs. Nb/Y (Winchester & Floyd, 1977) diagram, based on immobile elements. (d) Immobile element ratios diagram of Zr/Al_2O_3 vs. Al_2O_3/TiO_2, showing the main units in tight fields. (e) TiO_2 vs. Zr plot showing the existence of a possible fractionation trend and a well defined alteration line. Note the discrimination of the two clusters of felsic rocks marked by dashed ovals. (f) Plot Cr vs Zr highlighting the existence of two groups of mafic rocks.

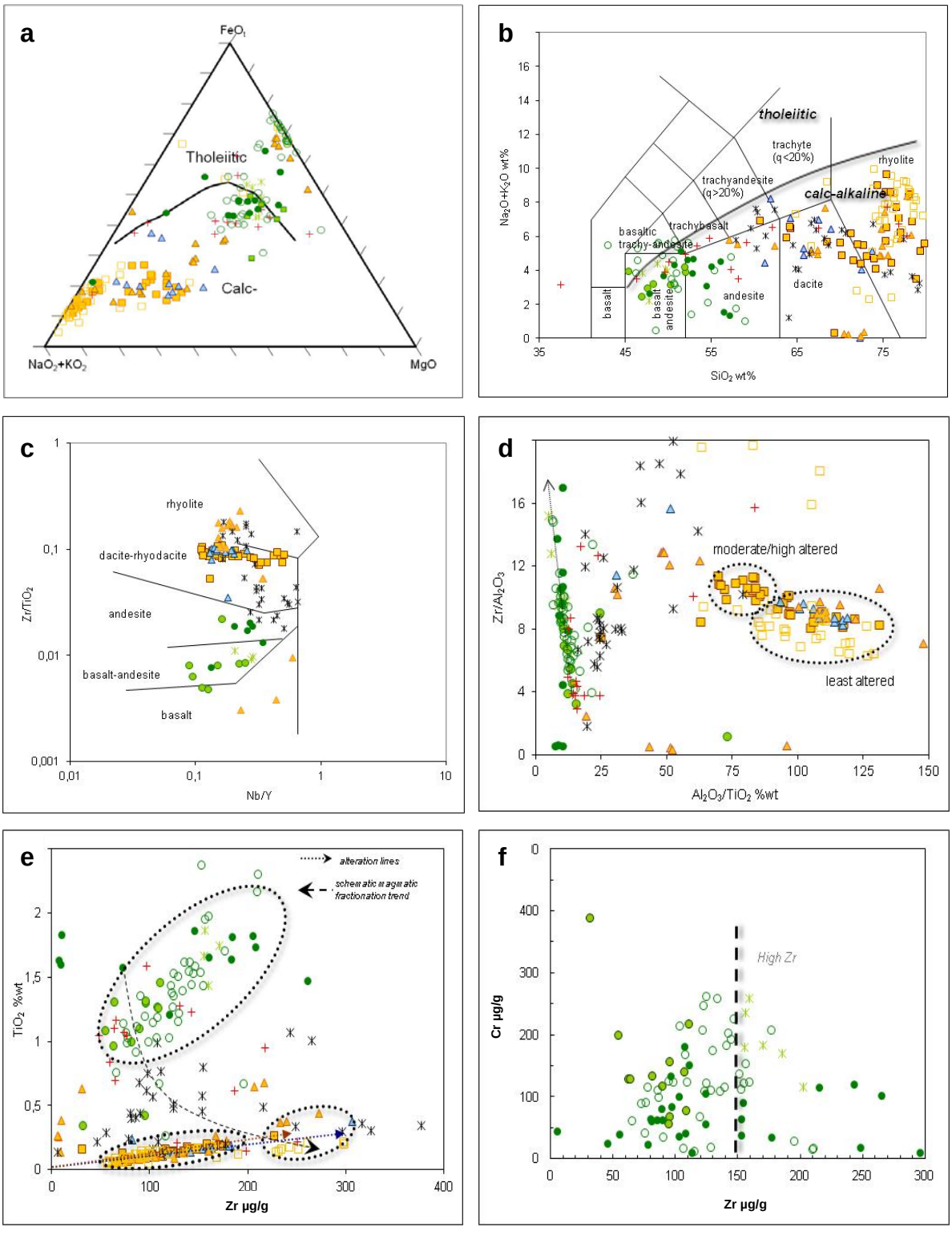

IGME and Costa samples
- Felsic Unit (masive)
- Felsic Unit (volcaniclastic)
- Mafic Unit
- Mafic Unit (high Zr-Ti)

Boulter samples
- BO Felsic rocks
- BO Mafic rocks
- BO Sedimentary rocks

Halsall (1990)
- Felsic Unit
- Mafic Unit
- Intrusive rocks

and Zr contents. In detail, the TiO_2 vs. Zr diagram shows high variable Zr contents; in fact, this diagram permits the discrimination of a group of felsic rocks with Zr contents values between 50 to 200 µg/g that is found in the Odiel river and Campillo areas and in Corta Atalaya, and a second group of high Zr felsic rocks, with values between 225 and 300 µg/g that dominate in the northern part of the Rio Tinto area (see Fig. 13e). Preliminary mapping and crosscutting relationships suggest that the low Zr rhyodacite is younger than the high Zr felsic rocks.

The coherent rocks belonging to the Mafic-Siliciclastic Unit have a composition close to that of basaltic andesite, as has been shown in previous studies (Boulter et al., 2004). However, the contents in immobile elements suggest that there are two different types of mafic rocks, a basaltic andesite and a high Ti-Zr basalt (Fig. 13e) that have not been distinguished petrographically due to the high degree of hydrothermal alteration that has masked the primary features. The Zr/Al_2O_3 vs. Al_2O_3/TiO_2 binary plot shows that both groups spread along a unique fractionation trend (Fig. 13d). These two groups are also clearly discriminated on a Cr versus Zr diagram (Fig. 13f). Significaly, the high Zr mafic rocks (> 150 µg/g) mainly correspond to intrusive dolerite and/or basalt lava from the sourthern limsb of the Rio Tinto anticline (El Campillo and south of Nerva areas). These results can be interpreted in a similar manner to the mafic rocks near El Almendro by Rosa (2009).

The REE chondrite-normalized patterns (McDonough et al., 1995) of the felsic rocks are characterized by a steep slope with enrichment of LREE vs. HREE ($[La/Yb]_N$= 4.67) with a relatively flat HREE pattern and a clearly defined negative Eu anomaly. The profiles are similar in both the massive and volcaniclastic felsic rocks (Fig. 14a). Here, three of the plotted samples show a minor negative Eu anomaly corresponding to the Zr-high rhyodacite – barren rocks - but it is more pronounced in the low-Zr rhyodacite or the hosted rocks, in a way similar to the described by Valenzuela et al., (2011b). All these patterns are typical of the calc-alkaline rocks, and they are consistent with an evolutionary

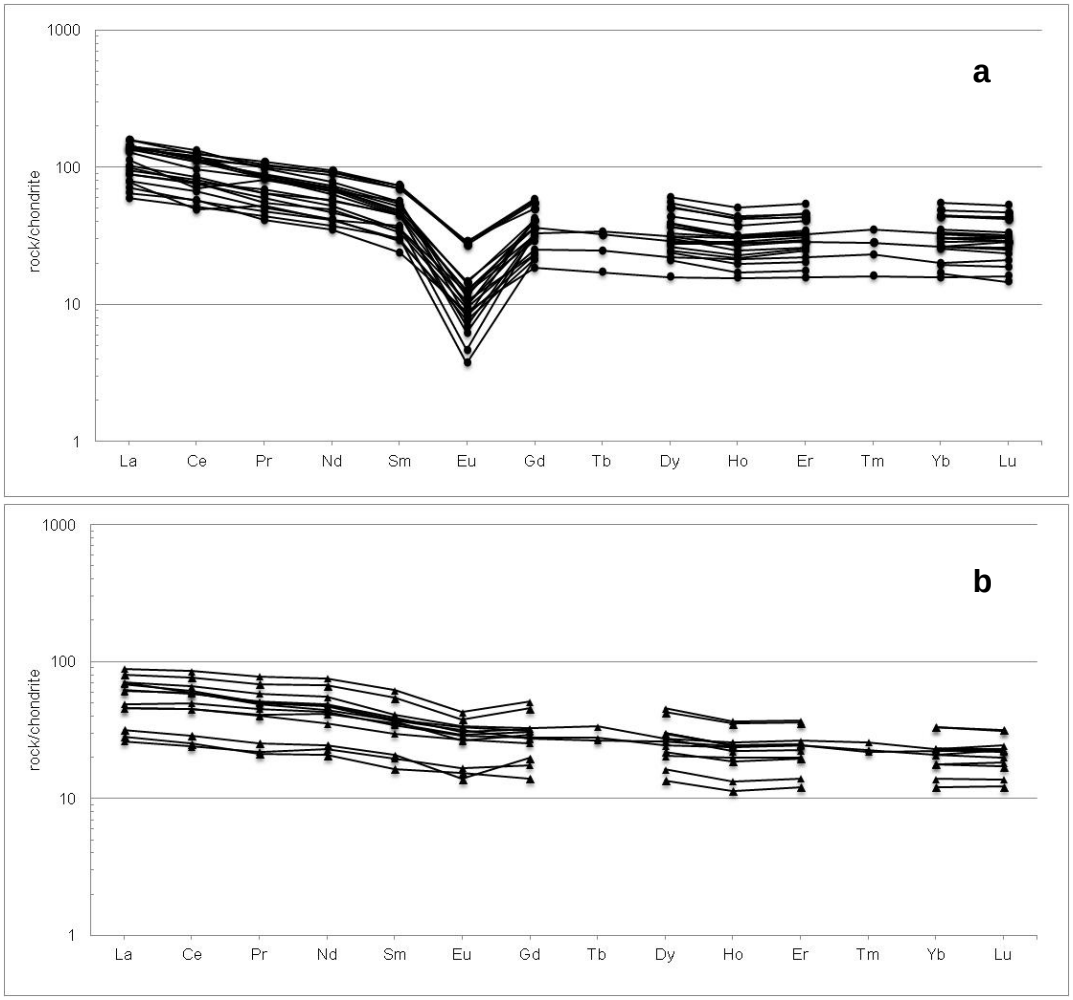

Figure 14. Chondrite-normalized to primitive mantle (McDonough et al., 1995) plots for the representative rock types at Río Tinto. (a) The least altered rhyodacite rocks showing two main groups, the Zr-high rhyodacite (minor Eu anomaly) and the rest of the coherent and volcaniclastic felsic rocks with an accentuated Eu anomaly. (b) Plot of the mafic rocks, showing the characteristic REE flat patterns.

process dominated by the fractionation of plagioclase. Minor vertical variations in the REE patterns could be caused by sampling or differences in the fractionation. In contrast, basalt and basaltic andesite show almost flat patterns with $[La/Yb]_N$ values between 1.6 and 2.75 (Fig. 14b). This is consistent with their tholeiitic affinity, characteristic of the most basaltic rocks from the IPB (Mitjavila et al., 1997) and confirms that the mafic character of some of the rocks in Rio Tinto is not due to hydrothermal alteration (chloritization) but is primary in origin.

The degree of hydrothermal alteration can be quantified by plotting the composition of the rocks in the Alteration Box plot proposed by Large et al. (2001); this diagram is able to

discriminate between different trends of hydrothermal alteration of igneous and derived rocks. It is based on the variation of two multi-component ratio indexes, the Alteration Index (AI) of Ishikawa et al. (1976) and the CCPI (Chlorite-Carbonate-Pyrite index) proposed by Large et al. (2001). The alteration index tracks the chemical variations associated with the chlorite- and sericite-rich alterations (Ishikawa et al., 1976); however, it does not take into account the carbonate alteration and is unable to discriminate chlorite from sericite alteration. This problem was resolved by Large et al. (2001) by formulating the CCPI index, that includes the content in FeO in addition to the MgO, Na_2O, and K_2O values previously considered by Ishikawa et al. (1976). The combination of these parameters in a bivariant plot is an effective tool for discriminating different trends relate to hydrothermal and diagenetic alteration. Within this diagram (Fig. 15), the samples from Rio Tinto can be grouped in two set of unaltered rocks (rhyodacite and basalt) and at least five different alteration trends. The most altered samples plot towards the upper-right corner (AI>90 and CCPI>95) and correspond to the mafic and felsic rocks with pervasive chloritic alteration located immediately beneath the massive sulphide orebodies in the Atalaya and Cerro Colorado open pits. While the mafic rocks seem to be directly replaced by the chloritite during a single metasomatic zone (Tornos, 2006), the evolution of the felsic volcanic rocks is more complex and there seems to be a metasomatic zoning from rocks with negligible alteration towards those with sericitic alteration and a later chloritic one; this is represented by the two different trends identified by the vectors 1 and 2 (Fig. 15). The increasing sericite alteration is defined by the vector 1 that tracks the depletion in Na and Ca, whereas the CCPI index is kept in a constant value. In hydrothermally altered rocks, the array becomes vertical (trend 2) due to an increase in the CCPI index associated with the the enrichment in Fe and Mg due to the intense chlorite alteration. In general, the felsic volcaniclastic rocks are more easily altered than the coherent ones. The third vector (3) track displays the weak sericite alteration observed in that the massive and volcaniclastic felsic rocks located in the distal areas away from the feeder zones. The vector 4 defines the trend of early albitization. A weak chlorite-albitization alteration is

marked by the vector 5. Both 4 and 5 vectors track the changes experimented in the felsic rocks during the low temperature alteration as described during seawater-volcanic rock interaction. Here, the igneous rocks experiment a spilitization process with the plagioclase and mafic minerals being replaced by albite and chlorite and/or epidote, respectively.

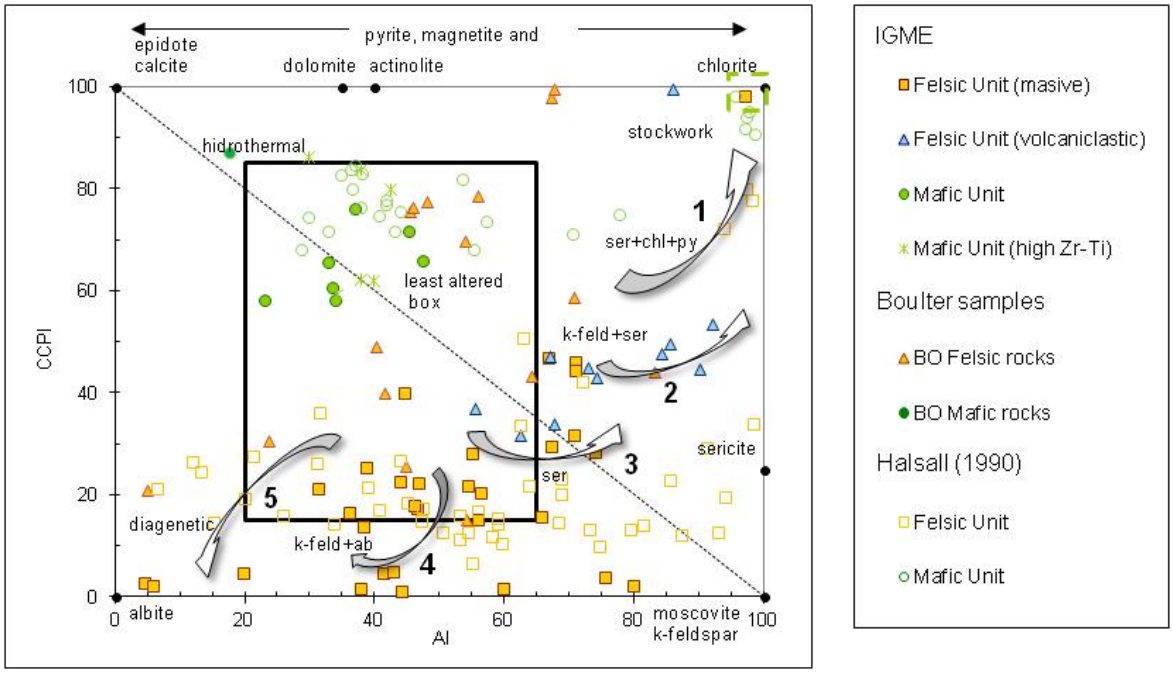

Figure 15. Bivariant AI-CCPI alteration box plot for the Rio Tinto area samples showing the existence of five different trends of hydrothermal alteration (see text for details). ($AI=100(K_2O+MgO)/(K_2O+MgO+Na_2O+CaO)$ and $CCPI=100(Mg+FeO)/(MgO+FeO+Na_2O+K_2O)$ (Large et al., 2001).

3. The mineralization

The Rio Tinto mining area hosts the major massive sulphide mineralization of the world with more than 1500 Mt of massive sulphides with 45%S, 40%Fe, 0.8%Cu, 2.1%Zn, 0.8%Pb, 0.5 g/t Au and 26 g/t Ag, and about 2000 Mt mineralized altered rock (García Palomero, 1992).

The main orebodies are aligned E-W in both limbs of the Rio Tinto structure with the Cerro Colorado stockwork cropping out in the core of the antiform (Fig. 2) (Williams et al., 1975). Earlier works interpreted the whole of them as a single lens of massive sulphides

(5 km long, 750 m wide and 40 m thick) that was subsequently folded, weathered and eroded, leaving only the orebodies located north and south of the structure (Williams et al., 1975). These deposits have been interpreted as classical seafloor exhalative deposits by Williams (1962) and the later works of Williams et al. (1975), Solomon et al. (1980), Badham (1982) and Eastoe et al. (1986).

The mineralization can be arranged in five major groups: (1) *stratiform deposits* within the southernmost part of the district (Filón Sur and San Dionisio); (2) lensoidal massive sulphide deposits in the northern limb of the structure wrapped by stockwork north of Cerro Colorado (Filón Norte, Salomón, Lago, Dehesa and Quebrantahuesos); (3) the easternmost massive sulphides (Planes-San Antonio); (4) the large outcrops of stockwork of Cerro Colorado; and, (5) a large gossan formed by the supergene alteration of the massive sulphides and stockwork. Beside this, there are some other small massive sulphide lenses such as Valle.

The massive sulphides are hosted both by altered volcanic rocks (Filón Norte orebodies) and by the shale of the Upper Sedimentary Unit (Filón Sur) (Fig.4). This feature, along with the regional mapping (Fig. 2) indicates that both groups of deposits do not correspond to the same unit and, thus, there is no straightforward relationship between the Filón Norte and Filón Sur orebodies (Tornos, 2006). The host rock, structure and texture of the massive sulphides are dramatically different suggesting that the situation was more complex. In fact, the shale hosting the massive sulphides in Filón Sur does not crop out in the northern limb of the anticline due to the configuration of the nappes.

The massive sulphides of Filón Sur form several stratiform lenses averaging 40 m thick in the contact between a dome complex of the Felsic Unit and the shale of the overlying Upper Sedimentary Unit and originally were traced for more than 3 km. These orebodies

have been mined through the showy Atalaya open pit (Fig. 3) and the large Filón Sur open cut, nowadays filled with waste.

The massive sulphides are mostly formed by fine grained pyrite with accessory chalcopyrite, sphalerite and galena with traces of other sulphides such as tetrahedrite-tennantite, arsenopyrite, pyrrhotite, cassiterite and, exceptionally and restricted to the stockworks, bismuth (bismuthinite, nuffeildite and aikinite) and cobalt minerals (Marcoux and Leistel, 1996). García Palomero (1992) has distinguished two different ore facies in the Filón Sur area: banded ore enriched in sphalerite-chalcopyrite in the base of the orebodies and fine grained and rich in the pyrite in the top; the amount of quartz increases upwards. The ore is mostly massive and with widespread recrystallization. Rarely, there are some primary features such as sedimentary layering with local graded bedding, shale soft clasts and sedimentary breccias. Ore textures include massive, banded, breccia, framboidal and colloform ones. The lowermost massive sulphides can retain also some primary features such as zoned crosscutting veins, with an edge of colloform pyrite and a core of fine grained sphalerite and chalcopyrite; locally they show ghosts of likely sulphate crystals. They are interpreted as the continuation of the feeder veins of the uppermost massive sulphides and related with the refining of the sulphide pile. The reason of the almost total absence of primary features and the marked metal zoning of the massive sulphides is hydrothermal refining, that likely masked early features leading to a homogeneous mass of pyrite with small lenses and veinlets of base metal sulphides, as has been described elsewhere (see Large, 2001). The most conspicuous structure is a widespread tectonic banding, better developed close to major shear bands. The hanging wall contact is sharp with a white chert cap while the footwall, when not sheared, is gradational to the stockwork. In the footwall, pervasively chloritized shale is gradually replaced by coarse grained pyrite, leaving remnants of the unreplaced host rock (Fig. 16a). These massive sulphides are rooted in a large stockwork hosted by the rhyodacite of the Felsic Unit.

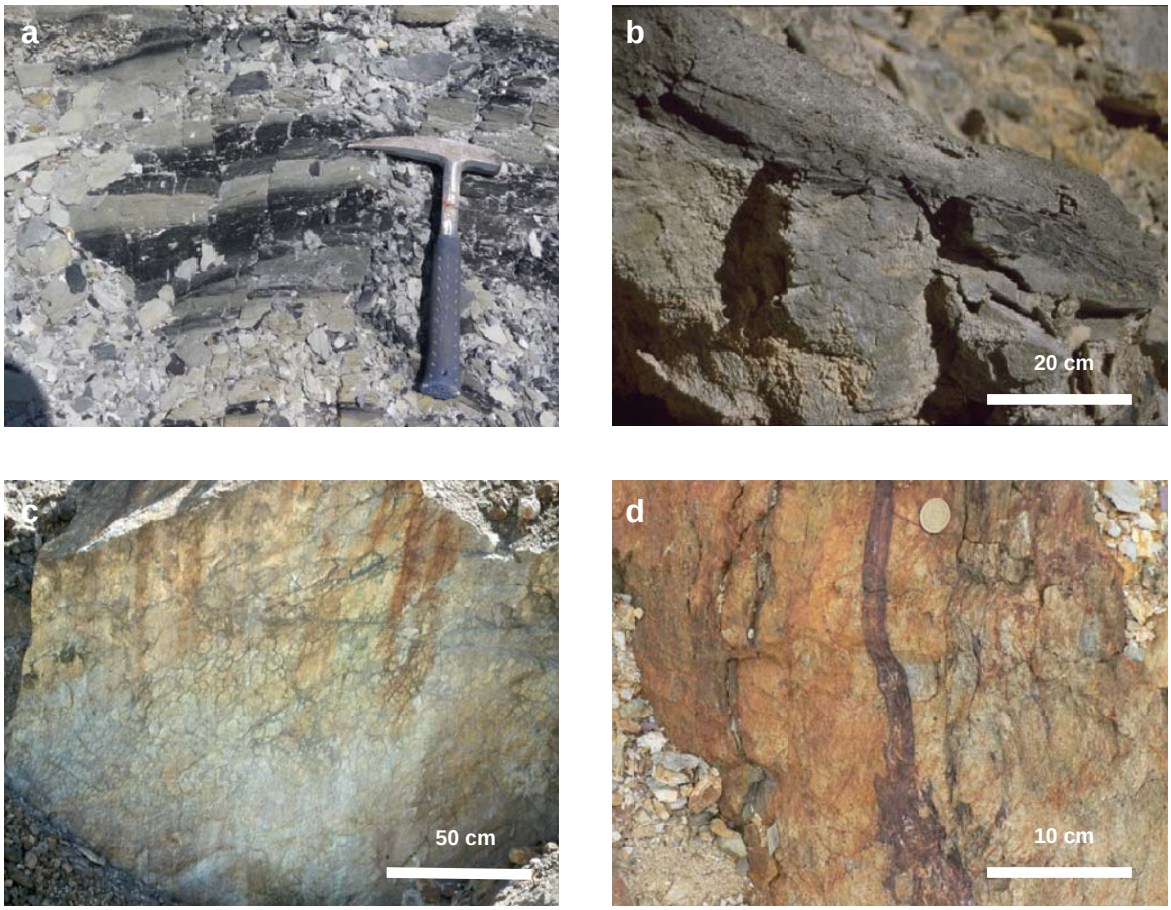

Figure 16. Photographs of the mineralization in the Rio Tinto district. (a) Weak to pervasive chloritic shale with laminated sulphides (pyrite), showing remnants of the fresh rock (Corta Atalaya). (b) Lower contact of the massive sulphides showing major tectonic lamination ("mylonite") (Corta Atalaya). (c) Stockwork with pseudobreccia texture in pervasively sericitized and silicified rhyodacite (Filón Norte). (d) Pseudo-peperite formed by veins of red mudrock into rhyodacite below the massive sulphides (Corta Atalaya). The veins crosscut the regional cleavage and postdate the tectonic contact between the mudrock and the porphyry suggesting that they are late tectonic veins and not a peperite.

In Corta Atalaya, the massive sulphides occupy the core of a syncline that has been later affected by major shearing (Fig. 3). Here, the massive sulphides are tectonically thickened up to 130 m and the footwall contact is sheared, masking most of the features of the original contact (Fig. 16b). Tectonic-hydrothermal remobilization has produced a marked but irregular enrichment in Cu or Cu-Zn-Pb overlying a zone of sulphide-rich mylonite.

The Filon Norte orebodies were located in the north and north-eastern sector of the mine and nowadays they are partially covered by the dumps of the nearby Cerro Colorado

open cut. They include the old Salomon and Lago large pits, worked between 1874 and 1960; the surrounding stockwork has been mined between 2000 and 2002. Here, the massive sulphides occur as subvertical lenses hosted by hydrothermally altered rhyodacite crosscut by the stockwork (Fig 16c). In detail, the rhyodacite wrapping the massive sulphides is pervasively affected by seriticic alteration that is replaced by a pervasive quartz + sericite zone around the massive sulphides, with the size and frequency of the stockwork veins increasing gradually both in the footwall and hanging wall of the massive ore. In detail, the massive sulphides show remnants of the original stockwork with the fragments of the breccia also replaced by sulphides. The massive sulphides are formed by coarse grained pyrite with significant proportions of sphalerite, chalcopyrite and galena and abundant interstitial silicates, mostly quartz and sericite. These massive sulphides are massive to brechoidal with no evidences of primary layering.

The absence of shale hosting the massive sulphides, the absence of primary layering and the relationships with the host rocks strongly suggest that these massive sulphides formed by replacement of the volcanic rocks below the seafloor, probably glassy or porous rhyodacite that could host an aquifer and was more reactive than the surrounding coherent rocks (Tornos et al., 2015). These rocks could be located in the carapace of the dome of form local mass flows or pyroclastic flows as lateral aprons of the dome (Allen and Cas, 1990; Allen et al., 1996).

The Planes-San Antonio orebodies are located in the easternmost part of the Rio Tinto district. They are inaccessible nowadays but they have been thoughtfully studied by Williams et al. (1975) that have shown that they correspond to exhalative stratiform lenses hosted by volcaniclastic rocks and shale capping a stockwork with a massive sulphide breccia pipe in the core. These relationships strongly suggest that probably the orebodies within Filón Norte correspond to massive sulphides pipes aligned along a major feeder zone that underlined the nowadays eroded massive sulphide lenses.

Opposite to the views of Boulter (1993, 1996), our data show that the massive sulphides postdate both the Felsic and Mafic Units. Palynological data on the shale hosting the massive sulphides of Filón Sur (Pereira and González Clavijo, 2007) indicate that it is younger than the underlying dacite and thus, it was deposited after the dome complex grew up. Furthermore, the veins of red mudrock interpreted as peperites and indicative that the intrusion of the porphyry was coetaneous with the deposition with the red shale (Boulter, 1993; Boulter et al., 2003) probably correspond to syn-Variscan veins as evidenced by the crosscutting relationships with the regional cleavage and the fact that they underlie a major tectonic contact (Fig. 16d). Its reddish colour is due to the syntectonic oxidation of the rocks. They are widespread all through the IPB and crosscut both volcanic and volcaniclastic rocks.

The area was supergenically altered and eroded during Cenozoic times (Amorós et al., 1981; García Palomero 1986; Núñez et al., 1987; Velasco et al., 2013). Originally, here there was a gossan (Cerro Colorado) 10-70 m thick, with an average of 30 m. Only some remnants are left, mostly in the southern part of the pit and below the ancient smelter. The gossan in situ is enriched in Au, Ag, Pb, Sb and Bi and depleted in Cu and Zn. The grades are about 79% Fe oxides, 1.2%Pb, minor Cu and Zn, 1.8-2.5 g/t Au and 35-45 g/t Ag. There is a transported gossan (Tortonian-Messinian, Velasco et al., 2013) with abundant heterolithic pebbles but negligible metal contents east of Rio Tinto (Alto de la Mesa) that is up to 10 m thick and interpreted as surficial chemical precipitates formed along a fluvial basin controlled by a fault (Sobol et al., 1997). The cementation zone below the gossan was small and almost completely mined in ancient times. Due to acid leaching, rocks are pervasively kaolinitized.

4. Discussion: the genetic model of the Rio Tinto deposit

The giant massive sulphide and stockwork orebodies at Rio Tinto represent a large zone of submarine hydrothermal activity. The massive sulphides probably formed on both

the seafloor and replacing underlying volcanic rocks, along major E-W trending faults, that were identified as major feeder zones by Solomon et al. (1982). The ratio of replacive vs. exhalative massive sulphides is likely about 2:1, indicating that replacive massive sulphides underlying stratiform ore can form a significant part of the total deposited sulphides, as has been quoted in present day oceanic systems (Humphris et al., 1995). Recently, Martín Izard et al. (2015) have proposed that the Rio Tinto mineralization formed in a small basin limited by NW and SE trending faults, most of them where later reactivated during the Variscan orogeny. This basin was infilled with the mafic and felsic volcanic rocks and the interbedded sediments. This idea was first proposed by Badham (1992), tracking the contact between the Mafic-Siliciclastic Unit and the Felsic Unit as a marker horizon predicted the existence of a third order basin, 5 km in size.

However, the regional mapping carried by the IGME (IGME, 1982) and Junta de Andalucía (2004) shows that the Mafic-Siliciclastic and Felsic Units can be mapped laterally for several tens of kilometers and, thus, they are not restricted to the Rio Tinto structure. The data suggest that the Rio Tinto deposits formed in a complex and active zone with widespread syn-sedimentary tectonics. Likely, there were several small, km-sized and short-lived third order anoxic basins in which the sedimentary rocks were deposited – and only the upper one was mineralized-.

If compared with other shale-hosted massive sulphides of the Iberian Pyrite Belt, what makes Rio Tinto strikingly different is the timing of formation. Most of the dated shale-hosted massive sulphides are of Strunian (late Devonian) age. This holds true for the deposits located in the southern part of the belt such as Aznalcóllar, Tharsis, Sotiel-Migollas or Neves Corvo (Pereira et al., 1996; González et al., 2002; Oliveira et al., 2003). However, at Rio Tinto both radiometric and palynological ages suggest that the massive sulphides are significantly younger, likely early Tournaisian, and coetaneous with those of the northern part of the belt (Tornos, 2006; see chapter I). This means that Rio Tinto is probably the only early Carboniferous exhalative deposit of the IPB and represents a

transition between the older exhalative deposits in the southern zone and the younger replacive ones in the northern IPB; it formed ca. 15 Ma after almost all the other shale-hosted massive sulphides were formed.

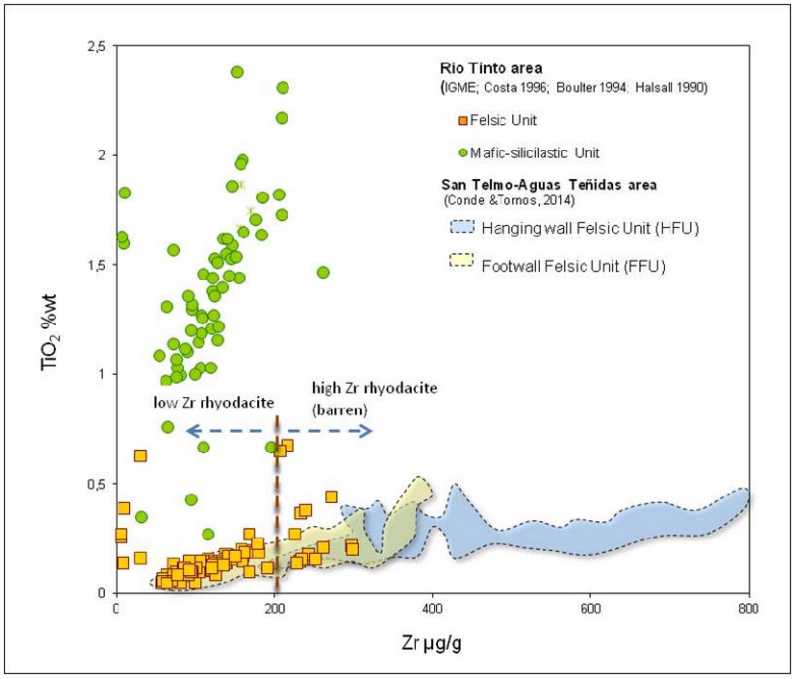

Figure 17. Immobile element (TiO2 vs. Zr) plot comparing the geochemistry of the felsic rocks of Rio Tinto and its comparison with equivalent rocks from the northern IPB. FFU: Footwall Felsic Unit; HFU: Hanging wall Felsic Unit (modified from Conde & Tornos, 2014).

The shale-hosted massive sulphides of Filón Sur and Planes-San Antonio show evidences of an exhalative origin on the seafloor (Tornos, 2006). Evidences for an exhalative origin include the stratiform nature of the orebodies and the local presence of inherited sedimentary structures. Formation by plume fallout has been proposed by Solomon et al. (1980), Badham (1992) and Boulter (1993); the relatively low Zn and Pb grades are interpreted by Badham (1992) as due to the spill out of hydrothermal fluids out of a brine pool and loose of the more soluble ones metals. The brine pool model for these deposits has been later on refined by Solomon et al. (2002) on the basis of the saline nature of the vented fluids. The likely environment of formation was a third order anoxic basin with the reducing conditions attained due to the displacement of seawater by vented saline hydrothermal fluids (Solomon et al., 2002).

Besides, the fluid inclusion data from quartz in the stockwork presented by Nehlig et al. (1992) indicate that vented fluids were aqueous and with salinities of 2-10 wt% NaCl equiv. Such fluids at temperatures near 130-230ºC should have negative buoyancy after mixing with seawater and would pond on the seafloor. $\delta^{34}S$ values of the massive sulphides are systematically lower (-6 to +8‰) than those of the stockwork (+6 to +12‰; Eastoe et al., 1986) indicating that the sulphur had a dual origin, one derived from the leaching of underlying rocks, likely the PQ Group, and a second source of biogenic origin, likely due to the reduction of seawater sulphate by bacteria/archea within the brine pool (Velasco et al., 1998; Tornos, 2006; Tornos et al., 2008).

Massive sulphides hosted by volcanic rocks are likely replacive. These massive sulphides probably formed by rapid cooling and fluid mixing in zones of high fluid flow when approaching the seafloor due to the mixing of deep fluids with reduced seawater (Tornos, 2006). $\delta^{34}S$ values indicate that sulphur has the same origin that in the exhalative ores. Stable isotope indicates that hydrothermal fluids at Rio Tinto were enriched in $\delta^{18}O$ and had δD values between 0 to 8‰ and -45 to 5 ‰ (Tornos et al., 2008). These values have been considered as due to the mixing of fluids exsolved from a deep igneous source with seawater. However, recent Sr and Nd data suggest that more likely these signatures are derived from the equilibration of fluids with the underlying reservoir, the PQ Group (Tornos, 2006; Tornos et al. 2008).

The massive sulphides of Rio Tinto are hosted in the likely younger rhyodacite having low Zr contents (<200 µg/g) and a pronounced negative Eu anomaly while the nearby high-Zr felsic rocks showing a small Eu anomaly are barren. The low Zr contents in the distal and barren areas (e.g. Odiel River and Campillo) could be interpreted as the felsic rocks in these areas being part of a separate dome complex unrelated to that cropping out in Rio Tinto. A similar relationship between mineralization and felsic domes has also been observed in the northern IPB, where the low-Zr rocks are the mineralized ones (Conde &

Tornos, 2014; chapter I). It is also consistent with the geochemical data shown by Valenzuela et al. (2011b) that describe a chemical contrast between the two felsic facies with different Zr/Ti ratios, being the mineralized felsic rocks of Corta Atalaya poor in Zr (Fig. 17). These geochemical results show that the ore-hosting felsic rocks are Zr-poor and, thus, not the most evolved of the area. As a whole, these geochemical data can be interpreted as reflecting the existence of a unique magma chamber where the felsic melts interacted with mafic primitive melts and had subsequent fractionation processes.

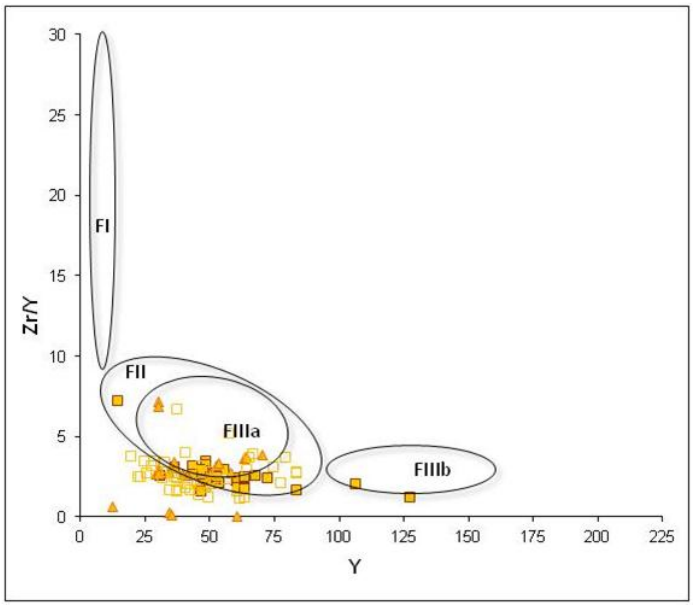

Figure 18. Zr/Y vs Y discrimination diagram for the felsic rocks from Río Tinto showing a FII affinity related to the rhyolite discrimination diagram of Hart el al. 2004 and Piercy 2010.

Thus, in the Iberian Pyrite Belt the ore-bearing felsic rocks are not related to the hottest and more fractionated magmatic rocks as it has been described in similar provinces (Barrie, 1995; Barrett et al., 2005). These results contradict recent studies that show that volcanogenic massive sulphide mineralization is related to zircon-rich felsic rocks (Barrie, 1995). Since the solubility of Zr in a magma depends on the temperature of generation of the melt, high Zr values should reflect the existence of super-heated melts that when intrude in the upper crust are able to form larger convective hydrothermal cells. However, these models apply only for volcanogenic massive sulphide deposits formed by seawater convection, which seems not to be the case of the VMS deposits of the northern Iberian Pyrite Belt. However, this discrimination is not clear when using the classification of felsic rocks proposed by Hart et al. (2004) and Gabour & Pearson (2008), but they permit to

show that the whole felsic rocks fall in FII rhyolite field which is typical of Phanerozoic and Proterozoic VHMS (Lesher et al., 1986; Lentz, 1998) (Fig 18).

The huge unusual size of Rio Tinto deposit compared to other VHMS elsewhere can be explained by the large amounts of biogenically sulphur from organic matter in combination with its geological setting of volcanism and tectonic active during a short time -1 to 2 Ma- (Solomon 2008, Tornos 2006; Menor et al., 2010)

5. Conclusions

The VS Complex of the Rio Tinto district includes large felsic dome complexes separated by two shaly sequences, the lower one capping a mafic-siliciclastic that marks the base of the volcanic unit. There are nine orebodies which occur in two different positions within the upper part of the sequence; a replacive mineralization in the hanging wall of a rhyodacite dome complex and shale-hosted mineralization deposited in an small, anoxic, third order basin located in the top of the dome complex. All the sequence shows a pervasive hydrothermal alteration with selective replacement of the felsic rocks by a sericite alteration and of the mafic rocks and shale by the chloritic alteration; both types of alteration host a large stockwork. Both the replacive and the exhalative mineralization are early Tournaisian in age; the shale rocks that mark the Devonian-Carboniferous transition does not show evidences of mineralization in marked contrast with the deposits located in the southern part of the IPB.

The geology and geochemistry show the existence of two different types of felsic rocks; later domes characterized by low Zr contents and a pronounced negative Eu anomaly are related to the mineralization while those having high Zr contents are barren, in a scheme similar of the northern IPB.

Acknowledgements

This work was financed by the project CICYT-FEDER 2003-0290 of the Spanish Government. We would like to thanks Mantesur and EMED-Tartessus companies for their collaboration and allowe the field and sampling works, and in particular to José Robredo and Angelo Farci. And extend our thanks to Nick Badham, Mike Solomon, David Mellado, Emilio González Clavijo and Alejandro Díez Montes by their constructive discussions and advices.

References

Allen, R.L., Cas, R.A.F., 1990. The Rosebery controversy: distinguishing prospective submarine ignimbrite-like units from subaerial ignimbrites in the Rosebery–Hercules Zn–Cu–Pb massive sulphide district, Tasmania. 10th Australian Geological Convention. 25. Geological Society Australia, 31-32.

Allen, R.L., Weihed, P., Svenson, S., 1996b. Setting of Zn–Cu–Au–Ag massive sulfide deposits in the evolution and facies architecture of a 1.9 Ga marine volcanic arc, Skellefte district, Sweden. Economic Geology 91, 1022-1053.

Amorós, J.L., Lunar, R., Tavira, P., 1981. Jarosite: a silver bearing of the gossan of Río Tinto (Huelva) and La Unión (Cartagena). Mineralium Deposita 16, 205–213.

Avery, D., 1974. Not on Queen Victoria's birthday; the story of the Rio Tinto mines. Collins, London, 464 pp.

Baboury, D., Pearson, V., 2008. Rhyolite geochemical signatures and association with volcanogenic massive sulfide deposits: Examples from the Abitibi Belt, Canada. Economic Geology 103, 1531-1562

Badham, J. P. N., 2001, Physical and chemical paleogeography of the Rio Tinto area during ore deposition, En: GEODE Workshop "Massive sulphide deposits in the Iberian Pyrite Belt: New advances and comparison with equivalent systems", Tornos, F., Pascual, E., Saez, R., Hidalgo, R. (eds.), 4, En: GEODE Workshop "Massive sulphide deposits in the Iberian Pyrite Belt: New advances and comparison with equivalent systems", Tornos,F., Pascual,E., Saez,R., Hidalgo,R. (eds.), 4.

Badham, J.P.N., 1982. Further data on the formation of ores at Rio Tinto, Spain. Transactions Institution Mining Metallurgy 91, B26-B32.

Blanco, A., Rothenberg, B., 1981. Exploraición Arqueometalúrgica de Huelva. Labor, Barcelona, 312-314.Barrett, T.J., MacLean, W.H. 1994. Chemostratigraphy and hydrothermal alteration in exploration for VHMS deposits in greenstones and younger

volcanic rocks, in Alteration and Alteration Processes. Lentz, D.R. (ed.); Geological Association of Canada, Short Course Notes, Volume 11, 433-467.

Barrett, T.J., MacLean, W.H. 1999. Volcanic sequences, Lithogeochemistry, and hydrothermal alteration in some bimodal volcanic-associated massive sulfide systems, in Volcanic-associated massive sulfide deposits: processes and examples in modern and ancient settings. C.T. Barrie and M.D. Hannington (eds.); Society of Economic Geologists, Reviews in Economic Geology, Volume 8, 101-131.

Barrie, C.T., Amelin, Y., Pascual, E., 2002. U-Pb geochronology of VMS mineralization in the Iberian Pyrite Belt. Mineralium Deposita, 37, 684-703.

Barriga, F.J.A.S., 1983, Hydrothermal metamorphism and ore genesis at Aljustrel, Portugal, unpublished PhD thesis, University of Western Ontario, 368p

Boulter, C.A., 1996. Extensional tectonics and magamatism as drivers of convection leading to Iberian Pyrite Belt massive sulfphide deposits? Journal of the Geological Society of London 153, 181-184

Boulter, C.A. 1993a Comparison of Río Tinto, Spain and Guaymas Basin, Gulf of California: An explanation of a supergiant massive sulfide deposit in an ancient sill-sediment complex. Geology 21, 801-804

Boulter, C.A., 1993b. High level peperitic sills at Rio Tinto, Spain: implications for stratigraphy and mineralization. Transactions-Institution of Mining and Metallurgy. Section B. Applied Earth Science 102, 30– 38.

Boulter, C.A., Hopkinson, L.J., Ineson, M.G., Brockwell, J.S., 2004. Provenance and geochemistry of sedimentary components in de Volcano-Sedimentary Complex, Iberian Pyrite Belt: discrimination between the sill-sediment complex and volcanic-pile models. Journal of the Geological Society of London, 161, 103-115.

Boulter, C.A. Soriano, C., Simman, P. 2001. The Iberian Pyrite Belt: a mineralized system dismembered by voluminous high-level sills. Terra Nova 13, 99-104.

Busby-Spear, C.J., White, J.D.L., 1987. Variation in peperite textures associated with differing host-sediment properties. Bulletin of Volcanology 49, 765-775.

Conde, C., Tornos, F., 2014. Volcanic stratigraphy and geochemistry of the VS complex in the northern Iberian Pyrite Belt. Macla 19.

Costa, I.M.S.R., 1996. Efeitos mineralogicos e geochimicos de alteraçao mineralizante en rochas vulcanicas felsicas de Rio Tinto (Faixa Piritosa Iberica, Espanha). Unpublished MSc Thesis, Universidad de Lisboa, 200 pp.

Dunning, G.R., Díez Montes, A., Matas, J., Martín Parra, L.M., Almarza, J., Donaire, M., 2002. Geocronología U/Pb del volcanismo ácido y granitoides de la Faja Pirítica Ibérica (Zona Surportuguesa). Geogaceta, 32: 127-130.

Eastoe, C.J., Solomon,M., García Palomero,F., 1986. Sulphur isotope study of massive and stockwork pyrite deposits at Rio Tinto, Spain. Trans. IMM, 95, B201-207.

Franklin, J.M., Sangster, D.M., Lydon, J.W., 1981. Volcanic associated massive sulfide deposits. Economic Geology, 485– 627 (75th Anniversary Volume).

García Palomero, F., 1990. Rio Tinto deposits –geology and geological models for their exploration and ore-reserve evaluation, in Sulphide Deposits-Their origin and processing, Gray, P.M.J., Bowyer, G.J., Castle, J.F. Vaughan, D.J., Warnes, N.A.(Ed) The Institution of Mining and Metallurgy, 17-36.

García Palomero, F., 1992. Mineralizaciones de Riotinto (Huelva): geología, génesis y modelos geológicos para su explotación y evaluación de reservas minerales. In: Recursos Minerales de España, Textos Univ., 15, CSIC, pp.1325-1352

García Palomero, F., 1980. Caracteres geológicos y relaciones morfológicas y genéticas de los yacimientos del anticlinal de Rio Tinto. Instituto de Estudios Onubenses "Padre Marchena". Excma. Diputación de Huelva. 262 pp.

Gemmell, J.B., Fulton, R., 2001. Geology, genesis, and exploration implications of the footwall and hanging-wall alteration associated with the Hellyer volcanic-hosted massive sulfide deposit, Tasmani, Australia. Economic Geology, 96, 1003-1035.

González-Clavijo, E., Díez-Montes, A., 2010. Porpuesta de estructura geológica para el depósito gigante de sulfuros masivos volcanogénicos de Río Tinto, Faja Pirítica Ibérica. Geogaceta 48, 204-206.

González, F., Moreno, C., Saez, R., Clayton, J., 2002. Ore genesis age of the Tharsis Mining District (Iberian Pyrite Belt): a palynological approach. Journal Geological Society London, v. 159, p. 229-232.

Gonzalo y Tarín, J., 1888. Memoría de la Comisión del Mapa Gelógico de España: Descripción física, geológica y menera de la provincia de Huelva, 2 volumenes, Madrid.

Gumiel, J.C., 1988. Estudio geológico y metalogénico de la mineralización de W-Sn-Bi-Mo asociada a la cúpula granítica de San Nicolás, Valle de la Serena (BAdajox). Unpublished Martes thesis, Universidad Complutense de Madrid, 221 pp.

Gumiel, P., Sanderson, D.J., Campos, R., Roberts, S., 2001. Fractal geometry of the Cerro Colorado stockwork, Rio Tinto Mine (Iberian Pyrite Belt). GEODE Workshop "Massive sulphide deposits in the Iberian Pyrite Belt: New advances and comparison with equivalent systems", Tornos, F., Pascual, E., Saez, R., Hidalgo, R. (eds.), 23-24.

Halsall, C.E., 1989. The relationship between intrusive magmatism, volcanism and massive sulphide mineralisation at Río Tinto, Spain. Unpublished Doctoral Thesis, Univ. of London, 298 pp.

Halsall, C.E. Sawkins, F.J., 1989 Magmatic-hydrothermal origin ofr fluids involved in the generation of massive sulphide deposits at Río Tinto (Spain). In: Miles, D. (Ed)., Water-Rock Interaction, Balkema, Rotterdam, 285-288.

Hart, T.R., Gibson, H.L., Lesher, C.M., 2004. Trace element geochemistry and petrogenesis of felsic volcanic rocks associated with volcanogenic massive Cu-Zn-Pb sulfide deposits. Economic Geology 99, 1003-1013.

Humphris, S.E., Herzig, P.M., Miller, D.J. et al., 1995. The internal structure of an active seafloor massive sulphide deposit. Nature, 377, 713-716.

IGME (1982): Síntesis Geológica de la Faja Pirítica del SO de España. Instituto Geológico y Minero de España, Madrid, 106.

Irvine, T.N., Baragar, W.R.A., 1971. A guide to chemical classification of the common volcanic rocks. Canadian Journal of Earth Sciences 8, 523-548.

Ishikawa, Y., Sawaguchi, T., Iwaya, S., Horiuchi, M., 1976. Delineation of prospecting targets for Kuroko deposits based on modes of volcanism of underlying dacite and alteration halos. Mining Geology 26, 105-117.

Junta de Andalucía, 2004. Mapa de Edad Geológica de Andalucía, E 1:400.000, Conserjería de Medio Ambiente. Junta de Andalucía, Sevilla, España.

Kokelaar, B.P., 1982. Fluidization of wet sediment during the emplacement and cooling of various igneous bodies, Journal of the Geological Society London, 139, 21-33.

Lafrance, B., Mueller, W.U., Daigneault R., Dupras, N., 2000. Evolution of a submerged composite arc volcano: volcanology and geochemistry of the Normétal volcanic complex, Abitibi greenstone belt, Quebec, Canada. Precambrian Research 101, 277-311.

Large, R.R., Gemmell, J. B., Paulick, H., Huston, D.L., 2001. The Alteration Box Plot: A Simple Approach to Understanding the Relationship between Alteration Mineralogy and Lithogeochemistry Associated with Volcanic-Hosted Massive Sulfide Deposits. Economic Geology 96, 957-971.

Large, R.R., 1992. Australian volcanic-hosted massive sulfide deposits: features, styles and genetic models. Economic Geology 87, 471–510.

Le Bas, M.J., Le Maitre, R.W., Streckeisen, A., Zannetin, B. 1986. A chemical classification of volcanic rocks based on the total alkali-silica diagram. Journal of Petrology, 27: 745-750.

Lecólle, M., 1977. La ceinture sud-ibérique: un example de province à amas sulfurés volcanosédimentaries (tectonique, métamorphism, stratigraphie, volcanism, paléogeographie et metallogenie). Unpublished PhD thesis, Universite Pierre et Marie Curie, 609 p.

Leistel, J.M., Marcoux, E., Thieblemont, D., Quesada, C., Sa´nchez, A., Almodóvar, G.R., Pascual, E., Sáez, R., 1998. The volcanic- hosted massive sulphide deposits of the Iberian Pyrite Belt. Review and preface to the special issue. Mineralium Deposita 33, 2-30.

Lentz, D.R., 1999. Petrology, geochemistry and oxygen isotope interpretation of felsic volcanic and related rocks hosting the Brunswick 6 and 12 massive sulfide deposits, Brunswick Belt, Bathurst Mining Camp, New Brunswick, Canada. Economic Geology 94, 57-86.

Lydon, J.W., 1984. Volcanogenic massive sulfide deposits. I. A descriptive model. Geoscience Canada, 11, 195-202

MacLean, W.H., Barrett, T.J., 1993. Lithogeochemical techniques using immobile elements. Journal of Geochemical Exploration 48, 109-133.

Marcoux, E., 1998. Lead isotope systematics in the giant massive sulphide deposits in the Iberian Pyrite Belt. Mineralium Deposita 33, 45-58.

Marcoux, E., Leistel, J.M., 1996. Mineralogy and geochemistry of massive sulphide deposits, Iberian Pyrite Belt. Boletín Geológico y Minero 107, 117-126.

McDonough, W.F., Sun, S.S., 1995. Composition of the Earth. Chemical Geology 120, 233-253.

Mellado, D., González Clavijo, E., Tornos, F., Conde, C., 2006. Geología y estructura de la Mina de Río Tinto (Faja Pirítica Ibérica, España). Geogaceta, 40, 231-234.

Menor-Salvan C., Tornos, F., Fernández-Remolar, D., Amils, R., 2010. Association between catastrophic paleovegetation changes during Devonian-Carboniferous bounday and the formation of giant massive sulphide deposits. Earth and Planetary Science Letters 299, 398-408.

Mitjavila, J., Marti, J., Soriano, C., 1997. Magmatic evolution and tectonic setting of the Iberian Pyrite Belt volcanism. Journal of Petrology 38, 727-755.

Moreno, C., 1993. Post-volcanic Paleozoic of the Iberian Pyrite Belt: an example of basin morphologic control on sediment distribution in a turbidite basin. Journal of Sedimentary Petrology 63, 1118-1128.

Moreno, C., Sierra, S., and Sáez, R., 1996. Evidence for catastrophism at the Famennian-Dinantian boundary in the Iberian Pyrite Belt, in Strogen, P., Somervilee, I. D., and

Jones, G. L., eds., Recent advances in Lower Carboniferous Geology, 107. Special Publication, Geological Society London, p. 153-162.

Munhá, J., 1990. Metamorphic evolution of the South Portuguese/Pulo do Lobo Zone. In: Dallmeyer, R.D., Martínez García, E. (Eds.), Pre-Mesozoic Evolution of Iberia. Springer Verlag, 363-368.

Munhá, J., 1983. Hercynian magmatism in the Iberian Pyrite Belt. Memorias Servicio Geologico Portugal 29, 39-81.

Nehlig,P., Cassard,D., Marcoux,E., 1998: Geometry and genesis of feeder zones of massive sulphide deposits: constraints from the Rio Tinto ore deposit (Spain). Mineralium Deposita, 33, 1-2, 137-149.

Núñez, C., Roca, A., Espiell, F., 1987. Improved gold and silver recovery from Spanish gossan ores by sulphidization prior to cyanidation. Trans Inst Min Metal C-96: C171

Oliveira, J.T., 1983. The marine Carboniferous of south Portugal: a stratigraphic and sedimentological approach. In: Sousa, L.D., Oliveira, J.T., (Eds.) The Carboniferous of Portugal. Memórias dos Serviçios Geológicos de Portugal 29, 3-37.

Oliveira, J.T., Pereira, Z., Carvalho, P., Pacheco, N., Korn, D., 2003. Stratigraphy of the tectonically imbricated lithological succession of the Neves Corvo Mine Region, Iberian Pyrite Belt, Implications for regional basin dynamics. Mineralium Deposita 39, 422-436.

Oliveira, J.T., Pacheco, N., Carvalho, P., Ferreira, A., 1997. The Neves Corvo Mine and Palaeozoic geology of Southwest Portugal. In: Barriga, F.J.A.S., Carvalho, F., (Eds.), Geology and VMS deposits of the Iberian Pyrite Belt. Guide Book Series 27, SEG, 21-71.

Oliveira, J.T., Quesada, C., 1998. A comparison of stratigraphy, structure and paleogeography of the South Portuguese zone and Southwest England, European Variscides. Geoscience in South-West England, The Scott Simpson Lecture, Annual Conference of the Ussher Society, vol. 9, 141– 150.

Onézime, J., Charvet, J., Faure, M., Chauvet, A., Panis, D., 2002. Structural evolution of the southernmost segment of the West European Variscides: the South Portuguese zone (SW Iberia): Journal of Structural Geology 24, 451–468.

Pascual, E., Donaire, T., Valenzuela, A., Sáez, R., Tornos, F., 2001 Geology of Riotinto and Río Odiel areas. In: Riotinto-Río Odiel Field Trip Guide. Geode Workshop, Aracena, España.

Pereira, Z., González-Clavijo, E., 2007. New Palynological ages improveing the geological background of the Río Tinto area (Spanish part of the Iberian Pyrite Belt). In: Ed. Pereira, Z., Oliveira J.T., Wicander, R. CIMP Lisbon'07. Ineti, Lisbon., 105-107.

Pereira, Z., Saez, R., Pons, J.M., Oliveira, J.T., Moreno, C., 1996: Edad devónica (Struniense) de las mineralizaciones de Aznalcóllar (Faja Pirítica Ibérica) en base a palinología. Geogaceta, 20-7,1609-1612.

Quesada, C., 1998. A reappraisal of the structure of the Spanish segment of the Iberian Pyrite Belt. Mineralium Deposita 33, 31-44.

Quesada, C., 1999. Tectonostratigraphic evolution of the Iberian Pyryte Belt. Post-Conference Field Trip. XV Reunión de Geología del Oeste Peninsular. International Meeting on Cadomian Orogens. J. Conf. Abstracts 4, 1032-1034.

Rambaud, F. (1969): El sinclinal carbonífero de Riotinto (Huelva) y sus mineralizaciones asociadas. Memorias IGME, 71, 229 pp.

Rodriguez, R.M., Diez, A., Leyva, F., Matas, J., Almarza, J., Donaire, M. (2002): Datación palinoestratigráfica del volcanismo en la sección de la Ribera del Jarama (Faja Pirítica Ibérica, Zona Surportuguesa) Geogaceta, 32,247-250.

Rosa, C.J.P., 2007. Facies architecture of the Volcanic Sedimentary Complex of the Iberian Pyrite Belt, Portugal and Spain. Ph.D. thesis, University of Tasmania, 357 pp.

Rosa, C.J.P., McPhie, J., Relvas, J.M.R.S., 2010. Type of volcanoes hosting the massive sulphide deposits of the Iberian Pyrite Belt. Journal of Volcanology and Geothermal Research 194, 107-126.

Rosa, C.J.P., McPhie, J., Relvas, J.M.R.S, Pereira, Z., Oliveira, T., and Pacheco, N., 2008. Facies analyses and volcanic setting of the giant Neves Corvo massive sulphide deposit, Iberian Pyrite Belt, Portugal. Mineralium Deposita 43, 449-466.

Rothenberg, B. and Blanco-Freijeiro, A., 1981. Ancient Mining and Metallurgy in South-West Spain, IAMS

Rothenberg, B., Pérez, J.A., 1987. Excavaciones de urgencia en la necrópolis de Stock de Gossa (Riotinto, Huelva). Anuario Arqueológico de Andalucía/1985, III. Actividades de Urgencia, 187-191. Conserjería de Cultura. Dirección General de Bienes Culturales, Junta de Andalucía, Sevilla.

Routhier, P., Aye, F., Boyer, C., Lecólle, M., Moliere, P., Picot, P., Roger, G., 1980. Le ceinture sud-iberíque a amas sulfures dans sa partie espagnole médiane. Memoire du BRGM 94, 265 pp.

Sáez, R., Tornos, F., Pascual, E., 2001. Cross-seciton on the Riotinto mining district. In: Pascual, E., Donaire, T., Valenzuela, A., Sáez, R., Tornos, F., Geology of Riotinto and Río Odiel areas. In: Riotinto-Río Odiel Field Trip Guide. Geode Workshop, Aracena, España.

Sánchez España, J., Velasco, F., 1999. Constraints on the Hercynian metamorphism in the northern IPB: Ore textures and phyllosilicate cristallinity: Boletin Sociedad Española Mineralogia, v. 22-A, 103-104.

Schlatter, D., 2007. Volcanic stratigraphy and hydrothermal alteration of the Petiknäs south Zn-Pb-Cu-Au-Ag volcanic-hosted massive sulfide deposit, Sweden Luleå: Luleå tekniska universitet. Doctoral thesis / Luleå University of Technology.

Schlatter, D., 2005. Volcanic stratigraphy, chemical stratigraphy, and hydrothermal alteration of the Petiknäs South Volcanic-hosted massive sulfide deposit, SwedenLuleå: Luleå tekniska universitet. Licentiate thesis / Luleå University of Technology.

Schermerhorn, L.J.G., 1975. Spilites, regional metamorphism and subduction in the Iberian Pyrite Belt: some comments. Geologie en Mijnbouw 54, 23-35.

Schermerhorn, L.J.G., 1971. An outline of the stratigraphy of the Iberian Pyrite Belt. Boletín Geológico y Minero 82, 239-268.

Silva, J.B., Oliveira, J.T., Ribeiro, A., 1990. Structural outline of the South Portuguese Zone. In: Dallmeyer, R.D., Martínez García, E. (Eds.), PreMesozoic Geology of Iberia. Springer Verlag, pp. 348-362.

Sobol, F., Toscano, M., Castro, J.A., Saez, R., 1997: A field guide to the Riotinto Mines. Geology and VMS deposits of the Iberian Pyrite Belt. SEG Fieldbook Series 27, 158-164.

Solomon, M., 2008. Brine pool deposition for the Zn-Pb-Cu massive sulphide deposits of the Bathurst mining camp, New Brunswick, Canada. I. Comparisons with the Iberian pyrite belt. Ore Geology Reviews 33: 329-351.

Solomon, M., Tornos, F., Gaspar, O.C., 2002. Explanation for many of the unusual features of the massive sulfide deposits of the Iberian Pyrite Belt. Geology 30, 87-90.

Solomon, M., Walshe, J.L., García Palomero, F., 1980: Formation of massive sulfide deposits at Rio Tinto, Spain. Trans.Inst.Min.Met., 89, Feb.1980, 16-24

Soriano, C., Casas, J.M., 2002. Cross section through the central part of the Iberian Pyrite Belt, South Portuguese Zone, Spain. In: Martínez Catalán, J.R., Hatcher, R.D., Arenas, R., Díaz García, F. (Eds.), Variscan Appalachian Dynamics: The Building of the Late Paleozoic Basement, Special Paper-Geological Society America, 364, 183– 197.

Soriano, C., Martı´, J., 1999. Facies analysis of volcano-sedimentary successions hosting massive sulfide deposits in the Iberian Pyrite Belt, Spain. Economic Geology 94, 867-882.

Thieblemont, D., Pascual, E., Stein, G., 1998. Magmatism in the Iberian Pyrite Belt: petrological constraints on a metallogenic model. Mineralium Deposita 33, 98-110.

Tornos, F., Conde, C., Chiaradia, M., Velasco F., 2015. Evolving subduction-related basins control the formation of VMS deposits in the Iberian Pyrite Belt. SEG Conference, Hobart, Tasmania.

Tornos, F., Heinrich, C.A., 2008, Shale basins, sulfur-deficient ore brines, and the formation of exhalative base metal deposits. Chemical Geology, 247, 195-207

Tornos, F., 2006. Environment of formation and styles of volcanogenic massive sulphides: The Iberian Pyrite Belt. Ore Geology Reviews 28, 259-307.

Tornos, F., Conde, C., 2007. The Rio Tinto district. Field trip guide of the Pre-sympositum trip to southern Spain. "23rd International Applied Geochemistry Sumposium" Oviedo 14th-19th June, 2007.

Tornos, F., Relvas, J. M. R. S., Ruiz de Almodovar, G., 2003. Field Trip Guide, GEODE-Global Comparison Massive Sulphide Project Field Workshop: The geology of the Volcanic Hosted Massive Sulphides of the Iberian Pyrite Belt,

Tornos, F., 2001. The Río Tinto district. GEODE Workshop “Massive sulphide deposits in the Iberian Pyrite Belt: New advances and comparison with equivalent systems. Field trip guide. Marzo 2000. Aracena, Huelva.

Valenzuela, A., Donaire, T., Pascual, E., 2002. Secuencia de facies volcánicas en el área del río Odiel (Faja Pirítica Ibérica, España). Geogaceta 32, 131-134.

Valenzuela, A., Donaire, T., Gonzalez-Roldan, M.J., Toscano, M., Pascual, E., 2011a. Volcanic architecture in the Odiel river area and the volcanic environment in the Riotinto-Nerva Unit, Iberian Pyrite Belt, Spain. Journal of Volcanology and Geothermal Research 202, 29-46.

Valenzuela, A., Donaire, T., Pin, C., Toscano, M., Hamilton, M.A., Pascual, E., 2011 b. Geochemistry and U-Pb dating of felsic volcanic rocks in the Riotinto-Nerva unit, Iberian Pyrite Belt, Spain: crustal thinning, progressive crustal melting and massive sulphide genesis. Journal of the Geological Society 168, 717-731.

Velasco, F., Sánchez España, J., Boyce, A., Fallick, A.E., Sáez, R., Almodóvar, G.R., 1998. A new sulphur isotopic study of some Iberian Pyrite Belt deposits: evidence of a textural control on some sulphur isotope compositions. Mineralium Deposita 34, 1-18.

Velasco, F., Herrrero, J.M., Suárez, S., Yusta, I., Alvaro, A., Tornos, F., 2013. Supergene features and evolution of gossans capping massive sulphide deposits in the Iberian Pyrite Belt. Ore Geology Reviews 53, 181-203

Williams, D., 1966. Volcanism and Ore Deposits. Leipzig: Freiberger Forsch. C120

Williams, D., 1934. The geology of the Rio Tinto mines, Spain. Transactions of the Institution of Mining and Metallurgy 43, 593-678.

Williams, D., Stanton, R.L., Rambaud, F., 1975. The Planes–San Antonio pyritic deposit of Rio Tinto, Spain: its nature, environment and genesis. Transactions-Institution of Mining and Metallurgy. Section B. Applied Earth Science 84, 73-82.

Williams, D., 1990. Further reflections on the origin of the porphyries and ores of Riotinto, Spain: Transactions Institution Mining Metallurgy.

CAPITULO III

Geology and geochemistry of the volcanic succession hosting the massive sulphides in the SE Iberian Pyrite Belt (Spain): the Aznalcóllar-Las Cruces zone

Geología y geoquímica de la secuencia volcánica encajante de los sulfuros masivos del SE de la Faja Pirítica (España): la zona de Aznalcóllar-Las Cruces

Abstract

The Aznalcóllar-Las Cruces mining district is the largest accumulation of massive sulphides in the SE part of the Iberian Pyrite Belt. The mineralization occurs as shale-related stratiform bodies located above (crypto)-domes of rhyodacite, sometimes located beneath the sediments of the Guadalquivir Basin. The Aznalcóllar-Los Frailes mining district includes two outcropping (Aznalcóllar and Los Frailes) and several blind massive sulphide orebodies. Las Cruces deposit is the easternmost known orebody and one of the richest copper deposits worldwide due to the presence of a high grade zone of supergene enrichment.

Detailed lithostratigraphic and mapping studies of the host sequence show that it is similar in the three deposits and characterized by the presence of three main units: (1) The *Lower Unit* that comprises coherent massive porphyritic dacite-rhyolite and associated hyaloclastite and interbedded crystal-rich volcanic sandstone with dark shale to the top of the unit. The massive sulphides are hosted by these late sedimentary rocks. This unit usually shows intense hydrothermal alteration. The hanging wall consists of: (2) the *Intermediate Unit*, dominated by a thick sequence of felsic rocks. In Aznacóllar-Los Frailes area contains two different subunits separated by a peculiar level including shale, purple siltstone, pumice and, locally, basaltic intrusions. The *subunit (A)* is dominated by fragmental and coherent porphyritic felsic rocks, and the aforementioned marker horizon; and, the *subunit (B)* that is more heterogeneous; in Aznalcóllar it is dominated by polymictic breccia, felsic volcaniclastic sandstone and shale capped by a thick package of coherent felsic rocks and a proximal volcaniclastic breccia that is present in Los Frailes area. In the Las Cruces deposit, the *Intermediate Unit* is a thick package made up of heterogeneous volcaniclastic breccias and rich-crystal sandstone interpreted as a large mass flow. Here, it also has a similar layer containing pumice-rich fragments that has been traced over the whole area, capped by a late dacite-rhyodacite dome complex with associated fragmental rocks, autoclastic and transported breccia. (3) The *Upper Unit*

contains shale and sandstone and a small level of felsic volcaniclastic sandstone and breccia which is intruded by dacite sills. The contacts are peperitic suggesting that the sills intruded early in unconsolidated sediments.

Geochemically, this volcanic sequence ranges from basalt-andesite to rhyodacite without major compositional gaps. In the Aznalcóllar area, the rocks of *Lower Unit* are classified as rhyodacite-rhyolite while those of the *Intermediate Unit* are dacite to rhyodacite. However, most samples from Las Cruces fall in the andesite to the rhyodacite fields, something that does not correlate with the petrography. The REE chondrite-normalized patterns of these volcanic rocks also show some differences between the Aznalcóllar-Los Frailes and the Las Cruces footwall sequence, which is here interpreted as a consequence of the pervasive hydrothermal alteration, which is more intense in Las Cruces.

The shale is a rather significant component of the whole sequence and the immediate host rock to the orebody. Mineralized shale is enriched in elements typically present in anoxic settings, something consistent with the Mn-Fe-V and (V/(V+Ni) = 0.69-0.92) ratios. However, barren shale formed in sub-oxic to oxic conditions.

The palaeogeographic evolution of the VS Complex in the area includes the formation of an early dacite to rhyodacite dome complex broadly synchronous with the Devonian-Carboniferous boundary and likely marks the onset of the volcanism in the area. The massive sulphides are located as stratiform bodies in the shale and volcaniclastic sandstone within the hanging wall of the dome complex, probably in a small third order anoxic basin. The post-mineralizing sequence includes a second felsic volcanic event that produced the *Intermediate Unit (A)* which consists of similar (crypto-)dome complexes. The upper part of this unit is characterized by explosive volcanism that produced abundant pumice-rich rocks that form a marker level in the area. The third volcanic episode is also mainly felsic and recorded by the presence of thick layers of volcanic

breccia lateral to dacite-rhyodacite dome complexes interbedded fine-grained sediments. The sequence is capped by a late felsic sill complex intruding in a sequence dominated by shale interbedded with volcaniclastic rocks.

Keywords: SE Iberian Pyrite Belt; Aznalcóllar, Las Cruces, volcanogenic massive sulphides; geochemistry; volcanic architecture.

1. Introduction and geologic setting

The South Portuguese Zone is an allochthonous terrane in the Variscan Belt of Europe that comprises the southern part of the Iberian Massif (Julivert et al., 1974). The prolifically mineralized Iberian Pyrite Belt (IPB) is the central of the three subdomains of the South Portuguese Zone (Routhier et al., 1980; Oliveira, 1983; Quesada, 1996, 1998). The Iberian Pyrite Belt is composed primarily of volcanic and volcaniclastic rocks ranging in composition from basalt to rhyolite interlayered with detrital and chemical sediments (Munhá, 1983; Mitjavila et al., 1997; Thieblement et al., 1998). It is bound to the north by the Middle to late Devonian Pulo do Lobo Accretionary Prism and to the south by the early Carboniferous flysch deposits of the the Baixo Alentejo Group. The basement to the IPB is unknown (Strauss, 1970; Schermerhorn, 1971).

The stratigraphy of the Iberian Pyrite Belt is in turn divided into three units. The basal unit is a homogeneous detrital sequence called the Phyllite and Quartzite (PQ) Group (Schermerhorn, 1971). It comprises at least 2000 m of a monotonous detrital sequence composed of shale, quartzarenite and quartzwacke. This sequence is interpreted to have been deposited on a shallow marine continental platform adjacent to a hinterland (Moreno et al., 1996). The gradational top of the PQ Group is marked by limestone lenses and thick quartzarenite layers, sometimes with evidences of being deposited in a shallow marine to continental environment. Fossils in the limestone have yielded late Famennian ages (Van den Boogaard and Schermerhorn, 1975).

The PQ Group is conformably overlain by the Volcanic Sedimentary Complex (VS Complex). The VS Complex is characterized by the presence of a continuous suite of volcanic rocks ranging in composition from basalt to rhyolite intercalated with pumice- and glass-rich volcaniclastic rocks, epiclastic sediments and detrital and chemical sediments including jasper, chert, manganese-rich layers and massive sulphides (Oliveira, 1990; Mitjavila et al., 1997; Soriano & Martí, 1999; Tornos, 2006). The thickness of the VS Complex varies between 0 and 1300 metres. Zircon U-Pb geochronology of igneous rocks

and palynological studies yield ages between late Famennian to middle Visean (Oliveira 1990; Pereira et al., 1996; Nesbitt et al., 1999; Barrie et al., 2002). From north to south there are systematic changes in the distribution of rock types in the VSC. The northern sector is characterized by massive volcanic and volcaniclastic rocks with only some accessory shale (Valenzuela et al., 2002; Tornos, 2006; Conde, see previous chapter). In contrast, the southern sector is dominated by shale and siliciclastic sedimentary rocks with intercalated volcanic rocks (Strauss, 1970; Soriano & Martí, 1999; Conde et al., 2003, 2007). The VS Complex Is dated as late Famennian – early Visean (Oliveira, 1990).

The VS Complex is the principal host to massive sulphide mineralization throughout the IPB. A geographic trend in the style of mineralization reflects the variation in the lithofacies distribution (Tornos, 2006). In the southern IPB, most massive sulphides occur as shale-related stratiform bodies, whereas volcanic-hosted replacive and stratabound mineralization occurs in the northern sector. The shale-associated orebodies (e.g., Aznalcóllar-Los Frailes, Las Cruces, Neves Corvo, Sotiel-Migollas and Tharsis) are interpreted to have formed in anoxic brine pools within third order basins, whereas the volcanic-hosted orebodies (e.g., Aguas Teñidas, Concepción, San Platón, La Zarza or Aljustrel) are interpreted to have formed by sub-seafloor replacement of pumice and glass-rich volcaniclastic rocks (Tornos, 2006; Conde in previous chapter).

The Baixo Alentejo Flysch Group is the uppermost sedimentary unit of the IPB. It is a thick package of syn-Variscan turbiditic epiclastic sedimentary rocks, including shale, arenite and minor conglomerate. The Baixo Alentejo Flysch Group is interpreted as a flysch sequence that was deposited on a prograding submarine continental platform (Moreno, 1993; Oliveira, 1990) and has an age of late Visean-Moscovian (Oliveira et al., 2006; Pereira et al., 2008).

Subsidence during deposition of the Iberian Pyrite Belt occurred within pull-apart basins generated by left lateral strike-slip faulting, currently interpreted as driven by oblique collision of the South Portuguese Zone with the Iberian Massif (Silva et al., 1990;

Quesada et al., 1991; Oliveira & Quesada, 1998; Onézime et al., 2003). The structural architecture of the Iberian Pyrite Belt is dominated by an E-W to NE-SW structures. The Variscan deformation of the IPB caused a thin-skinned, south-verging, asymmetric fold and thrust belt (Silva et al., 1990; Quesada, 1991, 1998; Soriano, 1997; Onézime, 2002). Variable, but generally low grade, regional metamorphism from prehnite-pumpellyite to greenschist facies accompanied this deformation and was associated with widespread penetrative foliation (Munhá, 1979, 1990). Previous researchers have suggested that variations in the intensity of metamorphism were related to strain partitioning along shear zones (Saéz et al., 1996; Sánchez España, 2000), and not a geographic distribution (Munhá, 1990).

2. Mining activity in the southeastern Iberian Pyrite Belt

The Aznalcóllar-Las Cruces mining district is the largest accumulation of massive sulphides in the SE part of the Iberian Pyrite Belt and it is close to the edge with the Tertiary Guadalquivir Basin. The district includes two outcropping (Aznalcóllar and Los Frailes) and several blind massive sulphide orebodies (Cuchichon, Higuereta, Silillos and Caridad) that have been systematically mined during the XXth century, as well as the large and recently discovered Las Cruces deposit, located beneath the sediments of the Guadalquivir Basin (Fig. 1). The giant Aznalcóllar-Los Frailes group is the largest of these and had an original global resource of 160 million tonnes (Mt) of massive sulphide ore. The Aznalcóllar lense contained original reserves of 43 Mt @ 0.44% Cu, 1.43% Pb, 2.70% Zn, 47.27 g/t Ag and 0.44 g/t Au. Related stockwork mineralization comprises an additional 47 Mt @ 0.58% Cu, 0.40 Zn and 10 g/t Ag. The nearby Los Frailes orebody is composed of two discrete massive sulphide lenses with combined reserves of 71 Mt @ 0.34% Cu, 2.17% Pb, 3.85% Zn, 60 g/t Ag and 0.4 g/t Au. The Las Cruces deposit had original resources of 20.7 Mt @ 3.2% Cu, 1.1% Zn and 0.4% Pb of primary massive sulphides as well as 17.6 Mt @ 6.2% Cu of cementation ore that is currently mined.

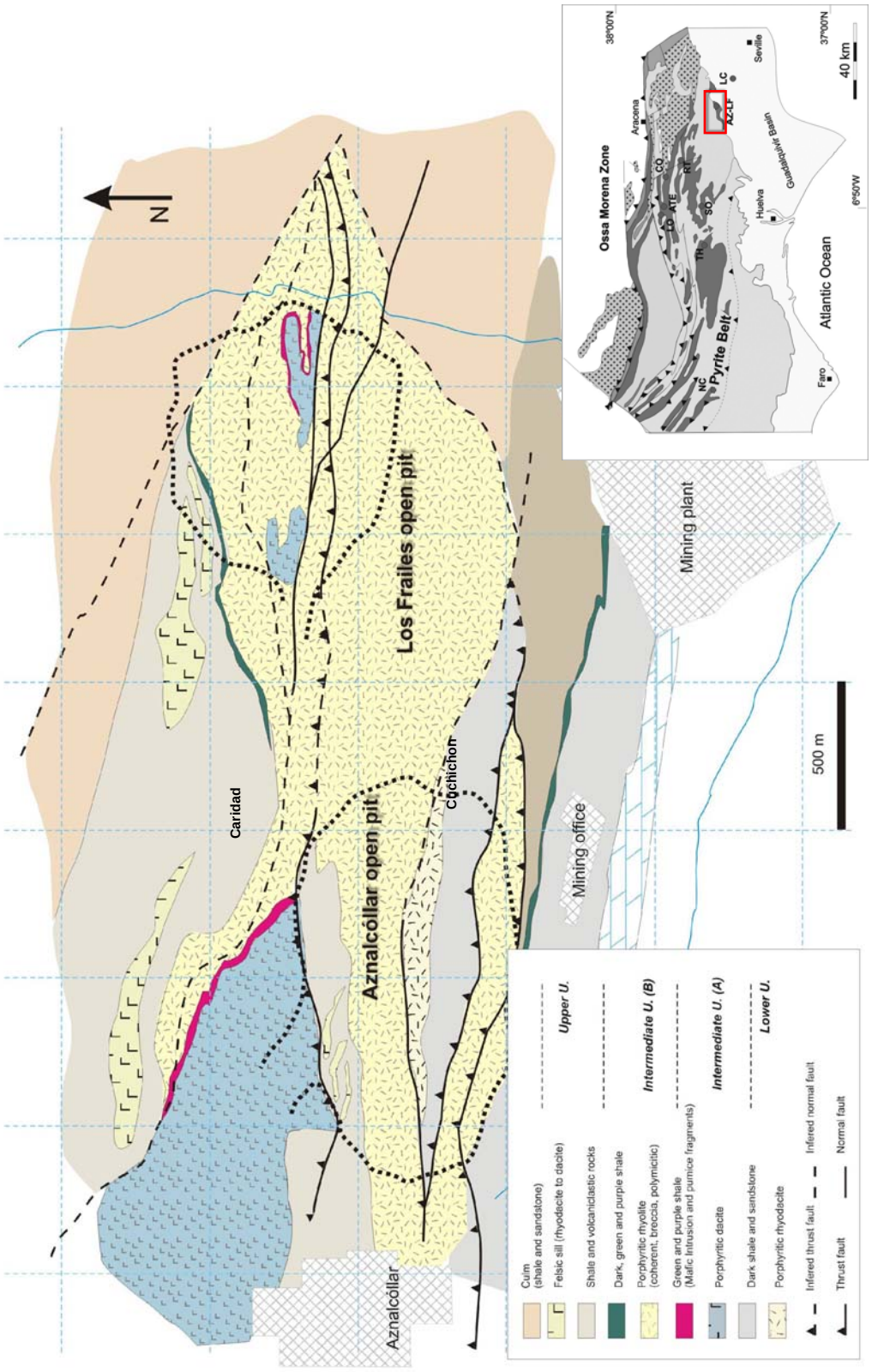

Figure 1. Simplified geological map of the Aznalcóllar area showing the location of the main orebodies (modified after Fernández, 2001).

Archaeological research has shown that the mining activity in the Aznalcóllar area started prior to 3000 BC. Early mining was mainly of the Roman period and evidence of this activity is still evident in the Aznalcóllar open pit. In the first half of the 20th century the outcropping massive sulphides were worked by an English company (Seville sulphur). The property changed hands and Andalucía de Piritas, S.A. (APIRSA) began the underground working of the Silillos-Higuereta orebodies and opened the Aznalcóllar open cut in the 1960's. In 1987, APIRSA was purchased by Boliden AB, who continued to operate the Aznalcóllar pit and targeted exploration on a gravimetric anomaly at Los Frailes. This geophysical target had already been identified the decade before, but had not been explored until that time. The Aznalcóllar pit was shut down in 1997 as the open pit of Los Frailes was brought on line. The mine was closed in September 2001 because of the drop of the base metal prices and the environmental issues arising from the April 1998 rupture of the Aznalcóllar tailings dam.

Las Cruces deposit is the easternmost known orebody of the Iberian Pyrite Belt. In the 1990's, Riomin Exploraciones (a branch of Rio Tinto plc) began a systematic exploration programme east of the IPB. By 1994, this program had revealed a large gravity anomaly in the Faralaes II area (close to Seville, between Gerena and Guillena). Exploration thereafter was focussed on the drillhole testing this anomaly. An early drillhole revealed a considerable amount of primary sulphides and, importantly, a large high grade secondary zone of copper enrichment. The Las Cruces project was bought by Cobre Las Cruces SL, a Spanish subsidiary company of MK Gold in 1999, who pushed the project toward operational feasibility. Subsequently, a 70% of stake was acquired by INMET Mining Corporation, and permitting was completed in early 2005. The last two years have been dedicated to building the hydrometallurgical plant and stripping overburden from the orebody. The construction phase and stripping are due was completed in 2009, after which the project had an expected mine life of 15 years. Actually, First Quantum Minerals

Ltd. (Canadian company), is the owner of the copper mine, with an estimated production of 72,000 t/y of refined copper.

There has been significant previous research describing the geology, structure and metallogeny of the Aznalcóllar district, notably that of Pinedo Vara (1963), Coullaut et al., (1975), IGME (1976), Hofstetter et al. (1979), Hernández Enrile (1981), Sierra (1984a , 1984b), Sierra et al. (1985), Pascual et al. (1994), Toscano et al. (1997), Almodóvar et al. (1998), Donaire et al. (2002), Fernández (2001), and Allen (2001). However, there are wide discrepancies between the interpretations of the stratigraphic sequences and origins of the mineralization presented by these authors. Previous studies of the Las Cruces ore deposit have been focussed on a general overview of the deposit (Knight, 2000), the secondary alteration (Capitan, 2006; Blake 2008; Tornos et al., 2014; Yesares et al., 2014) and the general mining operation (Doyle 1993; Doyle et al., 1998, 2003).

The main aim of this study is to reconstruct the volcanic sequence of Volcanic Sedimentary Complex in the Aznalcóllar-Los Frailes-Las Cruces area. This has been approached through the detailed mapping of the lithofacies and structure, with special attention paid to the contact relationships between facies, and the correlation of lithologic units and marker horizons. This field investigation is complemented by the petrology and geochemical analyses that supports interpretation of the nature of the volcanic rocks, shale depositional processes and the hydrothermal alteration, proposing a genetic model for the genesis of the primary massive sulphides.

3. Facies analysis of the VS Complex in the SE IPB

3.1. Aznalcóllar district (Aznalcóllar-Los Frailes)

The Aznalcóllar and Los Frailes deposits occur within a thick sequence of felsic massive and volcaniclastic rocks, dark shale and minor mafic rocks latterly folded and sheared during the Variscan orogeny. In general, the VS Complex here has large amounts of sedimentary rocks (shale) that are not so abundant in the northern part of IPB.

Detailed mapping of the open pits (Aznalcóllar and Los Frailes) and adjacent areas has allowed for distinguishing three main units (Figs. 1 and 2): (1) the *Lower Unit* that comprises coherent massive porphyritic rhyolite-dacite and interbedded crystal-rich volcaniclastic sandstone with dark shale in the top of the unit. The massive sulphides are hosted by these late sedimentary rocks. This unit usually shows intense hydrothermal alteration; (2) the *Intermediate Unit*, dominated by a thick sequence of felsic rocks contains two different subunits separated by a peculiar level including shale, purple siltstone, pumice and, locally, basaltic intrusions. The *subunit (A)* is dominated by fragmental and coherent porphyritic felsic rocks, and the aforementioned marker horizon; the *subunit(B)* is in Aznalcóllar dominated by polymictic breccia, felsic volcaniclastic sandstone and shale and by a thick package of coherent felsic rocks and a proximal breccia in Los Frailes area. (3) The *Upper Unit* contains shale, sandstone and a small level of felsic volcanic sandstone and breccia sequence which is intruded by felsic sills.

The *Lower Unit* crops out in the narrow band (<15 m) at the centre part of Aznalcóllar open pit and seems to be thicker in several deep drill holes of Los Frailes deposit (<50 m) (Fig. 1). This unit consists of massive volcanic rocks (Allen, 2001; Hernández, 2001) interbedded with volcanic sandstone and dark shale on the top, where the massive sulphides are hosted. This volcanic unit is composed by a coherent and autobrecciated porphyritic rhyodacite, characterized by the presence of 15-25% of feldspar + quartz ± biotite phenocrysts in a dark fine grained groundmass. Commonly, it shows a pervasive sericitic or/and chloritic hydrothermal alteration, and locally, sulphide disseminated and veins (stockwork?). Despite widespread hydrothermal alteration, the drillcore of the Los Frailes area shows abundant in situ breccia structures that are interpreted as in situ and reworked hyaloclastite. The upper part of this volcanic package is dominated by a felsic breccia containing detritic fragments and small shale clasts. This architecture suggests that this deposit is located on the margin of a dome complex while Aznalcóllar is located in more internal facies.

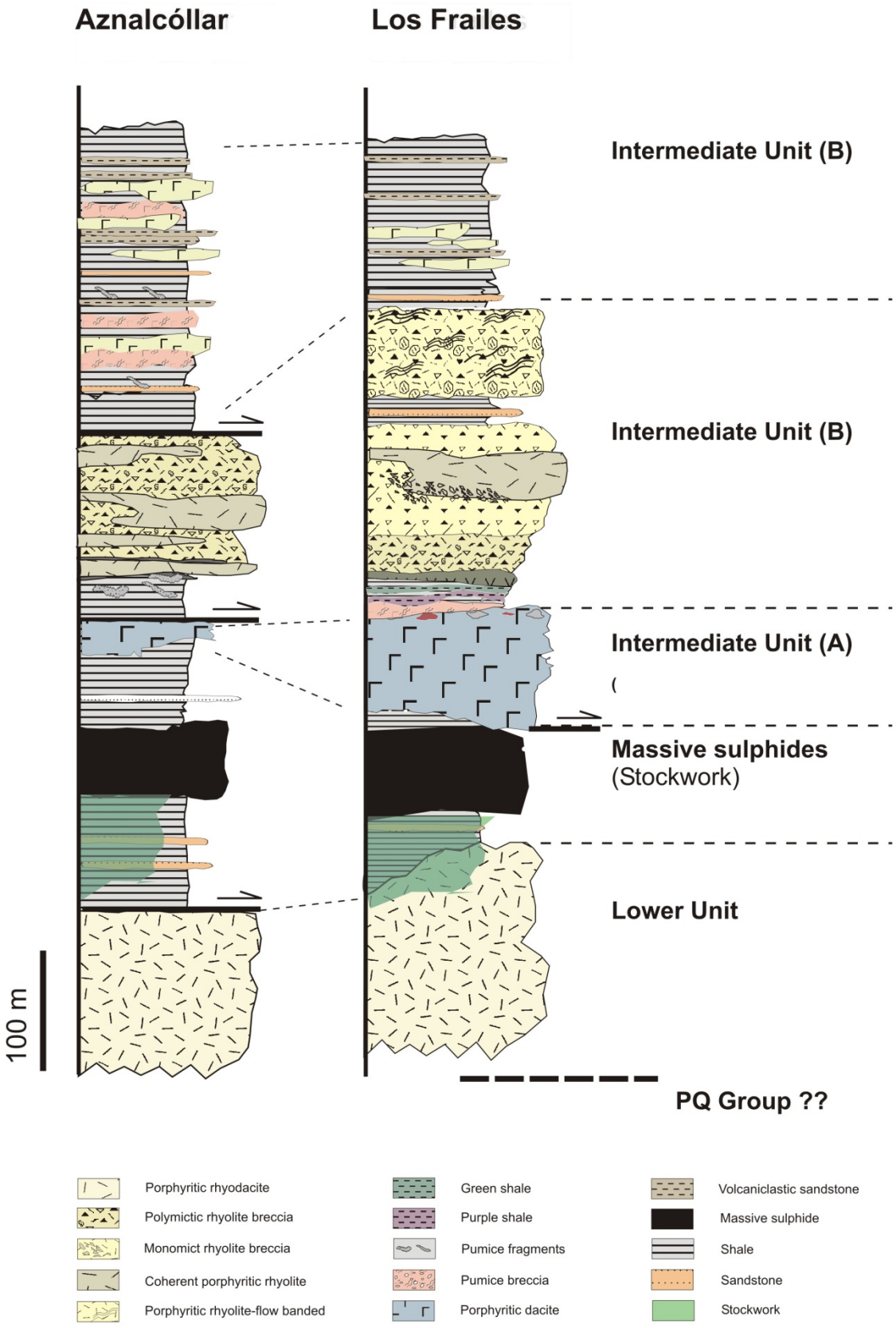

Figure 2 Detailed stratigraphic columns of the sequence at Aznalcóllar and Los Frailes open pits.

The unit passes gradationally to be dominated by sedimentary rocks. The transitional zones is dominated by alternating crystal-rich volcaniclastic sandstone and dark shale showing abundant sedimentary structures that are the host of the mineralization.

Previous works (Saéz et al., 1996; Almodóvar et al., 1998) have proposed a very different stratigraphic sequence considering this unit as part of the "V_{A1}" episode (Pons et al., 1993) and consisting of "*crystal and vitric tuffs and black shale*" in a sequence with reversed stratigraphy. This description is drastically different to that exposed by Allen (2001), Fernández (2001) and Conde et al. (2003) in later studies. The detailed geological study shows that these contrasting opinions are based on the interpretation of the stratigraphic younging and the structural facing determinations. The cross sections and the reconstruction of the lithological sequence show that the main structures consist of a series of overturned north dipping asymmetric folds. Generally, these folds have associated shear zone and faults, mainly thrusts, which are subsequently reactivated as normal faults. The existence of these tectonic structures explains the inversion of the sequence, the variable thickness of the different units and the stacking of the massive sulphide lenses. This is evident in Los Frailes open pit where the massive sulphide lense is intensely deformed (Fig. 3a), and in Aznalcóllar, where the stockwork overthrusts on the massive sulphides (Pons, 1993) (Fig.3).

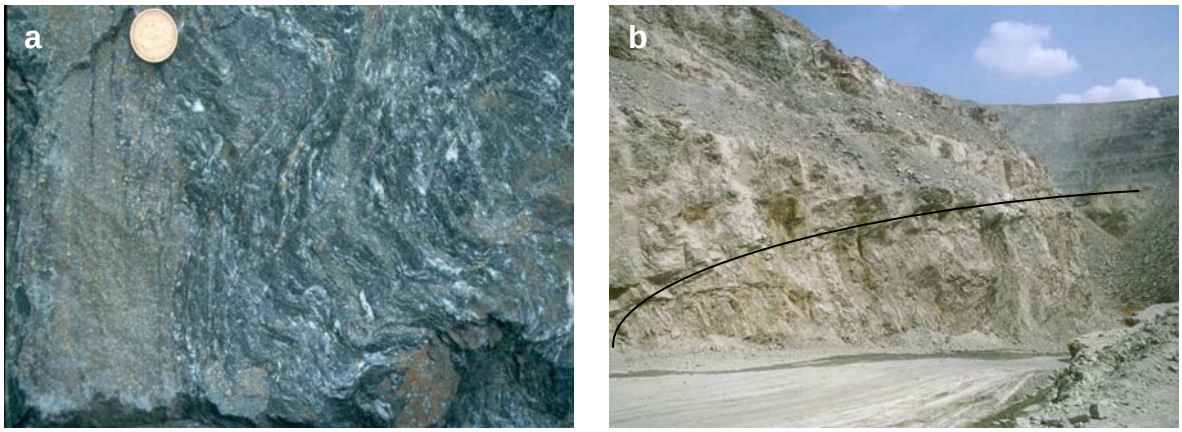

Figure 3. Photographies showing the structural complexity of this area. (a) Los Frailes open pit: intensely foliated mineralized stockwork; (b) Aznalcóllar open pit: mineralized stockwork overthrusted on the massive sulphides.

The cross sections and the drillcore logging reveal that the dark shale hosting the massive sulphides has a variable thickness between 5 and 90 m. In Aznalcóllar, the footwall contact is gradational but in Los Frailes it varies from sharp to gradational. In Los Frailes, the cropping out shale below the massive sulphides is commonly chloritized and silicified, something that suggests that is part of the stockwork. In both deposits, the upper contact is sharp and usually tectonic, but locally there are evidences of a primary and gradational contact where the overlying dark shale and volcaniclastic sandstone. Palynological dating of the shale shows a lattermost Devonian age (Strunian; Pereira et al., 1996), an age similar to that of other deposits of the southern IPB such as Tharsis, Neves Corvo, or Sotiel Migollas (González, 2005).

The orebody in Los Frailes occurs in a tight and overturned antiform which is thrusted between two shear zones following a structural scheme similar to that described in other areas of the IPB (Silva et al., 1990; Onézime et al. 2002). To the south-west, in the Aznalcóllar deposit, there are several large thrusts with E-W trend that cut the asymmetric folds, repeating the sequence and overthrusting the stockwork above the massive sulphides (Fig. 1).

The massive sulphides form a lensoidal orebody dominate by fine grained pyrite with minor chalcopyrite, sphalerite and galena (Hofstetter, 1980; Sierra, 1984a, 1984b; Almovodar et al., 1998). Almodovar et al. (1998) differentiate three ore types: polymetallic, pyritic and Cu-pyritic, which define a clear zonation with a Cu-enrichment in the centre of orebody and a high concentration of Zn and Pb in the upper and lateral parts. In detail, the mineralization shows a banded structure where the different types of mineralization alternate. The massive sulphides show abundant evidences of deformation, including S-C structures, widespread tectonic foliation usually related with the remobilization of the most ductile sulphides (sphalerite, chalcopyrite and galena) and abundant sulphide veins in the host rocks.

The mineralization shows evidences of replacement, including the presence of abundant relicts of the hydrothermally altered protolith with replacive contacts, in the lower part (Fig. 4a) and in the underlying stockwork zone (Fig. 4b). However, the uppermost part include primary lamination with graded bedding, sedimentary breccias (Figs. 4c and 4d), and alternating sulphides and unalterated dark shale that suggest deposition as exhalative chemical sediments.

Above the alternating shale and volcaniclastic sandstone that cap the massive sulphides occur a thick volcanic unit, the *Intermediate Unit* with two distinct subunits, (A) a crystal-rich porphyry felsic sequence; and, (B) a thick felsic unit with only some sediments

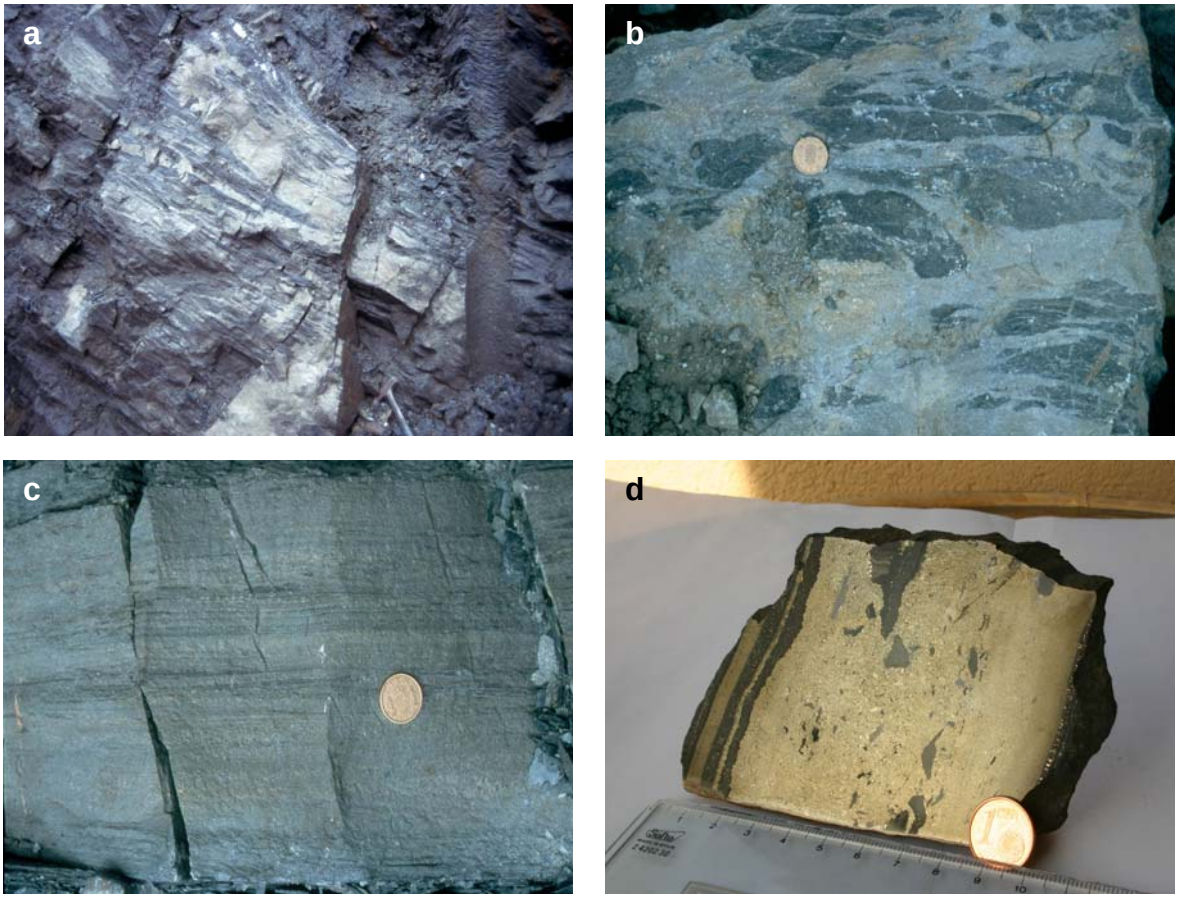

Figure 4. Representative photographs of outcrops and sample of the massive sulphides. (a) Outcrop of the footwall of the massive sulphides displaying replacive textures; semi-massive to massive sulphides replace highly altered shale (Los Frailes open pit). (b) Stockwork vein system in the chloritized footwall shale below the massive sulphides (Los Frailes open pit). (c) Banded mineralization showing evidences of graded bedding on the top of Los Frailes orebody. (d) Representative sample of the hanging wall of the Aznalcóllar orebody with sedimentary breccias and graded bedding (sample from Pablo Gumiel)

(shale and volcanic sandstone) interbedded with rhyolite breccia from monomictic to polymictic composition.

The *Intermediate subunit (A)* displays different characteristic in the Aznalcóllar and Los Frailes open pits suggesting that was deposited in a rather active setting.

In Los Frailes, it is composed by a feldspar and quartz (minor biotite)-phyric rhyodacite-dacite of 50 to 100 m in thickness (Fig. 5a). The proportion of phenocrysts varies between 15 to 30% in volume and range in size from 2 to 3 mm; they are usually subeuhedral to euhedral, but occasionally they are broken. The groundmass is cryptocristalline and composed of quartz, feldspar and phyllosilicates. Locally, there is a layer of rich-crystal sandstone with abundant sedimentary structures interbedded or included in porphyritic rhyodacite-dacite. Laterally and on top of it, it includes peculiar pumice-rich unit with abundant flattened fragments, 0.15-1 m in size composed by 70-80% quartz and feldspar phenocrysts within a glass matrix. They are supported by grey, green and purple shale or mudstone (Fig. 5b). This unit probably corresponds to an epoch of quiescent sedimentation. The presence of large pumice fragments supported by shale suggests that some of the eruption products floated on the sea, were transported and later deposited within fine grained sediments when they became saturated in water and sank. Its origin is unknown but could be either derived from explosive volcanism associated with the underlying rhyodacite or are exotic fragments derived from far, either subaerial or submarine, volcanism. Later dewatering, compaction and deformation flattened the original clasts. The uppermost part of the subunit includes dark, green and purple shale and a mafic intrusion, 8-10 m in thickness, which is interpreted as basalt-andesitic sill.

In the Aznalcóllar area, the porphyritic rhyodacite-dacite unit is significantly thinner and sometimes absent due to tectonic erosion related to the large shear zone that marks the hanging wall of the massive sulphides. The interbedded shale and sandstone on top of the massive sulphides is overlain by the foliated porphyritic rhyodacite to dacite (Fig. 5c) and a thick unit of the pumice-rich rocks. Here, the pumice clasts (0.5-70 cm) are located

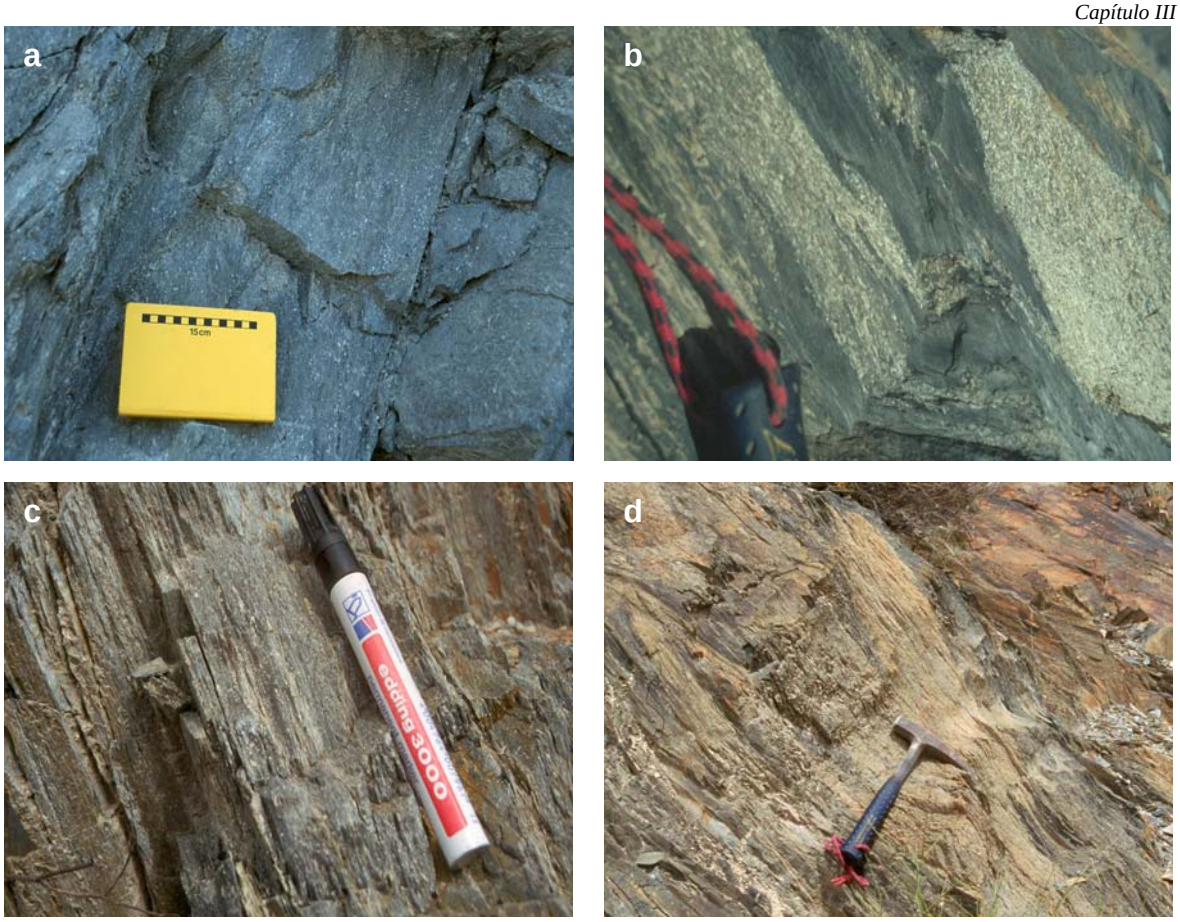

Figure 5. . Photographs of representative outcrops of the volcanic facies from the Intermediate subunit (A). (a) Outcrop showing a feldspar-quartz rich phyric dacite (Los Frailes open pit). (b) Irregular pumice fragments included in grey shale. Los Frailes open pit. (c) Foliated porphyric rhyodacite-dacite in the Aznalcóllar open pit, overlain by (d) a mass flow of pumice-fragments.

and supported in a thick sequence of irregularly distributed grey to dark shale with interbedded volcanic ash. Locally, there are large concentrations of these pumice-rich fragments and pumice-rich sandstones. As a whole, this unit is interpreted as related to an explosive extrusive dome complex that ended with a large explosion, with generation of large pumice fragments that were later eroded and reworked in pumice mass flows (Fig. 5d). The variability of the volume of the pyroclastic facies within both open pits reflects the proximity to the eruption.

The *Intermediated subunit* (B) is a thick package (150-250 m) dominated by breccias of dominant rhyolitic composition. In Aznalcóllar, this subunit is conformably or tectonically located above the Intermediate subunit (A) (Fig. 1). It composed by a poorly sorted clast-supported breccia with intense foliation. It contains polymictic clasts that range in size

from 5 to 40 cm. The composition of the clasts include different types of porphyritic rhyolite with white and pink colour and having 15-20% feldspar and quartz phenocrysts having 1-3 mm in size, aphyric rhyolite rich in amygdales and perlitic textures, elongated fragments of grey-green siltstone and ash lenses (Fig. 6a). This breccia alternates or laterally grades to similar reworked breccias with smaller fragments interbedded with shale and sandstone (Fig. 6b).

This unit is different in the Los Frailes area. Here, it consists of a complex rhyolite sequence, up to 200 m thick, dominated by vent-dominated facies. From base to top three facies are differentiated:

- Polymictic rhyolite breccia dominated by poorly sorted and clast supported white aphyric rhyolite clasts, green and red quartz- and feldspar-phyric rhyolite clasts and minor versicolour (green and purple) siltstone clasts (Fig. 6c). The clasts are sub-rounded and the size varies from a few centimeters (<15 cm) to 6 metres. Locally, they show evidences of crude stratification and graded bedding. As a whole, this unit is interpreted as a large mass flow.
- A rhyolitic hyaloclastite formed by a monomictic porphyritic rhyolite breccia with fragments of various colors (green, pink and beige) which shows abundant jig-saw fit and perlitic textures. This facies is intensely deformed and the clasts are flattened parallel to the foliation (Fig. 6d). In detail, some clasts show an irregular and gradual edge with the groundmass. They occur in layers 2-3 m thick and show evidences of limited sedimentary transport, including moderate sorting and normal graded bedding (Fig. 6e).These rocks overlie the coherent rhyolite described below. Restricted to the area south of the mine, the polymictic rhyolite breccia is overlain by a monomictic versicolour and stratified rhyolite breccia. They have similar characteristics to monomictic rhyolite breccia.

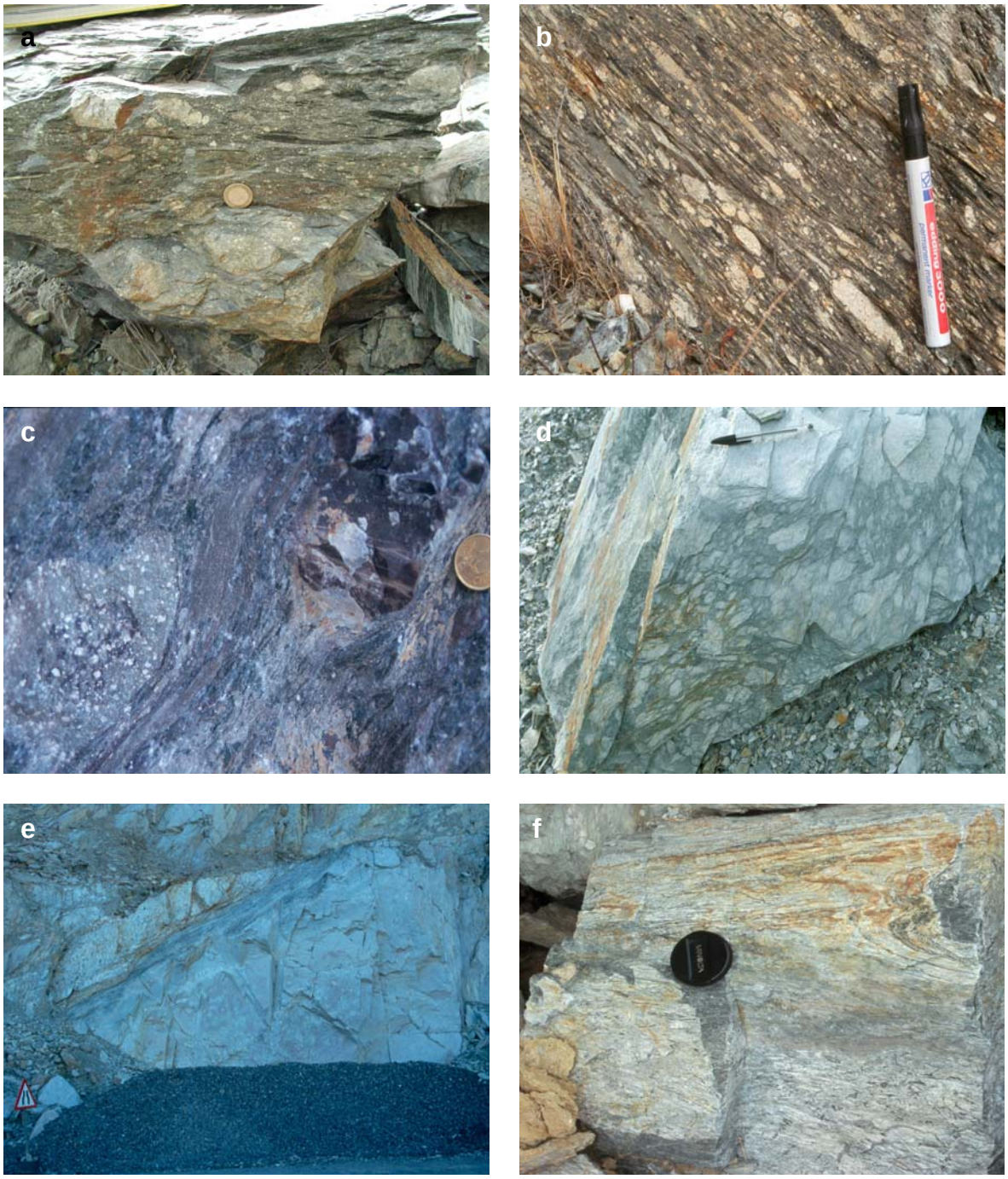

Figure 6. Representative photographs of the main lithofacies of the Intermedite Unit (B). Aznalcóllar open pit: (a) Coarse breccia composed of heterogeneous clasts of rhyolite and siltstone interbedded with ash lenses (coin for scale: 2.3 cm), that laterally graded to (b) foliated reworked polymictic breccia (marker for scale: 15.7 cm). In the Los Frailes open cut, this unit comprises: (c) polymictic rhyolite breccia with clasts of porphyritic and aphyric rhyolite and versicolour siltstone (coin scale: 2.4); (d) clast-supported monomictic hyaloclastite breccia showing clasts with cuspate margins (pen for scale: 14.50), which laterally grade into (e) transported polimictic breccia and shale layers (traffic sign scale: 2 m); (f) block of the coherent aphyric rhyolite showing flow banding marked by fine green and cream alternating bands (cover scale: 5 cm).

- Coherent porphyritic rhyolite, consisting of a porphyritic rhyolite with 2-15% phenocrysts of feldspar and quartz in a microcrystalline groundmass. The facies vary from almost aphyric with less than 2% phenocrysts to the dominant porphyritic facies with about 15% phenocrysts. The phenocrysts are subhedral crystals of 1-2 mm in size; the rock also includes abundant amygdales (2-4 mm) filled of quartz. The aphyric rocks have local fine flow banding and occasionally contain devitrification spherulites (Fig. 6f).

The Upper Unit forms the uppermost part of the sequence. The lower contact of this unit is marked by purple and green shale and the mafic sill. The Upper Unit is dominated

Figure 7. Panoramic and detailed photographs showing the main characteristics of the Upper Unit. (a) Dark and grey shale, interbedded by volcaniclastic breccias and intruded by felsic sill complex (Aznalcóllar open pit). (b) Subhhorizontal felsic sill intruding in a sequence of dark, grey and purple shale (N of Los Frailes open pit). (c) Peperite contact between dark shale and a rhyolitic subvolcanic intrusive body showing irregular and angular clasts in a black shale groundmass. (d) "*Globular peperite*" located in the contact upper contact of a rhyodacitic sill with the host shale.

by dark and grey shale and sandstone interbedded with crystal-rich volcanic sandstone and breccia. These late ones contain abundant pumice clasts and layers of glass shards which are commonly partially dismembered or broken and are especially abundant in the Aznalcóllar open pit. Finally, in both Aznalcóllar and Los Frailes open pits this sedimentary unit is intruded by a felsic sill complex composed of feldspar and quartz-phyric rhyodacite to dacite (Fig. 7a and b). These felsic intrusions show peperitic contacts with the host sedimentary rocks (Fig 7c and d). These late rocks have been described as a *globular peperite* by Donaire et al (2002).

3.2. Las Cruces Mine

The host sequence of the massive sulphides can be grouped into four main units (Fig. 8), in a similar manner to that of the Aznalcóllar area.

The *footwall* or *Lower Unit* (>300m) mainly consists of a porphyritic dacite dome with associated autoclastic breccia and hyaloclastite along the margins and the top. Commonly, it consists of a thick grey to green coherent dacite alternating with in situ-hyaloclastite consisting of a clast-supported breccia with monomictic, 0.5-10 cm fragments with angular to curviplanar shaped edges. The groundmass is fine grained and microporphyritic and includes microcrystalline aggregates and skeletal crystal of quartz and minor subhedral plagioclase. Lateral to the coherent facies and related hyaloclastite there are lenses of reworked transported breccia and sandstone of similar composition. Locally, these volcaniclastic rocks are intruded by a mafic sill which consist of fine-grained coherent massive basaltic-andesite, rarely weakly porphyritic to aphyric and intensely chloritized.

This felsic unit grades upwards into dark shale and crystal-rich sandstone which are the host of the primary mineralization. The rocks below the massive sulphides are affected by a pervasive and highly irregular hydrothermal alteration, consisting of chloritization, sericitization and silicification with a variable sulphide content in the form of disseminated

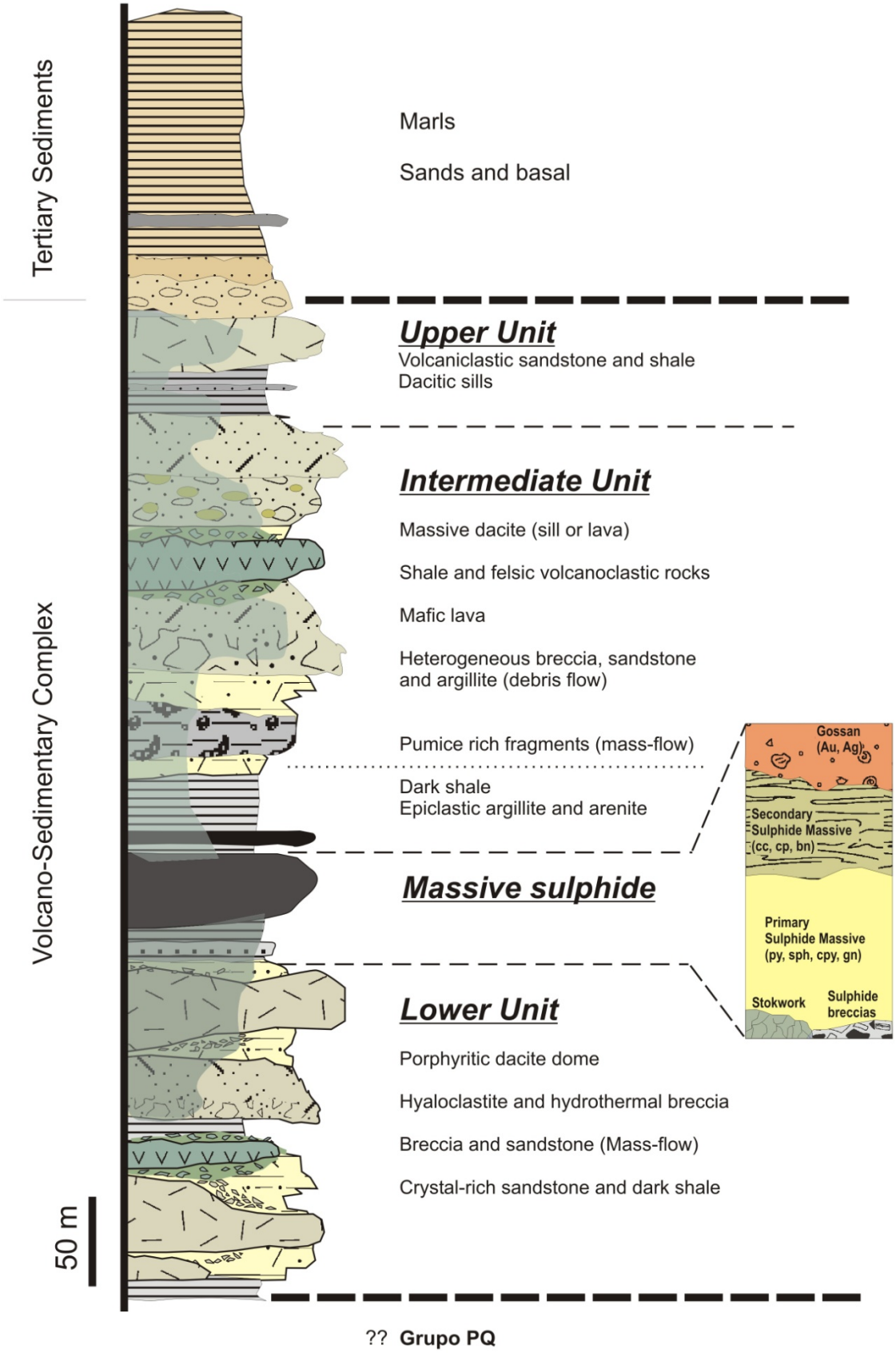

Figure 8 Detailed stratigraphic column of the ore-host sequence of the Las Cruces deposit (modified from Conde et al., 2007)**.**

grains, semi-massive lenses or veins. These rocks are interpreted as a stockwork or feeder zone. Despite most of the stockwork is hosted by the volcanic rocks, some of it is hosted by shale with chloritic alteration.

The massive sulphides form a stratiform lense (Knight 2000; Tornos et al., 2013, 2015) and are very similar to other deposits of the southern IPB. They are dominated by fine grained, massive to banded, pyrite with local enrichments in sphalerite, chalcopyrite and galena. These massive sulphides show local sedimentary structures such as parallel lamination, as well as a characteristic layer near the footwall and made up of syn-sedimentary breccias with fragments of massive sulphide, shale, chert and jasper (Fig. 9a). Furthermore, there are evidences of older sulphates being replaced by pyrite (Tornos,

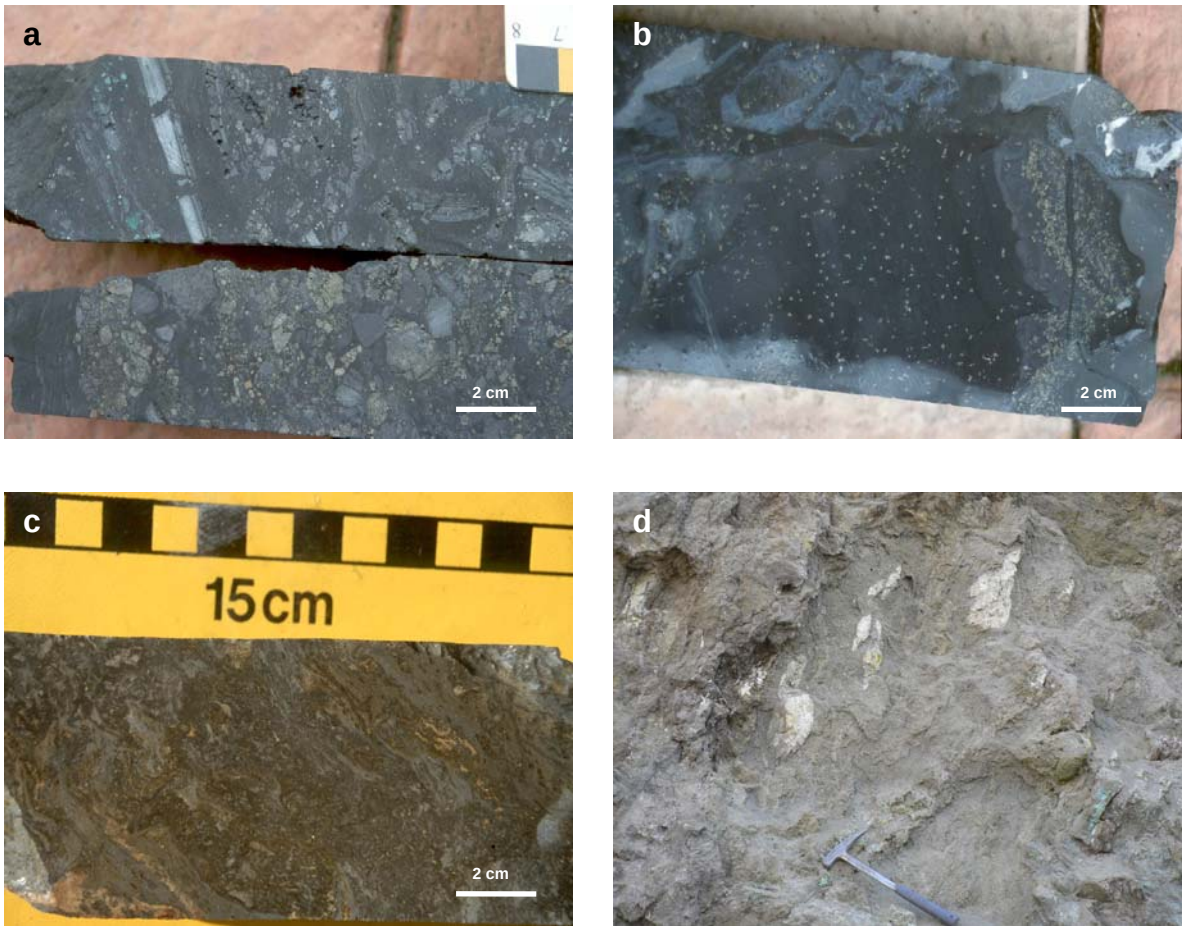

Figure 9. Photographs from drill core slabs of the primary massive sulphide and stockwork. (a) Polymictic breccia makes up sulphide and siltstone clasts included in dark shale. (b) Pyrite replacing sulphate in footwall mudstone. (c) Stringer (or stockwork) sulphide zones underlie the massive sulphides compose by sericite+chlorite+quartz+pyrite. (d) Sericitic felsic rocks replacive by massive sulphide (N of the open pit).

2006) (Fig. 9b). All these features indicate that the primary mineralization was dominantly exhalative onto the seafloor, probably within a third order anoxic basin. However, the footwall of the mineralization shows evidences of hydrothermal replacement and sometimes there are remnants of strongly sericitized and silicified dacite within the massive sulphides (Fig. 9c and d).

As quoted above, Las Cruces is characterized by a thick zone of secondary alteration. The cementation assemblage replaced the massive sulphides and also occurs as veins and breccia groundmass at the top of the massive sulphides. The mineralogy of the secondary zone includes chalcocite, covellite, bornite, chalcopyrite, pyrite and enargite. This peculiar mineral assemblage has recently been studied and described by Velasco et al. (2013), Tornos et al. (2015) and Yesares et al. (2015). The gossan that originally capped these rocks has been replaced by an unusual assemblage dominated by carbonates, galena, iron sulphides and a complex sulphide assemblage (Knight, 2000; Blake, 2008; Tornos et al., 2013; Yesares et al., 2014) that is thought to be of biogenic origin (Tornos et al., 2014).

Palynological ages of the host rocks at Las Cruces show that the massive sulphides formed during the Strunian (late Devonian) (Doyle, pers. comm., 2003) and contemporaneously with most of the shale-hosted massive sulphide deposits of the southern IPB (Tornos, 2006).

The hanging wall of the mineralization consists of a complex sequence (250-350 m) of felsic and intermediate volcanic rocks, including dome complexes, mass flow and pumice-rich breccia alternating with siltstone and shale, which dominate the upper part of the sequence. Three units can be distinguished:

- The *basal unit*, capping the massive sulphides, that includes dark shale alternating with epiclastic argillite and arenite with similar characteristics to the siliciclastic package located below and hosting the massive sulphides.

- The *Intermediate Unit* is a thick package made up of heterogeneous breccias and rich-crystal sandstone that probably correspond to a large mass flow; here there is a single layer containing pumice-rich fragments that has been traced over the whole area (Conde et al., 2003, see above) and a small dome complex of rhyodacite-dacite and associated autoclastic and transported breccia.

  The felsic mass-flow consists in monomictic breccia interbedded with sandstone and argillites which locally are interstratified by normal-graded polymictic breccia and coarse grained pumice rich sandstone with evidences of a transport and reworded (debris flow) (Fig 10 a to c). This polymictic pumice sandstone consists of quartz and feldspar crystal, pumice clasts, and felsic and siltstone clasts. This facies shows a diffuse laminated and normal graded.

  Near the footwall of the *Intermediate Unit,* there is a layer of dark shale and fine-grained felsic sandstone rich in compacted pumice clasts. The pumice clasts range between 1 cm and 50 cm in size. They are commonly porphyritic and contain quartz and plagioclase phenocrysts 1-2 mm in size, included in a cryptocrystalline groundmass. These clasts are irregular in shape and show a conspicuous white alteration halo on the external margin which is developed by the chemical reaction and temperature contrast between clast and shale (Fig. 10d). This peculiar layer shows similar lithological characteristics and the same position within the stratigraphic sequence that the pumice-rich facies at the Aznalcóllar-Los Frailes zone.

  These mass flow facies grade upwards to succession with alternating argillite and grey and beige crystal-rich sandstone of dacitic composition that are intruded by rare mafic dykes and a dacite sill (Fig. 10e). This coherent dacite consists in weakly to porphyritic dacite, with feldspar and minor quartz phenocrysts in a microcrystalline groundmass.

Figure 10. Photographs of the main facies of the hanging wall at Las Cruces deposit. (a) Interbedded volcaniclastic breccia, sandstone and siltstone. (b) Mass-flow deposits with clasts of dacite porphyry supported in a sand- to mud-matrix. (c) Coarse polimictic pumice sandstone composes by quartz and feldspar crystal, pumice fragments, and siltstone clasts. (d) Shale layer with pumice fragments rich in feldspar ± quartz phenocrysts in a microcrystalline groundmass of chlorite ± sericite. (e) Mafic sill or lava with pervasive chloritic alteration. (f) Peperite formed by interaction of felsic coherent rocks with shale.

- The uppermost part of the *Upper Unit* is composed of shale and felsic volcaniclastic rocks that are capped by a massive dacite that could either be a lava flow or a sill. This dacite is massive and commonly weakly porphyritic. The contacts with the host fine-grained sandstone and shale are locally peperitic (Fig. 10f), which imply their emplacement being into wet unconsolidated sediment and probably at shallow depths below the seafloor (Busby-Spear et al., 1987)

The hanging wall units show only a weak to moderate alteration (chloritization, sericitization, silicification, and carbonatization) but a widespread supergene alteration that consists of acid leaching and silicification.

Barrie et al. (2002) dated by U-Pb in zircon one of these dacite rocks within the hanging wall sequence, yielding an age of 353.97 ± 0.69 Ma.

In the area around Las Cruces these Palaeozoic rocks are covered by about 150 m of Tertiary conglomerate, sand and marl (Fig. 8).

4. Lithogeochemistry of volcanic rocks and shale

The geochemistry of volcanic rocks and shale is used here as tool for lithological discrimination and determination of the depositional conditions of the ore. 70 samples of volcanic rocks and 69 of shale from drill cores and outcrops were analyzed for major and trace elements by X-ray fluorescence (XRF) and ICP-MS at the Laboratorios Generales of the IGME (Appendix I). The shale was also analyzed for total organic carbon and sulphur.

4.1. Geochemistry of the volcanic rocks

Most of the rocks in the area, especially in Las Cruces, show a pervasive hydrothermal alteration and, thus, discrimination between lithological groups has been predominantly based on elements traditionally regarded as immobile (Al_2O_3, TiO_2 and Zr) (Mac Lean & Barrett, 1993; Barrett & MacLean, 1999).

The volcanic rocks have been plotted in the standard discriminating diagram (Zr/TiO_2 vs. Nb/Y and SiO_2 vs. Zr/TiO_2). They range in composition between basalt-andesite and rhyodacite without major compositional gaps. The geochemistry of the rocks in the Aznalcóllar zone show distinct patterns that allow the easy discrimination between units. The felsic rocks of the *Lower Unit* are classified as rhyodacite-rhyolite while those of the *Intermediate Unit* are rhyodacite to dacite (Fig. 11a). However, most samples from Las Cruces fall in the andesite to the rhyodacite fields, and even some rocks plot in the trachyandesite field, something that does not correlate with the petrographic characteristics of these samples (Fig. 11b). This problem has been discussed by Munhà (1983) and Rosa et al. (2004). These authors have interpreted these anomalous classification as due to the HFSE-depleted or low HFS concentrations in these rocks, something that has been also described in Bathurst District (Lentz, 1999).

The magmatic affinity has been tracked for both areas using the La-Yb diagram of Barrett & MacLean (1999). La and Yb contents of 7-30 µg/g and 1-3 µg/g, respectively, define a calc-alkaline trend.

At Las Cruces, the TiO2% vs. Zr and Nb/Zr ratios identify only one broad group of volcanic rocks with no major geochemical differences, suggesting that all the sequence represents different batches of an unique magmatic pulse and with no dramatic chemical breaks. However, in the Aznalcóllar zone, the samples plotted in the binary diagrams (Zr/Al_2O_3 vs. Al_2O_3/TiO_2; Fig. 13d) indicate that these rocks are probably represent a more magmatic differentiation process or different degrees of partial melting of an unique magmatic chamber.

The REE chondrite-normalized patterns (McDonough et al., 1995) of the volcanic rocks show some differences between the Aznalcóllar-Los Frailes and Las Cruces samples. The samples of Aznalcóllar-Los Frailes mainly display a steep slope pattern with enrichment of LREE vs. HREE ($[La/Yb]_N$= 4.67) and with a relatively flat HREE pattern and a clearly

defined negative Eu anomaly. In fact, both felsic Intermediate subunits can be discriminated on the basis of the Eu anomaly, that is small in the dacite of the *Intermediate Unit (A)* and significantly larger in the rhyodacite-dacite from the *Intermediate Unit (B)*. The mafic rocks show classical almost flat patterns compatible with a juvenile derivation with minor modifications. The chondrite-normalized REE spidergram for footwall (*Lower Unit*) and hanging wall (*Intermediate and Upper Units*) from Las Cruces show similar patterns for LREE with moderate slopes from La to Sm and weakly Eu anomaly. However, HREE patterns are different. While that for the rocks from *Intermediate and Upper Units* HREE patterns are flat, the footwall display a moderate slopes from Gd to Lu. This low content only is apparent and is caused by the dilution effect and therefore by the amount of mass gained as a consequence of significant hydrothermal alteration (Barrett et al., 1993).

All these patterns are typical of the calc-alkaline rocks, and they are consistent with an evolutionary process dominated by the fractionation of plagioclase. However, minor variations can be due to the intense hydrothermal and supergene alteration present in whole sequence in Las Cruces mine.

The degree of hydrothermal alteration can be assessed using the alteration box plot based on two multicomponent ratios indexes (AI and CCPI; Large et al., 2001) The data from Las Cruces confirm that both the footwall and the hanging wall are affected by hydrothermal processes but only the footwall rocks plot into the chlorite ± pyrite ± (sericite) field. The other rocks plot in two different trends (vectors 1 and 2 in the Figure 11e). These vectors define a Na and Ca depletion and Fe and Mg enrichment, respectively, typical tracks of an intense to strong hydrothermal alteration. Nevertheless, most of the samples of Aznalcóllar-Los Frailes area fall in unalterated box suggesting that scale of the alteration in Aznalcóllar-Los Frailes was significantly smaller than in Las Cruces. Only a dacite-rhyodacite sample located near the tectonic contact between the *Intermediate Units*

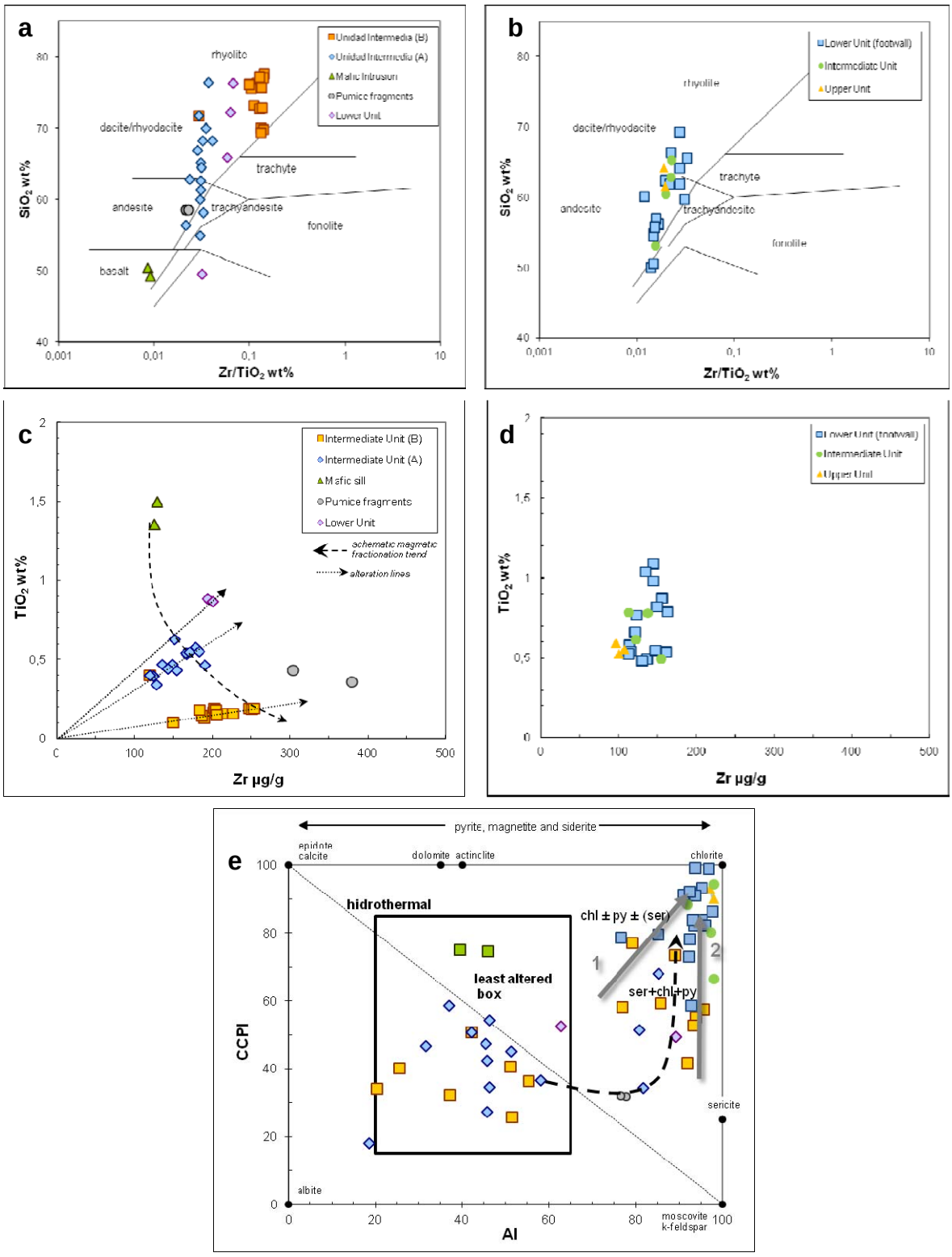

Figure 11. Geochemical diagrams of volcanic rocks of the Aznalcóllar district and Las Cruces deposit. (a) and (b) Compositional discrimination SiO_2 vs. Zr/TiO_2 diagrams for Aznalcóllar-Las Cruces samples (Winchester and Floyd, 1977). (c) Immobile element ratios diagram of Zr vs. TiO_2, showing the existence of a possible fractionation trend and alteration lines for the different units of Aznalcóllar area, and (d) a tight group for all samples of the Las Cruces deposit. (e) Bivariant Al-CCPI alteration box plot for the Aznalcóllar district and Las Cruces deposit showing the different trends of hydrothermal alteration (Large et al., 2001).

(A) and (B) in Los Frailes open pit and close to the upper contact of the massive sulphides shows a weak sericitic and chloritic alteration (Fig. 11e).

4.2. Geochemistry of the shale

As indicated in the lithostratigraphic study, shale is a rather significant component of the whole sequence and the immediate host rock to the Aznalcóllar, Los Frailes and Las Cruces orebodies. The analysis of the shale along the whole sequence reveals an important variability in some critical elements such as Fe, V, Cr, Mo and W. Mineralized shale is enriched in elements typically present in anoxic settings (e.g. V, Cr, Mo and W), but the grey and dark shale interbedded with the volcanic rocks in the hanging wall have low values. This variability could be a consequence of the hydrothermal input from the vented fluids in the basin but also could be indicative of the degree of anoxia of the environment where the massive sulphides formed.

The Mn-Fe-V and V/(V+Ni) ratios show that shale hosting the mineralization plot in the anoxic field, having the shale from the different deposits equivalent values (V/(V+Ni) = 0.73-0.89, Las Cruces; 0.72-0.92, Aznalcóllar; and 0.69-0.88, Los Frailes). This anoxic setting is also confirmed in the Mn and Fe plots, which also show that most of the shale plots in the suboxic to anoxic fields (Fig. 11b). However, these redox conditions are different in the barren shale in the units above the massive sulphides, where sub-oxic to oxic conditions are established (Fig. 12a and b). These different features confirm the evidences found in other massive sulphide deposits of the IPB. They show that the mineralization is related to local anoxic conditions that disappeared after the formation of the VMS and suggest that anoxia was established in direct relationship with the ore forming event, i.e., probably due to the input of upflowing hydrothermal fluids (Tornos et al., 2003).

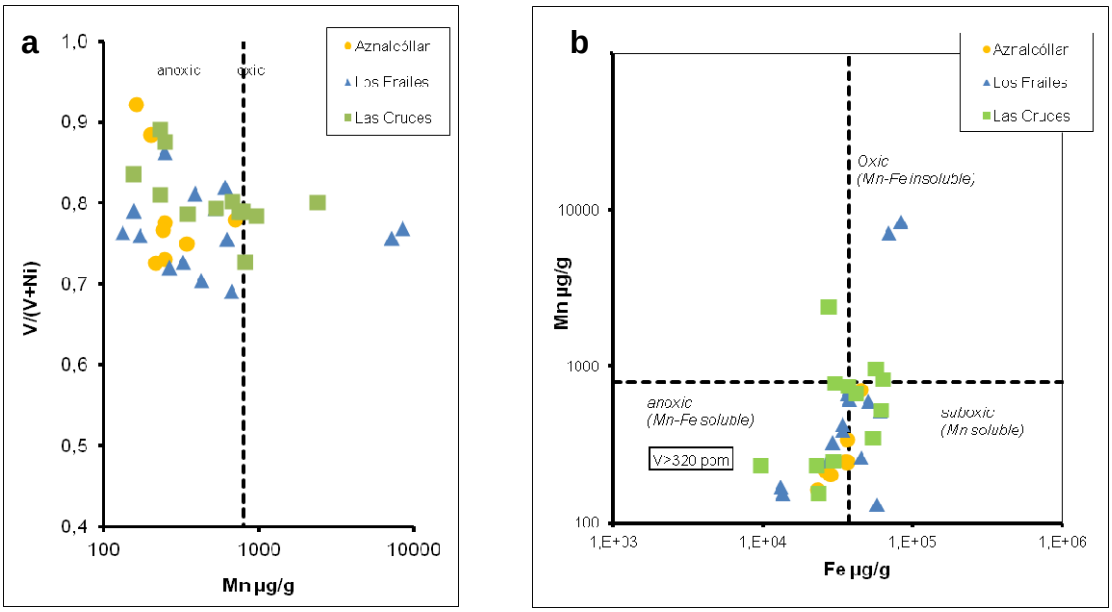

Figure 12. Geochemical plots of the shale from the Aznalcóllar-Los Frailes zone and Las Cruces deposit. (a) V/(V+Ni) vs. Mn plot indicating the redox environment of deposition of the shale; (b) Fe vs. Mn diagram showing the redox conditions of the shale on basis of Fe-Mn-V abundance (Quinby-Hunt and Wilde, 1994).

5. Evolution and interpretation of the palaeogeographic basin

The geologic evolution of the VS Complex in the SE Iberian Pyrite Belt comprises three major superimposed volcaniclastic units and some later subvolcanic intrusions (Fig. 13) that show characteristic lithological and geochemically features.

The first volcanic event (*Lower Unit*) was associated with the early formation of dacite to rhyodacite dome complex that where emplaced synchronously with the deposition of dark shale and volcaniclastic sandstone deposited below wave base. Laterally, the massive dome core facies located in the Aznalcóllar-Los Frailes zone pass to autoclastic, transported, reworked and resedimented mass flow breccia of the Las Cruces deposit. The massive sulphides are located as stratiform bodies in the shale and volcaniclastic sandstone in direct contact with the hanging wall of the dome complex, in small anoxic basins that hypothetically could correspond to zones of dome collapse or caldera. These events took place near the Devonian-Carboniferous boundary. Despite most of the mineralization is exhalative, the footwall of the deposits is interpreted as replacive in the uppermost part of the domes (see Fig. 4a and 9d).

The post-mineralizing sequence includes a second felsic volcanic event that produced the *Intermediate Unit* (A). It is composed of similar (crypto-)dome complexes intruding through a similar hosted sequence. The upper part of this unit includes abundant pumice-rich rocks product of explosive volcanism interbedded with dark and red shale revealing that they were emplaced during a change of the ambient of sedimentation in the basin. The setting changed from a deep water environment while the dark shale was deposited to a shallow water environment for the red/purple shale sedimentation. It is also supported by deposition of the peculiar pumice fragments facies, present in both areas.

The third volcanic episode is also mainly felsic and recorded by the presence of thick layers of volcanic breccia (hyaloclastite and autobreccia) associated to a third group of dacite-rhyodacite dome complexes. The sequence also includes polymictic breccia and sandstone that are interpreted as mass flows derived from different volcanic sources interbedded with fine-grained sediments that mark epochs of relative stability.

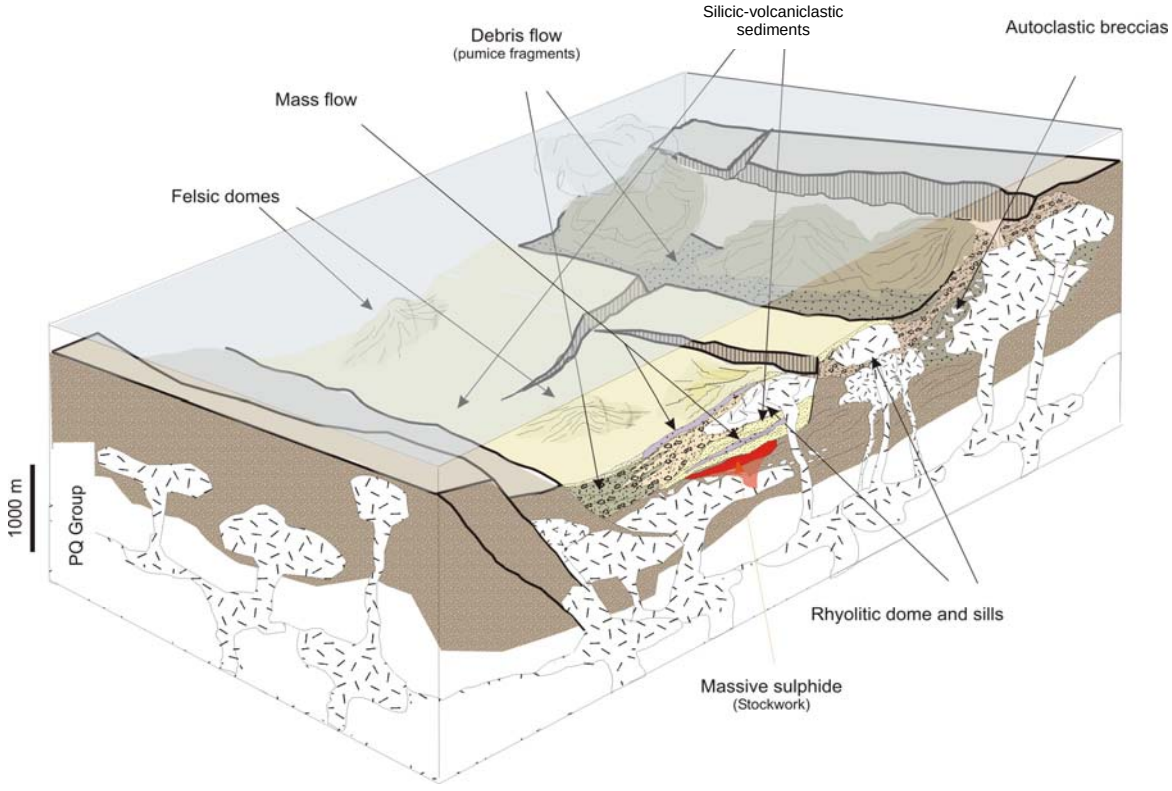

Figure 13. Schematic diagram representing the evolution of the VS Complex in the SE of the Iberian Pyrite Belt.

The sequence is capped by a late felsic sill complex intruding in a sequence dominated by dark, grey and purple shale interbedded with volcaniclastic sandstone and breccia, many of the contacts are peperitic suggesting that the sills intruded unconsolidated sediments deposited in a shallow water environment and variable oxidizing.

6. Conclusions

The detailed geological and geochemical study of the host sequence of the massive sulphides in the SE Iberian Pyrite Belt shows that the massive sulphides are hosted by a rather constant volcanic sequence and both the ore horizon and the environment of formation were the same at the district scale. The sequence is complex and includes several (crypto-)domes of dacite to rhyodacite with associated hyaloclastite, interbedded with volcaniclastic aprons of breccia and sandstone, siltstone and several thick shale units. The sequence was formed during three main superimposed volcanic events and later subvolcanic intrusions. The exhalative and replacive massive sulphides are located as stratiform bodies in the anoxic shale and volcaniclastic sandstone that cap the earliest dome complex. The post-mineralizing sequence includes two felsic volcanic episodes delimited by peculiar pumice-rich rocks, which form a marker level at the district scale. The sequence is capped by a late felsic sill complex intruding in a sequence dominated by shale interbedded with volcaniclastic rocks. The shale hosting the massive sulphides was formed in an anoxic setting while the other shale present all around the sequence was formed in sub-oxic to oxic conditions.

The volcanic sequence hosts rocks from basalt-andesite to rhyodacite without major compositional gaps. The original geochemistry, especially of the ore footwall sequence, has been severely modified by a superimposed hydrothermal alteration that is more conspicuous in the Las Cruces area, suggesting that the hydrothermal system was here significantly larger than that at Aznalcóllar-Las Cruces.

Acknowledgements

This work is a contribution to the Global Comparison of Massive Sulphides project (IGCP 502). The study was supported by BTE2003-0290 DGI-FEDER project and the IGME. We thank Cobre Las Cruces SA, APIRSA and Boliden for their help for handing and sampling the drill cores, and allowed land and mine access. We would like to thank Angel Maestre, Mike Doyle and Gobain Ovejero for help and especially to Jesús Fernandez for sharing his knowledge about the Aznalcóllar and Los Frailes mines.

References

Allen, R.L., 2001. Volcanic facies in VHMS districts and their use in reconstructing stratigraphy: an example from Los Frailes-Aznalcóllar, Iberian Pyrite Belt. GEODE workshop “Massive sulphide deposits in the Iberian: New advances and comparisons with equivalent systems”. Aracena (Huelva, Spain), 1-3.

Almodóvar, G.R., Sáez, R., Pons, J.M., Maestre, A., Toscano, M., Pascual, E., 1998. Geology and genesis of the Aznalcóllar massive sulphide deposits. Iberian Pyrite Belt, Spain. Mineralium Deposita 33, 111-136.

Barrett, T.J., MacLean, W.H., 1999. Volcanic sequences, lithogeochemistry, and hydrothermal alteration in some bimodal volcanic-associated massive sulphide systems. In: Barrie, C.T., Hannington, M.D. (Eds.) Volcanic-associated massive sulphide deposits: processes and examples in modern and ancient settings. Reviews in Economic Geology 8, 101-131.

Barrie, C.T., Amelin, Y., Pascual, E., 2002. U-Pb geochronology of VMS mineralization in the Iberian Pyrite Belt. Mineralium Deposita, 37, 684-703.

Blake, C., 2008. Themineralogical characterization and interpretation of a precious metalbearing fossil gossan, Las Cruces, Spain. PhD Thesis. Cardiff University, 330 pp.

Busby-Spera, C.J., White, J.D.L., 1987. Variation in peperite textures associated with differing host-sediment properties. Bulletin of Volcanology 49, 765-775.

Capitán, M.A., 2006.Mineralogía y Geoquímica de la alteración superficial de depósitos de sulfuros masivos en la Faja Pirítica Ibérica. PhD Thesis. Universidad de Huelva, 260 pp.

Conde. C., Tornos, F., Fernández, J. Doyle, M., 2003. Encuadre estratigráfico de los sulfuros masivos de la parte suroriental de la Faja Pirítica: Aznalcóllar-Los Frailes, y Las Cruces. Boletín Sociedad Española de Mineralogía 26, 161-162.

Conde, C., Tornos, F., Doyle, M., 2007. Geology and lithogeochemistry of the unique Las Cruces VMS deposit, Iberian Pyrite Belt. In: Andrew, C.J. et al. (Eds.) Digging Deeper, Biennial SGA Meeting, Dublin, (Ireland), 1101-1104.

Coullaut, J.L., Soler, M., Antón, J.A., 1975. Investigación de piritas y sulfuros complejos en la zona de Aznalcóllar. Jornadas Minero-Metalúrgicas, Bilbao, 2, 155-178.

Donaire, T., Sáez, R., Pascual, E., 2002. Rhyolitic globular peperites from the Aznalcóllar mining district (Iberian Pyrite Belt, Spain): physical and chemical controls, Journal of Volcanology and Geothermal Research 114, 119-128.

Doyle, M. (1996): Las Cruces copper project, Pyrite Belt, Spain: Boletín Geológico Minero, 107, 681-683.

Doyle, M., Moissey, C., Sharp, G., 1998. Discovery of the Las Cruces massive sulfide deposit, Andalucia, Spain. Pathways'98 Extended Abstracts. Society of Economic Geologist, Denver: 108-110.

Doyle, M., Morrissey, C., Sharp, G., 2003: The Las Cruces Orebody, Seville province, Andalucia, Spain, in The Geology and genesis of Europe's major base metal deposits, Kelly, C. G. et al. eds., Dublin, Irish Association for Economic Geology, 381-390

Gonzalez, F., 2005. Las pizarras negras del límite Devónico/carbonífero de la Faja Pirítica Ibérica (S.O. de España). Estudio bioestratigráfico e implicaciones sobre la paleogeografía de la cuenca y el origen de las mineralizaciones de sulfuros. Tesis Doctoral. Facultad de Ciencias Experimentales, Departamento de Geología, Área de Estratigrafía, Universidad de Huelva, 200 pp

Hernández Enrile, J.K., 1981. Marco geológico estructural de los yacimientos de sulfuros de Aznalcóllar (Región Oriental de la banda Pirítica Ibérica). Reunión de Xeología e Minería do Noroeste peninsular.

Hofstetter, J.P., 1980. L'amas sulfuré á Cu-Pb-Zn d'Aznalóllar (Sevilla), Espagne. Géologie, Paléogéographie et Métallogénie de l'extremité sud-orientale de la Ceinture Sud-Ibérique. Thése 3e Cicle. Université Pierre et Marie Curie, París, 192 pp

Hofstetter, J.P., Lécolle, M., Stoppel, D., 1979. Découverte et datation d'une faune du Viséen inférieur dans les calcaires du sud-est d'Aznalcóllar (Sevilla), Espagne. Conséquences pour l'intérpr- etation métallogénique del'amas sulfuré voisin. CR Acad Sci Paris 288, 855-858

IGME, 1978. Mapa Geológico de España, escala 1:50000, Hoja n° 961: Aznalcóllar

Julivert, M., Fontboté, J.M., Ribeiro, A., Conde, L.N., 1974. Mapa Tectónico de la Península Ibérica, Baleares y Canarias, Instituto Geológico y Minero de España, 1-110.

Knight, F.C., 2000. The mineralogy, geochemistry and genesis of the secondary sulphide mineralization of the Las Cruces deposit, Spain. PhD Thesis. Cardiff, University of Wales, 434 pp.

Large, R.R., Gemmell, J.B., Paulick, H., 2001. The alteration box plot –a simple approach to understanding the relationship between alteration mineralogy and lithogeochemistry associated with volcanic-hosted massive sulphide deposits. Economic Geology 96, 957-971

Lentz, D.R., 1999. Petrology, geochemistry, and oxygen isotope interpretation of felsic volcanic and related rocks hosting the Brunswick 6 and 12 massive sulfide deposits (Brunswick Belt), Bathurst mining camp, New Brunswick, Canada. Economic Geology 94, 57-86.

MacLean, W.H., Barrett, T.J., 1993. Lithogeochemical techniques using immobile elements. Journal of Geochemical Exploration 48, 109-133.

McDonough, W.F., Sun, S.S,. 1995. Composition of the Earth. Chemical Geology 120, 233-253.

Mitjavila, J., Martí, J., Soriano, C., 1997. Magmatic evolution and tectonic setting of the Iberian Pyrite Belt volcanism. Journal of Petrology 38, 727– 755.

Moreno, C., 1993. Post-volcanic Paleozoic of the Iberian Pyrite Belt: an example of basin morphologic control on sediment distribution in a turbidite basin. Journal of Sedimentary Petrology 63, 1118-1128.

Moreno, C., Sierra, S., and Saez, R., 1996. Evidence for catastrophism at the Famennian-Dinantian boundary in the Iberian Pyrite Belt, in Strogen, P., Somervilee, I. D., and Jones, G. L., eds., Recent advances in Lower Carboniferous Geology, 107. Special Publication, Geological Society London, p. 153-162.

Pererira, M.F., Chichorro, M., Williams, I.S., Silva, J.B., 2008. Zircon U-Pb geochronology of paragneisses and biotite granites from the SW Iberia Massif (Portugal): evidence for a paleogeographic link between the Ossa-Morena Ediacaran basins and the West African craton. In: Ennih, N., Liégois, J.P. (Eds.), The Boundaries of the West African Craton. Geologic Society, 297 p. Spec. Publ. London, 385-408.

Tornos, F., 2006. Environment of formation and styles of volcanogenic massive sulphides: The Iberian Pyrite Belt. Ore Geology Reviews 28, 259-307.

Tornos, F., Velasco, F., Miguelez, N.G., Escobar, J.M., 2013. Polyphase secondary alteration and the formation of complex Cu and Pb-Ag-Au-rich assemblages, Las Cruces copper deposit, SW Spain Mineral Deposit Research for a High Tech World - 12th SGA Biennial Meeting 2013. SGA, Uppsala, 587-589.

Tornos, F., Velasco, F., Escobar, J.M., Gomez, C., 2015. The role of geothermal activity in the upgrade of secondary copper ores, Las Cruces (Iberian Pyrite Belt) In: AS A-M, M C, Ph M, E P, S S (eds) From Source, Transport and Metal deposits to Mineral Resources in a Sustainable World. Proceeding of the 13th Biennial SGA Meeting, 24-27 August 2015, Nancy, France. Nancy, 1201-1204.

Munhá, J., 1979. Blue amphiboles, metamorphic regime and plate tectonic modelling in the Iberian Pyrite Belt. Contribution to Mineral and Petrology 107, 153-162.

Munhá, J., 1983. Hercynian magmatism in the Iberian Pyrite Belt. Memorias Servicio Geológico Portugal 29, 39–81.

Munhá, J., 1990. Metamorphic evolution of the South Portuguese/Pulo do Lobo Zone. In: Dallmeyer R.D. and Marínez García E. (Eds.) PreMesozoic Geology of Iberia. SpringerVerlag, Berlín, 363-368.

Nesbitt, R.W., Pascual, E., Fanning, C.M., Toscano, M., Sáez, R., Almodóvar, G.R., 1999. U\Pb dating of stockwork zircons from the eastern Iberian Pyrite Belt. J. Geol. Soc. (London, U.K.) 156, 7–10.

Oliveira, J.T., Quesada, C., 1998. A comparison of stratigraphy, structure and paleogeography of the South Portuguese Zone and Southwest England, European Variscides Geoscience in south-west England (The Scott Simpson Lecture, Annual Conference of the Ussher Society 1998, 141-159.

Oliveira, J.T., 1990. South Portuguese Zone: introduction. Stratigraphy and synsedimentary tectonism. In: Dallmeyer, R.D., Martínez García, E. (Eds.), PreMesozoic Geology of Iberia. Springer Verlag, 333– 347.

Oliveira, J.R., 1983. The marine Carboniferous of south Portugal: a stratigraphic and sedimentological approach. In: Sousa, L.,D., Oliveira, J.T., (Eds), The Carboniferous of Portugal. Memórias dos Serviços Geológicos de Portugal 29, 3-37.

Oliveira, J. T., Relvas, J., Pereira, Z., Matos, J., Rosa, C., Rosa, D., Munhá, J. M., Jorge, R., Pinto, A., 2006). O Complexo Vulcano-Sedimentar da Faixa Piritosa: estratigrafia, vulcanismo, mineralizações associadas e evolução tectono-estratigráficano contexto da Zona Sul Portuguesa. *In*: *Geologia de Portugal no contexto da Ibéria.* Dias, R., Araújo, A., Terrinha, P. & Kullberg, J.C. (eds). Univ. Évora, Évora, 207-243.

Onézime, J., Charvet, J., Faure, M., Bourdier, J. L., and Chauvet, A., 2003. A new geodynamic interpretation for the South Portuguese Zone (SW Iberia) and the Iberian Pyrite Belt genesis: Tectonics 22, 1–17.

Onézime, J., Charvet, J., Faure, M., Chauvet, A., Panis, D., 2002. Structural evolution of the southernmost segment of the West European Variscides: the South Portuguese zone (SW Iberia): Journal of Structural Geology 24, 451–468.

Pascual, E., Ruiz de Almodóvar, G., Sáez, R., Toscano, M., Donaire, T., 1994. Petrología y geoquímica de tobas vítreas del área de Aznalcóllar (Faja Pirítica Ibérica). Boletín Sociedad Española de Mineralogía 17, 155-156

Pereira, Z., Saez, R., Pons, J.M., Oliveira, J.T., Moreno, C., 1996: Edad devónica (Struniense) de las mineralizaciones de Aznalcóllar (Faja Pirítica Ibérica) en base a palinología. Geogaceta, 20-7,1609-1612.

Pinedo, I., 1963. Piritas de Huelva. Su historia, minería y aprovechamiento. Summa Editorial, Madrid. 1003 pp.

Quesada, C., 1991. Geological constraints on the Paleozoic tectonic evolution of tectonostratigraphic terranes in the Iberian Massif. Tectonophysics 185, 225-145

Quesada, C., 1996. Estructura del sector español de la Faja Pirítica Ibérica: implicaciones para la exploración de yacimientos. Boletín Geológico y Minero 107, 265-278.

Quesada, C., 1998. A reappraisal of the structure of the Spanish segment of the Iberian Pyrite Belt. Mineralium Deposita 33, 31-44.

Quinby-Hunt, M.S., Wilde, P., 1991. The provenance of low-calcic black shales. Mineralium Deposita 26, 113-121.

Rosa, D.R.N., Invierno, C.M., Oliveira, V.M.J., Rosa, C.J.P., 2004. Geochemistry of volcanic rocks, Albernoa Area, Iberian Pyrite Belt, Portugal. International Geology Review 46, 366-383.

Routhier, P., Aye, F., Boyer, C., Lecolle, M., Moliere, P., Picot, P., and Roger, G., 1980, Le ceinture sud-iberique a amas sulfures dans sa partie espagnole mediane: Memoire Bureau Recherches Geologiques Minieres 94, 265 p.

Sáez, R., Almodovar, G. R., Pascual, E., 1996. Geological constraints on massive sulphide genesis in the Iberian Pyrite Belt. Ore Geology Reviews 11, 429-451.

Sánchez España, F.J., 2000. Mineralogía y geoquímica de los yacimientos de sulfuros masivos en el área Nor-Oriental de la Faja Pirítica Ibérica, San Telmo–San Miguel–Peña del Hierro, Norte de Huelva, España. Unpublished Ph.D. thesis. Universidad del País Vasco, 307 pp.

Schermerhorn, L.J.G., 1971. An outline of the stratigraphy of the Iberian Pyrite Belt. Boletín Geológico y Minero 82, 239-268.

Sierra, J., 1984a. Geología, Mineralogía y Metalogenia del Yacimiento de Aznalcóllar. (Primera parte: Litoestratigrafía y Tectónica). Boletín Geológico y Minero 95, 440-455.

Sierra, J., 1984b Geología, mineralogía y metalogenia del yacimiento de Aznalcóllar (Segunda parte: Mineralogía y sucesioón mineral). Boletín Geológico y Minero 95, 553-568.

Sierra, J., Gumiel, P., Arribas, A., 198. Geología, mineralogía y metalogenia del yacimiento de Aznalcóllar (Tercera parte: Metalogenia). Boletín Geológico y Minero 96, 23-30.

Silva, J.B., Oliveira, J.T. Ribeiro, A., 1990. Structural outline of the South Portuguese Zone. In: Dallmeyer, R.D., Martínez García, E. (Eds.) Pre-Mesozoic Geology of Iberia. Springer-Verlag, Verlin, 348-362.

Soriano, D., Martí, J., 1999. Facies analysis of volcano-sedimentary successions hosting massive sulfide deposits in the Iberian Pyrite Belt, Spain. Economic Geology 94, 867-882.

Soriano, C., 1997. Vulcanisme i estructura de la Faja Piritica Iberica. Zona Sud Portuguesa Tesis Doctoral. Universitat de Barcelona (Spain), 265 pp.

Strauss, G.K., 1970. Sobre la geología de la provincia piritífera del suroeste de la Península Ibérica y de sus yacimientos, en especial sobre la mina de pirita de Lousal (Portugal). Mem. IGME 77, 266 pp

Thiéblemont, D., Pascual, E., Stein, F., 1998. Magmatism in the Iberian Pyrite Belt: petrological constrains on a metallogenic model. Mineralium Deposita 33, 259-307.

Tornos, F., 2006. Environment of formation and styles of volcanogenic massive sulphides: The Iberian Pyrite Belt. Ore Geology Reviews 28, 259-307.

Tornos, F., Velasco, F., Menor-Salván, C., Delgado, A., Slack, J.F., Escobar, J.M., 2014. Formation of recent Pb-Ag-Au mineralization by potential sub-surface microbial activity. Nature Commonictions 1-8.

Toscano, M., Sáez, R., Almodóvar, G.R., 1997. Evolución de los fluidos hidrotermales en la génesis de los sulfuros masivos de Aznalcóllar, Faja Pirítica Ibérica. Evidencias a partir de las inclusiones fluidas. Geogaceta 21, 211 –214.

Valenzuela, A., Donaire, R., Pascual, E., 2002. Secuencia de facies volcánicas en el área del río Odiel (Faja Pirítica Ibérica, España). Geogaceta 32, 131-134.

Velasco, F., Herrero, J.M., Suárez, S., Yusta, I., Alvaro, A., Tornos, F., 2013. Supergene features and evolution of gossans capping massive sulphide deposits in the Iberian Pyrite Belt. Ore Geology Reviews 53, 191-203.

Winchester, J.A., Floyd, P.A., 1977 Geochemical discrimination of different magma series and their differentiation products using immobile elements. Chemical Geology 20, 325-343.

Yesares, L., Ruiz de Almodóvar, G., Nieto, J.M., Sáez, R., Aiglsperger, R., Proenza, J.A., Gómez, C., Escobar, J.M., 2014. Mineralizaciones de oro en el depósito de Las Cruces, Faja Pirítica Ibérica. Macla 19.

Yesares, L., Aiglsperger, R., Sáez, R., Ruiz de Almodóvar, G., Nieto, J.M., Proenza, J.A., Gómez, C., Escobar, J.M., 2015. Gold behavior in supergene profiles under changing redox conditions: the example of the Las Cruces deposit, Iberian Pyrite Belt. Economic Geology 110, 2109-2126

CAPITULO IV

Laser Ablation-ICPMS analysis of trace elements in pyrite from the Tharsis massive sulphide deposit, Iberian Pyrite Belt (Spain).

Análisis de elementos traza por LA-ICPMS en pirita del depósito de Tharsis, Faja Pirítica (España)

Abstract

The high sensitivity Laser Ablation Inductively Coupled Plasma Mass Spectrometry (LA-ICPMS) has been utilized in the determination of trace elements in pyrite from the Tharsis VMS deposit, one of the most significant ore deposits in the southern Iberian Pyrite Belt. The study tracks the content and distribution of trace elements within the different facies of the massive sulphide orebody. Enrichment of elements such as Cu, Zn and Pb is interpreted to be due to the presence of nanoinclusions of chalcopyrite, sphalerite and galena, respectively. A second group of elements, including As, Au, Tl, Mn and Mo, shows significant chemical variations according to the type of mineralization and textural evolution of the pyrite. This behaviour is thought to be due to the fact that these metals are included in the lattice and controlled by the degree of crystallinity, the temperature and the redox conditions during the ore forming process. Early, spongiform and colloform pyrite is enriched in As and Au and interpreted to have formed from a high temperature and low fS_2 fluid in the stockwork zone; the pyrite of this facies has high Co contents. Tl, Mn and Mo are enriched in pyrite precipitated at lower temperature and higher oxidation state, i.e., in the exhalative part of the system. In general, both Co and Ni show an irregular distribution and do not have the sympathetic distribution observed in equivalent studies.

keywords: trace elements, Tharsis, massive sulphide, Iberian Pyrite Belt, LA-ICPMS

1. Introduction

Pyrite is the most common mineral in volcanogenic massive sulphide (VMS) deposits worldwide (Franklin et al., 1981, 2005; Lydon, 1988). This is especially relevant in the shale-hosted deposits of the southern Iberian Pyrite Belt (IPB), among which the giant Tharsis deposit (> 100 Mt) is one of the best examples. The deposit comprises several lensoidal sulphide bodies that are composed of >95% fine-grained pyrite with locally abundant sedimentary textures (Tornos et al., 1998).

Pyrite contains significant amounts of trace elements, both as mineral inclusions and as substitutions in its crystal structure, which can be detected and measured despite their low concentration levels by laser ablation inductively coupled plasma mass spectrometry (LA-ICPMS). The concentration and distribution of these components may serve as a sensitive proxy for variations in the geochemical conditions that prevailed during sulphide precipitation. They can be also used in mineral exploration and in the development of genetic models for mineral deposits (Huston et al., 1995; Raymond, 1996; Maier et al., 2005; Yamaguchi & Ohomoto, 2006; Large et al., 2009; Maslennikov et al., 2009; Koglin et al., 2010; Zhao et al., 2011).

In this paper, we present the first study of trace elements in pyrite from the Spanish sector of the IPB. Pyrite was analysed by LA-ICPMS combining a micro-solid laser ablation sampling system (LA) with a high sensitivity multi-element ICPMS. This is a modern microanalytical technique that yields much lower detection limits and much higher spatial resolution (e.g., Cook et al., 2009a, 2009b; Large et al., 2009; Koglin et al., 2010), that alternative available methods (e.g., electron microprobe, Huston et al., 1995; Belcher et al., 2004; Chouinard et al., 2005; or energy dispersive spectrometry (SEM) McClenanghan et al. 2004). For this, LA-ICPMS technique is an excellent analytical tool in order to improve our understanding of pyrite genesis and evolution.

Previous studies concerning massive sulphide deposits from similar metallogenic provinces and deposits such as Urals (Maslennikov et al., 2009); Kidd Creek (Canada) (Cabri et al., 1985) Queensland and Tasmania (Smith, 1992; Huston et al., 1995; Raymond, 1996), Bathurst Mining Camp (McClenaghan et al., 2004, 2009; Conde et al., 2008) and Neves Corvo, in the Portuguese sector of the Iberian Pyrite Belt (Serranti et al., 2002), have shown the importance of trace element distribution in pyrite, chalcopyrite and sphalerite as a geochemical tracer. This study provides the trace elements variations in pyrite from the different part of the massive sulphide to improve and support the peculiar genesis of Tharsis volcanic-hosted massive sulphide.

2. Geological setting of the Tharsis massive sulphide

The Tharsis deposit (Filón Norte orebody), with original reserves of over 100 Mt at 0.5 Cu %, 0.6 Pb %, 2.7 % Zn, 22 g/t Ag and 0.7 g/t Au (Tornos, 2006), is one of the most important deposits in the Iberian Pyrite Belt that with more than 2,500 Mt is considered as the major concentration of massive sulphide deposits in the world (Leistel et al., 1998b; Tornos, 2006). The deposit, located in the southern IPB (Fig. 1), is situated at the base of the Volcano-Sedimentary Complex (VS Complex) interbedded with shale and directly overlying the siliciclastic Phyllite-Quartzite (PQ) Group (shale and quartz sandstone) (Tornos et al., 1998; Tornos 2006). Particularly, the VS Complex in Tharsis is composed by a monotonous dark shale-rich sequence (Tharsis Fm.) tectonically overlayed by mafic and felsic volcanic rocks (Tornos et al., 1998; Tornos and Conde, 2002; Tornos et al. 2008) (Figure 1b and 1c). There are no volcanic rocks interbedded with the massive sulphides, although laterally away from the deposit, the mineralized stratigraphic levels are marked by thin felsic volcaniclastic beds. Below the massive sulphides there is an irregular and thick feeder zone or stockwork, up to 200 m thick, hosted by a zone of chlorite-rich hydrothermal alteration that transgresses both the lowermost VS Complex and the PQ Group (Figure 1c).

The Filón Norte massive sulphide ore (Figure 2a) forms a thick lens (≈ 130 m) that is comprised of tectonically stacked units of what was originally a single large sheet-like massive sulphide body (ca. 20x4 km^2) (Tornos et al., 1998). In detail, the mineralization is made up of (Figure 1d): (1) dominant monotonous *fine-grained pyrite* (< 400 μm) intergrown with minor amounts of chalcopyrite, sphalerite, galena, siderite, quartz, chlorite and other accessory minerals; (2) small and thin *conglomerate* beds that include subrounded clasts of massive sulphide and shale supported by fine-grained pyrite, that likely correspond to local debris flows (Figure 2b); (3) matrix-supported breccia with finely laminated pyrite, sphalerite and siderite in cm-sized angular fragments supported by coarse grained pyrite and siderite, occurring in the basal part of the deposit (*carbonate ore*) (Figure 2c); (4) the *laminated ore*, located in the uppermost part and in the contact with the hanging wall shale. It is made up of alternating shale and pyrite with abundant sedimentary structures (laminations, graded bedding, slumps, etc.) sometimes related to syn-sedimentary faults (Figure 2d) and beneath siliceous shale alternating with white and grey chert (Figure 2e); and, (5) the stockwork that consists in irregular veins composed by pyrite, minor quartz, Co-As-Fe-S minerals, and trace Bi-Pb-Cu-(Sb) sulphosalts, tellurides and native gold (Figure 2f) (Marcoux et el., 1996; Tornos et al., 1998) in chloritized shale.

3. Analytical methods

The analysis of trace elements in pyrite was carried out on the LA-ICP MS facility at the CODES Ore Deposit Research Centre (Hobart, Australia). Trace elements were analysed via LA-ICPMS of spots 80 μm wide and 90 μm deep on pyrite grains larger than 150 μm. The total analytical run times were between 90 to 100 s, with background integration times of 30-35 s and 40-45 s for real ablation data or laser on (Figure 3). Data were collected for 21 elements; ^{47}Ti, ^{51}V, ^{55}Mn, ^{57}Fe, ^{59}Co, ^{60}Ni, ^{65}Cu, ^{66}Zn, ^{75}As, ^{90}Zr, ^{95}Mo, ^{107}Ag, ^{111}Cd, ^{118}Sn, ^{121}Sb, ^{125}Te, ^{139}La, ^{197}Au, ^{205}Tl, ^{208}Pb and ^{209}Bi, corresponding to 2003). Further, Fe was used in the internal standard for quantification of pyrite, and the trace element

Figure 1. Geological setting maps of the Tharsis deposit. (A) Schematic map of Variscan Fold Belt in Europe (Oliveira and Quesada, 1998). (B) Detailed geological map of the Tharsis area and location of Filón Norte orebody (modified from Tornos et al., 2008). (C) General stratigraphic column of Filón Norte, Tharsis (IPB), showing the distribution of the different types of mineralization within the orebody (modified from Tornos and Conde, 2002; Tornos et al., 2008).

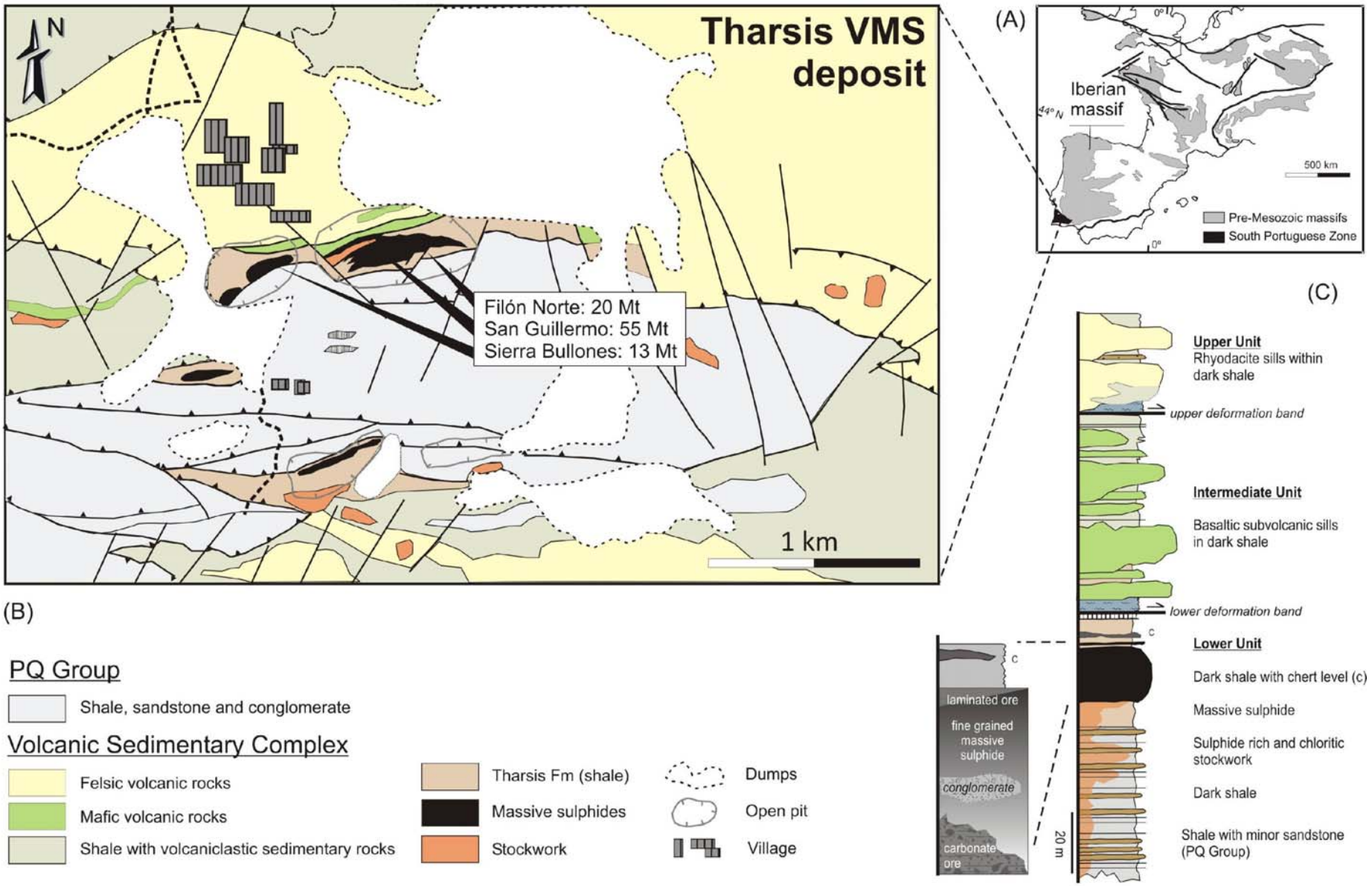
Tharsis VMS deposit
N
Filón Norte: 20 Mt
San Guillermo: 55 Mt
Sierra Bullones: 13 Mt
1 km
(A)
Iberian massif
44°N
500 km
Pre-Mesozoic massifs
South Portuguese Zone
(B)
PQ Group
Shale, sandstone and conglomerate
Volcanic Sedimentary Complex
Felsic volcanic rocks
Mafic volcanic rocks
Shale with volcaniclastic sedimentary rocks
Tharsis Fm (shale)
Massive sulphides
Stockwork
Dumps
Open pit
Village
(C)
Upper Unit
Rhyodacite sills within dark shale
upper deformation band
Intermediate Unit
Basaltic subvolcanic sills in dark shale
lower deformation band
Lower Unit
Dark shale with chert level (c)
Massive sulphide
Sulphide rich and chloritic stockwork
Dark shale
Shale with minor sandstone (PQ Group)
c
laminated ore
fine grained massive sulphide
conglomerate
carbonate ore
20 m

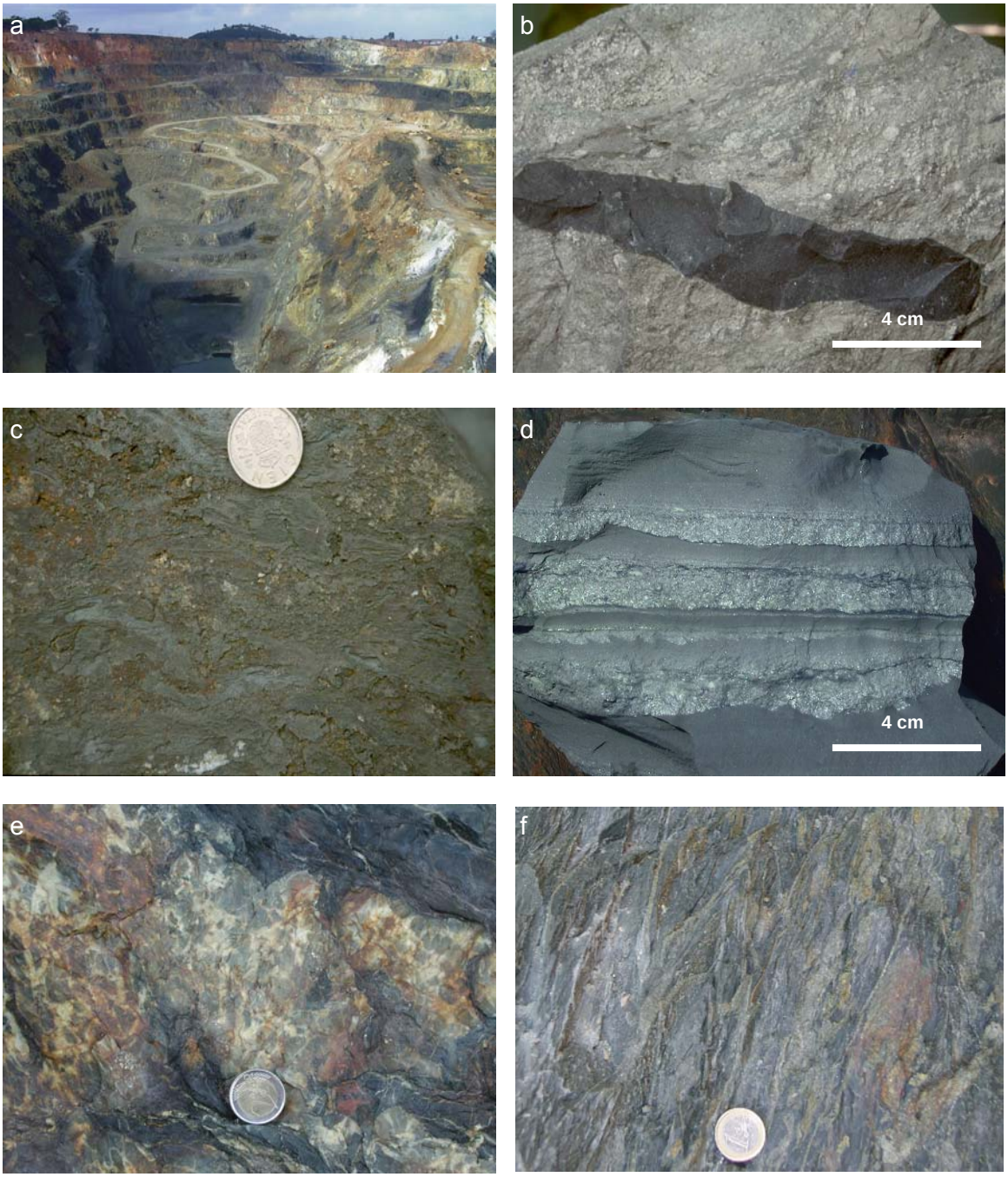

Figure 2. Representative photographs from outcrops on the Filón Norte orebody, Tharsis deposit. (a) Overview of Filón Norte open pit (Tharsis). (b) Large clast of siliceous shale supported by fine-grained pyrite in the conglomerate ore. (c) *Carbonate ore* showing fragments of fine alternating layers of siderite and sulphides (dominantly pyrite) cemented by coarse-grained pyrite + siderite (coin size, 2 cm). (d) Representative sample of the *laminated ore* showing a layering that includes shale with local replacement by ankerite in its uppermost part, fine-grained breccia similar to the carbonate ore; and finely layered pyrite with graded bedding. (e) Silicified shale in the hanging wall of the massive sulphides with lenses of chert (coin size, 2.5 cm). (f) Chloritized dark shale containing thin and irregular quartz and sulphide veins (stockwork) (coin size, 2.3 cm).

contents of the internal standard STDGL-1 (a borate glass with sulphide powered) as primary calibration standard (Norman et al., 1998; Danyushevsky et al., 2003). The S was calculated using the theoretical stoichiometry or the empirical formula. In order to obtain the optimum results, the standard (STDGL-1) was analyzed twice every one and fifteenth analyses to account for the instrument drift, with a 80 μm beam and at 10 Hz.

Analyses were performed on 12 polished samples representing each of the principal ore facies. Within each sample, three to five pyrite grains were selected depending on the size and quality of the sample, and in each grain we performed three analyses. In total, 105 determinations were carried out. Analyzed pyrite includes 4 grains from the laminated ore, 11 from the main fine-grained massive sulphide ore, 4 from the conglomerate ore, 13 from the carbonate ore, and 7 from the footwall stockwork (Table 1) (Appendix II).

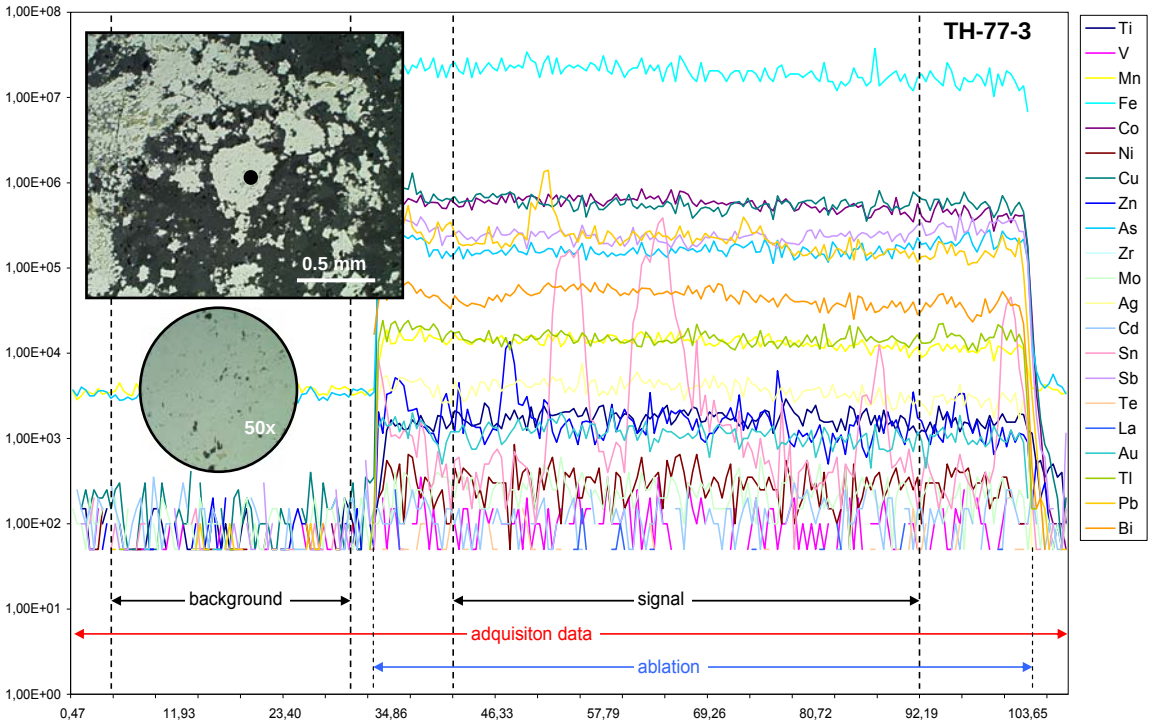

Figure 3. Representative single-spot LA-ICPMS spectra of one analyzed pyrite, showing the data acquisition times and spectra for all elements analyzed. Times is represented in the X-coordinate (in seconds), and Y-axis shows the concentration of elements (in µg/g).

Table 1. Summary of the concentrations of representative trace elements of pyrite grains from the different mineral types, from the Filón Norte ore, Tharsis deposit (Iberian Pyrite Belt). Analysis by LA-ICP MS. Concentration in µg/g**)**

		Ti	V	Mn	Co	Ni	Cu	Zn	As	Zr	Mo	Ag	Cd	Sn	Sb	La	Au	Tl	Pb	Bi
Laminated ore	*n=4*																			
	average	6.2	0.3	22.7	49.7	0.7	748.1	90.8	517.0	*<0.1*	0.8	15.7	0.3	13.2	219.5	*<0.01*	0.6	148.5	4 945.3	93.8
	max.	7.0	0.9	39.1	95.6	0.9	1 447.3	227.3	1 003.0	*<0.1*	1.9	35.6	0.5	23.8	315.0	*<0.1*	0.8	512.2	13 744.2	179.5
	min.	4.8	*<0.1*	4.4	2.2	0.4	160.2	19.4	105.0	*<0.01*	0.2	6.1	0.1	0.5	182.6	*<0.01*	0.5	3.9	1 683.0	45.7
	st. dev.	1.0	0.4	14.4	38.8	0.2	603.4	95.7	369.1	-	0.8	13.5	0.2	11.5	63.8	-	0.1	244.6	5 871.1	59.5
	>MDL (%)	100	100	100	100	100	100	100	100	100	100	100	75	100	100	100	100	100	100	100
Fine grained ms	*n=11*																			
	average	8.4	0.4	26.3	62.6	5.2	1 065.0	554.0	565.3	*<0.1*	0.6	22.1	1.5	13.9	481.5	*<0.01*	1.5	25.6	3 576.8	184.9
	max.	12.7	1.4	160.3	158.8	17.2	2 647.0	4 644.9	2 258.3	*<0.1*	3.2	116.0	10.1	94.6	1 975.6	*<0.1*	6.3	107.0	12 846.3	1 453.1
	min.	6.2	*<0.1*	4.3	0.2	0.3	55.1	1.4	6.5	*<0.1*	*<0.1*	0.1	0.2	0.2	1.8	*<0.01*	*<0.1*	*<0.1*	4.1	0.5
	st. dev.	1.7	0.4	46.5	52.5	5.6	947.8	1 371.8	658.0	-	0.9	38.4	2.9	27.1	609.6	-	1.9	43.6	3 921.9	424.6
	>MDL (%)	100	100	100	100	100	100	100	100	36	82	100	73	100	100	82	91	100	100	100
Conglomerate	*n=4*																			
	average	8.6	1.6	362.1	396.1	2.1	3 222.2	852.1	1 433.7	*<0.1*	0.3	10.0	1.8	6.0	209.5	*<0.1*	3.5	0.3	2 385.9	91.6
	max.	9.7	4.9	829.8	734.3	3.1	6 570.5	1 441.7	4 811.5	*<0.1*	0.5	16.5	2.7	10.1	308.6	*<0.1*	6.5	0.8	4 409.4	158.1
	min.	7.5	<0.1	4.4	157.4	1.3	1.6	1.1	221.9	*<0.1*	0.1	0.1	0.2	0.2	3.1	*<0.01*	*<0.1*	*<0.1*	6.9	0.2
	st. desv.	0.9	2.2	355.9	252.8	0.8	2 692.8	608.1	2 253.4	-	0.2	7.1	1.1	4.3	142.6	-	2.6	0.3	2 170.7	66.2
	>MDL (%)	100	100	100	100	100	100	100	100	75	100	100	100	100	100	75	100	100	100	100
Carbonate ore	*n=13*																			
	average	11.0	2.6	308.1	93.5	7.8	1 759.7	3 785.6	747.8	0.1	2.2	20.5	8.3	38.7	384.8	*<0.1*	2.2	32.2	3,467.3	58.8
	max.	43.7	11.9	1 348.4	260.5	40.2	4 888.8	18 297.0	3 131.0	1.4	19.2	113.5	39.3	134.2	753.3	*<0.1*	8.2	376.8	25 215.5	282.5
	min.	6.6	*<0.1*	4.5	3.3	0.5	192.9	7.2	277.4	*<0.1*	0.1	3.9	0.1	1.8	71.5	*<0.01*	0.2	0.3	133.9	19.4
	st. dev.	9.9	3.4	367.0	89.0	10.8	1 472.7	5 533.5	761.7	0.4	5.2	29.4	12.2	41.6	203.8	-	2.4	103.6	6 630.9	69.7
	>MDL (%)	100	100	100	100	100	100	100	100	77	85	100	85	100	100	85	100	100	100	100
Stockwork	*n=7*																			
	average	31.8	5.3	67.4	121.1	34.7	941.0	142.2	2 533.2	0.5	0.3	4.9	0.4	13.7	161.0	0.4	3.5	51.7	1 307.1	84.6
	max.	173.2	35.4	423.8	337.1	86.8	2 143.0	698.5	4 732.3	3.4	1.2	7.8	1.0	48.1	263.6	2.6	8.0	175.6	5 351.6	257.3
	min.	5.2	*<0.1*	2.1	8.4	0.7	185.7	3.5	1 656.6	*<0.01*	0.1	0.3	0.2	0.2	5.3	*<0.01*	1.2	*<0.1*	5.4	6.8
	st. dev.	62.4	13.3	157.3	132.2	38.0	827.1	251.8	1 223.7	1.3	0.4	2.9	0.3	19.8	101.0	1.0	2.4	81.4	1 963.4	92.0
	>MDL (%)	100	100	100	100	100	100	100	100	57	100	100	71	100	100	29	100	100	100	100

n= number of selected samples; max.= maximum; min.= minimum; st.desv.= standard deviation; >MDL(%)=percentage of analyses above the minimum detection limit

4. Evaluation and interpretation of the analytical results

Trace elements occur in pyrite in three modes: as inclusions and as stoichiometric and non-stoichiometric substitutions (Huston et al., 1995). Although inclusions exposed in the surface can be avoided, there always remains the possibility that the ablation pit intersects unobserved subsurface discrete nanoinclusions. Therefore, the samples analyzed can show an inhomogeneity ablation profile even on the single-spot scale (<100 µg/g).

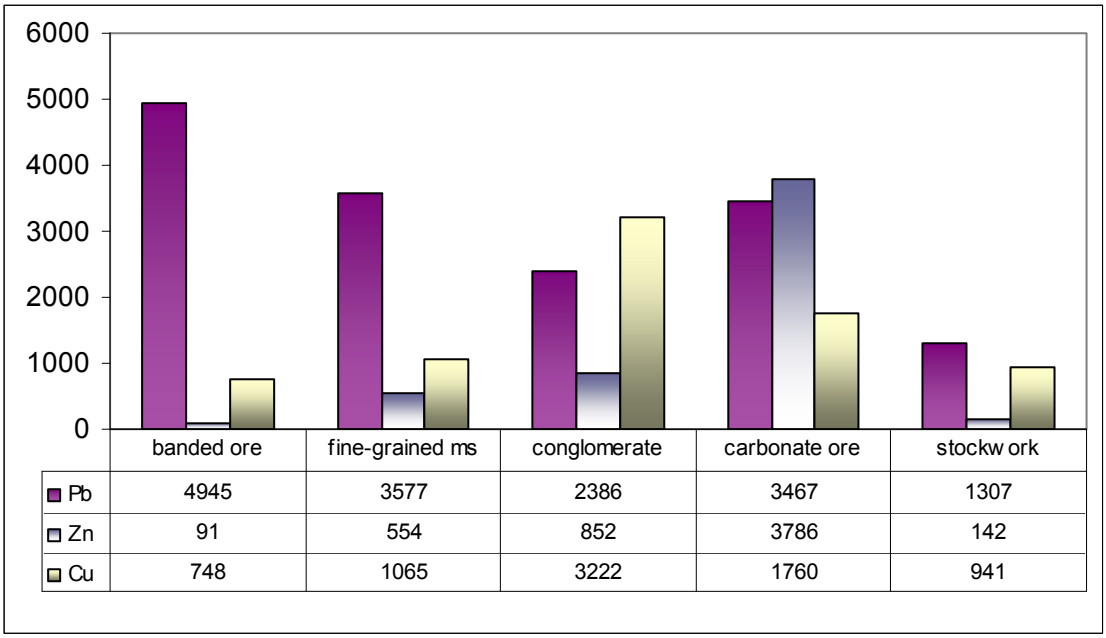

	banded ore	fine-grained ms	conglomerate	carbonate ore	stockwork
Pb	4945	3577	2386	3467	1307
Zn	91	554	852	3786	142
Cu	748	1065	3222	1760	941

Figure 4.- Histograms showing the distribution of Cu, Pb and Zn concentrations in pyrite of all mineral types from Filón Norte massive sulphide deposit. Y-coordinate indicates average value in µg/g, and dataset table shows a summary of Cu, Pb and Zn concentration (on average) in µg/g for all types of pyrite.

The contents of Cu, Pb and Zn in pyrite are erratic, but high for all ore facies (Table 2). Concentrations summarized as histograms in Figure 4 show high and variable concentrations in all the studied samples, with concentrations between 90 and 4900 µg/g; highest contents are observed in pyrite from the laminated ore, particularly in Pb (up to 5000 µg/g). However, all the analyzed pyrite grains show relatively moderate Cu (740-3230 µg/g) and Zn (90-3790 µg/g) contents. These concentrations are interpreted as reflecting of nanometer-sized sub-microscopic inclusions (<2 µm) of galena and, to a lesser extent, of chalcopyrite and sphalerite in pyrite throughout the entire deposit (Fig. 5).

Table 2. Summary of the correlation coefficients for selected trace elements in pyrite form the Filón Norte, Tharsis.

	Samples	*Ag&Pb*	*Ag&Cu*	*Pb&Bi*	*As&Au*	*Bi&Au*	*Co&Au*	*Co&Ni*	*Sn&Cu*	*Sn&Zn*
Total	41									
Banded ore	4	***0.98***	0.35	***0.95***	***0.64***	-0.18	-0.79	***0.92***	0.44	-0.60
Fine-grained ms	11	***0.90***	0.44	0.40	-0.12	***0.80***	0.02	0.31	0.58	***0.98***
Conglomerate	4	0.47	***0.98***	0.41	***0.76***	***0.99***	0.38	***0.72***	***0.90***	***0.94***
Carbonate ore	13	***0.95***	-0.32	***0.97***	***0.89***	-0.03	-0.22	0.01	0.31	-0.09
Stockwork	7	0.61	0.66	-0.394	-0.14	***0.94***	***0.73***	0.42	***0.78***	0.63

They seem to be a relationship between the concentrations of base metals and the texture in pyrite. The highest Cu, Zn and Pb values, on average, occur in early pyrite with spongiform and framboidal morphology or composed of aggregates of fine-grained euhedral crystals. In contrast, the Cu, Pb and Zn contents of individual and large euhedral crystals are never greater than 70 µg/g, probably because the microinclusions have been taken out by recrystallization events and coalesced in larger inclusions or individual grains (Large et al., 2009; McClenaghan et al., 2009). The basic correlation matrix between the analyzed elements shows that there is a strong general correlation between Pb and Ag in pyrite ($r = 0.98$, see Fig. 6a), except in the conglomerate facies wherein the Ag concentration is mainly positive correlated with that of Cu (Table 2). These relationships suggest that galena is of the dominant carrier of silver in the whole deposit except in the conglomerate facies that is a Ag-rich fahlore (freibergite?). The laminated ore and the carbonate ore show a positive correlation between Pb and Bi ($r > 0.9$, Figure 6b), possibly due to the presence of inclusions of Pb-Bi sulphosalts, such as wittichenite.

Arsenic is the most pronounced non-stoichiometric substitution in pyrite of this study. The highest As concentrations occur in pyrite from the stockwork, but are also occasionally high in the conglomerate and the massive sulphide facies (Figure 7). In the stockwork, the As content of pyrite ranges from 1650 to 4730 µg/g (Table 1), among which

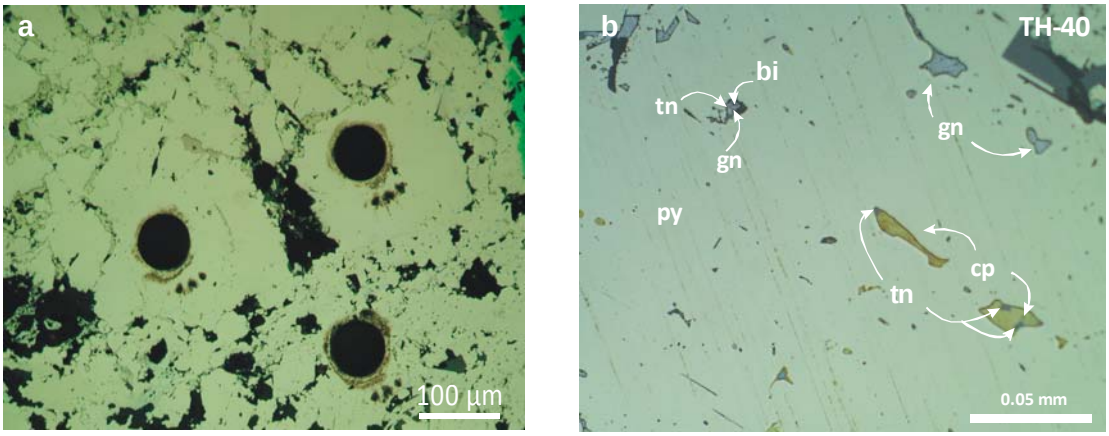

Figure 5. Reflected-light photomicrographs of pyrite from Filón Norte, Tharsis. (a) Example of subhedral hydrothermal pyrite abladed by laser ablation. (b) Subhedral pyrite showing microinclusions of galena, chalcopyrite, Pb-Bi sulphosalts and/or bismuth and tennantite-tetrahedrite (TH-40: carbonate ore). (Mineral abbreviations from: *http://www.unige.ch/sciences/terre/mineral/fontbote/opaques/ore_abbreviations.html*)

the highest values are recorded from the framboidal and colloform pyrite. Arsenic has been shown in previous VMS mineralogic studies to have a correlated between gold and trace elements (e.g., Cook and Chryssoulis, 1990; McClenaghan et al., 2004, 2009; Reich et al., 2005; Large et al., 2009). Here, the gold content of pyrite ranges from 1 to 8 µg/g (Table 1). Data from pyrite of the laminated ore, conglomerate and carbonate ore show a positive correlation between As and Au (Table 2), in contrast it is negative in pyrite from the fine-grained massive sulphide and the stockwork. Positive correlation is typical in the As-rich pyrite which usually occurs in the mineral assemblage of the Iberian Pyrite Belt massive sulphide deposits. The relationship between As enrichment and Au in pyrite is probably due to quick supersaturation of early pyrite formed at relatively low sulphur fugacities at high (>300ºC) temperatures. Rapid precipitation of pyrite led to both the colloform texture and to the incorporation of As and Au in the immature pyrite lattice. The As substitution for S^{2-} in the pyrite structure within sulphur-deficient conditions makes arsenical pyrite that occurs as metastable solid solution $Fe(As,S)_2$ (Huston et al., 1995) Regarding the negative correlation, some authors suggest a pattern association involving Au and Te that could be interpreted by presence of micro-inclusions of Au-bearing

tellurides (Maslennikov et al., 2009), which have not observed in the massive sulphides at Tharsis (Leistel et al., 1998a) Only a telluride mineral, joseite ($Bi_4(S,Te)_3$) has been identified in the stockwork (Marcoux et al., 1996; Tornos et al., 1998). Otherwise, the fine-grained massive sulphide and the stockwork have positive Bi and Au and Co and Au correlations (Table 2). Also, the conglomerate facies shows a good relationship between Bi and Au (r = 0.99). In this case, these data are supported by the presence of microinclusions of cobalt-bearing minerals (e.g., cobaltite, alloclasite and/or glaucodot) and Bi minerals (kobellite and/or bismuthinite), which are common in the mineral assemblage of Tharsis massive sulphide, particularly, within stockwork (Marcoux et al., 1996; Tornos et al., 1998).

Thallium also occurs in the pyrite lattice with concentrations that ranges from 0.01 to 512 µg/g. The highest contents are associated with framboidal or colloform pyrite (> 100 µg/g); however, the most significant enrichment (> 500 µg/g) was found in the euhedral and sub-euhedral pyrite from the laminated ore (Figure 7). The presence of Tl in pyrite is commonly product of the substitution of Fe^{3+} for Tl^{3+} in the As-rich pyrite (Cook et al.,

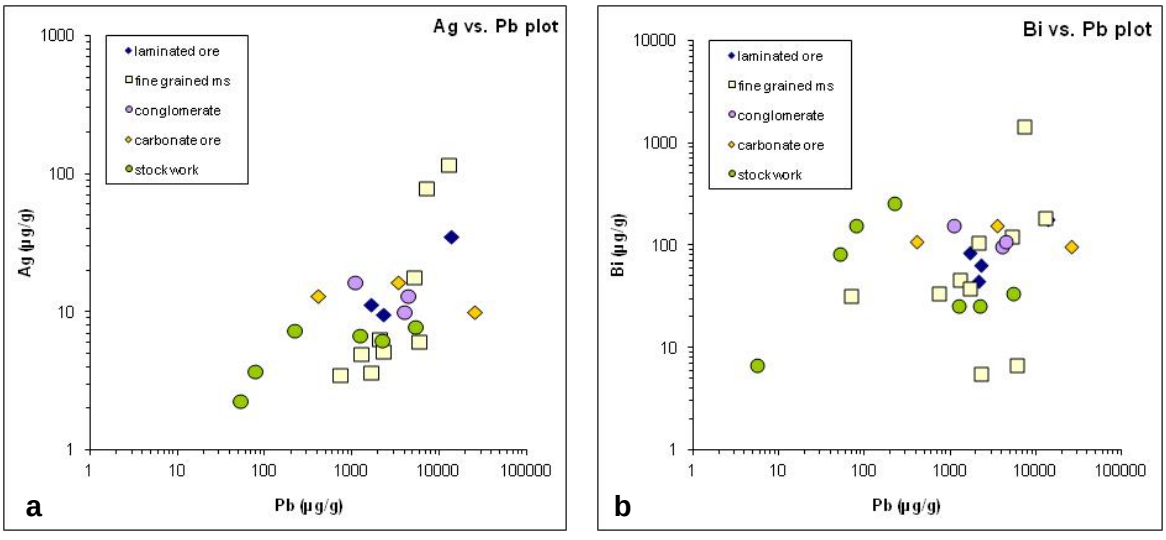

Figure 6. Binary plots of selected trace elements in pyrite. (a) Ag *vs*. Pb diagram showing a positive correlation trend, mainly in pyrite from laminated ore, carbonate ore and fine-grained massive sulphide (r > 0.90). (b) Plot of Bi *vs*. Pb displaying a correlation index higher than r = 0.95 in the laminated and carbonate ore.

1990), something supported by the positive correlation between Tl and As in the carbonate ore (r = 0.94). However, the Tl enrichment related to colloform pyrite shows a weak positive correlation of Tl and Pb. In this case, the presence of Tl is interpreted by the presence of galena micro-inclusions, which under conditions of low temperature could show significant substitution of $2Tl^{+}$ for Pb^{2+} (Maslennikov et al., 2009).

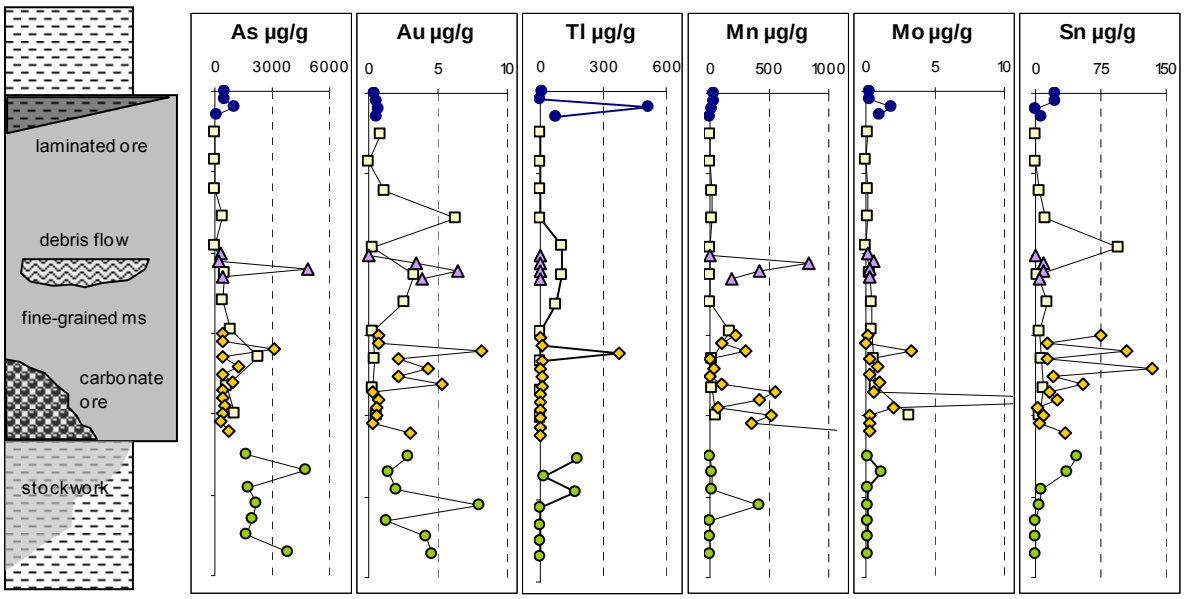

Figure 7. Section of the Filón Norte orebody (Tharsis) showing the distribution of selected trace elements in pyrite from the different mineralization types (in µg/g). Graphic symbols: laminated ore, blue circle; fin-grained massive sulphide, light yellow square; debris flow, lilac triangle; carbonate ore, yellow diamond; and stockwork, green circle

The concentration of Mn ranges between tens to a few hundred µg/g (Table 1). The Mn concentration is highest in the pyrite - specially in the early finely laminated pyrite from the carbonate ore, and is occasionally elevated in the conglomerate facies, with average concentrations of >300 µg/g and 360 µg/g, respectively (Figure 7). In the coarse grains it could be interpreted to presence of Mn-bearing carbonate inclusions -especially in carbonate ore - but in this case the geochemical data and texture support that probably the enrichment in Mn occurs by the simple cation exchange between Fe^{2+} by Mn^{2+} and rarely by intergrown, which is interpreted as due to the precipitation at low temperatures and especially at relatively high oxidation states. Mn-rich pyrite in the conglomerate facies potentially originated from the reworking of the carbonate ore.

Generally, the pyrite of the carbonate ore is enriched in Mo (avg. 2.2 µg/g) with respect to the other facies (0.3 - 0.8 µg/g). The incorporation of small amounts of Mo in the structure of pyrite is thought also to be related to the redox conditions, with Mo enrichment under oxidizing conditions and perhaps during the late hydrothermal recrystallization (Huston et al., 1995).

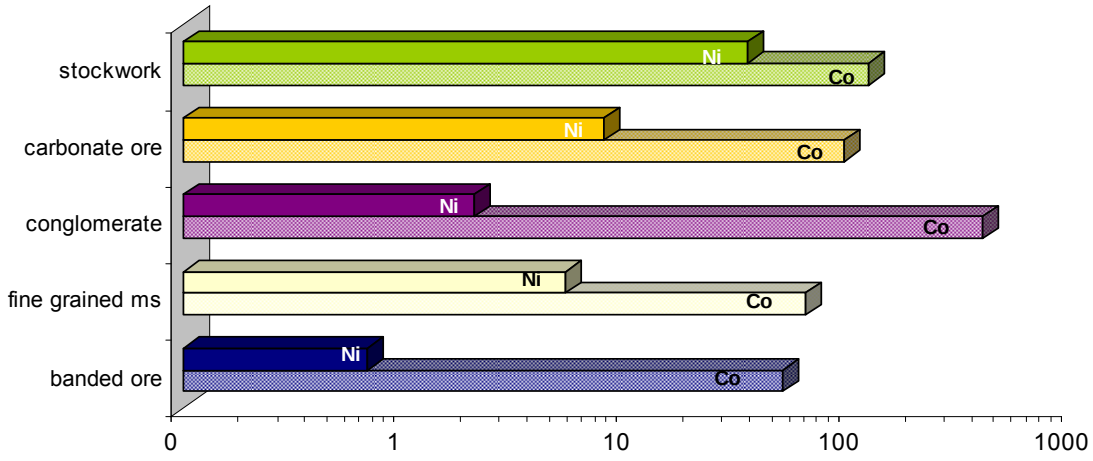

Figure 8. Histogram showing the distribution of Co and Ni in pyrite of whole massive sulphide (in µg/g).

The Ti content is broadly uniform in all ore facies, and exhibits concentrations from 6 to 11 µg/g. One analysis from the stockwork zone yielded a highly anomalous value of 170 µg/g, which is likely due to record ablation of a rutile or ilmenite inclusion.

In general, the massive sulphide deposits of the Iberian Pyrite Belt have more Sn than other massive sulphide deposits elsewhere (Solomon et al., 2002). This is especially visible in the Neves Corvo deposit (Portugal) where the massive sulphides contain average contents of 2.2% Sn and include local zones of almost massive cassiterite (>8% Sn) (Relvas, 2000; Serranti et al., 2002). In Tharsis, all of our analyses record measureable Sn, with an average concentration of 13 µg/g Sn, but there is an anomalous enrichment of up to 130 µg/g in pyrite of the carbonate ore (Table 1). Stannite has been described previously as an accessory mineral at Tharsis (Tornos et al., 1998), but our results indicate that there is not always a good correlation between Cu and Sn within the

pyrite (Table 2). Thus, stannite cannot be the sole, and perhaps not even the principal, Sn-bearing phase in the pyrite. Alternatively, the Sn budget may be accounted by Sn held in solid solution in pyrite as has been suggested by Cabri et al. (1985) for the elevated Sn content in massive sulphides at Kidd Creek. This could be possible at Tharsis, but petrography indicates that the high Sn contents are largely due to the presence of SnO_2 (cassiterite) inclusions in sphalerite, which coprecipitated with pyrite at intermediate fS_2 values (Tornos et al., 1998). Thus, is likely that the high Sn contents are due to the presence of nano inclusions of cassiterite in pyrite.

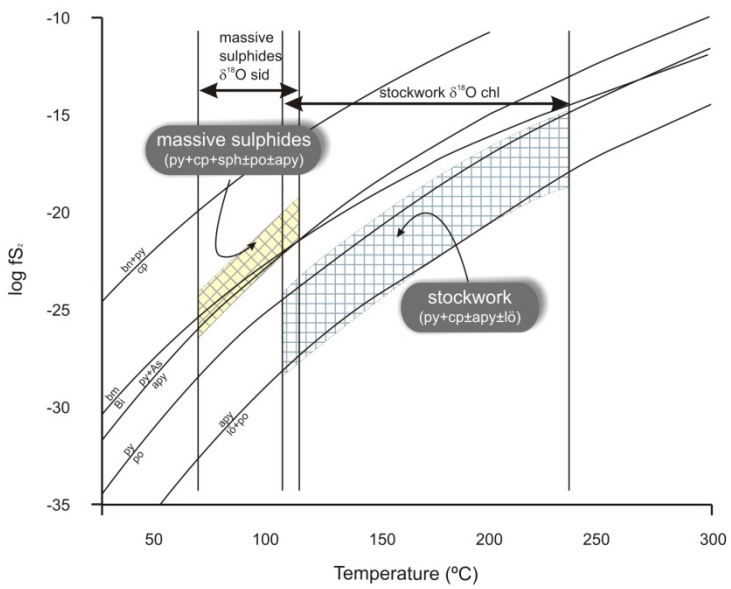

Figure 9. Log fS_2 *vs.* T (ºC) diagram showing conditions of pyrite formation in stockwork and massive sulphide (modified after Tornos et al. 2008)

Co and Ni are the most common trace elements in pyrite, and are the elements that have been most widely investigated as possible tracers of the origin and conditions of precipitation of the pyrite (Walshe and Solomon, 1981; Roberts, 1982; Brill, 1989; Huston et al., 1995; Raymond, 1996; Clark et al., 2004; Koglin et al., 2009). In some cases, the Co:Ni ratio has been employed to discriminate the environment of formation (Hawley and Nichol, 1961; Bajwah et al., 1987), although the robustness of this classification has also been questioned (Campbell and Ethier, 1984). Both Co and Ni usually occur as stoichiometric substitutions in pyrite, wherein they substitute the Fe lattice sites since they

are isomorphous and chalcophile (Springer et al., 1964). At Tharsis, the highest concentrations of Co (avg. 120 µg/g) occur in the footwall stockwork zone and in the conglomerate facies (avg. 360 µg/g). In both ore facies, the highest values are in the aggregates of fine pyrite crystals and porous pyrite. Pyrite in the laminated ore contains the lowest average Co (< 50 µg/g). Ni contents are systematically lower than Co concentrations. Pyrite in most of the ore facies contains less than 8 µg/g Ni, except in the footwall stockwork where Ni concentrations exceed 85 µg/g (Table 1). Enrichment of Co and Ni in pyrite is here likely attributable to the higher temperatures and lower fS_2 conditions of the stockwork zone (Figure 9), that favour the replacement of Fe by Co in the lattice. Locally, cobaltite has also been observed in the stockwork mineral assemblage (Tornos et al., 1998).

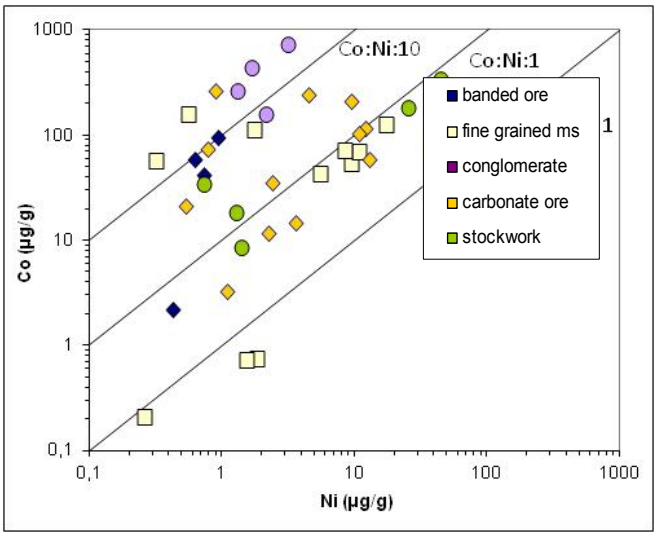

Figure 10. Binary plot of Co *vs*. Ni content showing the distribution of Co/Ni ratios of pyrite from the Filón Norte massive sulphide.

The petrogenetic interpretation of the Co and Ni contents in pyrite has been discussed by Bralia et al. (1979), Brill (1989) and Bajwah et al. (1987), which propose diagrams showing the relationship between these contents and the style of mineralization. In such diagrams (Figure 10), the pyrite at Tharsis shows a widely variable Co:Ni range and the values field, from sedimentary environment (< Co / Ni = 1) to volcano-exhalative pyrite (> Co / Ni = 10). However, these models are probably only indicative, unless the system is

saturated in both Co and Ni. That is, pyrite coexists with Ni- and Co-rich phases and the amount of hosted Ni and Co depends exclusively on their concentrations in fluids and the conditions of formation (temperature and fS_2). Since cobaltite is the only discrete Co-rich phase at the Tharsis stockwork and is only locally present, it is unlikely that Co and Ni can be used as petrogenetic indicators here.

5. Discussion and conclusions

The detailed geochemical study of pyrite from the Tharsis massive sulphide deposit shows the existence of a systematic enrichment in some trace elements. The results show a coherent distribution according to the texture and type of mineralization. The anomalously high concentrations of Cu, Pb, Zn, Ag, Sn and Ti are interpreted to be due to the presence of sub-microscopic inclusions of different phases that are also present as discrete grains within the deposit. The concentration of As, Mn, Mo, Tl, Ni, Co and Au is more irregular and was probably controlled by the temperature of the fluid, fO_2-fS_2 conditions and the degree of crystallinity of the host mineral. Whereas Mo, Mn and Tl are enriched in the apparently more oxidized and cooler zones, As, Co and Au concentrate preferentially in the low-fS_2 environments. The latter are concentrated in the pyrite from the stockwork and, less commonly, in the conglomerate. In general, early pyrite precipitated at higher temperatures and showing lower crystallinity index– probably due to rapid precipitation induced by supersaturation or microbial precipitation- has higher concentrations of these metals; major enrichment occurs in pyrite with the most primitive textures (framboidal and colloform), showing a strong depletion in the more mature euhedral pyrite. An evolution from an early, high temperature, reduced and sulphur-poor system, represented by the stockwork, to a S_2-rich, oxidized and cooler environment in the massive sulphides is consistent with the observed variation in the Co, Ni and the other lattice-related elements.

These results demonstrate that the trace elements concentration in the pyrite could be of help to define a strategic signature in the mining exploration. They would allow distinguishing the proximal and distal zone of the volcanic massive sulphides, as stockwork zones and late remobilizations veins, because the trace elements precipitation is highly determined to specific physicochemical and redox conditions.

Acknowledgements

This work has been funded by the CICYT-FEDER project BTE2000-0161-CO2 of the Spanish Government and is part of the Global Comparison of Massive Sulphides Project (IGCP 502). It is part of the Ph. D. thesis of the first author. Additional funds have been provided by a research scholarship from IGME, with additional funding from the McKinstry Grant of the Society of Economic Geologists (SEG). We especially thank the analytical team at CODES (University of Tasmania) for the execution of the laboratory work and A. Castillo for facilitating sample collection at Tharsis. We would like to thank Ross Large and Michel Solomon for his valuable comments and suggestions.

References

Bajwah, Z.U., Seccombe, P.K., Offer, R., 1987. Trace element distribution, Co:Ni ratios and genesis of the Big Cadia iron-copper deposit, New South Wales, Australia. Mineralium Deposita 22, 292-300.

Belcher, R. W., Rozendaal, A., Przybylowicz W. J., 2004. Trace element zoning in pyrite determined by PIXE elemental mapping: evidence for varying ore-fluid composition and electrochemical precipitation of gold at the Spitskop deposit, Saldania Belt, South Africa. X-Ray Spectrometry 33, 174-180.

Bralia, A., Sabatini, G., Troja, F., 1979. A revaluation of the Co/Ni ratio in pyrite as geochemical tool in ore genesis problems. Mineralium Deposita 14, 353-374.

Brill, B., 1989. Trace-element contents and partitioning of elements in ore minerals from the CSA Cu-Pb-Zn deposit, Australia. Canadian Mineralogist 27, 263-274.

Cabri, L.J., Campbell, J.L., Laflamme, J.H.G., Leigh, R.C., Maxwell, J.A., Scott, J.D., 1985. Proton-microprobe analysis of trace elements in sulfides from some massive-sulfide deposits. Canadian Mineralogist: 23, 133-148.

Campbell, F.A., Ethier, V.G., 1984. Nickel and cobalt in pyrrhotite and pyrite from the Faro and Sullivan orebodies. Canadian Mineralogist 22, 503-506.

Chouinard, A., Paquette, J., Williams-Jones, A. E., 2005. Crystallographic controls on trace-element incorporation in auriferous pyrite from the Pascua epithermal high-sulfidation deposit, Chile-Argentina. Canadian Mineralogist 43, 951-963.

Clark, C., Grguric, B., Schmidt Mumm, A., 2004. Genetic implications of pyrite chemistry from the palaeoproterozoic Olary Domain and overlying Neoproterozoic Adelaidean sequences, northeastern South Austrlia. Ore Geology Review 25, 237-257.

Conde, C., Lentz, D.R., Walker, J.A., Huard, A., Tornos, F., 2008. Petrology and geochemistry of the Cu-rich zone at the Brunswick No. 6 Zn-Pb-Cu-Ag VMS deposit, Bathurst Mining Camp, New Brunwick (Canada). 33rd International Geological Congress, Oslo.

Cook, N.J., Ciobanu, C.L., Mao, J.W., 2009a. Textural control on gold distribution in As-free pyrite from the Dongping, Huangtuliang and Hougou gold deposits, North China Craton, (Hebei Province, China). Chemical Geochemistry 204, 101-121.

Cook, N.J., Ciobanu, C.L., Pring, A., Skinner, W., Shimizu, M., Danyushevsky, L., Saini-Eidukat, B., Melcher, F., 2009b. Trace and minor elements in sphalerite: A LA-ICPMS study. Geochimica et Cosmochimica Acta 73, 4761-4791.

Cook, N.J., Chryssoulis, S.L., 1990. Concentrations of invisible gold in the common sulfides. Canadian Mineralogist: 28, 1-16.

Campbell, F.A., Ethier, V.G., 1984. Nickel and cobalt in pyrrhotite and pyrite from the Faro and Sullivan orebodies. Canadian Mineralogist 22 503-506.

Danyushevsky, L.V., Robinson, P., McGoldrick, P., Large, R.R., Gilbert, S., 2003. LA-ICPM of sulfides: evaluation of an XRF glass disc standard for analysis of different sulphide matrixes. 2003 Goldschmidt Conference, Japan: Geochemica Cosmochimica Acta, 67, p. A73.

Franklin, J.M., Sangster, D.M., Lydon, J.W., 1981. Volcanis-associated massive sulphide deposits. In: Skinner, B.J, (eds) Econimic Geology Seventy-Fifth Anniversary Volume, Society of Economic Geologists, 485-627.

Franklin, J.M., Gibson, H.L, Galley, A.G., Jonasson, I.R., 2005. Volcanigenic Massive Sulfide Deposits. In: Hedenquist, J.W., Thompson, J.F.H., Goldfarb, R.J., Richards, J.P. (eds) Economic Geology 100th Anniversay Volume. Society of Economic Geologist, 523-560.

Hawley, J.E., Nichol, I., 1961. Trace elements in pyrite, pyrrhotite and chalcopyrite of different ores. Economic Geology, 56, 467-487.

Huston, D.L., Sie, S.H., Suter, G.F., Cooke, D.R., Both, R.A., 1995. Trace elements in sulfide minerals from eastern Australia volcanic-hosted massive sulphide deposit. Economic Geology 90, 1167-1196.

Koglin, N., Frimmel, H.E., Lawrie, W.E., Brätz, H., 2010. Trace-element characteristics of different pyrite types in Mesoarchaean to Palaeoproterozoic placer deposits. Mineralium Deposita 45, 259-280.

Large, R.R., Danyushevsky, L., Hollit, C., Maslennikov, V., Meffre, S., Gilbert, S., Bull, S., Scott, R., Emsbo, P., Thomas, H., Singh, B., Foster, J., 2009. Gold and trace element zonation in pyrite using a laser imaging technique: implications for the timing of gold in orogenic and Carlin-style sediment-hosted deposits. Economic Geology 104, 635-668.

Leistel, J.M., Marcoux, E., Deschamps, Y., Jourbert, M., 1998a. Anthitetic behaviour of gold in the volcanogenic massive sulphide deposits of the Iberian Pyrite Belt. Mineralium Deposita 33, 82-97.

Leistel, J.M., Marcoux, E.,Thieblemont, D., Quesada, C., Sanchez, A., Almodóvar, G.R., Pacula, E., Sáez, R., 1998b. The volcanic-hosted massive sulphide deposits of the Iberian Pyrite Belt: Review and preface to the special issue. Mineralium Deposita 33, 2-30.

Lydon, J. W., 1988. Volcanogenic Massive Sulphide Deposits, Part 1, A Descriptive Model. In: Roberts R.G. & Sheahan P.A. (eds.) Ore Deposit Models. Geoscience Canada, Rep. Ser. 3, GAC, St. John's, Newfoundland, 45-153.

Maier, R.C., 2005. Pyrite trace element halos to northern Australian sediment-hosted Zn-Pb-Ag deposits. In: Mao, J. and Bierlein, F.P (eds) Mineral Deposit Research: Meeting the Global Challenge. Proceedings of the Eighth Biennial SGA Meeting, China, 18-20.

Marcoux, E., Moelo, Y., Leistel, J.M., 1996. Bismuth and cobalt minerals: indicators of stringer zones to massive-sulfide deposits, South Iberian Pyrite Belt. Mineralium Deposita 31, 1-26.

Maslennikov, V.V., Maslennikova, S.P., Large, R.R., Danyushevsky L.V., 2009. Study of trace element zonation in vent chimneys from the Silurian Yaman-Kasy volcanic-hosted massive sulphide deposit (southern Urals, Russia) using Laser Ablaiton-Inductively Coupled Plasma Mass Spectrometry (LA-ICPMS). Economic Geology 104, 1111-1141.

McClenaghan, S. H., Lentz, Cabri, L.J., 2004. Abundance and speciation of gold in massive sulphides of the Bathurst Mining Camp, New Brunswick, Canada. The Canadian Mineralogist 42, 851-871.

McClenaghan, S. H., Lentz, D.R., Martin, J., Diegor, W. G., 2009. Gold in the Brunswick No. 12 volcanogenic massive sulphide deposit, Bathurst Mining Camp, Canada: Evidence from bulk ore analysis and laser ablation ICP-MS data on sulphide phases. Mineralium Deposita 44, 523-557.

Norman, M.D. Griffin, W.L. Prearson, N.J., García M.O., O'Reilly, S.Y., 1998. Quantitative analysis of trace element abundances in glasses and minerals: a comparison of laser ablation inductively coupled plasma mass spectrometry, solution inductively coupled plasma mass spectrometry, proton microprobe and electron microprobe data. Journal of Analytical Atomic Spectrometry 13, 477-483.

Raymond, O.L., 1996. Pyrite composition and ore genesis in the Prince Lyell copper deposit, Mt Lyell mineral field, western Tasmania, Australia. Ore Geology Reviews 10, 231-250.

Reich, M., Kesles, S.R., Utsunomiya, S., Palenik, C.S., Chryssoulis, S.L., Ewing, R., 2005. Solubility of gold in arsenian pyrite. Geochemica et Cosmochimica Acta 69, 2781-2796.

Relvas, J.M.R.S., 2000. Geology and metallogenesis at the Neves Corvo deposit, Portugal. Ph.D. thesis, Universidade de Lisboa, 319 pp.

Roberts, F.I., 1982. Trace element chemistry of pyrite: a useful guide to the occurrence of sulphide base metal mineralization. Journal of Geochemical Exploration 17, 49-62.

Serranti, S., Ferreini, V., Masi, U., Cabri, L.J., 2002. Trace-element distribution in cassiterite and sulfides from rubané and massive ores of the Corvo deposit, Portugal. Canadian Mineralogist 40, 815-835.

Smith, R.N., Huston, D.L., 1992. Distribution and association of selected trace elements at the Rosebery deposit, Tasmania. Economic Geology 87, 706-719.

Springer, G., Schachner-Korn, D., Long, J.V.P., 1964. Metastable solid dilution reactions in the system FeS2-CoS2-NiS2. Economic Geology 59, 475-491.

Solomon, M., Tornos, F., Garpas, O.C., 2002. Explanation for many of the unusual features of the massive sulphide deposit of the Iberian pyrite belt. Geology 30, 87-90.

Tornos, F., 2006. Enviroment of formation and styles of volcanogenic massive sulfides. The Iberian Pyrite Belt: Ore Geology Reviews 28, 259-307.

Tornos, F., González Clavijo, E., Spiro, B., 1998. The Filón Norte orebody (Tharsis, Iberian Pyrite Belt): a proximal low-temperature shale-hosted massive sulphide in a thin-skinned tectonic belt. Mineralium Deposita 33, 150-169.

Tornos, F., Conde, C., 2002. La influencia biogénica en la formación de los yacimientos de sulfuros masivos de la Faja Pirítica Ibérica. Geogaceta 32, 235-238.

Tornos, F., Solomon, M., Conde, C., Spiro, B.F., 2008. Formation of the Tharsis massive sulfide deposit, Iberian Pyrite Belt: Geological, Lithogeochemical, and Stable Isotope Evidence for Deposition in a Brine Pool. Economic Geology 103, 185-214.

Walshe, J.L., Solomon, M., 1981. An investigation into the environment of formation of the volcanic-hosted Mount Lyell copper deposits using geology, mineralogy, stable isotopes and a six-component chlorite solid solution model. Economic Geology 76, 246-284.

Yamaguchi, K.E., Ohmoto, H., 2006. Evidence from sulfur isotope and trace elements in pyrites for their multiple post-depositional processes in uranium ores at the Stanleigh Mine, Elliot Lake, Ontario, Canada. Geological Society of America Memoirs 2006, 143-156.

Zhao, H.X, Frimel, H.E., Jiang, S.Y., Dai, B.Z., 2011. LA-ICP-MS trace element analysis of pyrite from the Xiaoqinling gold district, China: Implications for ore genesis. Ore Geology Reviews 43, 142-153.

CAPITULO V

Modelización hidrodinámica de los sulfuros masivos de la zona sur de la Faja Pirítica Ibérica (España)

Hydrogeologic modelling of the hydrothermal process in the VHMS from the southern part of Iberian Pyrite Belt (Spain).

Resumen

La parte sur de la Faja Pirítica Ibérica (FPI) alberga algunos depósitos gigantes de sulfuros masivos volcanogénicos que se encuentran encajados en pizarras oscuras sobreyacentes a complejos tipo domo. La mineralización se interpreta como exhalativa y formada en cuencas marinas de tercer orden someras y restringidas de carácter anóxico-subanóxico. La precipitación de varios millones toneladas de sulfuros es resultado de la mezcla de fluidos hidrotermales profundos con agua marina modificada. Los fluidos profundos ascendieron a la superficie vía circulación convectiva producida por un flujo elevado de calor.

Este trabajo desarrolla dos modelos bidimensionales (2D) de alta resolución simulando la cuenca devónica en la que se forman las mineralizaciones. Se han supuesto dos casos extremos de composición química de las soluciones hidrotermales. El primer modelo fue testado para un supuesto tal que la unidad sedimentaria subyacente está saturada en agua “pura” (salinidad 0% peso NaCl), y en segundo lugar, en fluidos salinos con entrada de agua del mar. El modelo numérico tiene como objetivo verificar si se puede generar un campo de flujo cuantitativamente suficiente como para formar la mineralización por convección térmica, y establecer cual es la influencia de la salinidad en el desarrollo de estos sistemas hidrotermales. Los modelos han sido desarrollados mediante el programa CSP, “Complex System Platform” (Matthäi et al., 2001, 2004) creado con el objetivo de resolver numérica y simultáneamente las ecuaciones matemáticas que controlan el flujo de fluido, y el transporte de calor y solutos, en un medio poroso. Las características geológicas (estratigrafía, tectónica y paleogeografía), así como la parametrización hidrológica del modelo corresponden a una cuenca restringida, similar a en la que se localizan la mayoría de los cuerpos de sulfuros masivos de la parte sur de la Faja Pirítica.

El modelo basado en la circulación de “agua pura” muestra ya en los primeros estadios, el desarrollo de una circulación convectiva capaz de conducir fluidos calientes y moderadamente salinos a la superficie del fondo oceánico. Los fluidos ascienden

principalmente a los largo de grandes fallas en el fondo oceánico. El modelo muestra que el campo de flujo convectivo generado es muy sensible a la salinidad del fluido (Caso 2). Se ha observado un gran cambio –en comparación con el Caso 1- respecto a los resultados obtenidos en la dinámica de los fluidos, la velocidad de la convección termohalina y la transferencia de solutos. El flujo de fluido termohalino requiere más tiempo para que el gradiente geotérmico anómalo desarrolle la circulación convectiva (el triple de tiempo de modelización que para el modelo con “agua pura”), y salvo en los primeros estadios, nunca llega a generar un campo de temperaturas elevadas y velocidades de flujo anómalas en el fondo oceánico.

En conjunto, el modelo numérico demuestra que la circulación hidrotermal que dio lugar a los sulfuros masivos en la zona sur de la Faja Piritica podría estar controlada por una circulación convectiva forzada, sin que sea necesaria una gran fuente de calor procedente de intrusiones someras para que se desarrolle; esto es, una fuente magmática no es necesaria en la formación de este sistema.

Keywords: modelización numérica, flujo de calor y fluido, fluido termohalino, Faja Pirítica Ibérica.

Abstract

The southern part of the Iberian Pyrite Belt hosts several giant VMS deposit. The massive sulphides are hosted by dark shale overlying a dacite dome. This mineralization is interpreted as exhalative on an anoxic-suboxic seafloor, within a restricted and rather shallow basin. The precipitation of these million tons of sulphides is result of the mixing between modified sea water and deep hydrothermal fluids. This deep fluid flows upward by a convective flow induced by a high heat flux

This study has developed a two high-resolution bidimensional (2D) model that reproduces the late Devonian basin where the mineralization occurs. Two extreme cases related to the chemical composition of the hydrothermal solutions have been tested. The first model tests involving the underlying sedimentary sequence saturated in pure water (salinity 0% wt. NaCl eq.), and a second, with a brine fluid and inflow of seawater. The numerical model has the goal to prove if it is possible produce a flow field quantitative enough to develop the mineralization by thermal convection and analyze the influence of the salinity in the development of the hydrothermal system. They have been performed using the CSP finite-element modelling code (Matthäi et al., 2001, 2004), program based on mathematical equations for fluid flow, heat transport and solute transport in porous media. The geological characteristics (stratigraphy, tectonic and palaeogeography), and the hydrologic parameters belong a restricted basin, similar to where the massive sulphide occur in the south part of the Iberian Pyrite Belt.

The pure water simulation shows that the first stages of thermal and fluid convection are able to drive moderate saline and hot fluids to the. These fluids are upwards by the major faults to the seafloor. The numerical model shows that salinity has a significant effect on the convection flow (Case2). The results reveal a big change –compared to Case 1- related to the result of the fluid dynamics, the velocity of and thermohaline convection, and transfers solution flow. This thermohaline fluid required a long time of anomalous geothermal gradient for beginning the convective flow, more than three times

that pure water, and except in the first stages, never the temperatures and velocity of fluid are able to up on the seafloor.

As a whole, the numerical model supports that the hydrothermal fluid flow that develop the massive sulphide in the south part could be controlled by a forced convection flow, and it is not necessary a huge heat source related to shallow intrusions to its development, thus, a magmatic source is not necessary.

Keywords: numerical modelling, heat and fluid flow, thermohaline fluid, Iberian Pyrite Belt

1. Introducción

El estudio de los procesos geoquímicos y termodinámicos relacionados con la génesis de los sulfuros masivos es un campo de interés creciente en los últimos años en la investigación de los yacimientos minerales. La simulación mediante modelos numéricos de flujo de fluido y calor, y el trasporte de solutos ha permitido un mejor entendimiento de los procesos físico-químicos que intervienen en los sistemas hidrotermales en los fondos marinos (Schardt & Large, 2009; Gruen et al., 2012). Sin embargo, pocos son los trabajos orientados a la modelización hidrodinámica de los procesos que han intervenido en la formación de la mayor provincia mundial de sulfuros masivos, la Faja Pirítica Ibérica (FPI) (Barrie et al., 2004; Conde et al., 2005).

La mayoría de los sulfuros masivos gigantes (>100 Mt) de la Faja Pirítica se encuentran en su sector meridional (Fig. 1). La FPI incluye una serie estratigráfica relativamente simple y de edad Devónico Superior-Carbonífero Inferior, en la que se han diferenciado tres unidades principales. Las rocas más antiguas, datadas como Givetiense-Fameniense, forman el Grupo Cuarzo-Filítico (Grupo PQ). Está formado por una potente serie detrítica (>2000 m) constituida por una alternancia de pizarras y areniscas ricas en cuarzo, depositadas en una ambiente de plataforma continental estable que evoluciona a techo hacia facies de mayor energía, como barras de arena sedimentos de flujo y caliza (Moreno et al., 1996). Estratigráficamente por encima, está el Complejo Volcano-Sedimentario (CVS), con un espesor variable de 0 a 1300 m (Tornos, 2006), y formado por una serie heterogénea compuesta por una alternancia de rocas volcánicas, subvolcánicas y volcanoclásticas de carácter bimodal (desde basalto a riolita), junto con pizarras y sedimentos químicos (jaspe). Desde el punto de vista paleogeográfico, se interpreta que el CVS fue depositado entre el Fameniense Superior y el Viseense Inferior, en una cuenca de tipo “pull-apart” formada durante la colisión oblicua de la Zona Sur-Portuguesa (Avalonia?) y el Terreno Ibérico (Gondwana?) (Silva et al., 1990; Quesada, 1998; Tornos et al., 2005; Onézime et al., 2012)

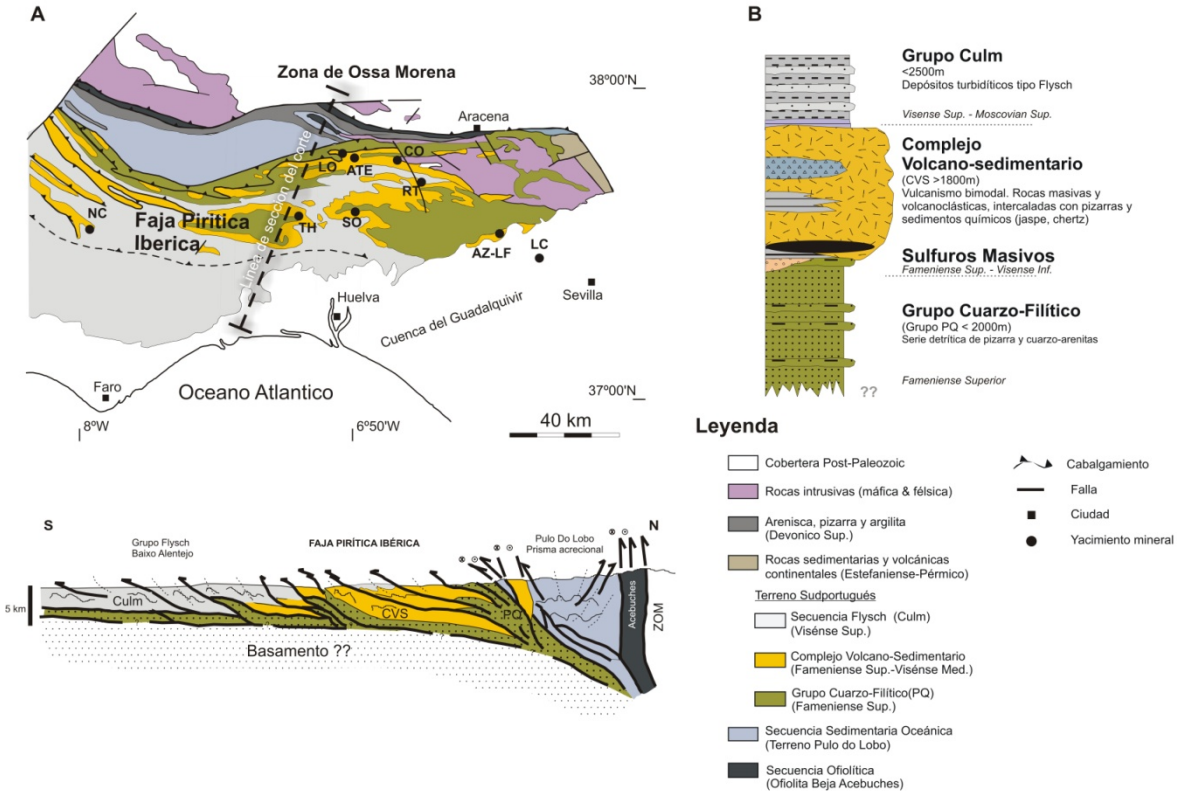

Figura 1. (A) Mapa geológico de la Faja Pirítica en el que se muestra un corte transversal (parte inferior) (modificado de Oliveira et al., 1990; Onézime et al., 2002) (B) Columna estratigráfica general de la Faja Pirítica (modificado de Tornos 2006). NC, Neves Corvo; Th, Tharsis; SO, Sotiel; AZ-LF, Aználcollar-Los Frailes; LC, Las Cruces; CO, Concepción; RT, Río Rinto; ATE, Aguas Teñidas; LO, Lomero Poyatos

autóctono sincrónico a la Orogenia Varisca (Silva et al., 1990; Quesada et al., 1998). La unidad superior, suprayacente a la unidad volcánica, es el Grupo Flysch de Baixo Alentejo, formado por una secuencia turbidítica tipo flysch muy potente (>3000 m), constituida por pizarras y grauvacas, y que se interpreta como producto de la colmatación de la cuenca y posterior inversión tectónica (Moreno, 1993).

Los depósitos más significativos de la zona sur de la FPI encajan en pizarras oscuras (ver Fig. 1). En algunos casos, estas pizarras se localizan directamente por encima del Grupo PQ (p.e.,Tharsis), o sobre una unidad félsica con complejos de tipo domo (p.e., Aznalcóllar-Los Frailes, Las Cruces, Sotiel, Valverde o Tharsis). Estos sulfuros masivos están caracterizados por su gran tonelaje, el alto contenido en pirita, y la presencia de estructuras sedimentarias que sugieren un probable origen ligado a procesos exhalativos

en una cuenca anóxica restringida (Tornos 2006; Tornos et al., 2008). Estos depósitos parecen ser coetáneos y limitados a un único nivel estratigráfico de 3 a 4 Ma (Fig. 2), y datado como Struniense Superior (Pereira et al., 1996; González et al., 2002; Oliveira et al., 2002). La caracterización geológica y geoquímica sugiere que los fluidos que originaron la mineralización proceden de la maduración diagenética de la unidad detrítica infrayacente (Grupo PQ) (Tornos & Heinrich, 2008) y que fueron incorporados a circuitos hidrotermales debido a la implantación de un alto gradiente geotérmico del basamento (Conde et al., 2005; Tornos, 2006).

La hipótesis de trabajo es que, a diferencia de otros muchos distritos de sulfuros masivos a escala global, los sulfuros masivos del sector meridional de la Faja Pirítica no están relacionados con rocas ígneas, las cuales solo sirvieron para elevar el gradiente geotérmico. La situación de este distrito sobre una potente secuencia siliciclástica hace improbable que los metales sean lixiviados de rocas ígneas subyacentes, como es el caso en muchos distritos (Galley et al., 1995; Doley & Allen, 2003; Goodfellow & McCutcheon, 2003; Huston et al., 2011) y en la mayor parte de los sistemas submarinos actuales desarrollados en zonas de MOR (de Ronde et al., 2003; Gruen et al., 2014). La ausencia de alteraciones hidrotermales de tipo ácido y la geoquímica isotópica también indican que una contribución de fluidos magmáticos es también improbable (Campbell et al., 1984; Barrie et al., 2001; Schardt et al., 2005, Ingesbritsen & Appold, 2012). Esta geoquímica isotópica indica que los fluidos estaban equilibrados con las rocas siliciclásticas o incluso un basamento continental (Tornos, 2006). Finalmente, está la cuestión de por qué estos depósitos se formaron en un periodo de tiempo relativamente corto (<1 Ma, durante el Estruniense) y de una manera coetánea coincidiendo con el límite Devónico-Carbonífero (Menor et al., 2010).

Por ello, las condiciones de formación de estos depósitos minerales son distintas de las de otros sulfuros masivos que involucran agua magmática y/o marina y forman células convectivas que se asocian a actividad magmática y que son distorsionadas por la

entrada de fluidos magmáticos sobrepresurizados (Ingebritsen & Appold, 2012;). Para ello, se ha desarrollado un modelo numérico de elementos finitos que sea capaz de verificar si el Grupo PQ puede ser la fuente del fluido hidrotermal que da lugar a la formación de los sulfuros masivos y cuál puede ser el mecanismo que da lugar a la formación de los depósitos gigantes en un corto lapso de tiempo.

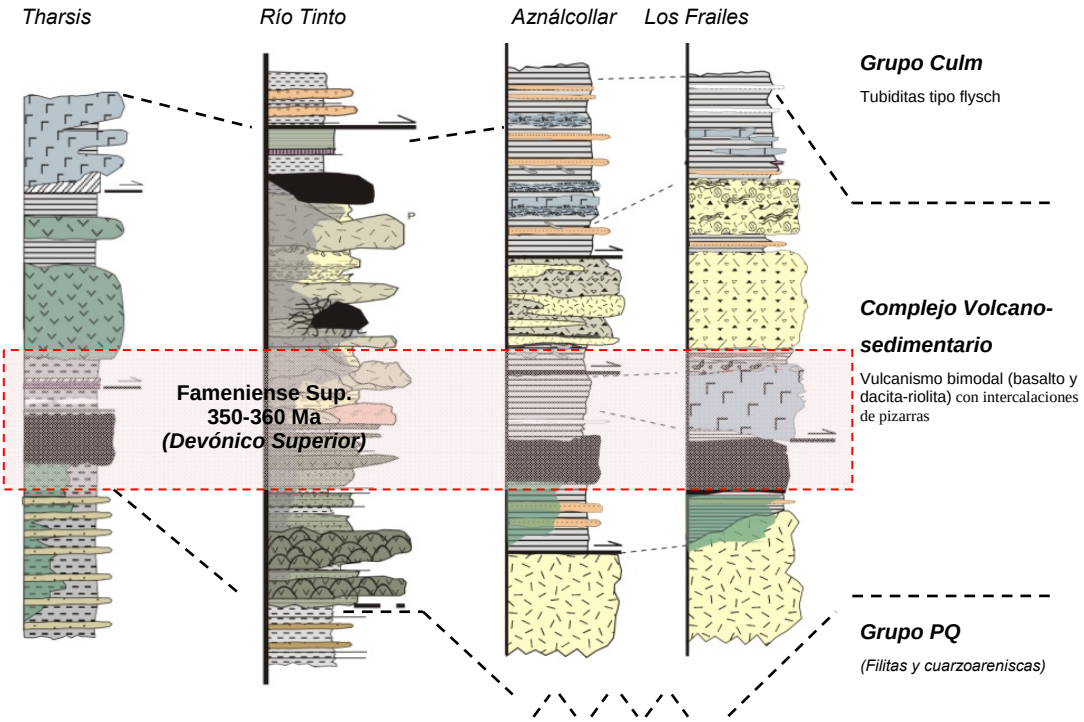

Figura 2. Columnas estratigráficas representativas de los principales depósitos encajados en pizarra de la zona sur de la Faja Pirítica (modificado de Tornos et al. 1998, Conde et al., 2003, Mellado et al., 2006, Conde et al., 2014).

2. Modelo numérico de flujo y transporte

El modelo de elementos y volúmenes finitos que se ha construido simula un flujo multifásico de agua y calor con un mecanismo de convección hidrodinámica y termohalina forzada por un gradiente de temperatura y densidad, que son a su vez inducidos por la existencia de soluciones con diferentes salinidades.

Los mecanismos de flujo de soluciones acuosas, la transferencia de calor y el transporte de solutos pueden ser descritos mediante *(1)* la ecuación de continuidad y la *(2)* ley de Darcy:

$$\emptyset \frac{\delta S_\infty}{\delta t} = -\nabla v_\infty + q_\infty \qquad (1)$$

∞=*fase*

$$v_\infty = -\lambda_\infty \kappa (\nabla p_\infty - \rho_\infty g) \quad (2)$$

donde ϕ es la porosidad de la roca (º%), ρ es la densidad (Kg/m^3) de fluido y *S* es la saturación de la fase acuosa (º%). La velocidad del fluido viene dada por la ecuación (2), donde λ es el ratio de movilidad ($\lambda_\infty = k_{r\infty}/\mu_\alpha$) relativo de la permeabilidad de la fase (κ) y su viscosidad (μ, Pa/s). La permeabilidad en el medio poroso es K, *p* es la presión (Pa) del fluido, y *g* (m/s^2) es la aceleración por gravedad.

La formulación del código numérico utilizada en este estudio implementa tres ecuaciones de estado (EOS):

a. <u>conservación de la masa de fluido</u>, teniendo en cuenta la fase líquida (l) y vapor (v);

$$\emptyset \frac{\partial \rho_f}{\partial t} + \rho_f \frac{\partial \emptyset}{\partial t} = -\nabla (v_v \rho_v) - (v_i \rho_i)$$

b. <u>conservación de la masa de soluto</u>, en relación a la conservación de la fracción de masa NaCl en el H_2O;

$$\emptyset \frac{\partial}{\partial t} \rho_f X_f = -\nabla \cdot v_v \rho_v X_v - \nabla \cdot v_l \rho_l X_l + D_l \nabla^2 \rho_l X_l + D_v \nabla^2 v X_v$$

c. <u>conservación de la energía</u>, definida por la capacidad calorífica de la fase líquida (c_{pl}) y conductividad térmica del medio poroso (*K*):

$$\left[(1-\emptyset)\rho_r c_{pr} + \emptyset\left(S_l \rho_l c_{pl} + S_v \rho_v c_{pc}\right)\right] \frac{\partial T}{\partial t} = -\nabla\left(v_v c_{pl} \rho_l T\right) - \left(v_l c_{pl} T\right) + K \nabla^2 T$$

Estas ecuaciones se basan en una serie de variables tales como la presión de fluidos (p_l), temperatura (T, en ºC), salinidad (X_l), saturación (S_l) y dispersión (D_l).

Uno de los objetivos de la modelización es estimar la velocidad del fluido y el flujo de calor a medida que se desarrolla el sistema convectivo y como este sistema es capaz de trasportar los fluidos salinos hidrotermales. Así, se considera como una variable importante a implementar en el modelo, la variación de la permeabilidad en profundidad. Por ello, se ha tenido en cuenta la ecuación que reproduce el cambio de la permeabilidad en función de la profundidad (Saar & Manga, 2004; Ingebritsen & Manning, 2010), y se ha implementado como "interrelation PermeabilityFromDepth":

$$k \approx 10^{-14} \times ((\exp(-3{,}2)) \times (sdepth/\max\ \_y))$$

La simulación numérica resuelve las ecuaciones de estado mediante el código "Complex System Platform "(CSP) (Matthäi et al., 2001), escrito en C++. Este software fue diseñado con el objetivo de resolver numéricamente, y de manera simultánea, las ecuaciones diferenciales de conservación de la masa y energía, pudiendo variar las condiciones y parámetros físico-químicos (permeabilidad, porosidad, salinidad y geometría, entre otros) que gobiernan el flujo de calor y fluido en un sistema hidrotermal termohalino (Geiger, 2004). La aplicación de este código numérico requiere de una parametrización representativa del medio (Fig. 3), y una discretización que permita implementar la variabilidad espacial de dicha parametrización y definir los puntos donde serán resueltas las ecuaciones. Así, para la construcción del modelo numérico se han cumplimentado una serie de módulos que han permitido desarrollar los siguientes requerimientos del código:

(1) *discretización* del dominio a simular de manera que se definan los puntos donde serán resueltas las ecuaciones anteriormente especificadas;

(2) identificación del *grupo de variables físicas* de los que deben ser calculadas;

(3) *parametrización inicial* de las variables físicas anteriormente definidas según una serie de parámetros propuestos en los "inputs" iniciales;

(4) identificación de las *ecuaciones diferenciales parciales* (PDEs, partial diferential equations) asignadas a cada uno de los nudos que forman parte de la malla y que simulan los mecanismos de acoplamiento espacio-temporales;

(5) "interrelations", módulo donde se consideran variables físicas aplicadas localmente y sin necesidad de un mecanismo de acoplamiento global;

(6) *"visitors"*, herramienta que permite un cambio en sistema de referencia;

(7) "*condiciones iniciales y de contorno"*, valores iniciales y de contorno de las variables físicas del modelo;

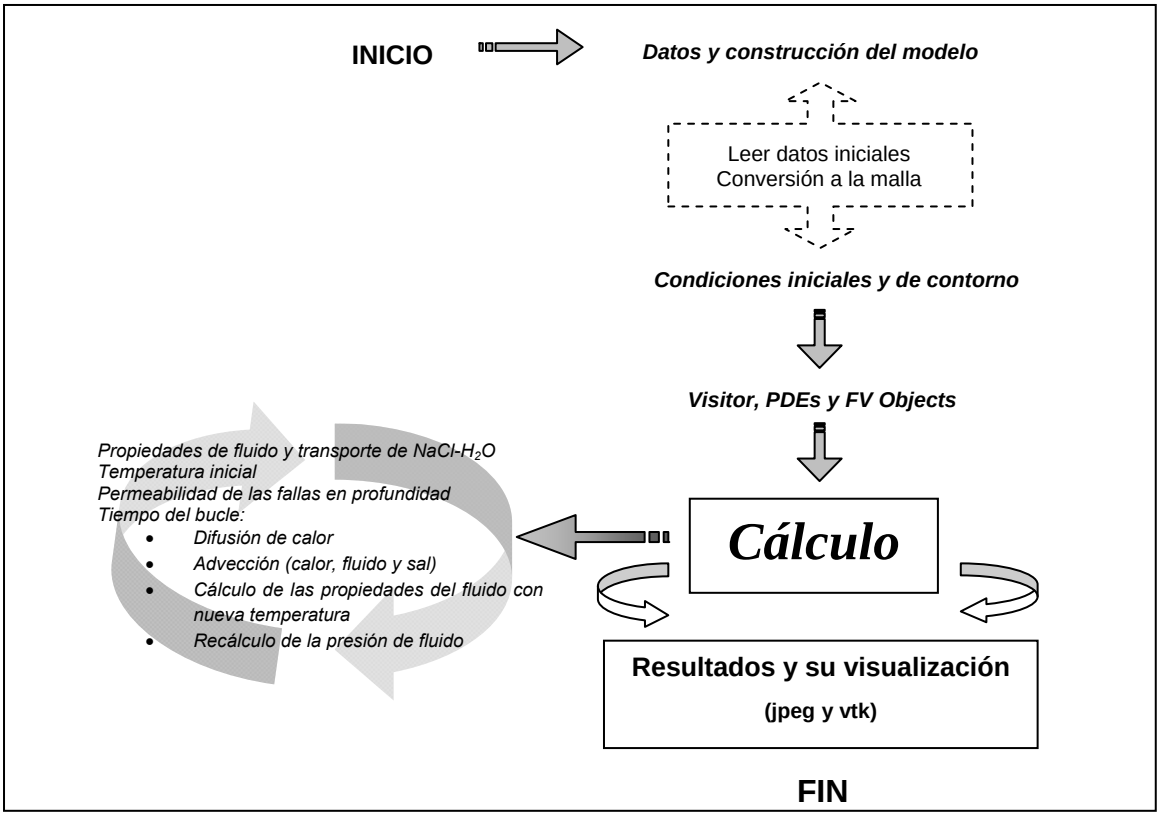

Figura 3. Esquema del proceso de modelización y cálculo informático empleado para el desarrollo de este trabajo. Hay que tener en cuenta que el resultado de la simulación debe ser interpretado en su contexto geológico.

(8) “input and output methods”, que convierte los resultados de los cálculos informático en datos legibles como gráficos, fotos, etc.

3. Modelo conceptual

La construcción del modelo conceptual está basada en el conocimiento de las características estratigráficas, estructurales y paleogeográficas de la zona sur de la FPI, que han sido previamente descritas en diversos estudios generales de la zona (Mitjavila et al., 1997; Leistel et al., 1998; Tornos, 2006), así como en trabajos enfocados al estudio de los sulfuros masivos encajados en pizarras zona sur de la Faja Pirítica (Tornos et al., 1998, y trabajos enmarcados en esta tesis). Un aspecto importante para la construcción del modelo numérico es el encuadre geotectónico en el momento de formación de las mineralizaciones. Con este fin, se ha tenido en cuenta las características paleogeográficas regionales interpretadas a partir del perfil sísmico IBERSEIS (Simancas et al., 2003) y estudios posteriores (Brown et al., 2012; Rubio et al., 2013) (Fig. 4A).

Litológicamente, el modelo conceptual incluye dos unidades principales: una unidad sedimentaria que representa al Grupo PQ (de 1500-2000 m de espesor), y una secuencia heterogénea suprayacente, compuesta por rocas volcánicas y sedimentarias (500-800 m), equivalente al Complejo Volcano-Sedimentario. Este conjunto está tectónicamente afectado por una serie de fallas extensionales y de desgarre, que dan lugar a la formación de zonas relativamente permeables y que canalizarían gran parte del flujo de fluido, y podrían compartimentar el sistema hidrodinámico.

En el modelo se han prefijado una serie de parámetros físicos e hidrológicos característicos de las dos grandes unidades que la constituyen y que dependen de la litología (Tabla 1). Para la alternacia de pizarras y areniscas del Grupo PQ se asume una permeabilidad y porosidad relativamente más alta que las del Grupo Volcano-Sedimentario. Los valores de estos parámetros han sido estimados a partir de la bibliografía y en base a los porcentajes estimados de cada tipo de roca que constituyen a

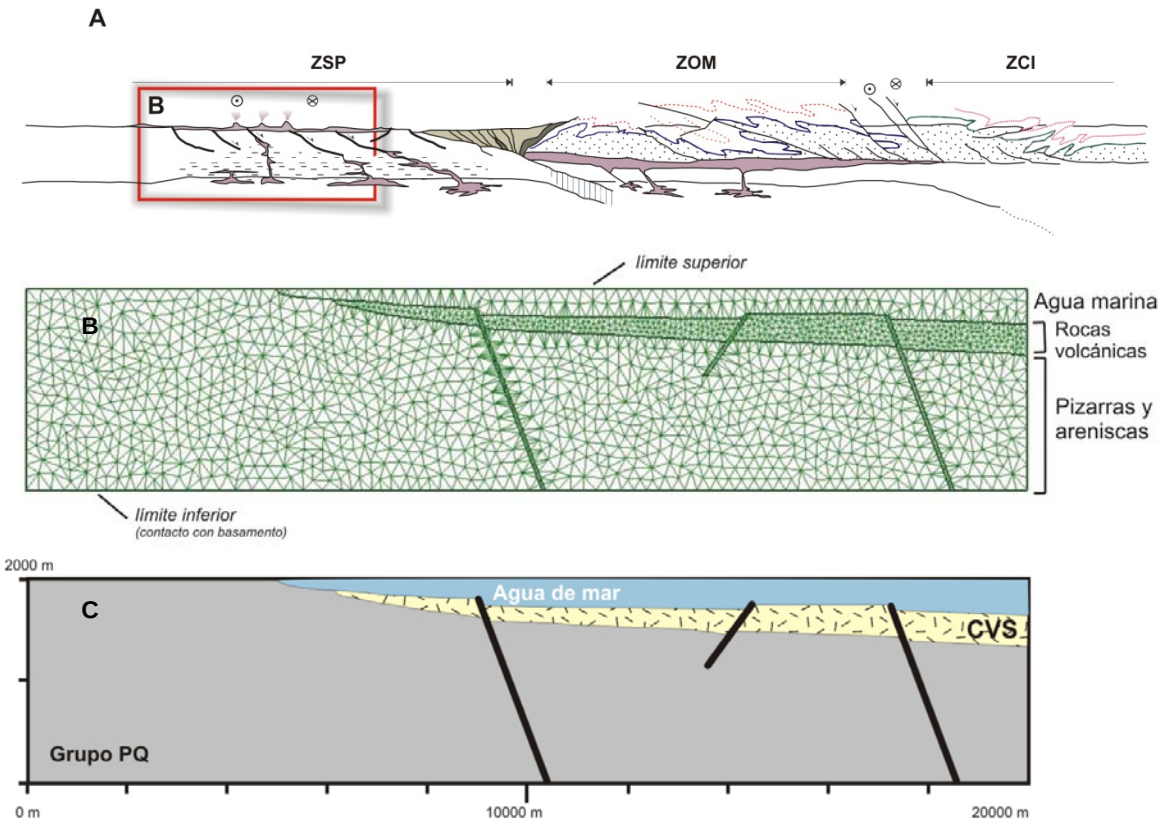

Figura 4. (A) Interpretación geológica del perfil sísmico profundo de reflexión IBERSEIS (Simancas et al., 2003); el recuadro muestra la zona modelizada. (B) Malla numérica de elementos y nodos del modelo para la zona sur de la Faja Pirítica; para cada uno de ellos se calcula el flujo de calor y fluido, así como velocidad, en función del tiempo y características de cada elemento. (C) Dimensiones, estratigrafía general y estructuras tectónicas del modelo.

la unidad litológica. El modelo ha sido realizado involucrando a dos fluidos con salinidades iniciales de 0 y 10% peso NaCl, respectivamente. Otras propiedades físicas de las rocas, como la capacidad calorífica y la conductividad térmica han sido determinadas a partir de los datos existentes para litologías equivalentes en contextos hidrodinámicos y geológicos similares (Bear, 1988; Domenico & Schwartz, 1990; Allen & Allen, 2004; Geiger, 2004; Matthäi et al., 2004). Para el Complejo Volcano-Sedimentario, unidad situada directamente bajo el fondo marino, los parámetros anteriormente citados se ha estimado promediando en base a las proporciones relativas de las rocas que lo componen (pizarra, riolita, dacita y basalto y sus equivalentes volcanosedimentarios); a grandes rasgos, esta unidad tiene una permeabilidad y una porosidad más bajas que las de la unidad infrayacente (Fig. 5).

Tabla 1. Valores de las propiedades iniciales consideradas en el modelo.

		Valores	Unidades	Referencia
Propiedades específicas de las unidades (permeabilidad[1])				
Complejo Volcano-Sedimentario		$1,0x10^{-15}$	m^2	estimado de:
Grupo PQ		$1,0x10^{-14}$	m^2	Freeze and Cherry (1979
Zona de falla		$1,0x10^{-12}$	m^2	Lewis 1989
Agua (océano)		$1,0x10^{-10}$	m^2	Smith & Chapman, 1983
Asignaciones generales de los materiales				
capacidad calorífica (roca)		880	J/kg K	
densidad (roca)		2700	Kg/m^3	
conductuvidad térmica		2.0	W/m ºC	estimado de:
comprensibilidad (roca)		$1,0x10^{-15}$	Pa^{-1}	
expansivad (roca)		$1,0x10^{-15}$	Pa^{-1}	Bear, 1972
fuente total		0		Domenico & Schwartz, 1990
fuente de fluido		0		Geiger, 2004
fuente de energía		0		Matthäi et al., 2004
fuente de salinidad		0		Allen & Allen, 2004
difusividad		$2,0x10^{-9}$	m^2/s	
porosidad		0,1	%	
Propiedades básicas de las unidades (porosidad)				
Zona de falla		0,3	%	
Grupo PQ		0,15	%	
Complejo Volcano-Sedimentario		0,1	%	
Propiedades especificas				
conductividad térmica (agua)		200	W/m ºC	
salinidad (agua)		3,2	% peso NaCl	
salinidad (PQ)[2]		0-10	% peso NaCl	Tornos 2006 Tornos & Heinrich 2011
Condiciones de contorno[3]				
temperatura	superior (*Dirichlet*)	23	ºC	
fuente de calor	inferior (*Neumann*)	$1,35x10^{-1}$	W	estimado de
salinidad	superior (*Dirichlet*)	3,2	% peso NaCl	Allen,P& Allen J, 1990
Salinidad[4]	inferior (*Dirichlet*)	5-15	% peso NaCl	Allen & Allen, 2004
presión de fluido	superior (*Dirichlet*)	101325	Pa	

[1] *Permeabilidad igual para componente vertical y horizontal.*

[2] *El valor de la salinidad del Grupo PQ varía en función del caso testado.*

[3] *Condiciones de contorno: Dirichlet (valor fijo) y Neumann (flujo fijo). Estas condiciones determinan la interacción del objeto con el medio que lo rodea.*

[4] *El valor de salinidad en la condición de contorno inferior varía según el caso testado.*

Las condiciones iniciales y de contorno consideradas en el modelo son:

(a) la *condición de contorno del margen inferior*, que representa la presencia de un basamento de muy baja permeabilidad intruido por rocas ígneas, y que se caracteriza por un alto flujo de calor, con valores entre 85 a 120 mW/m^2 estimados según valores calculados en cuencas de características y edades similares (Allen & Allen, 1990). Esta elevada fuente de calor da lugar al desarrollo de un alto gradiente geotérmico en la cuenca.

(b) la ***condición de contorno superior*** está definida por la superficie del agua marina, con una temperatura de 23ºC, una salinidad del 3,2 % peso NaCl, y presión de 1 atm.

Respecto a las condiciones iniciales y de contorno de la salinidad de las soluciones hidrotermales del Grupo PQ, se han postulado dos casos como ejemplos extremos que podrían reflejar las salinidades iniciales en las aguas de esta unidad. Con ello, se pretende observar la sensibilidad de los resultados –del flujo convectivo y de la temperatura- respecto a la salinidad. La primera hipótesis (Caso 1) asume que los fluidos en equilibrio con el Grupo PQ tienen una salinidad cero (agua pura), y una condición de contorno inferior con una salinidad del 5 % peso NaCl. En la segunda hipótesis (Caso 2), se ha tomado como condición inicial de salinidad de los fluidos en equilibrio con el Grupo PQ un valor de 10 % peso NaCl y una condición inferior de salinidad del 15 % peso NaCl. Esta salinidad está basada en la salinidad media de los fluidos hidrotermales relacionados con los sulfuros masivos del sector sur de la Faja Pirítica (Tornos, 2006; Tornos & Heinrich, 2008)

La discretización espacial del modelo numérico está ilustrada en la Figura 4B. Esta figura muestra una malla bidimensional de 3634 elementos triangulares que representa un corte geológico simple de dimensiones 20 x 40 km, y en el que quedan diferenciadas las dos unidades estratigráficas principales, las zonas de fallas y el agua del mar. La discretización temporal y espacial ha tenido en cuenta las limitaciones de los números de Peclet y Courant (de Marsily, 1986; Bear, 1988), para lo cual se realizaron pruebas con mallas preliminares para el cálculo de flujo, llegando a definir la malla final que ha sido utilizada en la modelización, así como los incrementos de tiempo implementados en el modelo. De este modo, para resaltar los cambios en el sistema, se ha realizado una discretización más fina en las zonas más susceptibles de experimentar cambios mayores en las variables. Así, se ha considerado que las unidades denominadas como “falla” y “rocas volcánicas” se dividirían en elementos más pequeños (tres veces menores respecto a las unidades “Grupo PQ” y “Agua”), porque son las zonas donde se espera

se produzcan las mayores tasas de flujo y transporte de calor y soluto.

Las simulaciones numéricas se han realizado para un tiempo total de 3 Ma, que es el intervalo máximo de duración de la mineralización y que corresponde al Estruniense Superior (González et al., 2002; Oliveira et al., 2002).

4. Resultados

La modelización realizada tiene como condición inicial una salinidad homogénea para el fluido contenido en cada unidad litológica, un campo de presiones hidrostáticas, y una temperatura dada por el gradiente geotérmico impuesto. Se debe tener en cuenta que, los cálculos modifican gradualmente el estadio inicial hipotético hacia una situación compatible con las condiciones de contorno impuestas. Posteriormente, el sistema hidrodinámico evolucionará transitoriamente hasta alcanzar las condiciones de flujo estacionario. En este sentido, los tiempos que se obtienen son solo estimativos y obtenidos a partir de las condiciones iniciales impuestas en el modelo. Sin embargo, son extremadamente útiles para evaluar cualitativamente los momentos hidrológicos clave, así como para comparar los tiempos relativos entre los dos supuestos testados.

4.1. Caso 1

El modelo numérico basado en que el Grupo PQ contiene agua no salina muestra que ya en los primeros años de simulación la circulación de fluidos empieza a desarrollar las primeras celdas convectivas. A los 300.000 años de iniciarse el proceso, se instaura una circulación convectiva generalizada en casi todo el sistema (Fig. 6), algo que permite descartar una circulación lateral confinada restringida a las rocas sedimentarias o a niveles especialmente permeables de la unidad volcánica, tales como niveles de pómez o vidrio o rocas volcanoclásticas. No es hasta cerca del 1 Ma cuando el sistema convectivo alcanza un estado quasi-estacionario caracterizado por una velocidad de fluido más constante, en torno a $2x10^{-8}$ m/s. En estos circuitos destaca el papel hidrodinámico de las fallas, las cuales actúan como vías preferentes de ascenso de los fluidos. Mientras que

pequeñas filtraciones se producen por zonas litológicamente permeables.

Los estadios iniciales de circulación hidrotermal en el modelo se caracterizan por el ascenso rápido de fluidos de alta temperatura (200-250ºC) y por elevadas velocidades de flujo que pueden alcanzar hasta $1{,}0x10^{-7}$ m/s. Posteriormente, estos pulsos calientes y veloces están acompañados de la circulación de fluidos con la mayor salinidad del ciclo (Fig. 7), algo que tiene lugar entre los 100.000 y 200.000 años. Después de este estadio inicial, el sistema entra en una fase más estable en la que gradualmente baja la temperatura y salinidad, probablemente como consecuencia de la mezcla del agua oceánica y fluidos salinos profundos (Fig. 6). Durante estas etapas, la distribución de la temperatura y salinidad tienen un patrón homogéneo en todo el modelo. En los últimos estadios, el sistema se estabiliza dando lugar a la formación de masas de agua poco salinos a techo del Grupo PQ. Trascurrido 1 Ma, las plumas de calor son menos vigorosas (Fig. 6) y, la temperatura con la que los fluidos ascienden es menor que la de los estadios anteriores (90-125ºC). Los resultados muestran el papel determinante de las fallas como vías de circulación preferente de los fluidos calientes con altas velocidades de flujo. Raramente se observa descenso de agua oceánica a través de las fallas; agua oceánica parece descender preferentemente a lo largo de discontinuidades menores y de zonas litológicamente más permeables.

4.2. Caso 2

En el segundo caso se ha supuesto que el fluido en equilibrio con las rocas que forman el Grupo PQ tiene salinidades y densidades intermedias (10 % peso NaCl). Los resultados muestran que el sistema convectivo que se genera se caracteriza por la presencia de celdas significativamente más pequeñas que en el caso anterior, y no es hasta pasado el millón de años cuando se observa la generación de celdas convectivas de mayores dimensiones, en torno a los 500-1000 m (Fig. 8).

Figura 6. Secuencias de distribución de la velocidad de flujo de fluido, temperatura y salinidad a los 300.000 años y 1 Ma iniciado el modelo (Caso 1), mostrando los cambios que el sistema experimenta a lo largo del transcurso del tiempo y de las condiciones variables del modelo. Las células convectivas se forman claramente desde los primeros años, destacando por su tamaño y velocidad ($\leq 2x10^{-8}$ m/s) a partir de los 300.000 años de iniciado el modelo.

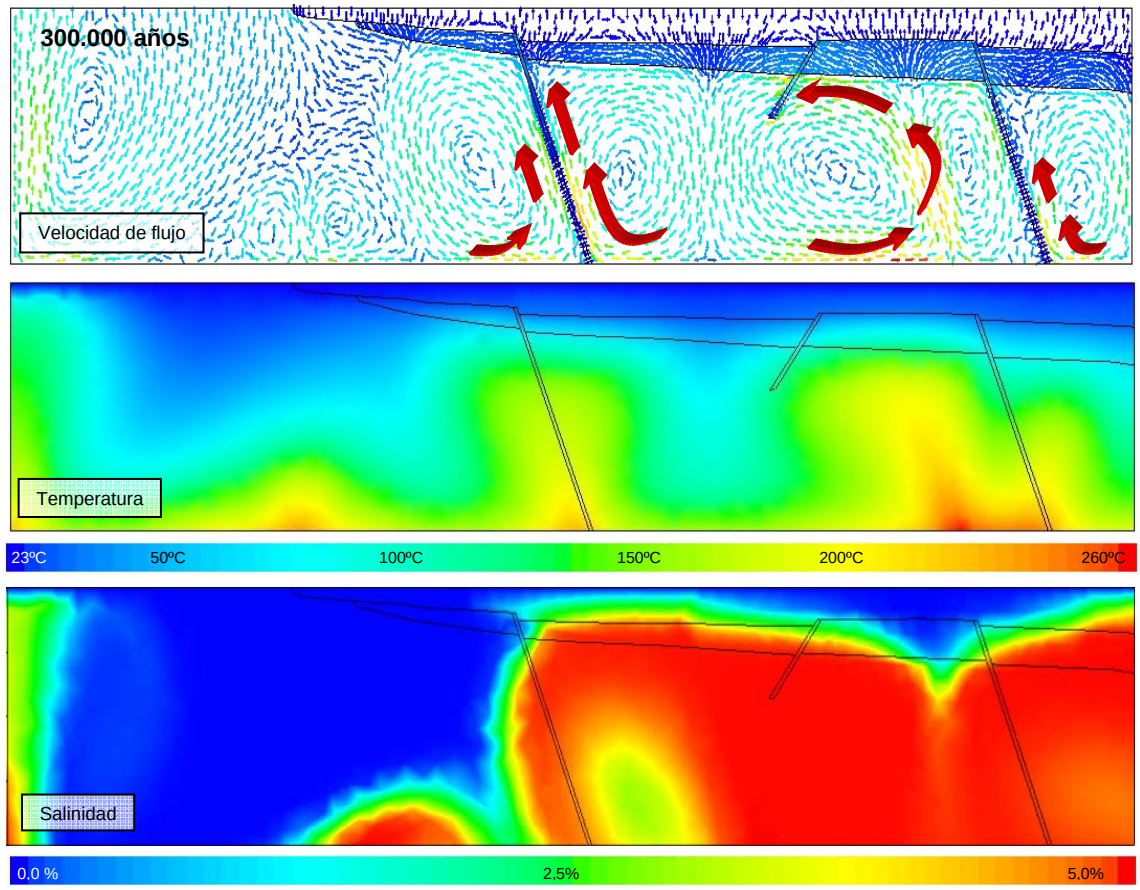
300.000 años
Velocidad de flujo
Temperatura
23ºC
50ºC
100ºC
150ºC
200ºC
260ºC
Salinidad
0,0 %
2,5%
5,0%

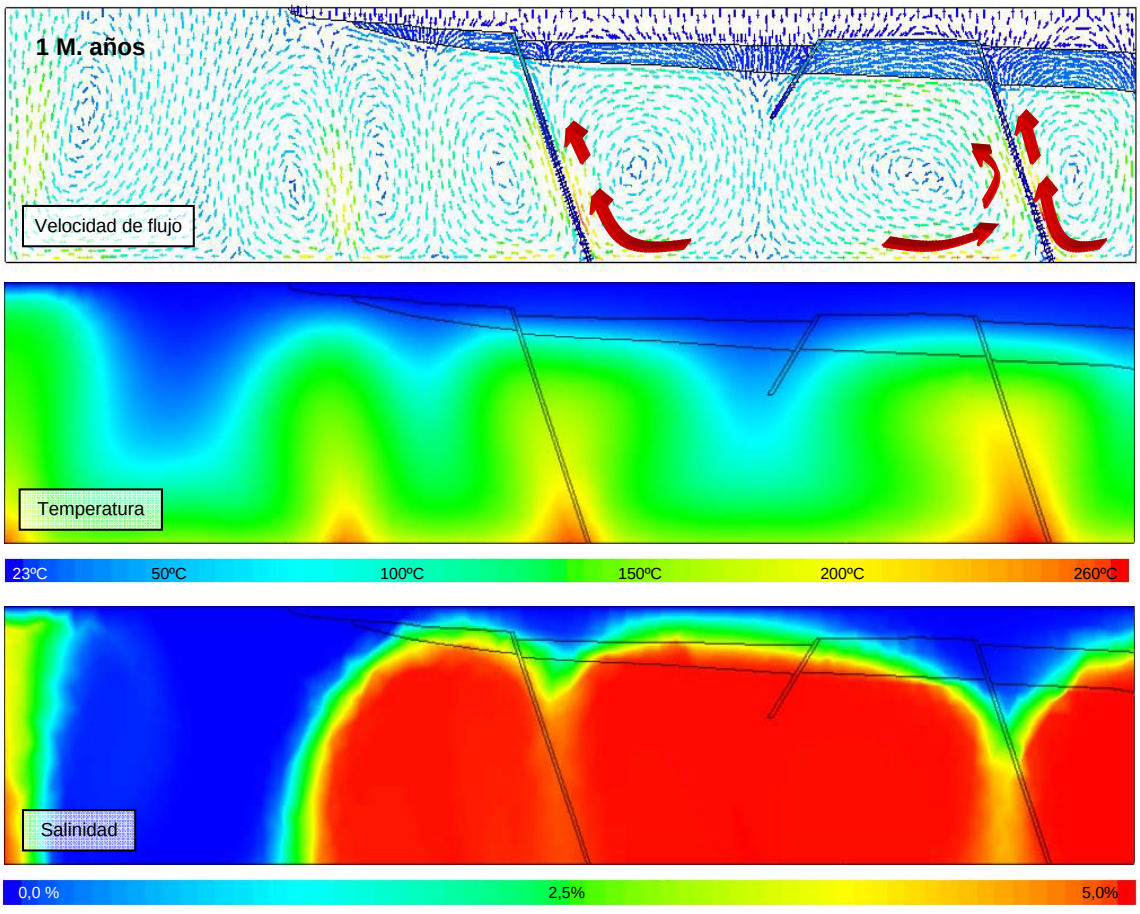
1 M. años
Velocidad de flujo
Temperatura
23ºC
50ºC
100ºC
150ºC
200ºC
260ºC
Salinidad
0,0 %
2,5%
5,0%

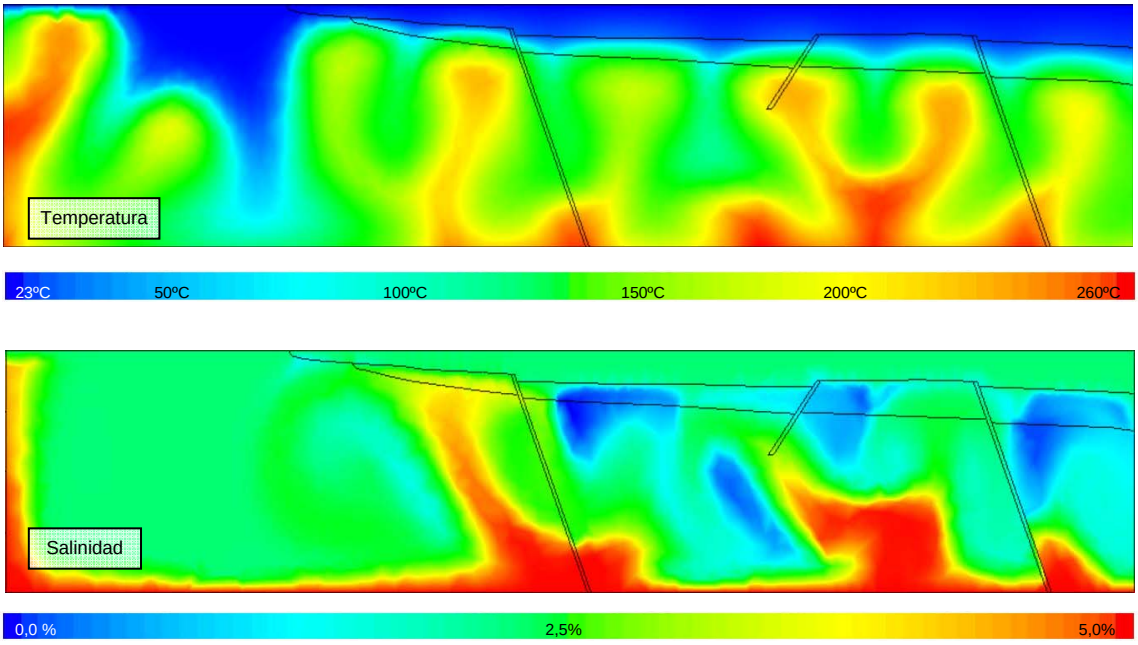

Figura 7. Distribución de la temperatura y salinidad del Caso 1 en estadios tempranos. (A) El trasporte de calor en el sistema, ya desde muy pronto (16.000 años de iniciado el test) da lugar al desarrollo de "finger" o pulsos de alta temperatura (≈200ºC). (B) Distribución de la evolución de la salinidad transcurridos 30.000 años (unidades salinidad % peso NaCl), mostrando grandes plumas con elevada salinidad.

Las velocidades del flujo de fluido son del orden de entre 10^{-9} y 10^{-11} m/s, con máximos locales que no superan los 10^{-8} m/s, esto es, estas celdas son entre uno y dos órdenes de magnitud más lentas que las formadas por fluidos poco salinos. Aquí es evidente como una mayor salinidad de las soluciones convectivas ralentiza el flujo, debido a una mayor densidad y viscosidad, lo que provoca a su vez una inercia y fricción mayor y, por tanto, una mayor resistencia al movimiento. Aunque el patrón evolutivo de flujo de calor y salinidad es similar al primer caso se aprecian, sin embargo, grandes diferencias. El modelo muestra que hay intensos pulsos de flujo de calor en estadios tempranos de la evolución convectiva (10.000 y 20.000 años), pero las propias características del fluido no permiten que se alcancen temperaturas superiores a los 160ºC en el fondo oceánico (Fig. 9A). Esta elevada salinidad también cambia las condiciones hidrodinámicas del

sistema y permite el descenso de fluidos más fríos y menos salinos provenientes del mar a través de las zonas de falla. Este hecho da lugar al trasporte rápido de agua fría hacia las partes profundas del sistema, lo que provoca que éste se enfríe más rápidamente. Así, una vez que el sistema alcanza el estado estacionario se observa un flujo de calor a temperaturas entre 200 y 250ºC pero que está restringido a la parte inferior del modelo. La salinidad tiene un comportamiento similar. Inicialmente, el flujo de calor origina la lenta circulación de fluidos salinos (10-15% peso NaCl) pero transcurridos estos primeros estadios la salinidad baja progresivamente como consecuencia de la mezcla del fluido profundo con el agua marina (Fig. 9B). Transcurridos los 3 Ma, el tamaño de las células convectivas disminuye a tamaños de 500-1000 m y la velocidad de flujo es muy baja (entre 10^{-9} y 10^{-13} m/s), quedando un sistema estable, donde no se producen grandes plumas de fluidos cálidos y salinos.

5. Discusión y conclusiones

La modelización numérica de los procesos hidrogeológicos que dan lugar a la formación de yacimientos de sulfuros masivos de la FPI muestra que el flujo de fluido está controlado por una circulación convectiva y no por el flujo lateral, demostrando que la circulación estratofúgica es poco relevante en estos sistemas. Estos resultados son consistentes con estudios previos (Bitzer 1997; Garven et al., 2001) que también muestran que el flujo por compactación pura de los sedimentos no es suficiente para transportar los solutos necesarios para generar depósitos minerales, aun a partir de disoluciones muy saturadas. Los resultados también muestran que no es necesario el emplazamiento de intrusiones ígneas someras para el desarrollo de las células convectivas, ni que la intrusión es un factor condicionante para que se formen grandes células. Con gradientes geotérmicos normales en una zona de extensión pueden darse lugar células convectivas suficientes. Sin embargo, la salinidad parece ser el condicionante crítico del desarrollo del sistema. Controla la temporalidad y tamaño de las células convectivas, y por tanto, sería un factor decisivo en la ubicación y edad de las

Figura 8. Secuencias de distribución de la velocidad de flujo de fluido, temperatura y salinidad en el Caso 2 para los 300.000 años y 1 Ma. Las células convectivas se desarrollan muy tarde y con velocidades muy bajas, del orden de 10^{-9} y 10^{-11} m/s. Raramente se observan pequeños pulsos de fluidos que llegan hasta temperaturas de unos 150ºC. A partir de 1 Ma de la simulación, se observan flujos de fluido descendente (flecha azul), generalmente asociado a las fallas, provocando un descenso de temperatura en el sistema. En los estadios finales, las células convectivas son pequeñas, de morfología vertical y velocidad baja, posiblemente debido a la alta salinidad del sistema en ese momento.

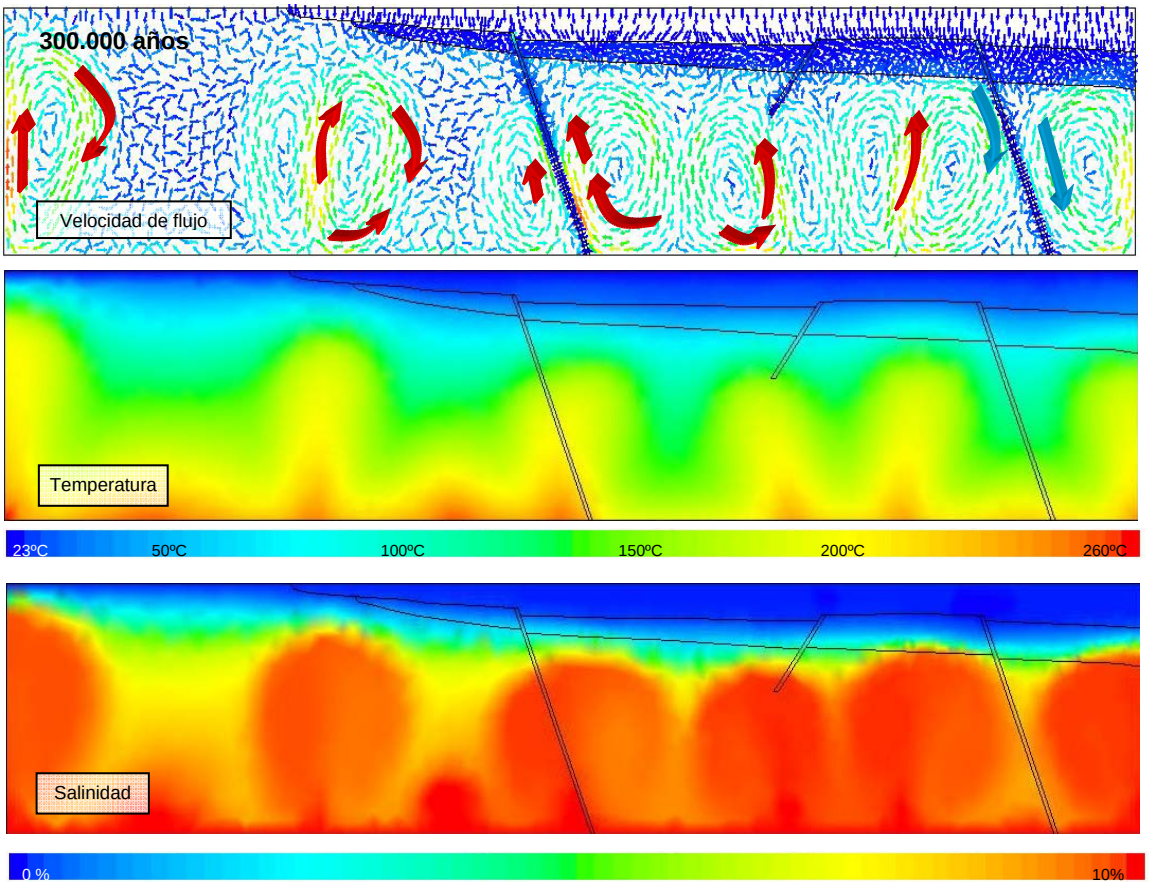
300.000 años
Velocidad de flujo
Temperatura
23ºC
50ºC
100ºC
150ºC
200ºC
260ºC
Salinidad
0 %
10%

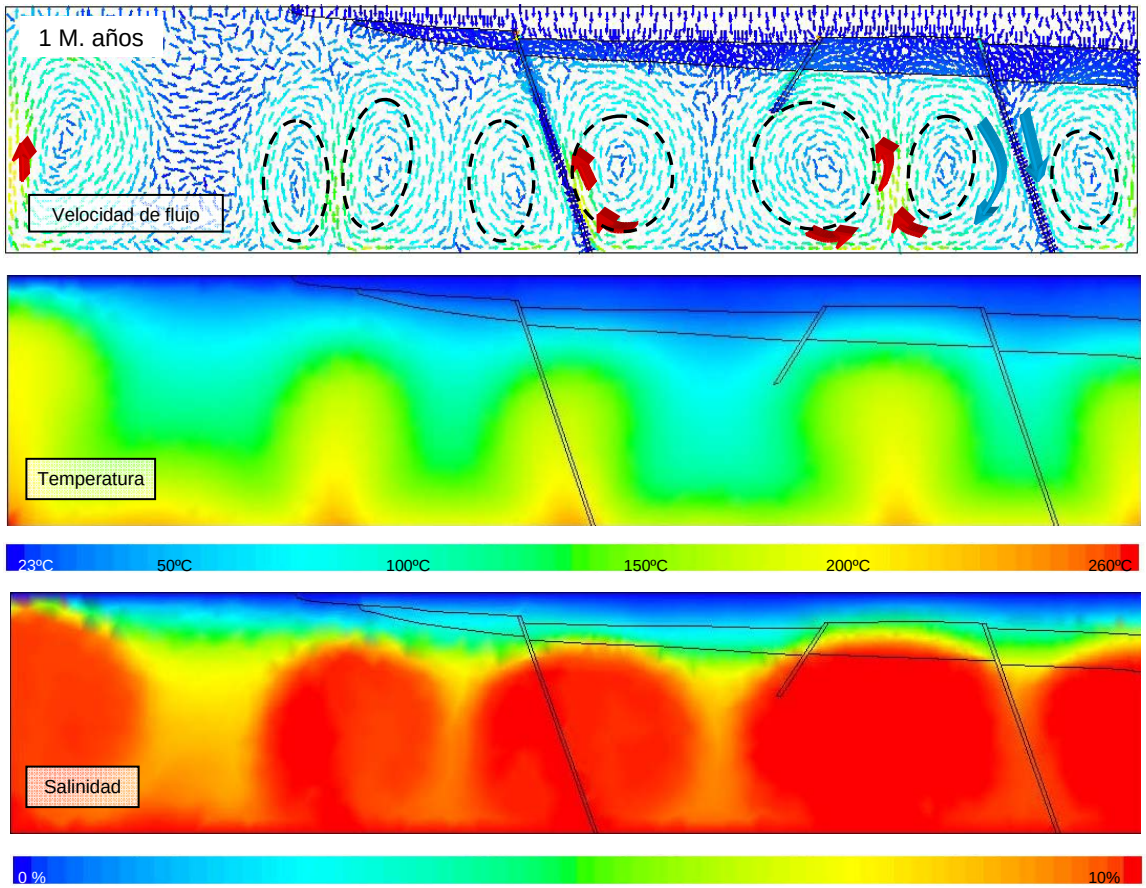
1 M. años
Velocidad de flujo
Temperatura
23ºC
50ºC
100ºC
150ºC
200ºC
260ºC
Salinidad
0 %
10%

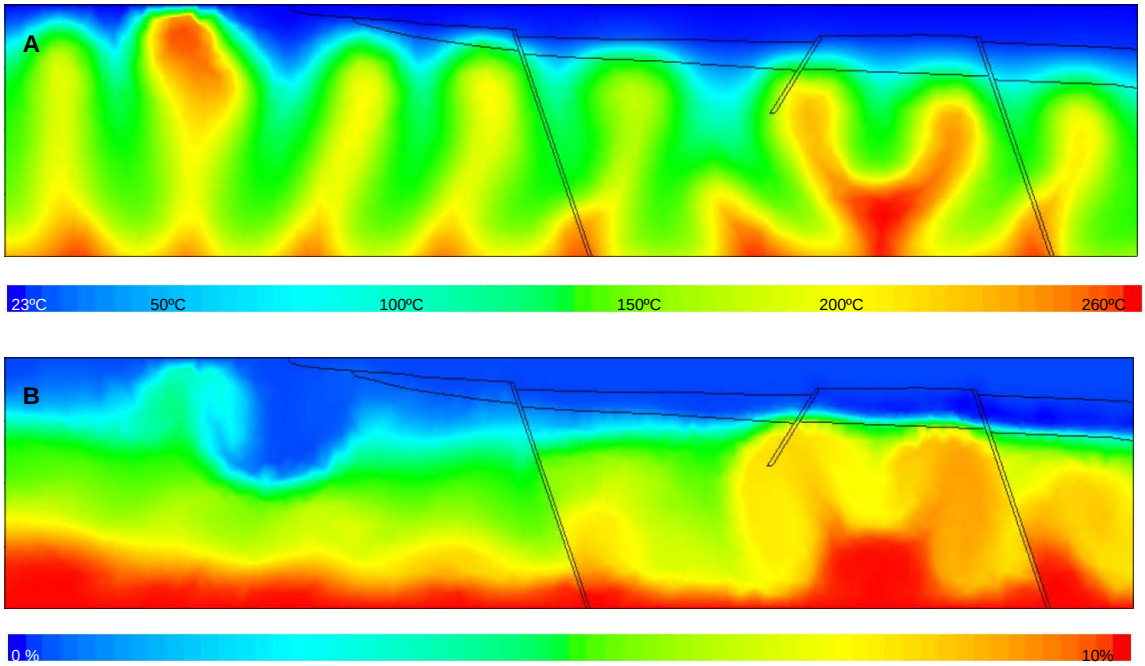

Figura 9. Distribución de temperatura y salinidad en la modelización del Caso 2. (A) El flujo de calor en el sistema salino evolución lentamente en los primeros estadios (16.000 años del inicio) y apenas si se forman pequeños pulsos de fluidos calientes (150ºC). (B) Distribución de la evolución de la salinidad en primeros estadios (30.000 años del inicio) (Leyenda: salinidad expresada en % peso NaCl).

zonas de exhalación hidrotermal y por ello de la distribución, tamaño y edad de los cuerpos de sulfuros masivos. El segundo factor determinante es la existencia de grandes estructuras tectónicas que son las que controlan la distribución de las células y la compartimentación del flujo.

El resultado más significativo de ambos modelos numéricos es que los fluidos más salinos y de mayor temperatura son los primeros en ascender y ser exhalados en el fondo marino. Dichos eventos tienen lugar tan pronto como se desarrollan las primeras células hidrotermales convectivas durante los primeros estadios de la evolución hidrodinámica de la cuenca y tan pronto como se produce un incremento del gradiente geotérmico. En estas células se alcanzan salinidades de 4-5% peso NaCl y temperaturas de 150-250ºC. Estas temperaturas y salinidades son similares a las que se han determinado en los stockwork de algunos sulfuros masivos del sur de la Faja Pirítica (Tornos, 2006; Relvas, 2000; Relvas et al., 2006; Tornos & Heinrich, 2008). Teniendo en cuenta la relación

directa entre la salinidad y temperatura y la solubilidad de los metales transportados como complejos clorurados (e.g., Eugster, 1986; Brimhall y Crerar, 1987), es probable que estos flujos convectivos sean los que transportaron los metales desde el basamento y dieron lugar a los sulfuros masivos de la zona sur por mezcla con aguas anóxicas y enriquecidas en azufre biogénico que se acumularían en subcuencas restringidas (Solomon et al., 2004; Tornos, 2006, Menor et al., 2010; Tornos et al., 2015).

El modelo numérico también es coherente con la formación de los sulfuros masivos en un intervalo relativamente corto de tiempo. Los dos casos estudiados muestran que la circulación de los fluidos calientes y salinos se restringe a los momentos posteriores a la instauración del sistema y que no llegan a durar un millón de años. Esto explicaría la corta duración, la sincronicidad y gran tamaño de los sulfuros masivos del sector meridional de la Faja Pirítica. Si no hay modificación del sistema hidrotermal o entrada de fluidos magmático-hidrotermales en la base del sistema, los sistemas hidrotermales pasarían a estar dominados por fluidos fríos y poco salinos de origen marino que tendrían poca capacidad de transporte de metales y que no serían capaces de formar depósitos. Probablemente ligados a esta etapa son los abundantes depósitos de jaspe y manganeso que hay en la Faja Pirítica (Sedler et al., 1997; Leistel et al., 1998).

Acknowledgements

Este estudio ha sido financiado por una beca Marie Curie del Comunidad Europea, los proyectos de investigación DGI-FEDER 2003-0290 y DGI2011-23214. Es una contribución al proyecto de Comparación Global de Sulfuros Masivos (IGCP 502). Quisiera agradecer especialmente al Dr. Stephan Matthäi y Dr. Sebastian Geiger por su gran ayuda con el Programa CSP (Complex Systems Paltform) y la compilación de los modelos propuestos, así como a Dr. Thomas Driesner, Dr. Richard Herrington y Dr. Joaquín Salas por sus constructivos comentarios y discusiones. Y al Dr. Carlos Ayora por su ayuda en el inicio de la formación y aprendizaje en el desarrollo de modelos numéricos.

Bibliografía

Allen, P.A., Allen J.R., 2004. Thermal history, In “Basin Analysis. Principles & Applications”, P.A. Allen and J.R. Allen, eds Balckwell Publishing, 282-305.

Barrie, C. T., Cathles, L. M., Erendi, A., Carr, P., Shosa, J., A., Ioannou, S., Spooner, E.T.C., 2001. Heat and Fluid Flow Modeling of Giant VMS Systems, Canadian Mining Industry Research Organization Final Report, 431 p.

Barrie, C.T., Amelin, Y., Pascual, E., 2002. U-Pb Geochronology of VMS mineralization in the Iberian Pyrite Belt. Mineralium Deposita, 37-8, 684-703.

Barrie, C. T., Erendi, A., Cathles, L. M., 2004. A Crustal Scale Heat and Fluid Flow Model for the Giant Rio Tinto VMS District, Iberian Pyrite Belt. Eos. Trans. AGU 85(19), Joint Assambly Supple., Abstract V11B-02.

Bear, J., 1988. Dynamics of Fluids in Porous Media. Dover Publicatons, Inc. 764 pp.

Bitzer, K., 1997. A finite-element model lfor simulation of consolidation, fluid flow, solute transport and heat flow in sedimentary basisns. Proceedings IAMG’97. CIMNEmUPC, Barcelona : 579-584.

Brimhall, G.H, Crerar, D.A., 1987. Ore fluids: magmatic to supergene. Reviews in Mineralogy and Geochemistry 17, 235-321.

Domenico, P.A., Schwartz, F. W., 1997. Physical and Chemical Hydrogeology. Willey. New York. 506 pp.

Campbell, I. H., McDougall, T. J., and Turner, J. S., 1984. A note on fluid dynamic processes which can influence the deposition of massive sulfides: Economic Geology 79, 1905-1913.

Conde, C., Tornos, F., Fernández, J., Doyle, M., 2003. Encuadre estratigráfico de los sulfuros masivos de la parte suroriental de la Faja Pirítica: Aznalcóllar-Los Frailes, y Las Cruces. Boletin de la Sociedad Española de Mineralogía, 26-A.

Conde, C., Tornos, F., 2014. Volcanic stratigraphy and geochemistry of the VS complex in the northern Iberian Pyrite Belt. Macla nº19.

Conde, C., Matthäi, S., Geiger, S., Tornos, F., Herrington, R., 2005. Heat and fluid modeling of the shale-hosted massive in the Iberian Pyrite Belt, Spain. In Abst: GAC-MAC meeting Halifax 2005, v. 30, 31-32.

de Marsily, G., 1986. Quantitative Hydrogeology. Groundwater hydrology for engineers. Academic press, San Diego.

de Ronde, C.E.J., Massoth, G.J., Baker, E.T., Lupton, J.E., 2003b. Submarine hydrothermal venting related to volcanic arcs. Soc. Econ. Geol. Spec. Publ. 10, 1–110.Eugster, HP (1986) Minerals in hot water. American Mineralogist 71, 655-673.

Doyle,M.G., Allen, R.L., 2003. Subsea-floor replacement in volcanic-hostedmassive sulfide deposits. Ore Geol. Rev. 23, 183–222.

Freeze, R.A, Cherry, J.A., 1979. Groundwater. Prentice-Hall, Englewood Cliffs.

Galley, A.G., Watkinson, D.H., Jonasson, I.R., Riverin, G., 1995. The subsea-floor formation of volcanic hosted massive sulfide: evidence from the Ansil deposit, Rouyn-Noranda, Canada. Economic Geology 90, 2006–2017.

Garven, G., Bull, S.W., Large, R.R., 2001. Hydrohtermla fluid flow modles of strariform ore genesis in the McArthur Basin, Northern Territory, Asutralia. Geofluid 1, 289-311.

Geiger, S., 2004. Numerical simulations of the hydrodynamics and therodinamics of NaCl-H2O fluids. PhD Thesis, Swiss Federal Institute of Technology Zürich, 233 pp.

González, F., Moreno, C., Sáez, R., Clayton, G., 2002. Ore genesis age of the Tharsis Mining District (Iberian Pyrite Belt): a palynological approach. Journal of the Geological Society., London, Vol. 15: 229-232.

Goodfellow, W.D., McCutcheon, S.R., 2003. Geologic and genetic attributes of volcanic sediment-hosted massive sulfide deposits of the Bathurst Mining Camp, Northern New Brunswick — a synthesis. Econ. Geol. Monogr. 11, 245–301.

Gruen, G., Weis, P., Driesner, T., de Ronde, C.E.J., Heinrich, C.A., 2012. Fluid-Flow Patterns at Brothers Volcano, Southern Kermadec Arc: Insights from Geologically Constrained Numerical Simulations. Economic Geology 107:1595-1611.

Huston, D.L., Relvas, J.R.S., Gemmell, J.B., Drieberg, S., 2011. The role of granites in volcanic-hosted massive sulphide ore-forming systems: an assessment of magmatic–hydrothermal contributions. Mineral. Deposita 46, 473–507.

Ingebritsen, S. E., Appold, M. S., 2012. The physical hydrogeology of ore deposits, Economic Geology, 107, 559–584.

Leistel, J. M., Marcoux, E., Thieblemont, D., Quesada, C., Sanchez, A., Almodovar, G. R., Pascual, E., Saez, R., 1998. Mineralium Deposita, 33/1-2, 2-30.

Lewis, M. A., 1989. 'Water' in Earth Science Mapping for planning, development and conservation. Ed: McCall, J, Marker, B. Graham y Trotman.

Matthäi, S.K., Geiger, S., Roberts, S.G., 2001. The Complex Systems Platform CSP3D3.0: User's Guide, 3rd ed. Zurich, Switzerland: ETH Research Reports, 150 p.

Matthäi, S.K., Heinrich, C.A. Driesner, T., 2004. "Is the Mount Isa copper deposit the product of forced brine convection in the footwall of a major reverse fault?" Geology 32 (4): 357-360.

Mitjavila, J., Marti, J., Soriano, C., 1997. Magmatic evolution and tectonic setting of the Iberian Pyrite Belt volcanism. Journal of Petrology 38, 727– 755.

Mellado, D. González Clavijo, E., Tornos, F. Conde, C., 2006. Geología y estructura de la Mina de Río Tinto (Faja Pirítica Ibérica, España). Geogaceta 40, 231-234.

Menor–Salvan, C., Tornos, F., Fernandez-Remolar, D., Amils, R., 2010. Association beween ctastrophic paleovegetation changes during Devonian-Carboniferous boundary and teh formation of giant massive sulfphide deposits. Earth and Planetary Science Letters 299, 398-408

Moreno, C., 1993. Post-volcanic Paleozoic of the Iberian Pyrite Belt: an example of basin morphologic control on sediment distribution in a turbidite basin. Journal of Sedimentary Petrology 63, 1118- 1128.

Onézime, J., Charvet, J. Faure, M., Chauvet, A., Panis, D., 2012. Structural evolution of the southernmost segment of the West European Variscides: the South Portuguese Zone (SW Iberia). Journal of Structural Geology 24, 451-468.

Oliveira, D. P. S., Poujol, M., Robb, L. J., 2002. Revista Sociedad Geológica España, 15/1-2, 105-112.

Pereira, Z., Saez, R., Pons, J. M., Oliveira, J. T., Moreno, C., 1996. Geogaceta, 20-7, 1609-1612.

Quesada, C., 1998. A reappraisal of the structure of the Spanish segment of the Iberian Pyrite Belt. Mineralium Deposita 33, 31-44.

Relvas, J.M.R.S., Barriga, F.J.A.S., Longstaffe, F., 2006. Hydrothermal alteration and mineralization in the Neves-Corvo volcanic-hosted massive sulfide deposit, Portugal: II. Oxygen, hydrogen and carbon isotopes. Economic Geology 101, 791–804.

Sánchez-España J., Velasco F., Boyce, A.J., 2003. Source and evolution of ore-forming fluids in northern Iberian Pyrite Belt massive sulphide deposits (SW Spain): evidence from fluid inclusions and stable isotopes. Mineralium Deposita 38, 519–537.

Schardt, C., Yang, J., Large, R., 2005. Numerical heat and fluid-flow modeling of the Panorama volcanic-hosted massive sulfide district, Western Australia: Economic Geology, v. 100, p. 547-566.

Schardt, C., Large, R.R., 2009. New insights into the genesis of volcanic-hosted massive sulfide deposits on the seafloor from numerical modeling studies. Ore Geology Reviews 35, 333-351.

Sedler,I.K., Wipfler,E., Matheis,G., 1997. The formation of stratiform manganese deposits vs VMS deposits in the SW-Iberian Pyrite Belt. In Papunen,H. (ed.), Mineral deposits: research and exploration, Balkema, Rotterdam, 575-578

Silva, J.B., Oliveira, J.T. Ribeiro, A., 1990. Structural outline of the South Portuguese Zone. In: Dallmeyer, R.D., Martínez García, E. (Eds.) Pre-Mesozoic Geology of Iberia. Springer-Verlag, Verlin, 348-362.

Simancas, J. F., Carbonell, R., González Lodeiro, F., Pérez-Estaún, A., Juhlin, C., Ayarza, Kashubin, A., Azor, A., Martínez Poyatos, D., Almodóvar, G. R., Pascual, E., Sáez, R., Expósito, I., 2003. The Crustal Structure of the Transpressional Variscan Orogen of SW Iberia: The IBERSEIS Deep Seismic Reflection Profile. Tectonics 22 (6), 1962-1974.

Smith,L., Chapmann, D.S., 1983. On the thermal effects of groundwater flow, 1 Regional Sclae Systems. Journal Geophysic Res. 88, 593-608.

Tornos, F., 2006. Environment of formation and styles of volcanogenic massive sulphides: The Iberian Pyrite Belt. Ore Geology Reviews 28, 259-307.

Tornos, F., Casquet, C., Relvas, J.M.R.S. 2005. Transpressional tectonics, lower crust decoupling and intrusion of deep mafic sills: A model for the unusual metallogenesis of SW Iberia. Ore Geology Reviews, 27, 133-163.

Tornos, F., Heinrich, C.A., 2008. Shale basins, sulfur-deficient ore brines, and the formation of exhalative base metal deposits. Chemical Geology 247, 195-207.

Tornos, F., Solomon, M., Conde, C., Spiro, B.F., 2008. Formation of the Tharsis massive sulphide deposit, Iberian Pyrite Belt: geological, lithogeochemical, and stable isotope evidence for deposition in a brine pool. Economic Geology 103, 185-214.

Tornos, F., Conde, C., Velasco, F. (2015) Evolving Subduction-Related Basins Control the Formation of VMS Deposits in the Iberian Pyrite Belt. SEG Conference 2015, Hobart,Tasmania.

Apéndices

Apéndice I-I

Composición de las rocas volcánicas

Tabla I.I.1. Composición química de las rocas volcánicas (Capítulo I). (Cursiva: menor del límite de detección)

Cod. Lab	06/181-72	06/181-73	06/181-74	06/181-75	06/181-76	06/181-77	06/181-78
Muestra	FP-CC-01	FP-CC-02	FP-CC-05	FP-CC-06	FP-CC-07	FP-CC-08	FP-CC-10
%							
SiO_2	75,89	80,88	72,16	77,26	66,87	64,52	66,70
Al_2O_3	13,40	10,92	14,11	11,70	14,26	15,17	15,14
Fe_2O_3	1,83	1,00	2,96	2,10	4,88	5,93	5,92
CaO	1,68	0,52	0,51	0,11	1,92	4,16	0,47
TiO_2	0,17	0,13	0,29	0,17	0,44	0,59	0,61
MnO	*0,02*	*0,02*	*0,02*	*0,02*	0,05	0,07	0,07
K_2O	0,98	0,00	2,88	4,53	3,24	1,80	1,57
MgO	2,03	0,11	3,36	0,17	3,64	2,56	2,51
P_2O_5	*0,05*	*0,05*	*0,05*	*0,05*	*0,05*	0,07	0,05
Na_2O	1,25	5,96	0,54	3,30	1,01	2,97	2,90
PPC	2,77	0,48	3,20	0,65	3,71	2,17	4,04
TOTAL	100,1	100,1	100,1	100,1	100,1	100,0	100,0
µg/g							
Sc	14	11	10	5	18	21	19
V	6	7	35	4	92	99	93
Cr	25	161	39	115	68	111	42
Co	*2,41*	*2,41*	*2,41*	*2,41*	*2*	11,4	9,7
Ni	1,2	2,9	7,3	2,1	4,1	5,4	5,1
Cu	6,2	84,3	128	*1,35*	6,4	5,8	6
Zn	84,4	47,1	*247*	33,2	46,3	131,7	48,5
Ga	22,8	17,5	20,4	17,5	15,7	18,1	18,3
Ge	1	1,1	1,3	*0,9*	1	1,4	*0,6*
As	13	7,5	5,3	4,8	*2,6*	4,3	*1,9*
Se	*1*	1,1	*1*	*1*	*1*	*1*	*1*
Br	0,8	*0,7*	*0,8*	1	1	*0,7*	1,1
Rb	34,5	0,6	104,6	79,8	99,3	49,3	49,3
Sr	158,3	58,7	36,7	18,7	75,4	159,1	86
Y	68,9	55,8	72,1	64,4	17,7	30,4	28,5
Zr	210,5	138,6	178,4	309,5	115,6	159	173,8
Nb	16	13,2	13,1	12,9	5,2	7	6,4
Mo	*0,3*	2,6	*0,4*	1,1	*0,2*	1,2	*1*
Ag	*3,96*	*3,96*	*3,96*	*3,96*	*3,96*	*3,96*	*3,96*
Cd	*10*	*10*	*10*	*10*	*10*	*10*	*0,2*
Sn	7,2	5,9	*7*	5,5	*0,5*	*0,5*	2,4
Sb	5,7	3	4,7	4,3	*2,1*	*1,9*	3,4
I	4	*2,8*	4,4	*3,9*	7,4	7,1	4,1
Cs	*3,8*	*5,5*	*5,3*	*0,7*	*6*	*0,1*	*2,4*
Ba	160,5	105,5	1235	245,8	269,9	243,5	173,8
La	39,5	28	46,5	35,4	16	18,7	18
Ce	68,8	57,5	102,9	81,8	38,8	39,1	46,5
Nd	43,1	30,5	54,2	39,6	13,5	17,4	19,9
Sm	16,9	13	11,8	10,6	*0,9*	*5,7*	*1,6*
Hf	5,6	4,7	4,9	9,7	*2*	4,3	4,4
Ta	*0,9*	*1*	*0,8*	*0,5*	*2,47*	*0,3*	*2*
W	3,8	4,5	5,2	3,1	3,2	3,3	4,3
Tl	*0,4*	*0,7*	*0*	*1,4*	*0,8*	*1,4*	*0,5*
Pb	15,9	20	13,7	5,8	6,6	62	4,1
Bi	*0,2*	*0,6*	*0,7*	*0,8*	*1*	*1*	*1*
Th	14,6	10,6	16,6	11,5	7,2	7,1	6,4
U	3,5	4,9	3,2	1,9	1,1	1,9	*1*

Cod. Lab	06/181-79	06/181-80	06/181-81	06/181-82	06/181-83	06/181-84	06/181-85
Muestra	FP-CC-11	FP-CC-12	FP-CC-14	FP-CC-15	FP-CC-19	FP-CC-21	FP-CC-22
%							
SiO_2	76,84	72,05	61,10	55,32	75,70	76,06	64,01
Al_2O_3	10,83	13,37	16,42	16,20	12,82	12,91	16,84
Fe_2O_3	2,93	3,29	6,12	9,51	1,74	2,15	5,13
CaO	0,26	1,44	7,67	6,86	0,73	0,25	3,15
TiO_2	0,19	0,37	0,68	1,24	0,13	0,16	0,79
MnO	0,02	*0,02*	0,09	0,19	*0,02*	*0,02*	0,04
K_2O	3,22	2,83	0,69	0,76	5,12	1,68	2,96
MgO	2,14	2,08	2,57	3,62	0,11	2,18	1,26
P_2O_5	*0,05*	*0,05*	0,12	0,19	*0,05*	*0,05*	0,16
Na_2O	0,24	1,42	2,20	3,46	3,03	1,02	3,60
PPC	3,33	3,15	2,35	2,65	0,63	3,59	2,07
TOTAL	100,1	100,1	100,0	100,0	100,1	100,1	100,0
µg/g							
Sc	10	13	22	31	17	6	17
V	14	32	117	205	6	8	97
Cr	18	37	111	49	109	22	82
Co	*2,41*	*2,41*	9,5	33	*2,41*	*2,41*	8
Ni	4,6	6,7	11,7	10,2	2,1	3,2	7,5
Cu	10,7	9,2	11,2	9	*0,9*	*1,35*	13,7
Zn	52	51,8	60,4	89,3	30,9	30,5	63,3
Ga	15,4	18	19,3	18,6	17,6	15,5	20,6
Ge	1,2	1,4	1	1,3	1,6	1,1	1,3
As	4,9	4,3	3,2	6,8	7,7	*1,4*	18,5
Se	*1*	*1*	*1*	*1*	*0,1*	*1*	*1*
Br	0,8	*0,7*	1,3	2,9	*0,6*	1,8	0,9
Rb	128,2	117,1	26,2	20,5	153,2	77,3	95,1
Sr	14,6	121,4	426,3	199,7	47,9	56,2	183,7
Y	48,8	52,7	19,1	33,4	49,8	26,5	40,9
Zr	208,7	247	135,7	136,9	122,2	138,3	229,8
Nb	9	9,1	5,2	6,8	8,7	6	10,2
Mo	*0,1*	*1*	*0,5*	*0,1*	*0,4*	*0,6*	1
Ag	*3,96*	*3,96*	*3,96*	*3,1*	*3,96*	*3,96*	*3,96*
Cd	*10*	*10*	*2*	*7,3*	*0,7*	*10*	*10*
Sn	4,3	4,7	2,7	*0,3*	5,6	5,4	*2*
Sb	*0,7*	3,5	*1*	*2,37*	3,9	*2,3*	5
I	5,8	6,6	*2,2*	5,1	5,1	*3,2*	5,8
Cs	7,8	9,1	*5,1*	*6*	*1,2*	7,7	*1,5*
Ba	207,7	367,3	88,1	119,2	455,9	358,7	403,8
La	21,9	19,9	15,6	13,1	25,7	33	26,4
Ce	55,1	51,7	39	31,7	64,2	77,2	66,7
Nd	30,9	26,8	16,6	19,7	26,3	28,4	26,8
Sm	8,2	8,4	*2,7*	*4,1*	7,8	7,3	7,7
Hf	6,3	7,4	3,9	3,2	4,7	5,9	4,8
Ta	*0,4*	*1,5*	*0,4*	*0,3*	*1,7*	*2,2*	*2,47*
W	3,6	4,3	3,9	2,9	4,5	2,3	6,6
Tl	*0,6*	*0,3*	*1,6*	*0,2*	*0,4*	*0,2*	*1,1*
Pb	22,3	15,4	9,3	13,7	26,6	6,4	9,8
Bi	*0,6*	*0,5*	*1*	*1*	*0,9*	*1*	*0,3*
Th	9,8	10,4	4,8	3,7	12,2	12,1	8,4
U	2,3	1,8	1,8	1,2	2,3	1,8	1,8

Cod. Lab	06/181-86	06/181-87	06/181-88	06/181-89	06/181-90	06/181-91	06/181-92
Muestra	FP-CC-23	FP-CC-24	FP-CC-25	FP-CC-26	FP-CC-27	FP-CC-28	FP-CC-29
%							
SiO_2	71,95	72,29	57,44	57,48	95,22	79,60	76,26
Al_2O_3	14,39	14,82	22,81	15,62	1,22	11,37	12,91
Fe_2O_3	3,60	2,70	6,52	7,97	2,46	1,75	1,93
CaO	0,13	0,05	0,02	7,43	0,14	0,08	0,23
TiO_2	0,45	0,17	0,98	0,69	0,21	0,09	0,09
MnO	*0,02*	0,04	0,05	0,12	*0,02*	*0,02*	*0,02*
K_2O	3,08	4,78	5,11	0,88	0,17	0,70	3,43
MgO	0,85	1,25	1,18	4,54	0,18	0,24	1,23
P_2O_5	*0,05*	0,01	*0,05*	0,05	*0,05*	*0,05*	*0,05*
Na_2O	1,91	1,13	0,45	2,70	*0,07*	5,49	1,94
PPC	3,63	2,74	5,45	2,53	0,41	0,69	1,98
TOTAL	100,1	100,0	100,0	100,0	100,1	100,1	100,1
µg/g							
Sc	11	3	18	35	*1*	*2*	5
V	39	5	127	183	14	6	4
Cr	31	24	101	136	194	108	58
Co	*2,41*	*2,41*	10,5	24,3	*2,41*	*2,41*	*2,41*
Ni	3	*0,1*	36,4	9,4	6,3	2,2	1,6
Cu	35,2	*1,35*	1,6	3,2	4,3	*1,35*	*1,35*
Zn	53,4	54,7	27,7	48,8	18	16,7	28,5
Ga	18,4	29,4	29,8	16,6	3	14	17,3
Ge	*0,8*	2	1,7	1,2	*0,9*	*0,8*	*0,6*
As	22,5	*0,9*	*1,7*	6,4	3,8	*1,5*	4,9
Se	*1*	*1*	*0,1*	*0,3*	*1*	*1*	*1*
Br	0,9	*0,2*	*0,8*	1,2	*0,5*	*0,6*	*0,7*
Rb	126,8	125,7	200,2	30,3	9,1	15	147,2
Sr	28,5	38,6	27	135,7	4	47,2	53,6
Y	48	117,8	27,5	23,4	7,3	41,6	56,7
Zr	193,1	408,3	162,5	98,4	335,5	107,6	108,6
Nb	7,6	37,4	17,6	4,7	3,2	6	7,3
Mo	*0,3*	*0,3*	*0,1*	*0,5*	1,4	*0,6*	*0,5*
Ag	*3,96*	*3,96*	*3,96*	*3,96*	*3,96*	*3,96*	*3,96*
Cd	*0,3*	*0,1*	*10*	*2,6*	*0,5*	*10*	*10*
Sn	2,6	9,4	2,4	2,2	3,7	4,8	7,2
Sb	4,9	4,4	*0,7*	*0,2*	3,4	3,1	4,2
I	4,6	*3,4*	5,4	4,1	4,6	6,9	4,6
Cs	12,1	*5*	*6*	*6*	*6*	*6*	6,2
Ba	246,1	431,1	721,2	181,2	85,9	82,9	644,4
La	28,2	55,2	43,5	*4,9*	10,3	25	30,6
Ce	58,7	121,2	84,2	36,8	22,4	64,3	55,2
Nd	27,4	60	34,5	16,6	*5,5*	25,4	25,3
Sm	*4,5*	13,3	9,2	*2,8*	*2,6*	*5,5*	*6,4*
Hf	5,7	10,6	5	*2,5*	8,4	*2,9*	4,8
Ta	*2,47*	*1,3*	*0,1*	*2,47*	*1,2*	*2,47*	*0,6*
W	4	4,3	2,9	*2,2*	3,5	*1,6*	4,2
Tl	*0,7*	*0,2*	*1,6*	1,7	*0,8*	*0,3*	*0,5*
Pb	8,1	4	*0,3*	10,2	7,8	5,3	2,7
Bi	*1*	*0,6*	1,1	*0,8*	*0,7*	*0,1*	*1*
Th	8,6	14,5	15,8	3,8	3,4	11,6	12,9
U	1,5	1,8	1,8	1,7	*0,2*	1,2	1,1

Cod. Lab	06/181-93	06/181-94	06/181-95	06/181-96	06/181-97	06/181-98	06/286-097
Muestra	FP-CC-31	FP-CC-32	FP-CC-33	FP-CC-34	FP-CC-35	FP-CC-36	FP-CC-37
%							
SiO_2	63,57	50,91	72,36	46,84	60,16	72,53	75,20
Al_2O_3	10,84	13,60	14,16	13,35	21,12	13,83	12,96
Fe_2O_3	16,27	13,00	1,89	11,98	2,87	2,58	1,76
CaO	0,04	6,05	0,05	5,30	0,19	0,52	0,11
TiO_2	0,23	2,55	0,28	1,32	0,43	0,17	0,16
MnO	0,18	0,14	*0,02*	0,21	0,02	*0,02*	*0,02*
K_2O	0,44	1,00	7,20	2,00	6,88	5,71	5,30
MgO	4,39	5,81	0,33	12,56	2,73	1,02	0,38
P_2O_5	*0,05*	0,27	*0,05*	0,11	*0,05*	*0,05*	*0,05*
Na_2O	*0,07*	4,26	2,08	1,93	1,91	2,06	2,97
PPC	4,03	2,42	1,66	4,41	3,68	1,58	1,16
TOTAL	100,1	100,0	100,1	100,0	100,0	100,1	100,1
µg/g							
Sc	9	48	8	33	13	7	5
V	18	318	22	172	34	4	18
Cr	53	56	80	251	29	26	12
Co	31	49,6	*2,41*	58,9	*2,41*	*2,41*	27
Ni	1,9	15,8	1,5	105,9	3,7	*0,7*	3
Cu	60,7	37,4	*0,1*	30	9,6	5,3	*1,35*
Zn	79,5	60	10,2	202,7	15,7	47,9	26,6
Ga	17,6	22,5	19,1	16,4	28,5	21,2	16
Ge	1,8	1,1	1,2	1,4	*0,7*	1,2	2,7
As	139,3	6	10,1	10,8	7,6	5,3	*2,3*
Se	*1*	*1*	*1*	*1*	*1*	*0,1*	*1*
Br	*0,1*	1,1	*0,8*	*0,4*	*0,3*	*0,3*	1,5
Rb	18,2	40	182,1	36,1	300,4	185,2	179,2
Sr	1,6	141,4	36,9	88,8	34,9	46,8	25,4
Y	31,5	52,2	40,7	27,1	55,8	53,7	34,2
Zr	123,3	213,8	162,4	89,4	237,8	229,7	140,9
Nb	6,2	6,5	7,7	3	11,5	12	6,3
Mo	1,1	1,3	*0,4*	*0,2*	*0,1*	*0,1*	*0,3*
Ag	5,6	6,9	*3,96*	*1,6*	*3,96*	*3,96*	*3,96*
Cd	*8*	*7*	*10*	*6,7*	*10*	*10*	*10*
Sn	5	*1,5*	7,7	*2,1*	45	6,4	6,1
Sb	5,3	*1,8*	4,4	*0,2*	5,4	*2,2*	3,6
I	5,8	*3,6*	4,3	5,4	6,6	4,4	4,1
Cs	*3*	*6*	*2,6*	*6*	7,1	16,8	6,1
Ba	128,7	73,4	744,7	121,8	532,9	431,2	371,3
La	20,3	9,2	26,8	7	36,7	34,6	28,6
Ce	51,6	41,3	60,1	15,6	89,7	67,6	58,4
Nd	21,1	24,4	22,3	13,4	33,3	37,4	22,8
Sm	8,6	*5*	*4,5*	7,3	7,9	11,7	*4,3*
Hf	*1,6*	4,7	5,5	3,3	5,8	8,9	3,3
Ta	*2,47*	*0,3*	*0,8*	*1*	*1*	*1,7*	*1*
W	6,2	3,9	4	2,7	3,4	4,7	193,4
Tl	2,8	*0,5*	*1,4*	*1,2*	2	*1,3*	*1,6*
Pb	4,3	2,3	17,8	12,8	2	11,5	6,1
Bi	*1*	*1*	*1*	*0,6*	1,7	*1*	*1*
Th	10	3,8	10,5	*1,1*	18	16,7	13,5
U	1,2	1,3	2,3	*1,2*	3,8	2,2	2,4

Cod. Lab	06/286-098	06/286-099	06/286-100	06/286-101	06/286-102	06/286-103	06/286-104
Muestra	FP-CC-38	FP-CC-39	FP-CC-41	FP-CC-42	FP-CC-72	FP-CC-118	FP-CC-119
%							
SiO_2	77,67	65,90	65,74	77,70	64,00	82,16	63,47
Al_2O_3	11,43	16,55	16,08	11,59	15,23	10,03	14,29
Fe_2O_3	1,98	3,68	4,80	1,93	7,94	1,56	9,73
CaO	0,08	0,24	2,24	2,96	0,96	0,67	0,43
TiO_2	0,14	0,33	0,32	0,25	1,32	0,13	1,44
MnO	*0,02*	0,03	0,04	*0,02*	0,09	0,03	*0,02*
K_2O	4,94	5,43	3,47	1,56	0,12	0,75	4,17
MgO	0,32	3,76	2,01	0,41	2,04	0,22	1,46
P_2O_5	*0,05*	0,06	0,08	0,05	0,35	*0,05*	0,09
Na_2O	2,63	0,26	1,27	2,29	5,78	3,77	1,94
PPC	0,81	3,76	3,95	1,25	2,16	0,68	2,98
TOTAL	100,1	100,0	100,0	100,0	100,0	100,0	100,0
µg/g							
Sc	4	11	13	9	19	*2*	27
V	9	25	28	18	100	3	149
Cr	12	12	20	19	18	13	222
Co	34,2	6,8	13,6	34,8	29	28	28,1
Ni	*1*	2,7	4,6	1,6	8,4	*0,7*	32,2
Cu	*1,35*	*0,4*	8	*1,35*	209,8	5,3	6,5
Zn	22	51,7	45,9	13,1	495	25,3	79,6
Ga	13,1	22	21	16,5	22,1	15,6	27
Ge	2,7	1,3	2,1	4,7	2,4	2,8	2,2
As	3,4	*2*	*2,4*	10,3	65,9	4,1	*2,4*
Se	*1*	*1*	*1*	*1*	*1*	*1*	*1*
Br	1,4	1,6	1,9	1,7	1,4	1,4	2,1
Rb	150,4	223,2	141,3	65,4	3,9	21,7	162,3
Sr	25,9	6	104,9	153,6	95,4	66,2	39,3
Y	31,9	47,1	44,8	34,9	75,4	54,6	72,6
Zr	119,9	190,6	180,8	146,8	479,9	193,6	125,6
Nb	5,2	9,9	8,3	6	12,9	11,2	7,9
Mo	*0,2*	*0,3*	*0,2*	*0,1*	*0,2*	*0,6*	1,4
Ag	*3,96*	*3,96*	*3,96*	*3,96*	*3,96*	*3,96*	*3,96*
Cd	*10*	*10*	*10*	*10*	*7,4*	*10*	*10*
Sn	2,1	4,1	5,1	3,7	4,6	5,9	*2,1*
Sb	*1,9*	*0,8*	2,5	2,4	15,4	3	*2*
I	6,7	4,6	5,4	4,2	*3*	4,6	6,1
Cs	*2,8*	*2,1*	8,7	*0,8*	*3,5*	*5,2*	*6*
Ba	326,6	238	761,2	258,8	104,8	117,6	1288,9
La	27,2	38,6	41,3	26,4	27	42,3	70,7
Ce	50,6	79,4	84,8	50,8	76,1	59	122,9
Nd	20,9	33,3	30,1	22,5	47,2	36,2	66,4
Sm	9,2	8	7,4	9,8	10,3	10,4	15,3
Hf	*1,5*	4,9	6,9	*2,5*	10,2	4,6	*2,3*
Ta	*2,47*	*0,8*	*0,6*	*2,47*	*2,47*	*2,47*	*2,47*
W	234,4	78,1	83,8	243,9	62,3	202,9	73,7
Tl	*0,2*	*1,4*	*0*	*0,5*	2,4	*0,1*	*0,1*
Pb	7,4	4,3	6	6,8	35	14,1	39,5
Bi	*0,8*	*0,5*	*0,7*	*0,2*	*1*	*1*	*1*
Th	10,7	15,5	13,9	9	7,5	11,7	2,6
U	1,7	1,3	2,8	1,7	2,2	1,8	3,1

Cod. Lab	06/286-105	06/286-106	06/286-107	06/286-108	06/286-109	06/286-110	06/286-111
Muestra	FP-CC-120	FP-CC-121	FP-CC-122	FP-CC-123	FP-CC-126	FP-CC-130	FP-CC-131
%							
SiO_2	70,37	75,55	61,39	78,07	69,31	76,93	56,53
Al_2O_3	14,34	12,01	18,18	11,04	13,24	11,33	13,73
Fe_2O_3	2,34	2,50	4,09	2,14	4,65	2,28	9,82
CaO	0,52	0,36	1,21	0,19	0,75	1,05	4,62
TiO_2	0,17	0,18	0,33	0,21	0,44	0,17	2,05
MnO	*0,02*	*0,02*	0,15	*0,02*	*0,02*	0,03	0,11
K_2O	4,76	5,90	5,92	4,84	2,19	4,54	0,37
MgO	3,85	0,50	3,96	0,27	4,45	0,29	5,54
P_2O_5	*0,05*	*0,05*	*0,05*	*0,05*	*0,05*	*0,05*	0,20
Na_2O	0,15	2,06	0,90	2,14	1,19	2,58	3,67
PPC	3,50	0,95	3,88	1,10	3,79	0,81	3,38
TOTAL	100,1	100,1	100,0	100,1	100,1	100,1	100,0
µg/g							
Sc	4	9	16	6	11	10	41
V	12	4	14	10	22	8	263
Cr	10	10	8	9	15	20	152
Co	*2,41*	29,5	5,9	28,8	6,1	33	40
Ni	8,8	1,1	13,1	*0,5*	1	1,1	28,9
Cu	*1,35*	*0,5*	12,5	*1,1*	6,7	15,8	59,2
Zn	38,9	56,9	104,2	30,3	63,8	47,8	110
Ga	18,8	20,4	27,6	13,6	20,9	15,6	19,2
Ge	*0,8*	2,9	1,8	2,7	1,2	2,4	1,4
As	*0,4*	8,8	29,8	*2,3*	5	3,2	28,2
Se	*1*	*1*	*1*	*1*	*1*	*1*	*1*
Br	1,8	1,2	0,8	1,5	4,6	1,7	1,8
Rb	126,1	209,7	332,3	98,3	128,5	72,2	10,7
Sr	27,4	38	102,7	40,6	59	97	139,3
Y	48,8	78,4	74,6	52,3	84,5	64,8	41,9
Zr	148,3	301,1	404,7	237,4	313,8	288,6	168,4
Nb	8,7	15	16,3	9,7	12,2	14,4	4,7
Mo	*1*	*0,1*	*1*	*0,3*	*1*	*0,5*	*0,4*
Ag	*3,96*	*3,96*	*3,96*	*3,96*	*3,96*	*3,96*	*3,96*
Cd	*10*	*10*	*10*	*10*	*10*	*10*	*0,9*
Sn	7,4	5,4	6,2	5	7,1	7,1	*0,4*
Sb	3,9	*2*	5,2	*1,8*	*2,2*	4,3	3,1
I	5,2	4,1	5,3	4,6	4,2	4,4	7,7
Cs	*4,2*	11,5	31,7	7	12,6	*2,3*	*6*
Ba	238,4	464,3	816,7	348,2	328	342,3	128,3
La	34,3	44,8	50,9	28,9	39,1	41,1	13,2
Ce	63,3	92,8	104,2	56	89,6	81,1	37,9
Nd	33,4	46,2	51,4	29	38,4	37,8	16,9
Sm	11	14,1	10,1	*6,9*	*6,9*	*6,9*	7,1
Hf	3,4	8,6	12,2	8	11	6,3	4,4
Ta	*2,47*	*0,1*	*0,7*	*1,2*	*1,4*	*0,5*	*0,7*
W	14,8	205,8	45,4	221,2	49,8	232,7	38
Tl	*1,6*	*0,9*	*1,1*	*0,3*	*1*	2,6	1,7
Pb	10,4	20,3	14,4	16,6	20,7	15,2	23,3
Bi	1	*0,5*	*0,8*	*1*	*0,2*	*0,4*	*1*
Th	14,3	11,7	15,6	14,2	14,7	11,6	1,5
U	*1*	1,5	*0,1*	2	3,3	2,8	*1,2*

Cod. Lab	06/370-01	246-24	246-25	246-26	246-27	246-28	246-29
Muestra	FP-CC-134	FP-CC-142	FP-CC-143	FP-CC-144	FP-CC-145	FP-CC-146	FP-CC-148
%							
SiO_2	62,75	69,90	74,79	70,48	72,70	63,24	69,59
Al_2O_3	18,68	12,10	13,20	16,14	13,72	14,95	14,81
Fe_2O_3	3,50	3,71	1,87	1,76	2,98	6,64	5,35
CaO	0,10	7,10	1,01	0,21	2,43	5,99	0,13
TiO_2	0,27	0,40	0,13	0,16	0,31	0,74	0,42
MnO	0,16	0,07	0,03	0,03	0,03	0,11	0,04
K_2O	1,43	0,32	3,09	4,45	2,01	0,89	2,16
MgO	6,01	1,89	2,28	1,88	1,44	3,22	1,09
P_2O_5	0,01	*0,05*	*0,05*	*0,05*	*0,05*	0,06	0,12
Na_2O	2,24	1,62	1,29	2,25	2,38	1,48	3,06
PPC	4,24	2,89	2,33	2,65	1,98	2,67	3,25
TOTAL	99,4	100,0	100,1	100,1	100,0	100,0	100,0
µg/g							
Sc	10	17	7	9	8	26	18
V	12	91	6	12	24	129	19
Cr	23	82	8	6	19	96	14
Co	*2,41*	32,1	3,4	8,9	15,9	28,1	8,1
Ni	4,3	20,2	2,4	2,4	3,4	16	8,1
Cu	*1,35*	29,9	6,3	16,9	18,4	16,5	11,7
Zn	76,7	40,3	35,9	38	38,7	68,3	60,7
Ga	30,8	15,4	16,7	22,7	15,7	16,1	18,6
Ge	*1*	*0,8*	*1*	*1*	*1*	*1*	*1*
As	4,8	3,3	13,6	10	10,3	4,9	*1,5*
Se	*1*	*0,6*	*1*	*1*	*0,1*	*0,5*	*1*
Br	2,6	9,7	*0,8*	1	1,4	3,2	0,8
Rb	62,9	12,2	147,5	205,9	97,8	40,5	80,5
Sr	153,9	51,1	67,8	34	189,7	158,1	88,5
Y	128,6	11,9	45,9	39,7	31,6	25,6	42,4
Zr	438,7	80,6	117,9	144,6	147,4	158,6	224,2
Nb	20,6	4,1	6,4	7,1	6,1	7,6	10,6
Mo	*0,5*	*0,8*	*0,4*	*0,3*	*0,6*	*0,5*	1,4
Ag	*3,96*	*3,96*	*3,96*	*3,96*	*3,96*	*3,96*	*3,96*
Cd	*10*	*10*	*10*	*10*	*10*	*10*	*10*
Sn	14,5	5,3	8	10,1	7	5,6	7,4
Sb	4,3	4,5	4,8	4,6	5,8	5,1	5
I	*1,1*	*0,7*	*3,95*	*3,95*	*3,95*	*0,3*	*0,6*
Cs	7,3	*6*	12,2	13,7	*5,1*	*5,3*	*2,2*
Ba	257,3	84,1	295,4	358,5	325,4	253,2	306,2
La	81,8	*4,3*	21,4	16,7	14,8	14	39,8
Ce	135,6	25,2	58,5	52,5	49,9	50,2	93,7
Nd	80,2	11,4	23	22,6	19,8	19	41,5
Sm	20,2	*0,7*	8,4	*5,3*	10,5	*1,9*	10,1
Hf	14,5	*2,5*	4,4	3,8	3,8	2,9	*2,4*
Ta	*1,4*	*1,6*	*1,5*	*2,47*	*1,2*	*0,5*	*2,47*
W	5,2	134,5	87,6	134	125,2	70,2	30,4
Tl	*1,3*	*1,6*	*0,2*	*1,4*	*0,4*	*1,2*	*0,7*
Pb	14,3	21,6	22,4	9,4	15,1	16,2	10,2
Bi	2	*0,6*	1,1	1,4	1,6	1,8	1,6
Th	25,7	4	13,5	16,3	8,3	7,7	11
U	1,3	1,4	3	3,2	3,5	3,1	4

Cod. Lab	246-30	246-31	246-32	246-33	246-34	246-35	246-36
Muestra	FP-CC-149	FP-CC-150	FP-CC-151	FP-CC-152	FP-CC-153	FP-CC-154	FP-CC-155
%							
SiO_2	65,61	64,90	52,85	72,45	72,29	70,16	80,79
Al_2O_3	14,46	14,18	19,27	13,44	14,65	14,69	9,22
Fe_2O_3	4,83	5,81	8,56	3,26	2,44	2,52	2,12
CaO	4,88	4,31	4,91	0,20	0,14	0,99	0,38
TiO_2	0,53	0,66	0,67	0,30	0,23	0,24	0,15
MnO	0,06	0,08	0,05	0,03	0,02	0,04	0,02
K_2O	1,49	2,67	2,84	3,91	7,31	2,72	0,50
MgO	2,33	2,77	3,29	1,74	0,50	4,35	3,22
P_2O_5	*0,05*	*0,05*	*0,05*	*0,05*	*0,05*	*0,05*	*0,05*
Na_2O	3,00	2,16	1,93	2,73	0,53	0,60	0,85
PPC	2,81	2,46	5,64	1,95	1,91	3,69	2,75
TOTAL	100,0	100,0	100,0	100,0	100,1	100,1	100,1
µg/g							
Sc	28	25	33	11	10	10	5
V	119	116	118	46	6	8	3
Cr	48	91	48	24	8	9	8
Co	34,5	29,3	18,4	23,6	*2,41*	*2,41*	*0,1*
Ni	6,4	15,6	15,1	3,8	1,4	3,4	2,5
Cu	14,6	15,9	2	3,6	4,8	7	*1,35*
Zn	75,1	60	100,3	25,4	41,5	75,4	56,2
Ga	13,9	15,8	19,4	15,6	27,3	24	14,9
Ge	*1*	*1*	*1*	*1*	*1*	*1*	1,2
As	20,7	6,6	*2,8*	6,2	5,7	7,4	*2,8*
Se	*0,2*	*1*	*0,2*	*1*	*0,5*	*0,2*	*1*
Br	0,8	*0,6*	*0,8*	*0,4*	0,9	*0,1*	*0,4*
Rb	35,1	79,7	48,7	122,5	333,4	202,7	40,8
Sr	104,6	144,9	93,9	46,1	31,4	57,3	43,8
Y	18,1	26,8	23,2	22,1	86,8	77,1	42,7
Zr	114,8	161,5	126,4	117	312,4	306,8	190,1
Nb	5,7	7,8	6,7	6,2	12,8	12,7	7,6
Mo	1,1	*0,9*	1	*0,4*	*0,4*	*1*	*1*
Ag	*3,96*	*3,96*	*3,96*	*3,96*	*3,96*	*3,96*	*3,96*
Cd	*10*	*10*	*10*	*10*	*10*	*10*	*10*
Sn	5,4	5,6	5,2	6,2	13,5	10,1	6
Sb	4,9	4,7	5,2	3	5,9	*1,5*	*0,6*
I	*3,95*	*2,3*	*3,95*	*1,3*	*2,8*	*1,7*	*0,4*
Cs	*6*	*3,2*	*0,1*	*3,3*	12,8	17,3	9,6
Ba	217,4	306,9	90,3	378,5	642,8	572,6	250,2
La	12,1	15,6	14,8	21,6	41,3	37,4	12,2
Ce	39,7	53,7	50,8	61,5	99,9	123,1	50,3
Nd	13,8	24,4	21,2	24,2	40,8	54,3	19,6
Sm	*4,6*	*5,7*	*2,4*	*2,6*	13,1	8,6	*5,6*
Hf	*2,7*	5,4	3,8	*2,8*	10,2	10,8	5,4
Ta	*0,3*	*2*	*1,4*	*0,3*	*0,8*	*1,2*	*1,4*
W	138,1	95,9	23,3	159,2	55,6	41,6	62,5
Tl	*1,3*	*0,7*	*1,6*	*0,8*	1,7	*0,6*	*0,4*
Pb	47,2	15,7	9,7	4,6	12,4	16	8,5
Bi	1	1,7	*0,4*	1	2,3	1,6	*0,7*
Th	5,8	8,3	7,3	11,2	20,8	19	11,7
U	3,4	3	*1*	3,2	5,2	3,1	1,7

Cod. Lab	246-37	246-38	246-39	246-40	246-41	246-42	246-43
Muestra	FP-CC-156	FP-CC-159	FP-CC-160	FP-CC-161	FP-CC-162	FP-CC-163	FP-CC-167
%							
SiO_2	83,13	67,55	78,92	69,47	64,26	59,74	65,70
Al_2O_3	7,22	14,65	10,73	15,23	17,81	19,90	13,65
Fe_2O_3	2,32	4,10	2,84	3,07	3,55	7,75	7,35
CaO	0,64	1,91	0,28	0,07	0,47	0,22	0,72
TiO_2	0,12	0,27	0,31	0,25	0,31	1,04	1,69
MnO	0,03	*0,02*	0,03	0,08	0,10	0,13	*0,02*
K_2O	0,32	2,41	*0,10*	0,90	0,56	3,46	3,82
MgO	3,29	4,90	0,15	4,99	6,09	2,08	1,82
P_2O_5	*0,05*	*0,05*	*0,05*	*0,05*	*0,05*	0,08	0,20
Na_2O	0,37	0,37	5,84	1,59	2,04	0,75	1,44
PPC	2,57	3,84	0,90	4,35	4,79	4,85	3,61
TOTAL	100,0	100,1	100,2	100,0	100,0	100,0	100,0
µg/g							
Sc	4	10	6	9	10	22	29
V	4	7	24	6	16	151	180
Cr	14	8	12	10	18	115	197
Co	9,9	*2,41*	48,4	*2,41*	*2,41*	31,3	18,5
Ni	2,2	2,9	3,1	3,5	6,1	56,4	22,3
Cu	*1,35*	*1,35*	4,2	10,3	6	43	4,6
Zn	64,5	83,2	42,4	79	85,7	107,2	82,7
Ga	12,4	23,3	16,5	23,1	28,6	26,1	19,4
Ge	1,8	2,8	3	1,3	*0,9*	1,9	2,3
As	4,1	19,8	6,8	3,7	5,9	4,4	6,1
Se	*1*	*1*	*1*	*1*	*0,3*	*1*	*0,1*
Br	*0,3*	*0,5*	*0,2*	*0,3*	*0,7*	*0,4*	1,3
Rb	21,4	131,4	1,1	62,6	38,5	154,4	146,5
Sr	27,9	81,9	28,1	61,9	101,7	79,7	42,4
Y	35,5	80,6	70,1	57,6	95	34,8	113,6
Zr	139	323,1	248,5	309,8	373,4	209,2	127
Nb	6,6	12,6	10,6	12,5	15,9	16,9	6,2
Mo	*0,1*	*0,3*	*0,3*	*1*	*0,1*	*1*	*0,6*
Ag	*3,96*	*3,96*	*3,96*	*3,96*	*3,96*	*3,96*	*3,96*
Cd	*10*	*10*	*10*	*10*	*10*	*0,3*	*2,1*
Sn	3,7	10,9	6,3	8,9	10,1	4,3	*1,7*
Sb	*1,8*	*0,6*	*0,4*	*0,9*	*0,5*	*2,37*	*0,5*
I	*1,1*	*3,95*	*3,95*	*0,6*	*2,8*	*0,6*	*3,95*
Cs	*4,1*	13,2	*4,9*	12,6	*3,7*	*5,8*	*6*
Ba	80,6	155,5	38,9	277	199,2	517,2	586,1
La	12	43,4	29,1	13,8	50,4	30,5	62,3
Ce	46,9	115,9	66,8	196,2	118,5	80,5	130,9
Nd	17,2	46,1	31,1	23	51,5	38,8	63,7
Sm	9,5	14,1	9	*4,3*	15,2	10,8	15,3
Hf	4,2	9,4	5,1	9,9	11,2	4,9	3,5
Ta	*0,4*	*0,3*	*2,47*	*1,7*	*0,4*	*0,8*	*2,47*
W	103	22,7	278,9	18,3	14,3	35,9	42,5
Tl	*0,5*	*1*	*1,6*	*0,4*	*1,1*	*1,4*	*0,9*
Pb	11,5	27,1	11,4	6,7	13,9	9,3	21,7
Bi	*0,4*	1	*0,*9*	*0,8*	*0,5*	*0,9*	1,3
Th	8,9	18,8	14,1	19,2	23,5	14,8	*0,9*
U	1,4	*0,3*	2,4	1,4	*1,2*	3,3	3

Cod. Lab	246-44	246-45	246-46	246-47
Muestra	FP-CC-168	FP-CC-169	FP-CC-170	FP-CC-171
%				
SiO_2	74,64	72,46	74,05	73,81
Al_2O_3	12,53	14,14	13,44	12,37
Fe_2O_3	2,98	2,60	2,42	2,83
CaO	1,27	0,61	0,43	0,71
TiO_2	0,25	0,23	0,19	0,37
MnO	0,02	*0,02*	0,11	0,03
K_2O	2,30	4,06	2,79	4,07
MgO	2,42	2,30	1,33	1,85
P_2O_5	*0,05*	*0,05*	*0,05*	*0,05*
Na_2O	1,06	0,20	2,77	1,97
PPC	2,54	3,40	2,47	2,00
TOTAL	100,1	100,1	100,1	100,1
µg/g				
Sc	9	8	4	10
V	20	18	5	47
Cr	12	7	11	13
Co	*2,41*	*2,41*	7,8	17,7
Ni	4,8	4	6,5	4,2
Cu	1,8	9,3	2,3	17,9
Zn	69,7	37,9	64,9	58,6
Ga	18,8	17,3	21,2	13,9
Ge	2,2	*0,9*	2,2	1,5
As	3,1	*0,1*	3,1	131,4
Se	*1*	*1*	*1*	*1*
Br	*0,7*	*0,4*	*0,1*	*0,3*
Rb	75,7	163,6	92,4	115,7
Sr	125	35,5	66,3	67,6
Y	53,3	45,6	111,4	29,6
Zr	206,5	203,8	289,5	167,2
Nb	10,5	7,5	17,2	5,7
Mo	*1*	*1*	*1*	*0,2*
Ag	*3,96*	*3,96*	*3,96*	*3,96*
Cd	*10*	*10*	*10*	*10*
Sn	3,8	4,6	8,5	3,1
Sb	*1,8*	*0,7*	*0,8*	3,1
I	*2,2*	4,1	*1,8*	*3,95*
Cs	6,9	*1,4*	8,7	*6*
Ba	426,3	423,9	379,1	343,8
La	20,1	25,7	41,6	10,3
Ce	72,5	65	104,8	35,9
Nd	30,9	26,6	48,9	17,8
Sm	*6,9*	7,1	12,5	*2,3*
Hf	6,6	7,1	9	5,6
Ta	*2,47*	*0,6*	*2,3*	*1,8*
W	40,9	30,7	97,1	133,2
Tl	*0,3*	*0,6*	*0,2*	*1,6*
Pb	9,3	22,1	11,7	11,1
Bi	*1*	1,3	1,5	*0,5*
Th	13,5	13,9	16	8,6
U	2,7	3,1	1,8	1

Tabla I.I.2 Composición química de las rocas volcánicas (Capítulo II). (Cursiva: menor del límite de detección)

Cod. Lab	05/317-01	05/317-02	05/317-03	05/317-04	-	-	-
Muestra	PBM-018	PBM-019	PBM-022	PBM-025	PBM-029	PBM-030	PBM-031
%							
SiO_2	63,68	79,60	69,50	75,31	70,66	67,76	78,70
Al_2O_3	16,96	8,31	8,47	13,79	8,02	10,40	11,96
Fe_2O_3	2,81	3,97	13,37	1,78	13,09	11,28	2,49
CaO	2,25	0,00	0,00	0,32	0,04	0,04	0,01
TiO_2	0,20	0,07	0,14	0,14	0,09	0,10	0,10
MnO	0,06	0,01	0,15	0,02	0,15	0,13	0,02
K_2O	5,14	2,57	0,00	2,37	0,20	1,35	3,15
MgO	2,28	0,35	5,01	0,46	3,77	4,07	0,85
P_2O_5	0,03	*0,02*	*0,02*	*0,02*	*0,05*	*0,05*	*0,05*
Na_2O	0,81	0,11	0,00	4,17	0,18	0,11	0,00
PPC	5,79	3,45	3,40	1,65	3,81	4,77	2,72
TOTAL	99,7	98,1	98,7	99,8	100,0	98,9	100,0
µg/g							
Sc	12	*2*	*2*	8	4	5	5
V	15	5	13	6	7	5	5
Cr	52	137	78	79	98	60	74
Co	*2,41*	*2,41*	37,6	*2,41*	37,5	24,4	*2,41*
Ni	4,4	3,1	4	5	1,6	1	*0,8*
Cu	2,3	*1,35*	4,9	*1,1*	991,9	25,4	10,3
Zn	38,1	9666	82,6	133,2	394,5	465,4	21,2
Ga	22	16	12,1	22,3	11,9	14,9	15,7
Ge	1	*1*	1,2	1	*1*	*0,3*	*1*
As	129	543,3	4,4	80,7	27,6	28,3	21,5
Se	0,6	0,2	0,1	0,5	3,1	4,1	*1*
Br	0,5	1,7	0,3	*0,4*	*0,7*	*0,5*	*0,4*
Rb	212,4	87,7	2,2	156,8	9,5	55,6	118,3
Sr	102	14,8	1,1	126,2	13,6	15,4	28,5
Y	48	28	23,4	46,2	28,6	38,4	27,2
Zr	170,8	67,9	71,6	138,3	74,6	93,2	99,2
Nb	7,2	3,1	3	6,3	3,7	4,5	5,4
Mo	2	2,2	0,9	0,5	*1*	1,4	2,8
Ag	*3,96*	*3,96*	*3,96*	*3,96*	*3,96*	*3,96*	*3,96*
Cd	*4*	13,7	*4*	*4*	*4*	*4*	*4*
Sn	8,2	20,3	5	6,8	9,9	15,1	27
Sb	11	73,3	0,5	4,2	4,5	4,5	2,8
I	1,4	*3,65*	*3,65*	*3,65*	*0,1*	*3,65*	*2,7*
Cs	16,2	15,9	0,8	4,7	*5,1*	*3,1*	*2,4*
Ba	1553,4	3121	195,6	966,5	264,8	525,1	2622,6
La	33,5	17,8	16,1	25,4	18,8	25,2	11,9
Ce	68,3	5,7	42,8	49,1	38,7	52	22,5
Nd	27,6	18,3	15,6	24,5	14,2	23,5	7,7
Sm	9,2	6,7	2,6	6	*4,4*	11,9	*1,4*
Hf	5,9	*2,87*	5,1	4,8	*2,87*	*2,6*	3,9
Ta	0,4	*2,47*	1,7	0,6	*2,47*	*0,4*	*1,6*
W	3	1,9	7,3	3,9	3,5	5,6	4,8
Tl	23,8	29,4	1,8	5,2	2,6	6,1	*1,3*
Pb	20,3	990,6	7,6	15,4	8,3	11,8	18,7
Bi	0,8	2,4	1,6	0,7	5,7	26,6	1,6
Th	15,6	7,6	8,3	15,2	8,3	10,6	11,9
U	4,6	*1,2*	2,8	11,8	1,2	3,1	4,1

Cod. Lab	-	-	-	-	-	-	-
Muestra	PBM-032	PBM-033	PBM-034	PBM-035	PBM-036	PBM-037	PBM-038
%							
SiO_2	68,28	73,54	55,19	27,59	73,68	61,91	76,81
Al_2O_3	8,03	14,17	11,71	17,19	13,89	20,15	13,01
Fe_2O_3	14,11	2,52	18,36	32,57	1,80	2,77	1,31
CaO	0,01	0,02	0,10	0,05	1,81	1,57	0,31
TiO_2	0,08	0,12	1,19	1,81	0,12	0,18	0,11
MnO	0,17	0,11	0,28	0,40	0,04	0,03	0,01
K_2O	0,14	3,47	0,00	0,00	4,13	6,16	3,33
MgO	4,51	2,91	7,39	9,70	0,63	1,45	0,19
P_2O_5	*0,05*	*0,05*	0,07	0,07	*0,05*	*0,05*	*0,05*
Na_2O	0,16	0,18	0,00	0,00	1,05	2,06	3,76
PPC	4,50	2,98	5,70	9,70	2,85	3,72	1,16
TOTAL	100,0	100,1	100,0	99,1	100,1	100,0	99,9
µg/g							
Sc	3	7	26	36	8	12	6
V	3	6	213	304	10	16	7
Cr	67	52	141	307	76	52	106
Co	48,8	*2,41*	58,9	145,1	*2,41*	*2,41*	*2,41*
Ni	1,6	1,3	7,9	48,8	3	13	2,2
Cu	112,8	*1,35*	164,2	7661	20,5	*1,35*	6,7
Zn	92	113,2	257,2	1735,9	49,7	102,6	24,9
Ga	14,3	18,1	17,2	23,8	18,1	28,7	13,7
Ge	*0,3*	*1*	*1*	*1*	*1*	1,1	*0,4*
As	38,9	*1,8*	40,9	70,6	*2,2*	3,6	86,5
Se	2,9	*0,3*	1	8,5	*0,5*	*0,6*	*1*
Br	*0,1*	*0,5*	*0,6*	1,5	*0,2*	*0,4*	*0,5*
Rb	8	143,7	2	1,4	180,8	236,9	92,3
Sr	4	24,3	6,4	24,4	71,5	59	85,5
Y	27,1	46,2	26,2	38,6	39,1	46,5	48,3
Zr	76,1	122,3	109,4	190,6	117,4	182,2	112,6
Nb	3,7	6,1	6,8	7,5	5,7	8,9	5,4
Mo	3,1	1,4	1,5	1,1	*0,3*	*0,5*	*0,4*
Ag	*3,96*	*3,96*	*3,96*	*2,8*	*3,96*	*3,96*	*3,96*
Cd	*4*	*4*	*4*	*2,5*	*4*	*4*	*4*
Sn	9,9	10,5	18,9	21,8	7,4	9,2	6,3
Sb	4,4	3,6	*1,7*	*2,37*	3,1	3,9	*2,4*
I	*3,65*	*3,9*	*3,65*	*0,6*	*3,65*	*3,5*	*3,65*
Cs	*1,5*	*3*	*6*	*6*	11,9	22,7	8,9
Ba	539,2	840,2	25,1	56,5	1654,3	536,3	851,7
La	17,2	25,5	8,7	*5,08*	29,3	42,3	28,5
Ce	44,6	65,8	29,6	23,6	50,4	79,3	45,7
Nd	19,9	25,4	12,6	*5,3*	19,8	33,2	20,9
Sm	*4*	12,1	*2,9*	*1,1*	*5,8*	9,9	7
Hf	3,3	5,7	4,2	*2,87*	3,4	5,7	3,5
Ta	*1,7*	*2,47*	*0,5*	*2,47*	*2,47*	*0*	*0,3*
W	6,2	*1,8*	23,5	57,8	*2,5*	*2*	3,9
Tl	*0,2*	6,2	1,5	2,9	11,1	2,8	*1,4*
Pb	11	4	18,4	30,8	10,9	14,7	18,3
Bi	*0,9*	*1*	1,9	11,8	*0,5*	*0,1*	1,2
Th	8,4	14,2	2	4	13,5	21,2	13,5
U	2,8	4,3	2	4,6	2,3	*0,5*	3,1

Cod. Lab	-	-	-	-	-	-	-
Muestra	PBM-039	PBM-040	PBM-041	PBM-042	PBM-043	PBM-044A	PBM-045
%							
SiO_2	64,18	68,90	66,59	56,33	67,49	69,25	72,42
Al_2O_3	17,49	16,16	16,33	7,27	16,50	8,58	15,14
Fe_2O_3	2,32	2,67	4,15	23,52	2,45	12,58	1,46
CaO	1,46	0,23	0,79	0,02	1,36	0,04	0,06
TiO_2	0,17	0,14	0,18	0,08	0,16	0,09	0,13
MnO	0,03	0,04	*0,01*	0,07	0,04	0,09	0,04
K_2O	5,54	4,16	4,99	0,00	3,89	0,21	3,55
MgO	3,02	2,64	0,99	3,39	1,70	5,14	1,84
P_2O_5	*0,05*	*0,05*	*0,05*	*0,05*	*0,05*	*0,05*	*0,05*
Na_2O	1,54	2,29	0,23	0,08	3,13	0,12	0,53
PPC	4,25	2,76	5,16	8,38	3,28	3,92	4,82
TOTAL	100,0	100,0	99,5	99,2	100,0	98,8	100,0
µg/g							
Sc	10	9	10	4	9	*2*	8
V	8	10	10	12	11	5	10
Cr	53	43	49	107	65	89	82
Co	*2,41*	*2,41*	*2,41*	321,1	*2,41*	32,4	*2,41*
Ni	8,3	4,9	1,8	1,1	3,7	1,7	1,6
Cu	1,9	*1,35*	91,2	8782	7,3	27,6	3,6
Zn	50,2	170,5	102,6	156,8	17,3	209,1	12,8
Ga	22,5	20,8	22,2	4,1	21,1	12,5	19,4
Ge	*0,8*	*0,9*	1,9	*1*	*1*	*0,1*	*1*
As	7,3	11,7	374,6	1271,5	10,3	13,6	16
Se	*0,1*	*0,6*	1,3	55,5	*0,6*	*0,4*	1,2
Br	*0,7*	*0,3*	*0,4*	*0,6*	*0,7*	*0,7*	*0,1*
Rb	221,4	164,4	217,6	1,2	161,8	6,8	118,2
Sr	77,2	77,4	46,4	*0,4*	146,2	2,5	52,7
Y	31,6	46,1	39,1	27,2	53	30,2	45,2
Zr	162,8	141	159,3	72,6	153,3	79,7	132,1
Nb	8	6,4	7,8	0	6,8	3,8	6,6
Mo	*0,4*	*0*	2,7	11,1	*0,4*	1,9	3,2
Ag	*3,96*	*3,96*	*3,96*	*3,96*	*3,96*	*3,96*	*3,96*
Cd	*4*	*4*	*4*	6,2	*4*	*4*	*4*
Sn	7,6	8,9	12,2	7,9	8,2	7,8	7,3
Sb	4	6,8	20,2	231,2	4,1	3,9	12,1
I	*0,5*	*3,65*	*3,65*	*3,65*	*3,65*	*1,5*	*3,65*
Cs	16	17,9	6	*6*	13,1	*2,2*	7,1
Ba	558,6	658,3	7520,8	165	1338,9	444,4	817,3
La	32,3	41,4	38,6	22,2	37,1	16	31,2
Ce	60	86,7	58,7	36,3	82	34,6	63,5
Nd	26,5	35,6	24,5	19,1	36,1	16,7	26,5
Sm	7,9	9,5	*5,4*	*4*	*4,4*	*6,1*	*6,3*
Hf	6,4	4,4	4,9	*2,87*	4,5	3,8	5,3
Ta	*1,4*	*2,47*	*2,47*	*2,47*	*0,8*	*0,6*	*0,2*
W	*2,6*	*1,8*	*2,7*	7,3	*2,3*	6,2	*2*
Tl	2,2	2	43,4	2,7	12,3	*1,4*	7
Pb	9,9	10,3	52,5	75,5	17,5	21	29,7
Bi	*0,2*	*0,9*	1,3	3619,8	5,1	3,7	*0,9*
Th	18,4	16,9	14,9	36,1	15,5	8,9	13,8
U	*0,5*	2	2,7	7,8	1	3,5	3,7

Cod. Lab	-	-	-	-	-	-	-
Muestra	PBM-046B	PBM-047A	PBM-048	PBM-049B	PBM-050	PBM-052	PBM-053
%							
SiO_2	65,74	41,78	59,89	72,96	52,99	69,93	71,18
Al_2O_3	18,78	16,06	19,37	7,49	12,48	15,50	15,18
Fe_2O_3	2,27	23,80	7,25	12,40	20,27	2,10	1,96
CaO	0,09	0,04	0,18	0,06	0,17	0,83	0,88
TiO_2	0,18	0,19	1,03	0,13	1,27	0,13	0,14
MnO	0,02	0,12	0,05	0,07	0,18	0,04	0,06
K_2O	4,33	0,17	4,36	0,15	0,00	3,37	1,94
MgO	3,41	10,05	2,98	3,26	7,00	2,94	2,16
P_2O_5	*0,05*	*0,05*	0,12	*0,05*	0,09	*0,05*	*0,05*
Na_2O	0,58	0,12	0,30	0,12	0,12	2,32	4,25
PPC	4,60	7,67	4,48	3,32	5,36	2,85	2,26
TOTAL	100,1	100,1	100,0	100,0	97,9	99,8	99,9
µg/g							
Sc	11	8	18	7	26	6	6
V	9	19	176	13	210	7	9
Cr	77	26	127	74	141	54	67
Co	*2,41*	71,4	9,1	34,3	59,2	*2,41*	*2,41*
Ni	1,4	2,1	43,8	1,6	6,3	5,1	6,8
Cu	2,9	1328,6	15,7	449,6	467,1	*0,5*	1,7
Zn	27,8	504,6	34,6	53,4	186,2	51,5	45,6
Ga	23,8	21,6	26,3	8,9	16	19,4	17,9
Ge	*1*	*0,2*	*1*	*1*	*1*	1,3	*0,3*
As	36	74,2	24,2	35,5	28,4	9,4	7
Se	1,8	*0,7*	*0,2*	*0,5*	*0,8*	*1*	*1*
Br	*0,4*	*0,1*	*0,3*	*0,5*	*0,4*	*0*	*0,3*
Rb	136,7	8,3	156,8	7,1	4,2	129,1	74,7
Sr	60,9	2,2	30,8	1,8	3,2	84,3	127,4
Y	45,8	50,4	29,7	32,6	20,4	46,6	59,7
Zr	180,6	169,2	235,2	163,6	106,9	129,2	138
Nb	8,7	7,7	18	5,8	4,5	6,3	6,5
Mo	2,4	4,8	1,1	1,4	2,1	*0,1*	*0,5*
Ag	*3,96*	*3,96*	*3,96*	*3,96*	*3,96*	*3,96*	*3,96*
Cd	*4*	*0,7*	*4*	*4*	*4*	*4*	*4*
Sn	10,1	19,3	6,2	9,9	6,7	7,7	7,8
Sb	15,7	3,7	*2*	4,4	*1,6*	*2,5*	2,9
I	*1,9*	*3,65*	*1,5*	*3,65*	*3,65*	*3,65*	*1,4*
Cs	7,7	*3,6*	*0,7*	*0,5*	*6*	10	10,9
Ba	730,4	177,9	765	55,9	20,2	475,5	361,6
La	39,5	30,9	43,9	17,3	6	27,1	26,8
Ce	84,2	75,4	75,9	40,7	14,8	68,1	58,7
Nd	35,9	29,5	30,3	20,3	*6*	24,4	25,7
Sm	*6,7*	*4*	*6,3*	*4,1*	*2,4*	*6*	9,9
Hf	5,5	3,2	6,8	*2,7*	*2,87*	5,1	5,7
Ta	*0,9*	*2,47*	*2,4*	*2,47*	*2,47*	*1,5*	*1,6*
W	3	9,7	5,6	3,3	5,6	3,3	4,4
Tl	8,2	2,3	7,6	2,9	*1,5*	*1,1*	1,7
Pb	17,3	16,8	3,8	7,8	7,6	13,3	11,4
Bi	6,4	9,2	1,5	2,8	*0,1*	*0,5*	1,1
Th	15,9	18,6	14,9	5	2,5	15,3	15,7
U	5,5	4,3	3	1,6	*1*	1,7	1,7

Cod. Lab	-	-	06/181-60	06/181-61	06/181-62	06/181-63	06/181-64
Muestra	PBM-054	PBM-055	PBM-074	PBM-075	PBM-078	PBM-079	PBM-080
%							
SiO_2	52,55	68,13	79,12	75,82	72,86	78,23	57,47
Al_2O_3	12,38	15,31	11,67	12,51	13,77	12,19	14,34
Fe_2O_3	19,65	7,03	1,38	2,61	2,96	1,87	11,06
CaO	0,05	0,05	0,04	0,07	0,60	0,20	0,50
TiO_2	1,04	0,29	0,14	0,16	0,18	0,16	1,13
MnO	0,30	0,12	*0,02*	*0,02*	0,04	*0,02*	0,09
K_2O	0,00	3,15	2,65	3,70	2,99	0,73	0,03
MgO	7,86	1,83	0,84	1,45	2,05	0,31	6,57
P_2O_5	*0,05*	*0,05*	*0,05*	*0,05*	*0,05*	*0,05*	0,14
Na_2O	0,14	0,18	2,08	0,38	1,59	5,38	3,38
PPC	6,00	3,87	2,08	3,31	2,96	0,94	5,29
TOTAL	100,0	100,0	100,1	100,1	100,0	100,1	100,0
µg/g							
Sc	29	10	4	5	6	*2*	29
V	201	66	*2*	*1*	*3*	3	252
Cr	135	39	58	36	53	91	34
Co	64,1	9,9	*2,41*	*2,41*	*2,41*	*2,41*	27,2
Ni	22,4	9,7	*0,9*	*0,6*	6,8	*0,9*	6,9
Cu	88,4	156,8	22,6	2	4,6	2	75,1
Zn	374,4	71,3	19,2	39,2	95,9	39,8	105
Ga	17,1	17,2	18,9	21,1	23,9	19,9	19,5
Ge	*0,7*	*0,1*	1,1	*0,9*	1,4	1,4	*0,1*
As	59	32,7	3,2	*1,8*	4,7	2,9	9,6
Se	*0,4*	*0,2*	*1*	*1*	*1*	*1*	*1*
Br	*0,4*	*0,6*	*0,5*	*0,1*	*0,8*	*0,2*	*0,6*
Rb	2	112,1	97,6	105,7	76,5	16,1	1,5
Sr	4,6	18,6	25,3	15,7	63,3	55,7	40,7
Y	22,4	26,3	63,2	79,1	102,1	72,5	20,3
Zr	83,5	116,8	238	311,2	391,1	291,3	91,6
Nb	3,8	4,8	13,6	17,4	29	28	5,9
Mo	1,1	1,3	*0,1*	*0,7*	*0,3*	*0,5*	1,2
Ag	*3,96*	*3,96*	*3,96*	*3,96*	*3,96*	*3,96*	*1,1*
Cd	*4*	*4*	*10*	*10*	*10*	*0,3*	5,8
Sn	10,5	18,9	7,6	9	6,8	6,9	*1,1*
Sb	*1*	*1,8*	2,5	2,9	*1,7*	3	*2,37*
I	*3,65*	*3,65*	*3,9*	5,4	4,1	*3,6*	*0,6*
Cs	*6*	*0,4*	*5,5*	8	8	*3,4*	*6*
Ba	22,8	773,4	106,9	334,1	415,6	93,3	13
La	*3,1*	20,5	33,8	48,5	81,4	48,2	*5,3*
Ce	*0,2*	49,3	78	85,6	95	93,3	14,7
Nd	*5,6*	18,2	36,6	43,6	78,5	47,8	*4,5*
Sm	*2,8*	*5,7*	14,1	11,9	23,4	15,4	*1,5*
Hf	2,87	3,3	6,6	8,6	11,8	8,7	*2,1*
Ta	*2,47*	*2,47*	*2,47*	*0,4*	*0,6*	*1*	*0,5*
W	27,1	*2,5*	3,5	3,2	3,2	3,8	3,7
Tl	*1*	2,7	*1*	*0,6*	*0,3*	*0,7*	*1,6*
Pb	14,1	35,4	3,4	5,4	10	6,5	2,6
Bi	*0,9*	1,6	*0,4*	*0,2*	1,2	*1*	*1*
Th	*1,1*	6,5	13,7	14,7	13,4	12,4	*1,3*
U	1,8	2,6	2,3	3,1	2,6	1,2	*0,2*

Cod. Lab	-	-	-	-	06/181-71	06/286-112	06/286-113
Muestra	PBM-083	PBM-087	PBM-090	PBM-091	PBM-097	PBM-098	PBM-099
%							
SiO_2	48,96	60,75	83,38	51,76	64,92	76,32	75,17
Al_2O_3	13,17	10,37	3,99	12,07	14,06	11,71	12,46
Fe_2O_3	23,67	18,80	7,21	17,29	6,59	2,29	2,76
CaO	0,07	0,02	0,01	0,17	0,17	0,05	0,78
TiO_2	1,11	0,43	0,16	1,00	0,67	0,15	0,18
MnO	0,25	0,20	0,10	0,17	0,18	0,03	0,03
K_2O	0,00	0,00	0,01	0,00	1,02	4,74	1,93
MgO	7,15	4,70	2,80	10,62	5,79	1,10	1,63
P_2O_5	0,07	*0,05*	*0,05*	0,11	0,07	*0,05*	*0,05*
Na_2O	*0,07*	*0,07*	*0,07*	*0,07*	2,37	1,44	2,56
PPC	5,56	4,74	2,34	6,82	4,15	2,17	2,50
TOTAL	100,0	100,0	99,4	100,0	100,0	100,0	100,0
µg/g							
Sc	27	11	3	27	24	4	5
V	189	88	38	173	129	7	4
Cr	118	56	69	134	44	7	10
Co	72,3	58,6	11,7	50,3	2,6	6	5,2
Ni	21,9	14,1	15,6	21,2	2,3	1,8	1,2
Cu	237	873,5	12,1	4,4	3,3	1,9	1,4
Zn	351,4	215,1	245,7	268,3	126,3	56,7	94,2
Ga	20,4	18,3	6,8	15,1	16,7	17,9	20,2
Ge	-	-	-	-	*0,3*	*1,9*	*1,8*
As	29,1	62,5	10,6	19,9	12,5	3,7	*2,2*
Se	*0,5*	2,5	*1*	*1*	*1*	*1*	*1*
Br	1,1	0,8	*0,5*	*0,7*	1	1,5	1,2
Rb	*0,3*	1,2	0,7	*0,1*	31	88,3	57,7
Sr	10,6	11,3	1	2,2	37,2	27,6	77,7
Y	34	21,1	5,2	18,9	27,5	65,9	70
Zr	89,1	94,1	29,8	81	168	234,8	305,2
Nb	3	3,4	4,1	2,8	6,4	10,8	13,2
Mo	*0,4*	3,6	*0,5*	*0,5*	*0,9*	*1*	*1*
Ag	10,4	4,2	*3,96*	5,8	*3,96*	*3,96*	*3,96*
Cd	12	7,2	*1,6*	*7,1*	*0,3*	*10*	*10*
Sn	9,7	3,8	5,4	18,5	3,7	4,9	8,1
Sb	*2,2*	*2,37*	*0,7*	*0,8*	*0,5*	*2,2*	*3,6*
I	6,4	5,1	4,4	5,6	5,6	*2,8*	4,9
Cs	*6*	*1*	*3,6*	*6*	*1*	*6,9*	*6,7*
Ba	*7,4*	41,3	*2*	*5,8*	138,4	360,7	311,5
La	*3,2*	*0,3*	5,6	*4,2*	11,1	34	37
Ce	17,5	13,9	17,3	15,8	35,1	80	64,4
Nd	12,9	6,7	9,7	*5,7*	15,8	33,2	35,8
Sm	*1,8*	*7,23*	*5*	*3,1*	*1,7*	*13*	*8,3*
Hf	*2,87*	*2,87*	*0,9*	*2,87*	3,8	8,1	7,9
Ta	*2,47*	*2,47*	*0,1*	*2,47*	*2,47*	*2,1*	*1,1*
W	24,8	11,7	5,6	7,8	5,2	91,2	75,9
Tl	*1,2*	1,7	*1,2*	*1,4*	*1,1*	*0,9*	*1,3*
Pb	6,9	15,3	3,5	10,4	4,2	8,9	10,3
Bi	*0,5*	3,9	*0,2*	*0,3*	*0,7*	*0,1*	*0,3*
Th	*1,5*	3,3	3,1	*0,7*	4,5	11,2	13,1
U	*0,7*	1,4	*1,2*	*1,2*	*0,7*	2	2,5

Cod. Lab	06/286-114	06/286-115	06/286-116	06/286-117	06/286-118	06/286-119	06/286-120
Muestra	PBM-100	PBM-101	PBM-102	PBM-107	PBM-108	PBM-109	PBM-111
%							
SiO_2	76,10	51,22	55,79	74,72	79,65	64,97	63,09
Al_2O_3	13,22	16,40	15,23	13,77	9,95	17,97	15,55
Fe_2O_3	1,59	8,89	10,31	2,34	2,58	3,32	5,86
CaO	0,13	8,51	1,34	0,13	0,22	1,63	2,87
TiO_2	0,20	1,25	2,02	0,17	0,17	0,29	0,65
MnO	*0,02*	0,09	0,10	*0,02*	*0,02*	*0,02*	0,06
K_2O	2,76	0,19	4,07	1,45	1,24	3,82	2,37
MgO	0,84	6,34	4,30	2,68	1,51	2,55	2,92
P_2O_5	*0,05*	0,12	0,07	*0,05*	*0,05*	*0,05*	0,10
Na_2O	2,76	3,40	0,93	1,51	0,80	1,62	4,11
PPC	2,40	3,61	5,86	3,23	3,88	3,84	2,42
TOTAL	100,1	100,0	100,0	100,1	100,1	100,1	100,0
µg/g							
Sc	5	31	32	7	7	13	23
V	10	199	262	9	20	11	93
Cr	14	116	17	14	16	6	137
Co	13,1	42,7	37,5	*0,4*	*2,41*	*2,41*	24
Ni	1,9	44,3	2,9	3,3	4,2	1,7	29,4
Cu	1,6	55,2	12	*1,3*	66,7	28,8	5,4
Zn	32,1	78,1	65,6	33,1	125,7	78,8	62,1
Ga	20,9	17,7	19,9	17,6	12,8	25,3	17,4
Ge	*2,6*	*1,3*	*1,1*	*1,1*	*1*	*1,6*	*1*
As	3,3	9	3	*0,4*	8,2	*1,7*	4,5
Se	*1*	*1*	*0,1*	*1*	*1*	*1*	*1*
Br	1,7	1	1	0,8	8,7	2,3	2,4
Rb	86,5	3,7	90,3	32,1	38,4	153,8	50,8
Sr	17,8	170,8	13,1	75,6	24,3	92,4	135,3
Y	86,7	30,8	28,9	18,3	51,7	56,1	30
Zr	298,2	128,1	156,3	142,7	103,1	275	160,5
Nb	11,4	4,4	5,5	5,8	5,1	10,7	7,6
Mo	*1*	*0,5*	*0,2*	*0,5*	*0,4*	*0,6*	*0,1*
Ag	*3,96*	*3,96*	*3,96*	*3,96*	*3,96*	*3,96*	*3,96*
Cd	*10*	*3,8*	*2,4*	*10*	*10*	*0,7*	*10*
Sn	6,3	2,2	*0,6*	5	4,3	8,5	2,9
Sb	*4,7*	*1*	*0,5*	*2,2*	*3,2*	*4,4*	*2,1*
I	5,3	4,6	6,3	6,8	6,3	5,9	*0,3*
Cs	*2*	*6*	*6*	*3,5*	8,5	*5,2*	*6*
Ba	169,4	47,8	36,2	397,5	234,8	584,2	390,5
La	43,7	7,9	9,6	31,7	78,9	52,3	26
Ce	94,9	29,7	33,5	68,6	148,8	104,6	55,2
Nd	50,5	16,5	17,6	24	72,4	43,8	28,1
Sm	*11,7*	*1,5*	*6,9*	10,6	16,3	12,4	7,4
Hf	8,8	4,4	3,8	4,8	*2,3*	8,1	3,4
Ta	*1*	*0,6*	*1,4*	*1*	*2,47*	*0,8*	*0,1*
W	149,5	32,3	45,4	58,4	45,8	38,7	71,2
Tl	*0,6*	*0,7*	*0,3*	*1,6*	*0,4*	*1,6*	*0,4*
Pb	2,9	6,2	2,3	4,6	21,3	12,2	7,7
Bi	*1*	*0,2*	*1*	*1*	*0,9*	*0,7*	*1*
Th	11,5	1,8	1,8	12,3	8,8	17,3	7,3
U	1,2	*1,2*	*0,1*	2,4	1,8	4,7	1,5

Cod. Lab	06/286-121	06/286-122	06/286-123	06/286-124	06/286-125	06/286-126	06/286-127
Muestra	PBM-112	PBM-114	PBM-117	PBM-118	PBM-119	PBM-122	PBM-123
%							
SiO_2	65,87	73,83	56,80	66,46	67,23	78,37	75,80
Al_2O_3	16,29	13,97	17,71	15,89	13,77	11,13	13,04
Fe_2O_3	4,87	2,44	7,39	6,20	6,18	2,13	2,07
CaO	4,17	0,83	5,71	2,83	1,92	0,34	0,10
TiO_2	0,46	0,24	0,89	0,50	0,69	0,18	0,21
MnO	0,03	0,02	0,11	0,04	0,13	*0,02*	*0,02*
K_2O	1,07	0,48	2,01	1,27	1,53	3,69	2,69
MgO	1,72	1,85	3,38	1,13	2,53	0,23	0,94
P_2O_5	0,11	*0,05*	0,10	0,08	0,10	*0,05*	*0,05*
Na_2O	3,01	3,03	2,24	1,16	3,67	3,18	2,31
PPC	2,41	3,31	3,66	4,45	2,25	0,74	2,85
TOTAL	100,0	100,1	100,0	100,0	100,0	100,1	100,1
µg/g							
Sc	17	8	29	23	18	7	8
V	46	9	137	20	83	4	9
Cr	19	8	63	10	19	19	11
Co	9,9	*2,41*	21,6	10,2	18,9	39,2	*1,6*
Ni	3,4	2,4	11,8	3,4	2,9	1,3	1,2
Cu	5,3	22,7	10,4	7,7	4,3	*0,77*	4
Zn	58,4	54,4	79	78,5	66,3	29,9	34,5
Ga	20,7	17,7	20,5	20,5	17,9	17,3	18,2
Ge	*1,5*	*1,6*	*1,6*	*0,9*	*1,4*	*3,2*	*2,4*
As	*1,7*	4,7	6,1	*0,4*	3,4	4,4	3,6
Se	*1*	*1*	*1*	*1*	*1*	*1*	*1*
Br	1,8	1,8	1,2	1,1	1,4	0,9	1,3
Rb	37	23	79,6	52,2	30,5	83,4	121,2
Sr	190,3	96,6	162	130,2	104	39,4	22,2
Y	39,6	44,3	26,5	46,9	39	50,7	56,6
Zr	221,2	215,6	153,2	248,2	187,5	244,1	191,3
Nb	9,6	8,3	9,8	12,6	7,2	10,1	7,6
Mo	*0,4*	*1*	*0,7*	*0,2*	*0,4*	*0,6*	*1*
Ag	*3,96*	*3,96*	*3,96*	*3,96*	*3,96*	*3,96*	*3,96*
Cd	*10*	*10*	*1,8*	*1,1*	*10*	*10*	*10*
Sn	4,3	6,6	2,1	4,2	*1,4*	7,8	4,2
Sb	*4,2*	*5,3*	*0,3*	*1,7*	*<LD*	*1,9*	*4,8*
I	5,1	*3,8*	4,7	*3,4*	5,9	5,9	5,2
Cs	*3,5*	*4,9*	*0,3*	*6*	*6*	*6*	*6*
Ba	301,5	224,8	300,5	355,1	209,2	448,7	221,2
La	32	33,3	21,1	69,5	22,5	30,8	38,2
Ce	71,6	73,3	55,7	113,1	50,7	64,1	71,4
Nd	33,4	30,7	21,7	57,6	21	28,1	33
Sm	*4*	11	*<LD*	*11,3*	*6,4<LL*	*12,3*	*5,2<LL*
Hf	6,3	5,5	4,2	5,2	4	7,4	6
Ta	*0,5*	*0,9*	*2,47*	*2,47*	*2,47*	*0,3*	*2,47*
W	51,4	36,7	24,4	25,9	49,3	248,4	74,5
Tl	*0,3*	*1,6*	*1*	*1*	*0,4*	*0,4*	*1,7*
Pb	12,2	17,3	14,4	18,5	5	14,2	6,4
Bi	*0,6*	*1*	*1*	*1*	*0,4*	1,5	*1*
Th	10,2	13,2	7,6	13,1	5,3	15,5	11,1
U	2,9	2,6	2,5	2,7	*0,6*	3,1	2

Cod. Lab	06/286-128	06/286-129	06/286-130	06/286-131	06/286-132	06/286-133
Muestra	PBM-124	PBM-125	PBM-*127	PBM-128	PBM-129	PBM-132
%						
SiO_2	75,63	76,96	77,04	70,17	72,69	75,07
Al_2O_3	12,49	11,63	11,75	14,10	13,25	12,79
Fe_2O_3	2,81	1,41	3,87	3,40	3,79	2,61
CaO	0,02	0,01	0,01	0,84	0,09	1,19
TiO_2	0,18	0,18	0,15	0,29	0,25	0,21
MnO	0,04	*0,02*	*0,02*	0,04	0,03	0,02
K_2O	3,85	7,98	3,06	3,51	4,17	3,81
MgO	1,46	0,15	0,91	3,00	1,65	0,87
P_2O_5	*0,05*	*0,05*	*0,05*	*0,05*	*0,05*	*0,05*
Na_2O	0,14	0,78	0,20	0,53	1,29	1,13
PPC	3,39	0,91	3,02	4,12	2,79	2,31
TOTAL	100,0	100,1	100,1	100,0	100,1	100,1
µg/g						
Sc	10	10	6	5	6	12
V	10	*2*	10	9	*3*	3
Cr	16	14	10	10	10	10
Co	6,3	29	16,9	*2,41*	*2,41*	*2,41*
Ni	1,5	*0,4*	2,4	1,2	*0,7*	1,1
Cu	209,9	*1,35*	36,4	13,6	1,9	3,1
Zn	78,3	16,5	20,1	124,2	57,9	39,6
Ga	18,3	16,5	14,7	25,4	22,2	28,6
Ge	*1,3*	*2,9*	*1,5*	*1,2*	*1,1*	*1,9*
As	31,9	*2,7*	8,3	3,3	*2*	3,7
Se	*1*	*1*	*1*	*1*	*1*	*1*
Br	1,4	0,9	1,3	*0,7*	0,9	*0,7*
Rb	139,7	129,4	91,2	100,3	123,3	132,5
Sr	3,1	11,8	7,6	66,9	7	53,4
Y	55,1	55,9	30,9	77,3	91,5	67,3
Zr	159	307,9	117,3	473	551,8	353,4
Nb	9,9	15,4	4,9	18,1	17,9	17,3
Mo	2,7	*0,4*	*0,7*	*0,1*	*1*	*1*
Ag	*3,96*	*3,96*	*3,96*	*3,96*	*3,96*	*3,96*
Cd	*10*	*10*	*10*	*10*	*10*	*10*
Sn	8	7	5,9	7,4	10,3	6,6
Sb	*3,9*	*4,1*	*2,4*	*2,3*	*2,5*	*1,7*
I	5,1	7,2	*2,5*	*2,5*	*2,7*	5
Cs	*6,7*	*3,6*	*6*	*7,6*	*7*	*6*
Ba	455,2	317,4	902,7	244,8	227,8	453,9
La	30,5	32,4	20	69,4	43,1	47,4
Ce	64,1	70,7	41	125,4	100,6	84
Nd	28,1	33,8	14,7	63,5	43,5	44,7
Sm	*10,5*	*7,7*	*5,6<LL*	*16,6*	*14,1*	*11*
Hf	5,2	9,5	4,7	14,3	16,7	8,8
Ta	*0,3*	*1*	*1,5*	*1,4*	*2,47*	*1,9*
W	98,9	223,5	116	20,2	40,6	52,3
Tl	*0,7*	*0,4*	*1,6*	*0,3*	*1,5*	*1,6*
Pb	82,9	8	4	25	3,1	15,5
Bi	*1*	*1*	*1*	*1*	*1*	1,2
Th	14,6	13,1	9,1	14,5	16,6	14,6
U	2	1,5	2,3	1,6	2,5	3,5

Tabla I.I.3. Composición química de las rocas volcánicas (Capítulo III). (Cursiva: menor del límite de detección)

Muestra	AZ-071	AZ-073	AZ-080	AZ-081	AZ-082	AZ-085	AZ-086
%							
SiO_2	77,57	50,43	65,11	54,95	61,30	69,92	66,82
TiO2	0,10	1,50	0,40	0,58	0,54	0,44	0,47
Al_2O_3	9,75	18,23	14,91	18,74	18,10	15,46	15,27
Fe_2O_3	2,07	8,60	4,55	8,03	4,63	2,34	4,28
MnO	0,02	0,13	0,02	0,07	0,07	0,01	0,05
MgO	4,44	7,25	1,41	3,55	2,58	0,77	1,67
CaO	0,55	3,77	0,94	0,43	1,97	1,01	2,18
Na_2O	0,24	4,92	1,42	2,28	4,61	4,07	4,80
K_2O	2,04	0,15	9,11	7,91	2,91	3,54	1,54
P_2O_5	0,04	0,15	0,16	0,12	0,10	0,07	0,07
PPC	3,22	4,88	1,99	3,34	3,2	2,38	2,7
TOTAL	100,04	99,99	100,00	100,00	100,00	100,00	99,85
µg/g							
Ba	157,0	758,0	606,0	434,0	433,0	192,0	269,0
Rb	72,0	11,0	145,0	169,0	71,0	83,0	38,0
Sr	21,0	364,0	57,0	41,0	236,0	77,0	289,0
Y	17,0	26,0	15,0	14,0	9,0	11,0	9,0
Zr	150,0	130,0	125,0	179,0	168,0	155,0	136,0
Nb	*10,0*	*10,0*	*10,0*	*10,0*	*10,0*	*10,0*	*10,0*
Pb	*10,0*	25,0	*10,0*	*10,0*	18,0	*10,0*	22,0
Zn	54,0	139,0	60,0	144,0	151,0	43,0	78,0
Cu	*8,0*	16,0	10,0	*8,0*	*8,0*	31,0	*8,0*
Ni	*10,0*	43,0	*10,0*	*10,0*	16,0	*10,0*	*10,0*
V	2,0	209,0	35,0	85,0	69,0	43,0	58,0
Cr	25,0	150,0	52,0	44,0	30,0	42,0	30,0
Sc	3,0	29,0	7,0	11,0	8,0	7,0	7,0
Co	2,0	36,0	7,0	9,0	15,0	7,0	11,0
Be	2,0	1,0	1,0	2,0	2,0	1,0	2,0
W	*10,0*	*10,0*	*10,0*	*10,0*	*10,0*	*10,0*	*10,0*
Sn	*5,0*	*5,0*	*5,0*	*5,0*	*5,0*	*5,0*	*5,0*
Mo	*4,0*	*4,0*	*4,0*	*4,0*	*4,0*	*4,0*	*4,0*
Ag	*1,0*	*1,0*	*1,0*	*1,0*	*1,0*	*1,0*	*1,0*
Cd	*2,0*	*2,0*	*2,0*	*2,0*	*2,0*	*2,0*	*2,0*
As	*10,0*	*10,0*	*10,0*	*10,0*	*10,0*	*10,0*	*10,0*
Sb	*10,0*	25,0	*10,0*	11,0	32,0	33,0	18,0
La	34,3	19,4	22,6	28,3	18,9	24,1	14,9
Ce	74,0	26,9	40,9	57,6	35,8	46,1	28,8
Pr	8,3	3,8	6,0	7,3	4,8	6,3	4,0
Nd	34,6	13,5	22,6	27,0	18,2	21,8	15,4
Sm	7,5	4,0	4,5	5,6	3,5	4,7	3,1
Eu	0,6	0,8	1,2	1,4	0,9	1,0	0,8
Gd	6,3	4,7	4,2	4,8	3,3	4,0	2,8
Tb	0,8	0,7	0,7	0,7	0,6	0,4	0,4
Dy	5,2	5,1	3,6	4,0	3,1	3,1	2,4
Ho	1,0	1,0	0,8	0,7	0,7	0,5	0,5
Er	2,7	2,9	2,1	2,0	1,8	1,7	1,4
Tm	0,3	0,3	0,3	0,3	0,3	0,2	0,2
Yb	3,8	2,7	1,8	2,4	1,7	1,9	1,3
Lu	0,5	0,3	0,3	0,3	0,3	0,2	0,2

Muestra	AZ-101	AZ-103	AZ-118	AZ-119	AZ-120	AZ-130	AZ-144
%							
SiO_2	49,27	59,96	76,01	76,25	75,51	64,47	77,03
TiO2	1,36	0,54	0,16	0,17	0,19	0,47	0,13
Al_2O_3	16,34	19,28	12,39	13,03	12,67	17,58	12,14
Fe_2O_3	8,40	4,43	1,96	2,01	2,47	3,33	1,68
MnO	0,18	0,04	0,02	0,02	0,06	0,06	0,02
MgO	7,04	1,26	1,74	0,18	1,05	1,38	1,54
CaO	6,07	1,43	0,14	0,35	0,62	1,43	0,35
Na_2O	4,79	3,52	0,40	2,68	5,76	4,52	2,89
K_2O	0,06	5,59	4,52	3,03	0,58	3,76	2,45
P_2O_5	0,14	0,13	0,04	0,04	0,04	0,08	0,04
PPC	6,11	3,82	2,66	2,29	1,11	2,94	1,76
TOTAL	99,74	99,99	100,04	100,04	100,05	100,01	100,04
µg/g							
Ba	78,0	684,0	450,0	440,0	140,0	574,0	271,0
Rb	9,0	138,0	196,0	153,0	27,0	96,0	116,0
Sr	286,0	148,0	19,0	99,0	88,0	221,0	90,0
Y	18,0	16,0	49,0	53,0	43,0	12,0	40,0
Zr	126,0	167,0	207,0	202,0	203,0	149,0	190,0
Nb	*10,0*	*10,0*	*10,0*	*10,0*	*10,0*	*10,0*	*10,0*
Pb	*10,0*	26,0	25,0	*10,0*	13,0	182,0	11,0
Zn	130,0	282,0	83,0	53,0	61,0	348,0	71,0
Cu	29,0	*8,0*	*8,0*	*8,0*	*8,0*	18,0	*8,0*
Ni	43,0	*10,0*	*10,0*	*10,0*	*10,0*	*10,0*	*10,0*
V	204,0	72,0	4,0	2,0	9,0	59,0	3,0
Cr	148,0	50,0	11,0	18,0	36,0	23,0	29,0
Sc	23,0	11,0	5,0	5,0	5,0	7,0	4,0
Co	41,0	14,0	3,0	2,0	4,0	10,0	2,0
Be	1,0	2,0	4,0	4,0	3,0	2,0	3,0
W	*10,0*	*10,0*	*10,0*	*10,0*	*10,0*	*10,0*	*10,0*
Sn	*5,0*	*5,0*	*5,0*	*5,0*	*5,0*	*5,0*	*5,0*
Mo	*4,0*	*4,0*	*4,0*	*4,0*	*4,0*	*4,0*	*4,0*
Ag	*1,0*	*1,0*	1,0	*1,0*	*1,0*	*1,0*	1,0
Cd	*2,0*	2,0	*2,0*	*2,0*	*2,0*	*2,0*	*2,0*
As	18,0	100,0	*10,0*	*10,0*	*10,0*	*10,0*	*10,0*
Sb	59,0	22,0	*10,0*	*10,0*	*10,0*	25,0	*10,0*
La	11,9	28,2	39,2	55,1	41,6	23,8	32,3
Ce	25,3	48,8	85,5	102,0	83,2	40,3	66,0
Pr	3,4	6,2	10,8	15,2	13,0	5,6	8,8
Nd	14,5	21,8	40,7	56,8	48,1	21,5	27,4
Sm	3,9	4,7	9,2	12,4	10,9	4,1	7,2
Eu	1,3	1,6	0,8	1,2	1,3	1,1	0,0
Gd	4,2	4,0	9,0	11,8	10,6	3,8	7,4
Tb	0,7	0,6	1,6	2,0	1,8	0,5	1,1
Dy	4,1	3,6	9,7	11,4	10,3	2,9	8,1
Ho	0,7	0,5	2,0	2,3	2,0	0,6	1,6
Er	1,8	1,4	5,9	6,6	5,5	1,7	4,8
Tm	0,3	0,3	0,9	1,0	1,0	0,3	0,6
Yb	2,2	2,0	5,6	6,2	5,6	1,5	4,4
Lu	0,2	0,1	0,9	1,0	0,7	0,3	0,6

Muestra	AZ-152	AZ-158	AZ-159	AZ-166	AZ-167	AZ-168	AZ-176
%							
SiO_2	73,16	68,26	62,66	56,35	72,75	76,39	62,49
TiO2	0,18	0,44	0,55	0,89	0,19	0,34	0,81
Al_2O_3	12,85	15,18	18,34	20,98	13,94	13,17	16,99
Fe_2O_3	2,81	3,17	4,19	6,59	2,26	1,12	9,60
MnO	0,03	0,03	0,05	0,08	0,03	0,01	0,02
MgO	3,25	1,85	2,29	0,97	2,19	0,37	1,04
CaO	0,49	1,68	1,18	0,54	0,46	1,34	0,27
Na_2O	1,34	3,68	4,10	0,39	3,86	5,14	0,82
K_2O	2,82	2,69	3,27	6,69	2,31	1,11	4,66
P_2O_5	0,04	0,09	0,10	0,05	0,04	0,05	0,11
PPC	3,07	2,93	3,29	6,48	2,02	0,97	3,19
TOTAL	100,04	100,00	100,00	100,01	100,04	100,00	99,99
µg/g							
Ba	298,0	677,0	441,0	559,0	327,0	160,0	457,0
Rb	126,0	59,0	70,0	152,0	107,0	46,0	185,0
Sr	46,0	175,0	233,0	47,0	63,0	145,0	69,0
Y	47,0	13,0	17,0	12,0	49,0	26,0	22,0
Zr	205,0	144,0	172,0	195,0	248,0	129,0	166,0
Nb	*10,0*	*10,0*	*10,0*	*10,0*	*10,0*	*10,0*	13,0
Pb	19,0	11,0	10,0	12,0	10,0	22,0	20,0
Zn	342,0	72,0	77,0	100,0	52,0	19,0	140,0
Cu	*8,0*	*8,0*	*8,0*	*8,0*	*8,0*	38,0	9,0
Ni	*10,0*	*10,0*	12,0	*10,0*	*10,0*	*10,0*	71,0
V	7,0	65,0	69,0	69,0	5,0	9,0	156,0
Cr	18,0	26,0	43,0	38,0	34,0	113,0	70,0
Sc	5,0	7,0	11,0	10,0	5,0	6,0	15,0
Co	3,0	12,0	13,0	14,0	3,0	4,0	25,0
Be	3,0	2,0	2,0	1,0	4,0	2,0	3,0
W	*10,0*	*10,0*	*10,0*	*10,0*	*10,0*	*10,0*	*10,0*
Sn	5,0	*5,0*	*5,0*	10,0	*5,0*	*5,0*	*5,0*
Mo	*4,0*	*4,0*	*4,0*	*4,0*	*4,0*	*4,0*	*4,0*
Ag	*1,0*	*1,0*	*1,0*	*1,0*	*1,0*	*1,0*	*1,0*
Cd	*2,0*	*2,0*	*2,0*	*2,0*	*2,0*	*2,0*	*2,0*
As	*10,0*	*10,0*	*10,0*	20,0	*10,0*	*10,0*	*10,0*
Sb	*10,0*	20,0	22,0	*10,0*	*10,0*	*10,0*	*10,0*
La	58,0	15,0	30,7	16,7	36,5	32,9	43,8
Ce	101,0	39,8	56,8	30,8	85,1	69,8	96,3
Pr	11,8	5,0	5,5	4,3	12,9	9,1	11,5
Nd	47,8	15,3	22,0	16,6	50,4	28,0	48,2
Sm	11,0	4,1	4,4	3,7	11,6	7,1	9,8
Eu	1,0	1,0	1,0	1,5	1,1	0,4	2,0
Gd	10,4	3,8	4,0	3,7	11,1	6,9	8,5
Tb	1,5	0,6	0,4	0,6	1,8	1,0	1,2
Dy	9,7	3,4	3,5	3,5	11,3	6,3	7,0
Ho	1,9	0,7	0,7	0,8	2,3	1,2	1,4
Er	5,5	2,1	2,0	2,2	6,9	3,7	3,9
Tm	0,7	0,3	0,2	0,4	1,0	0,5	0,5
Yb	5,2	1,8	2,4	2,0	6,9	3,6	3,9
Lu	0,7	0,4	0,2	0,4	1,0	0,5	0,5

Muestra	AZ-177	AZ-393	AZ-528	AZ-529	AZ-530	AZ-595	AZ-596
%							
SiO_2	68,92	63,75	77,12	72,81	58,52	89,34	76,08
TiO2	0,69	0,59	0,15	0,16	0,44	0,22	0,18
Al_2O_3	15,75	11,66	11,89	13,38	21,63	5,64	11,47
Fe_2O_3	5,17	12,20	1,65	2,17	3,16	1,18	3,06
MnO	0,05	0,17	0,02	0,02	0,01	0,01	0,01
MgO	1,19	4,41	1,27	3,85	1,84	0,75	3,48
CaO	0,32	0,13	0,59	0,39	0,66	0,13	0,24
Na_2O	0,51	0,07	4,21	0,78	2,12	0,47	0,92
K_2O	3,91	2,15	1,58	3,22	7,90	0,74	0,93
P_2O_5	0,04	0,06	0,04	0,04	0,06	0,04	0,04
PPC	3,44	4,89	1,54	3,23	3,67	1,51	3,61
TOTAL	100,00	100,07	100,04	100,04	100,00	100,03	100,04
µg/g							
Ba	367,0	780,0	203,0	326,0	298,0	287,0	292,0
Rb	158,0	88,0	80,0	110,0	266,0	37,0	43,0
Sr	55,0	14,0	55,0	41,0	45,0	34,0	75,0
Y	17,0	11,0	48,0	43,0	28,0	47,0	28,0
Zr	153,0	97,0	187,0	218,0	305,0	73,0	185,0
Nb	12,0	*10,0*	*10,0*	*10,0*	*10,0*	*10,0*	*10,0*
Pb	*10,0*	1627,0	*10,0*	*10,0*	57,0	30,0	12,0
Zn	139,0	154,0	39,0	48,0	49,0	221,0	98,0
Cu	15,0	*8,0*	*8,0*	*8,0*	26,0	27,0	23,0
Ni	81,0	23,0	*10,0*	*10,0*	15,0	11,0	*10,0*
V	133,0	113,0	3,0	3,0	31,0	42,0	12,0
Cr	73,0	130,0	44,0	22,0	30,0	47,0	18,0
Sc	14,0	16,0	4,0	5,0	11,0	4,0	5,0
Co	26,0	36,0	<2	2,0	8,0	4,0	5,0
Be	3,0	1,0	3,0	4,0	4,0	2,0	3,0
W	*10,0*	*10,0*	*10,0*	*10,0*	*10,0*	*10,0*	*10,0*
Sn	*5,0*	*5,0*	*5,0*	12,0	*5,0*	*5,0*	10,0
Mo	*4,0*	*4,0*	*4,0*	*4,0*	*4,0*	*4,0*	*4,0*
Ag	*1,0*	*1,0*	*1,0*	*1,0*	*1,0*	*1,0*	*1,0*
Cd	*2,0*	*2,0*	*2,0*	*2,0*	*2,0*	*2,0*	*2,0*
As	*10,0*	*10,0*	*10,0*	*10,0*	*10,0*	*10,0*	*10,0*
Sb	*10,0*	*10,0*	*10,0*	*10,0*	32,0	29,0	*10,0*
La	37,7	33,7	50,4	18,7	17,4	18,3	45,4
Ce	76,6	78,2	100,0	49,0	39,0	39,1	84,2
Pr	9,9	13,0	13,9	6,6	5,2	5,8	10,3
Nd	27,9	50,8	52,7	27,8	18,9	23,0	42,2
Sm	5,8	11,1	11,6	6,5	4,1	5,4	10,0
Eu	0,5	1,1	1,0	1,0	0,5	0,5	0,9
Gd	4,6	10,7	10,8	6,3	3,3	7,0	9,7
Tb	0,5	1,7	1,8	1,0	0,2	1,7	1,3
Dy	4,1	10,9	10,5	6,9	2,9	13,3	7,8
Ho	0,8	2,1	2,1	1,5	0,4	3,3	1,4
Er	2,6	6,4	6,2	4,4	1,7	10,1	3,6
Tm	0,3	0,9	1,0	0,6	0,0	1,5	0,4
Yb	2,5	6,2	6,3	4,4	2,1	9,1	3,2
Lu	0,3	0,9	1,0	0,6	0,1	1,3	0,3

Muestra	AZ-597	AZ-598	AZ-599	AZ-600	AZ-601	AZ-602	AZ-603
%							
SiO_2	65,79	68,21	76,27	69,93	58,48	57,09	71,74
TiO2	0,41	0,46	0,21	0,19	0,36	0,87	0,40
Al_2O_3	17,08	14,87	9,98	15,41	23,96	19,91	13,60
Fe_2O_3	3,74	6,54	4,04	3,03	2,71	6,33	4,09
MnO	0,04	0,03	0,03	0,03	0,02	0,08	0,03
MgO	3,50	1,86	3,90	3,23	1,66	2,91	1,85
CaO	0,21	0,56	0,57	0,08	0,21	0,38	0,67
Na_2O	0,27	0,34	1,12	0,24	2,28	3,76	3,90
K_2O	4,42	3,30	0,79	4,15	6,45	4,05	1,47
P_2O_5	0,04	0,04	0,04	0,04	0,05	0,13	0,06
PPC	4,54	3,81	3,1	3,7	3,84	4,5	2,18
TOTAL	100,04	100,00	100,04	100,04	100,00	100,01	100,00
µg/g							
Ba	554,0	282,0	210,0	774,0	524,0	428,0	313,0
Rb	162,0	129,0	39,0	149,0	250,0	94,0	37,0
Sr	25,0	48,0	92,0	31,0	86,0	101,0	290,0
Y	37,0	19,0	39,0	45,0	52,0	17,0	12,0
Zr	240,0	191,0	146,0	252,0	380,0	201,0	120,0
Nb	10,0	*10,0*	*10,0*	*10,0*	13,0	*10,0*	*10,0*
Pb	20,0	36,0	43,0	14,0	65,0	40,0	47,0
Zn	78,0	235,0	139,0	275,0	152,0	494,0	251,0
Cu	17,0	18,0	24,0	10,0	17,0	66,0	11,0
Ni	*10,0*	19,0	*10,0*	*10,0*	16,0	13,0	*10,0*
V	26,0	62,0	22,0	4,0	13,0	144,0	57,0
Cr	22,0	42,0	49,0	14,0	19,0	131,0	57,0
Sc	8,0	10,0	5,0	5,0	18,0	20,0	8,0
Co	6,0	9,0	5,0	4,0	7,0	11,0	7,0
Be	3,0	2,0	3,0	4,0	3,0	2,0	2,0
W	*10,0*	*10,0*	*10,0*	*10,0*	*10,0*	*10,0*	*10,0*
Sn	10,0	*5,0*	*5,0*	12,0	*5,0*	*5,0*	*5,0*
Mo	*4,0*	*4,0*	*4,0*	*4,0*	*4,0*	*4,0*	*4,0*
Ag	*1,0*	*1,0*	*1,0*	*1,0*	*1,0*	*1,0*	*1,0*
Cd	*2,0*	*2,0*	*2,0*	*2,0*	*2,0*	*2,0*	*2,0*
As	*10,0*	*10,0*	*10,0*	*10,0*	24,0	19,0	44,0
Sb	*10,0*	*10,0*	*10,0*	*10,0*	*10,0*	15,0	16,0
La	45,7	25,3	31,9	43,7	75,0	27,4	11,0
Ce	95,8	62,7	75,0	98,0	165,0	50,7	20,3
Pr	13,2	9,0	10,4	15,1	20,1	6,7	2,3
Nd	52,3	36,0	41,4	58,0	79,0	20,3	7,9
Sm	12,1	7,3	9,2	13,7	16,6	5,0	1,7
Eu	1,7	0,9	0,9	1,3	1,5	0,7	0,4
Gd	11,6	6,9	8,7	12,9	14,8	4,3	1,5
Tb	1,8	1,2	1,5	2,0	2,5	0,5	0,0
Dy	10,4	7,7	10,0	12,4	14,4	3,5	1,4
Ho	2,0	1,5	2,2	2,4	3,0	0,6	0,1
Er	5,6	4,5	7,2	7,3	8,6	2,2	0,6
Tm	0,7	0,7	1,2	1,1	1,3	0,2	0,0
Yb	5,1	4,3	7,6	7,2	8,0	2,3	1,2
Lu	0,7	0,6	1,1	1,1	1,2	0,2	0,0

Muestra	AZ-603*	AZ-604	AZ-605	AZ-606	AZ-607	AZ-713	AZ-714
%							
SiO_2	81,84	69,81	69,28	72,16	62,82	73,75	75,67
TiO2	0,12	0,16	0,19	0,23	0,63	0,36	0,31
Al_2O_3	9,91	14,07	15,92	13,80	17,42	6,80	6,54
Fe_2O_3	1,42	2,37	2,03	2,92	5,49	12,74	11,71
MnO	0,01	0,03	0,02	0,02	0,04	0,15	0,13
MgO	0,34	4,39	3,62	2,65	2,22	2,82	2,46
CaO	0,60	0,15	0,42	0,64	2,16	0,01	0,01
Na_2O	4,81	0,46	0,18	0,63	3,41	0,07	0,07
K_2O	0,09	4,85	4,68	3,55	2,59	0,10	0,10
P_2O_5	0,04	0,04	0,04	0,04	0,08	0,04	0,04
PPC	0,85	3,7	3,67	3,39	3,15	3,38	3,17
TOTAL	100,03	100,04	100,05	100,04	100,00	100,21	100,20
µg/g							
Ba	72,0	365,0	734,0	695,0	631,0	30,0	88,0
Rb	11,0	170,0	163,0	125,0	86,0	4,0	4,0
Sr	97,0	18,0	27,0	36,0	258,0	5,0	5,0
Y	91,0	38,0	45,0	62,0	17,0	6,0	5,0
Zr	163,0	227,0	254,0	149,0	152,0	53,0	52,0
Nb	*10,0*	*10,0*	*10,0*	13,0	*10,0*	*10,0*	*10,0*
Pb	22,0	19,0	*10,0*	*10,0*	67,0	*10,0*	*10,0*
Zn	48,0	99,0	67,0	114,0	312,0	176,0	151,0
Cu	*8,0*	10,0	*8,0*	11,0	*8,0*	188,0	91,0
Ni	*10,0*	*10,0*	*10,0*	20,0	*10,0*	29,0	25,0
V	3,0	3,0	4,0	24,0	97,0	92,0	91,0
Cr	141,0	24,0	20,0	36,0	66,0	58,0	58,0
Sc	4,0	5,0	6,0	13,0	16,0	6,0	5,0
Co	2,0	3,0	2,0	6,0	10,0	23,0	18,0
Be	2,0	4,0	4,0	3,0	3,0	1,0	1,0
W	*10,0*	*10,0*	*10,0*	*10,0*	*10,0*	*10,0*	*10,0*
Sn	*5,0*	*5,0*	7,0	*5,0*	*5,0*	*5,0*	*5,0*
Mo	*4,0*	*4,0*	*4,0*	*4,0*	*4,0*	*4,0*	*4,0*
Ag	*1,0*	*1,0*	*1,0*	*1,0*	*1,0*	*1,0*	*1,0*
Cd	*2,0*	*2,0*	*2,0*	*2,0*	*2,0*	*2,0*	*2,0*
As	*10,0*	*10,0*	*10,0*	*10,0*	12,0	*10,0*	*10,0*
Sb	*10,0*	*10,0*	*10,0*	*10,0*	*10,0*	*10,0*	*10,0*
La	39,7	37,7	41,9	23,1	21,1	26,1	42,2
Ce	79,5	81,7	92,7	45,2	44,2	52,4	91,9
Pr	8,8	10,5	12,1	5,8	6,0	6,3	12,6
Nd	35,3	36,4	42,3	21,2	23,2	23,2	49,4
Sm	8,8	8,3	9,4	5,5	5,4	4,7	10,1
Eu	0,8	0,7	0,8	0,6	0,5	1,3	1,0
Gd	10,8	7,5	8,4	5,6	5,6	4,3	9,3
Tb	2,0	1,0	1,3	1,0	0,7	0,5	1,5
Dy	15,2	7,4	9,3	6,7	6,5	3,9	9,5
Ho	3,4	1,4	1,8	1,4	1,3	0,8	2,0
Er	11,0	4,3	5,7	4,2	4,1	2,3	5,8
Tm	1,5	0,4	0,7	0,6	0,4	0,3	0,8
Yb	10,4	4,1	5,8	3,8	4,2	2,3	6,0
Lu	1,5	0,4	0,7	0,6	0,4	0,2	0,7

Muestra	AZ-636	AZ-637	AZ-665	LC-300	LC-312	LC-313	LC-317
%							
SiO_2	58,15	75,64	49,46	60,45	64,20	61,53	53,02
TiO2	0,55	0,15	0,22	0,78	0,52	0,55	0,78
Al_2O_3	20,11	13,15	8,45	15,15	11,25	12,34	12,26
Fe_2O_3	4,56	1,62	26,58	7,42	11,62	12,77	18,25
MnO	0,02	0,01	0,16	0,23	0,19	0,17	0,28
MgO	3,52	2,02	4,56	5,09	6,04	5,46	6,34
CaO	4,24	0,99	0,04	0,24	0,08	0,06	0,15
Na_2O	4,06	5,11	0,07	0,70	0,12	0,09	0,07
K_2O	1,34	0,09	0,08	5,60	1,17	1,88	1,37
P_2O_5	0,11	0,00	0,02	0,10	0,02	0,03	0,06
PPC	3,34	1,22	10,51	5,41	4,45	4,24	12,00
TOTAL	100,00	100,00	100,14	101,17	99,66	99,12	104,57
µg/g							
Ba	548,0	54,0	10,0	1084,0	739,0	665,0	170,0
Rb	34,0	5,0	1,0	142,0	45,0	56,0	53,0
Sr	507,0	158,0	2,0	37,0	29,0	30,0	18,0
Y	20,0	47,0	8,0	20,0	9,0	10,0	13,0
Zr	184,0	206,0	71,0	155,0	100,0	108,0	122,0
Nb	*10,0*	*10,0*	*10,0*	*10,0*	*10,0*	*10,0*	*10,0*
Pb	24,0	32,0	42,0	50,0	413,0	227,0	205,0
Zn	80,0	42,0	97,0	336,0	403,0	176,0	385,0
Cu	15,0	*8,0*	1160,0	*8,0*	1166,0	11,0	8,0
Ni	*10,0*	*10,0*	*10,0*	*10,0*	18,0	16,0	39,0
V	63,0	2,0	25,0	87,0	85,0	64,0	117,0
Cr	62,0	102,0	39,0	61,0	93,0	76,0	124,0
Sc	12,0	5,0	5,0	16,0	12,0	11,0	16,0
Co	9,0	2,0	40,0	19,0	27,0	29,0	56,0
Be	1,0	2,0	1,0	1,0	*1,0*	*1,0*	*1,0*
W	*10,0*	*10,0*	*10,0*	*10,0*	11,0	*10,0*	*10,0*
Sn	4,0	7,0	4,0	*5,0*	*5,0*	*5,0*	10,0
Mo	*2,0*	*2,0*	*2,0*	*4,0*	*4,0*	*4,0*	*4,0*
Ag	*1,0*	*1,0*	*1,0*	*1,0*	*1,0*	*1,0*	*1,0*
Cd	*2,0*	*2,0*	*2,0*	*2,0*	*2,0*	*2,0*	*2,0*
As	*10,0*	10,0	42,0	*10,0*	*10,0*	*10,0*	*10,0*
Sb	*10,0*	*10,0*	13,0	*10,0*	*10,0*	*10,0*	*10,0*
La	15,2	20,7	15,6	7,0	24,9	17,1	15,0
Ce	34,1	40,8	31,0	8,7	42,2	29,8	44,4
Pr	4,1	4,3	4,1	1,1	5,3	3,9	5,8
Nd	15,8	18,8	12,1	4,4	20,7	16,5	17,2
Sm	3,1	3,5	2,8	1,0	3,5	3,2	5,4
Eu	0,5	0,4	0,4	0,1	0,7	0,7	1,0
Gd	2,9	3,0	2,5	1,0	3,0	3,1	5,1
Tb	0,4	0,3	0,2	0,0	0,3	0,3	0,8
Dy	2,8	2,5	2,1	1,3	2,8	2,9	4,8
Ho	0,5	0,5	0,4	0,3	0,6	0,6	1,0
Er	1,7	1,3	1,1	1,0	1,7	1,7	2,8
Tm	0,2	0,1	0,2	0,1	0,2	0,2	0,4
Yb	1,7	1,3	1,2	1,3	2,0	2,0	1,9
Lu	0,2	0,1	0,2	0,0	0,1	0,1	0,4

Muestra	LC-342	LC-387	LC-513	LC-553	LC-554	LC-558	LC-271
%							
SiO_2	62,31	60,09	61,87	69,21	49,96	64,09	65,26
TiO2	0,58	1,09	0,54	0,54	0,87	0,49	0,49
Al_2O_3	11,18	16,12	12,93	12,78	13,75	13,13	10,79
Fe_2O_3	14,30	12,37	16,34	8,93	21,77	12,75	11,73
MnO	0,14	0,13	0,16	0,07	0,17	0,14	0,12
MgO	2,30	1,20	1,89	0,73	3,19	1,83	4,20
CaO	0,05	0,26	0,26	0,19	0,17	0,24	0,04
Na_2O	0,07	0,14	0,09	0,14	0,07	0,08	0,08
K_2O	2,58	3,65	1,67	3,10	1,57	2,77	1,86
P_2O_5	0,04	0,15	0,11	0,10	0,10	0,14	0,02
PPC	4,78	5,12	7,50	6,51	7,17	4,82	6,30
TOTAL	98,32	100,30	103,37	102,29	98,78	100,49	100,89
µg/g							
Ba	135,0	923,0	231,0	474,0	238,0	382,0	135,0
Rb	112,0	122,0	65,0	113,0	57,0	96,0	93,0
Sr	11,0	28,0	12,0	22,0	25,0	14,0	13,0
Y	11,0	10,0	14,0	11,0	12,0	9,0	9,0
Zr	113,0	130,0	149,0	148,0	121,0	135,0	113,0
Nb	*10,0*	*10,0*	*10,0*	*10,0*	*10,0*	*10,0*	*10,0*
Pb	14,0	*10,0*	91,0	206,0	292,0	82,0	129,0
Zn	98,0	106,0	466,0	740,0	624,0	503,0	173,0
Cu	*8,0*	*8,0*	*8,0*	8,0	34,0	77,0	13,0
Ni	*10,0*	*10,0*	*10,0*	*10,0*	*10,0*	16,0	31,0
V	69,0	174,0	70,0	81,0	151,0	62,0	96,0
Cr	97,0	79,0	27,0	48,0	100,0	34,0	135,0
Sc	11,0	13,0	4,0	5,0	17,0	6,0	15,0
Co	27,0	44,0	21,0	15,0	50,0	32,0	45,0
Be	*1,0*	*1,0*	*1,0*	*1,0*	*1,0*	1,0	*1,0*
W	*10,0*	*10,0*	*10,0*	10,0	*10,0*	*10,0*	*10,0*
Sn	19,0	13,0	17,0	34,0	59,0	23,0	1,0
Mo	*4,0*	*4,0*	*4,0*	*4,0*	*4,0*	*4,0*	4,0
Ag	*1,0*	*1,0*	*1,0*	*1,0*	*1,0*	*1,0*	*1,0*
Cd	*2,0*	*2,0*	*2,0*	*2,0*	*2,0*	*2,0*	*2,0*
As	19,0	11,0	10,0	27,0	37,0	13,0	14,0
Sb	*10,0*	*10,0*	*10,0*	*10,0*	*10,0*	*10,0*	*10,0*
La	7,7	13,7	19,4	15,6	12,7	23,0	19,0
Ce	19,6	37,0	39,5	31,0	30,8	42,0	58,4
Pr	2,5	4,8	5,1	4,1	4,0	6,3	7,8
Nd	7,9	15,6	16,5	12,1	12,5	25,3	25,2
Sm	2,1	4,0	4,3	2,8	2,7	5,4	5,9
Eu	0,3	0,6	0,7	0,4	1,0	2,4	2,5
Gd	2,0	3,4	3,5	2,5	2,4	4,9	5,4
Tb	0,4	0,6	0,5	0,2	0,4	0,8	0,8
Dy	2,4	3,5	3,1	2,1	2,4	4,3	4,9
Ho	0,5	0,7	0,7	0,4	0,5	0,9	1,0
Er	1,5	2,1	2,0	1,1	1,5	2,4	2,9
Tm	0,2	0,3	0,3	0,2	0,2	0,4	0,4
Yb	1,3	1,6	1,6	1,2	1,4	1,9	2,2
Lu	0,3	0,3	0,3	0,2	0,3	0,3	0,4

Muestra	LC-273	LC-301	LC-377	LC-389	LC-419	LC-450	LC-468
%							
SiO_2	62,74	52,18	59,66	55,67	62,28	54,77	54,44
TiO2	0,61	0,80	0,61	0,84	0,52	0,77	0,98
Al_2O_3	14,83	14,29	11,50	13,36	14,30	12,95	15,40
Fe_2O_3	8,71	10,58	17,49	19,45	14,60	20,43	13,56
MnO	0,14	0,43	0,09	0,12	0,13	0,20	0,26
MgO	5,25	5,68	1,76	2,07	1,85	2,91	3,85
CaO	0,03	0,28	0,02	0,17	0,21	0,04	0,22
Na_2O	0,14	0,36	0,18	0,09	0,08	0,07	0,12
K_2O	3,09	3,32	1,49	1,80	2,19	0,18	2,96
P_2O_5	0,03	0,09	0,03	0,12	0,15	0,05	0,11
PPC	3,67	7,65	8,10	7,39	4,13	4,09	4,22
TOTAL	99,23	95,66	100,93	101,09	100,46	96,44	96,12
µg/g							
Ba	1420,0	1075,0	306,0	237,0	1850,0	234,0	141,0
Rb	135,0	117,0	63,0	82,0	103,0	13,0	130,0
Sr	23,0	41,0	128,0	52,0	17,0	36,0	37,0
Y	15,0	13,0	9,0	11,0	15,0	11,0	14,0
Zr	138,0	131,0	92,0	129,0	164,0	114,0	145,0
Nb	*10,0*	*10,0*	*10,0*	*10,0*	*10,0*	*10,0*	*10,0*
Pb	76,0	113,0	12,0	21,0	41,0	15,0	19,0
Zn	222,0	1290,0	168,0	204,0	236,0	301,0	148,0
Cu	*8,0*	*8,0*	9,0	*8,0*	*8,0*	*8,0*	32,0
Ni	20,0	22,0	*10,0*	*10,0*	11,0	10,0	*10,0*
V	110,0	146,0	155,0	159,0	74,0	156,0	190,0
Cr	90,0	114,0	151,0	64,0	36,0	54,0	87,0
Sc	18,0	22,0	20,0	20,0	7,0	19,0	25,0
Co	16,0	27,0	36,0	50,0	21,0	36,0	16,0
Be	*1,0*	*1,0*	*1,0*	*1,0*	*1,0*	*1,0*	*1,0*
W	*10,0*	*10,0*	*10,0*	*10,0*	*10,0*	*10,0*	*10,0*
Sn	*1,0*	*1,0*	17,0	20,0	24,0	11,0	*1,0*
Mo	*2,0*	*2,0*	*2,0*	*2,0*	*2,0*	*2,0*	*2,0*
Ag	*1,0*	*1,0*	*1,0*	*1,0*	*1,0*	*1,0*	*1,0*
Cd	*2,0*	*2,0*	*2,0*	*2,0*	*2,0*	*2,0*	*2,0*
As	*10,0*	13,0	34,0	59,0	*10,0*	34,0	34,0
Sb	*10,0*	*10,0*	*10,0*	*10,0*	*10,0*	*10,0*	*10,0*
La	12,0	20,3	12,3	22,3	14,3	18,9	21,6
Ce	22,3	59,9	38,4	55,9	43,3	40,6	38,8
Pr	3,6	8,0	5,7	8,5	5,8	5,6	5,3
Nd	15,4	24,8	22,6	28,4	18,5	21,3	24,7
Sm	3,0	5,6	8,6	6,5	4,4	4,7	4,1
Eu	0,5	1,4	3,1	2,3	1,7	1,3	1,1
Gd	2,6	4,5	6,6	5,9	4,4	3,9	3,4
Tb	0,4	0,6	0,9	0,9	0,7	0,5	0,3
Dy	2,3	3,4	4,7	5,3	4,2	3,0	2,7
Ho	0,5	0,6	0,8	1,0	0,8	0,4	0,5
Er	1,4	1,8	2,1	3,1	2,3	1,0	1,5
Tm	0,2	0,3	0,3	0,5	0,3	0,2	0,2
Yb	1,3	1,5	1,6	2,6	1,9	1,6	1,8
Lu	0,3	0,3	0,3	0,4	0,3	0,0	0,1

Muestra	LC-508	LC-516	LC-557	LC-563	LC-609	LC-613	LC-619
%							
SiO_2	50,50	59,71	65,50	56,14	66,31	61,81	56,95
TiO2	0,79	0,53	0,48	0,82	0,55	0,66	1,04
Al_2O_3	11,85	13,46	13,31	16,26	12,82	13,80	18,14
Fe_2O_3	25,34	18,06	12,06	7,10	9,90	8,68	7,72
MnO	0,20	0,15	0,09	0,29	0,16	0,26	0,25
MgO	3,53	2,13	1,83	6,76	3,41	5,74	1,91
CaO	0,18	0,21	0,21	1,22	0,15	0,18	0,51
Na_2O	0,07	0,08	0,09	1,47	0,09	1,21	0,12
K_2O	0,13	1,45	2,35	2,07	2,55	2,27	6,11
P_2O_5	0,09	0,15	0,15	0,11	0,09	0,09	0,13
PPC	8,40	3,92	4,34	7,76	3,98	5,30	7,12
TOTAL	101,07	99,84	100,42	99,99	100,01	100,00	99,99
µg/g							
Ba	125,0	820,0	979,0	355,0	2050,0	336,0	184,0
Rb	10,0	65,0	103,0	94,0	117,0	110,0	132,0
Sr	13,0	13,0	18,0	68,0	20,0	49,0	30,0
Y	9,0	13,0	12,0	15,0	11,0	16,0	18,0
Zr	116,0	161,0	156,0	137,0	123,0	145,0	163,0
Nb	*10,0*	*10,0*	*10,0*	*10,0*	*10,0*	*10,0*	*10,0*
Pb	24,0	*10,0*	23,0	77,0	*10,0*	*10,0*	38,0
Zn	580,0	121,0	295,0	507,0	446,0	310,0	84,0
Cu	28,0	54,0	9,0	*8,0*	*8,0*	*8,0*	*8,0*
Ni	*10,0*	10,0	16,0	31,0	17,0	45,0	*10,0*
V	152,0	74,0	63,0	168,0	91,0	123,0	193,0
Cr	76,0	27,0	53,0	148,0	107,0	143,0	108,0
Sc	17,0	8,0	7,0	26,0	15,0	21,0	30,0
Co	33,0	20,0	32,0	22,0	25,0	27,0	21,0
Be	*1,0*	*1,0*	*1,0*	*1,0*	*1,0*	*1,0*	*1,0*
W	*10,0*	*10,0*	*10,0*	*10,0*	*10,0*	*10,0*	*10,0*
Sn	3,0	14,0	11,0	*1,0*	*1,0*	*1,0*	*1,0*
Mo	*2,0*	*2,0*	*2,0*	*2,0*	*2,0*	*2,0*	*2,0*
Ag	*1,0*	*1,0*	*1,0*	*1,0*	*1,0*	*1,0*	*1,0*
Cd	*2,0*	*2,0*	*2,0*	*2,0*	*2,0*	*2,0*	*2,0*
As	36,0	*10,0*	24,0	16,0	*10,0*	*10,0*	105,0
Sb	*10,0*	*10,0*	*10,0*	*10,0*	*10,0*	*10,0*	26,0
La	13,2	30,1	20,0	16,9	11,0	16,7	23,9
Ce	26,9	60,8	55,0	30,6	23,6	30,0	31,7
Pr	3,8	7,8	7,4	3,3	2,5	3,3	3,8
Nd	15,7	21,6	24,4	17,9	12,7	18,9	22,0
Sm	3,3	5,6	5,7	3,5	2,4	3,7	4,4
Eu	1,3	2,2	1,4	0,9	0,5	0,8	1,3
Gd	2,7	5,0	4,7	3,6	2,2	3,4	4,2
Tb	0,4	0,6	0,6	0,4	0,2	0,4	0,5
Dy	2,0	4,4	3,4	3,5	2,0	3,2	4,1
Ho	0,2	0,9	0,7	0,7	0,4	0,6	0,8
Er	0,7	2,4	1,9	2,1	1,3	1,9	2,5
Tm	0,1	0,4	0,3	0,3	0,2	0,3	0,4
Yb	1,0	2,0	1,5	2,4	1,6	2,1	2,7
Lu	0,0	0,3	0,2	0,2	0,1	0,2	0,3

Apéndice I-II

Composición de las pizarras

Tabla I.II.1 Composición química de las pizarras (Capítulo III). (Cursiva: menor del límite de detección)

Cod. Lab	03/295-70	03/295-71	03/295-72	03/295-73	03/295-74	03/295-75	03/295-60
Muestra	AZ-014	AZ-025	AZ-038	AZ-039	AZ-040	AZ-041	AZ-042
%							
SiO_2	60,23	35,32	57,11	55,66	78,82	27,23	85,20
TiO_2	0,92	0,46	0,92	1,05	0,31	0,57	0,18
Al_2O_3	20,52	8,83	18,00	20,06	6,39	10,64	3,72
Fe_2O_3	3,86	9,88	8,76	7,24	5,25	11,88	6,44
MnO	0,03	0,93	0,07	0,08	0,09	1,09	0,03
MgO	1,47	10,61	2,88	1,90	0,72	10,62	*0,01*
CaO	0,22	12,90	0,52	1,18	1,66	14,90	0,05
Na_2O	0,22	0,08	0,12	0,22	0,07	0,12	0,07
K_2O	7,14	1,43	5,60	6,52	2,41	1,97	1,05
P_2O_5	0,10	0,06	0,06	0,09	0,02	0,18	0,00
H_2O	5,30	19,50	5,97	6,01	4,27	20,74	3,26
Total	100,00	99,99	100,00	100,01	100,00	99,94	100,01
C%	1,54	5,67	1,18	1,52	0,85	6,27	0,32
C_{org}%	1,5	0,91	1,09	1,34	0,48	1,37	0,3
S%	0,71	2,58	1,52	1,35	3,4	3,5	3,59
Ba	3030	196	1350	1490	504	282	96
Rb	207	46	147	189	77	65	46
Sr	55	116	16	33	13	134	6
Y	13	25	11	15	11	32	3
Zr	155	87	169	185	68	101	37
Nb	15	*10*	*10*	13	*10*	*10*	*10*
Pb	277	367	570	1061	2550	375	296
Zn	72	149	623	805	2170	124	973
Cu	123	20	58	202	249	29	204
Ni	31	34	47	46	27	38	16
V	194	105	180	208	60	126	41
Cr	133	81	131	138	96	95	61
Sc	16	9	13	16	6	8	3
Co	10	7	15	14	7	8	7
Be	4	*1*	3	3	*1*	2	*1*
W	*5*	*5*	*5*	*5*	*5*	*5*	*5*
Sn	*5*	*5*	*5*	8	*5*	*5*	*5*
Mo	*4*	*4*	*4*	*4*	5	*4*	*4*
Ag	*1*	*1*	2	*1*	4	2	2
Cd	*2*	*2*	*2*	*2*	5	*2*	*2*
P	38	*20*	41	78	59	46	5680
As	36	27	51	65	64	32	83
Bi	1	3	2	2	4	4	4
Br	32	27	27	28	7	26	10
La	49	35	41	41	6	33	11
Ce	49	35	41	41	6	33	11

Cod. Lab	03/295-77	03/295-78	03/295-79	03/295-80	03/295-81	03/295-82	03/295-83
Muestra	AZ-096	AZ-131	AZ-132	AZ-133	AZ-134	AZ-135	AZ-136
%							
SiO_2	62,30	71,73	60,00	60,23	35,32	57,11	55,66
TiO_2	0,76	0,47	0,84	0,92	0,46	0,92	1,05
Al_2O_3	16,73	12,06	16,32	20,52	8,83	18,00	20,06
Fe_2O_3	4,04	4,88	8,18	3,86	9,88	8,76	7,24
MnO	0,03	0,05	0,02	0,03	0,93	0,07	0,08
MgO	0,31	1,66	0,62	1,47	10,61	2,88	1,90
CaO	0,14	1,17	0,18	0,22	12,90	0,52	1,18
Na_2O	0,30	0,08	0,19	0,22	0,08	0,12	0,22
K_2O	5,34	4,03	6,18	7,14	1,43	5,60	6,52
P_2O_5	0,24	0,03	0,06	0,10	0,06	0,06	0,09
H_2O	9,83	3,83	7,41	5,30	19,50	5,97	6,01
Total	100,00	100,00	100,00	100,00	99,99	100,00	100,01
C%	1,11	0,73	1,01	1,54	5,67	1,18	1,52
C_{org}%	1,09	0,54	0,98	1,5	0,91	1,09	1,34
S%	3,13	1,05	5,38	0,71	2,58	1,52	1,35
Ba	1005	558	1013	3030	196	1350	1490
Rb	183	118	190	207	46	147	189
Sr	192	16	22	55	116	16	33
Y	10	13	13	13	25	11	15
Zr	135	90	149	155	87	169	185
Nb	*10*	*10*	11	15	*10*	*10*	13
Pb	455	101	806	277	367	570	1061
Zn	1253	50	390	72	149	623	805
Cu	257	31	137	123	20	58	202
Ni	25	23	56	31	34	47	46
V	190	99	180	194	105	180	208
Cr	114	88	142	133	81	131	138
Sc	14	10	14	16	9	13	16
Co	8	8	14	10	7	15	14
Be	4	*1*	3	4	*1*	3	3
W	*5*	*5*	9	*5*	*5*	*5*	*5*
Sn	*5*	*5*	*5*	*5*	*5*	*5*	8
Mo	5	*4*	*4*	*4*	*4*	*4*	*4*
Ag	2	*1*	10	*1*	*1*	2	*1*
Cd	15	*2*	*2*	*2*	*2*	*2*	*2*
P	273	*20*	123	38	*20*	41	78
As	124	22	75	36	27	51	65
Bi	3	1	6	1	3	2	2
Br	36	27	33	32	27	27	28
La	68	42	44	49	35	41	41
Ce	68	42	44	49	35	41	41

Cod. Lab	03/295-84	03/295-85	03/295-86	03/295-87	-	03/295-88	03/295-89
Muestra	AZ-137	AZ-138	AZ-140	AZ-170	AZ-171	AZ-172	AZ-173
%							
SiO_2	78,82	27,23	85,20	67,54	57,86	72,92	71,66
TiO_2	0,31	0,57	0,18	0,71	0,97	0,73	0,73
Al_2O_3	6,39	10,64	3,72	14,45	18,92	14,58	14,59
Fe_2O_3	5,25	11,88	6,44	4,87	5,38	1,93	1,88
MnO	0,09	1,09	0,03	0,06	0,08	0,02	0,02
MgO	0,72	10,62	*0,01*	1,02	1,47	0,54	0,60
CaO	1,66	14,90	0,05	0,44	0,90	0,20	0,24
Na_2O	0,07	0,12	0,07	0,82	0,96	0,11	0,11
K_2O	2,41	1,97	1,05	4,14	6,29	4,77	4,96
P_2O_5	0,02	0,18	0,00	0,06	0,07	0,05	0,06
H_2O	4,27	20,74	3,26	5,90	7,11	4,15	5,17
Total	100,00	99,94	100,01	100,00	100,01	100,00	100,01
C%	0,85	6,27	0,32	1,76	-	1,02	1,05
C_{org}%	0,48	1,37	0,3	1,57	-	0,73	0,21
S%	3,4	3,5	3,59	0,41	-	0,19	0,24
Ba	504	282	96	396	549	592	597
Rb	77	65	46	159	215	186	189
Sr	13	134	6	76	88	100	102
Y	11	32	3	13	12	13	12
Zr	68	101	37	135	169	123	128
Nb	*10*	*10*	*10*	12	14	14	13
Pb	2550	375	296	50	36	111	118
Zn	2170	124	973	24	24	14	19
Cu	249	29	204	43	58	31	42
Ni	27	38	16	53	53	37	44
V	60	126	41	126	163	139	139
Cr	96	95	61	122	113	85	80
Sc	6	8	3	11	14	14	11
Co	7	8	7	14	15	22	25
Be	*1*	2	*1*	3	3	3	3
W	*5*	*5*	*5*	8	*5*	*5*	5
Sn	*5*	*5*	*5*	*5*	*5*	*5*	*5*
Mo	5	*4*	*4*	*4*	*4*	*4*	*4*
Ag	4	2	2	*1*	*1*	*1*	*1*
Cd	5	*2*	*2*	*2*	*2*	*2*	*2*
P	59	46	5680	52	51	56	62
As	64	32	83	29	23	49	71
Bi	4	4	4	1	0	0	0
Br	7	26	10	36	44	30	29
La	6	33	11	60	76	57	54
Ce	6	33	11	60	76	57	54

Cod. Lab	03/295-90	03/295-91	03/295-92	03/295-93	03/295-94	03/295-95	03/295-96
Muestra	AZ-174	AZ-175	LC-258	LC-259	LC-260	LC-261	LC-262
%							
SiO_2	77,97	69,81	68,60	65,84	64,42	61,27	61,40
TiO_2	0,57	0,72	1,17	1,17	1,04	0,92	1,00
Al_2O_3	12,04	13,99	18,48	18,91	18,53	16,43	17,58
Fe_2O_3	1,20	4,16	2,04	3,27	3,95	8,80	8,13
MnO	0,01	0,04	0,01	0,03	0,31	0,07	0,13
MgO	0,28	0,88	0,28	0,52	0,52	0,22	0,97
CaO	0,34	0,21	0,22	0,14	0,28	0,21	0,29
Na_2O	0,65	0,43	0,24	0,24	0,23	0,19	0,27
K_2O	3,32	4,65	5,54	5,46	5,22	5,02	4,43
P_2O_5	0,21	0,05	0,12	0,09	0,10	0,05	0,12
H_2O	3,42	5,04	3,31	4,33	5,31	6,82	5,68
Total	100,00	100,00	100,01	100,00	99,89	100,00	100,00
C%	0,78	1,42	0,72	0,76	0,79	0,94	1,18
C_{org}%	0,73	1,38	0,67	0,65	0,61	0,89	1,13
S%	0,3	0,09	0,57	0,29	1,25	4,55	0,86
Ba	346	563	1921	2246	5100	335	2470
Rb	134	178	185	183	184	148	137
Sr	126	43	115	137	101	123	93
Y	11	10	15	14	13	14	14
Zr	105	137	280	252	230	165	200
Nb	*10*	13	18	16	15	*10*	15
Pb	114	33	18	37	26	223	68
Zn	*10*	16	65	165	175	981	202
Cu	22	36	12	15	15	592	32
Ni	16	48	33	35	36	34	39
V	113	127	146	148	144	130	141
Cr	75	76	106	99	96	107	99
Sc	10	12	15	16	16	14	15
Co	9	18	13	15	15	43	16
Be	*1*	*1*	3	4	3	3	3
W	5	*5*	*5*	6	*5*	*5*	*5*
Sn	*5*	*5*	*5*	*5*	*5*	19	*5*
Mo	*4*	*4*	*4*	*4*	*4*	*4*	*4*
Ag	*1*	*1*	*1*	*1*	*1*	2	*1*
Cd	*2*	*2*	*2*	*2*	*2*	*2*	*2*
P	49	36	569	476	482	328	619
As	28	24	*20*	*20*	67	157	25
Bi	0	0	-	-	-	-	-
Br	26	35	-	-	-	-	-
La	43	63	46	45	44	31	44
Ce	43	63	90	89	85	65	85

Cod. Lab	03/295-97	03/295-98	03/295-99	03/295-100	-	-	-
Muestra	LC-264	LC-276	LC-282	LC-283	LC-284	LC-285	LC-321
%							
SiO_2	52,53	64,81	62,62	64,62	63,75	58,27	58,55
TiO_2	0,92	1,07	1,08	1,07	1,04	0,97	1,22
Al_2O_3	16,66	17,96	18,46	17,76	19,14	17,23	27,29
Fe_2O_3	9,03	4,34	6,00	5,29	3,35	7,81	0,61
MnO	0,11	0,10	0,09	0,10	0,02	0,05	*0,00*
MgO	0,72	0,62	1,76	1,46	0,64	1,65	0,36
CaO	0,20	0,30	0,28	0,36	0,29	0,43	0,10
Na_2O	0,34	0,24	0,39	0,38	0,43	0,40	0,19
K_2O	4,33	5,37	4,06	4,15	4,47	3,59	4,59
P_2O_5	0,16	0,09	0,10	0,09	0,12	0,14	0,20
H_2O	9,54	5,10	5,16	4,72	6,74	9,47	5,72
Total	94,54	100,00	100,00	99,99	100,00	100,01	98,85
C%	1,87	1,09	0,92	0,89	1,47	2,4	1,080
C_{org}%	1,83	1,03	0,87	0,84	1,43	2,33	0,970
S%	3,67	0,71	0,27	0,18	0,48	0,34	1,870
Ba	6390	1990	556	539	656	420	1377
Rb	143	195	131	126	143	121	167
Sr	151	70	90	84	107	73	459
Y	13	13	11	12	15	13	15
Zr	192	251	227	252	198	200	304
Nb	13	15	15	15	16	12	19
Pb	5110	39	11	12	22	22	41
Zn	33400	170	203	156	170	227	114
Cu	176	15	*8*	31	29	19	20
Ni	49	38	37	39	31	38	29
V	130	142	149	145	157	139	179
Cr	87	97	102	105	102	89	110
Sc	13	15	15	15	16	14	16
Co	18	14	14	13	13	13	18
Be	4	4	3	3	4	3	2
W	*5*	8	*5*	*5*	*5*	*5*	*10*
Sn	224	*5*	*5*	*5*	*5*	*5*	*10*
Mo	9	*4*	*4*	*4*	*4*	*4*	*4*
Ag	4	*1*	*1*	*1*	*1*	*1*	*1*
Cd	69	*2*	*2*	*2*	*2*	*2*	4
P	698	464	469	478	572	642	809
As	272	22	*20*	*20*	*20*	*20*	*1*
Bi	-	-	-	-	-	-	-
Br	-	-	-	-	-	-	-
La	37	41	38	32	46	37	53
Ce	73	80	77	68	87	73	114

Cod. Lab	-	-	-	-	-	-	-
Muestra	LC-333	LC-353	LC-355	LC-406	LC-438	LC-439	LC-440
%							
SiO_2	66,27	67,26	59,97	64,91	64,44	65,43	64,69
TiO_2	1,13	1,07	1,10	1,17	1,08	1,00	0,95
Al_2O_3	20,46	20,65	20,36	21,18	21,54	21,95	19,78
Fe_2O_3	0,87	0,70	4,20	1,37	0,96	0,65	1,59
MnO	0,00	0,00	0,03	0,03	0,00	0,00	0,00
MgO	0,17	0,09	0,61	0,48	0,20	0,19	0,65
CaO	0,10	0,12	0,15	0,25	0,08	0,07	0,07
Na_2O	0,26	0,22	0,30	0,27	0,30	0,28	0,18
K_2O	5,06	4,08	5,70	5,62	5,35	4,57	6,25
P_2O_5	0,11	0,15	0,15	0,10	0,10	0,09	0,04
H_2O	5,52	8,02	4,88	5,80	5,78	5,95	4,62
Total	99,96	102,37	97,45	101,17	99,82	100,17	98,82
C%	0,750	0,920	0,820	0,720	1,000	0,880	0,730
C_{org}%	0,740	0,900	0,730	0,710	0,960	0,880	0,700
S%	0,450	0,720	0,300	0,340	0,310	0,500	0,340
Ba	1015	1096	1970	936	1360	1247	831
Rb	181	149	169	204	175	157	226
Sr	117	115	161	104	173	204	120
Y	18	16	23	14	10	10	13
Zr	237	278	177	261	211	216	182
Nb	20	16	18	19	18	16	16
Pb	103	159	2130	11	366	417	145
Zn	208	233	9040	92	887	1255	64
Cu	15	16	604	19	11	10	47
Ni	35	28	27	22	26	17	29
V	165	138	189	178	164	136	160
Cr	95	86	102	104	95	81	90
Sc	19	16	15	19	18	15	15
Co	15	14	26	14	16	12	16
Be	2	3	5	3	3	2	3
W	*10*	*10*	-	*10*	*10*	*10*	*10*
Sn	*10*	*10*	48	*10*	*10*	*10*	*10*
Mo	*4*	*4*	*4*	*4*	*4*	*4*	*4*
Ag	*1*	*1*	5	*1*	*1*	*1*	*1*
Cd	*2*	*2*	11	*2*	4	*2*	41
P	577	733	802	467	510	385	245
As	*1*	*1*	5	*1*	*1*	*1*	*1*
Bi	-	-	-	-	-	-	-
Br	-	-	-	-	-	-	-
La	50	53	42	47	22	17	29
Ce	122	113	86	96	38	29	57

Cod. Lab	-	-	-	-
Muestra	LC-441	LC-442	LC-443	LC-464
%				
SiO_2	67,52	59,57	65,23	67,13
TiO_2	1,08	1,04	1,12	1,05
Al_2O_3	19,36	20,18	21,61	20,46
Fe_2O_3	1,63	5,94	0,87	0,72
MnO	0,01	0,00	0,01	*0,00*
MgO	0,33	0,30	0,22	0,11
CaO	0,10	0,08	0,11	0,10
Na_2O	0,34	0,23	0,23	0,23
K_2O	4,68	4,56	4,96	4,33
P_2O_5	0,08	0,08	0,13	0,12
H_2O	6,74	5,66	5,56	6,88
Total	101,86	97,65	100,04	101,12
C%	0,710	0,790	0,780	0,830
C_{org}%	0,630	0,700	0,660	0,740
S%	0,300	0,350	0,340	4,310
Ba	3434	557	1711	826
Rb	162	152	174	155
Sr	94	167	128	121
Y	16	9	12	16
Zr	251	154	272	263
Nb	17	16	17	17
Pb	106	70	347	310
Zn	423	59	1085	577
Cu	28	73	26	23
Ni	29	29	25	30
V	136	151	154	139
Cr	82	85	91	85
Sc	15	15	17	16
Co	13	28	13	19
Be	3	4	2	2
W	*10*	*10*	*10*	*10*
Sn	*10*	11	*10*	*10*
Mo	*4*	*4*	*4*	*4*
Ag	*1*	*1*	*1*	*1*
Cd	*2*	*2*	*2*	5
P	358	361	603	552
As	*1*	*1*	*1*	*1*
Bi	-	-	-	-
Br	-	-	-	-
La	37	34	42	44
Ce	82	74	86	96

Apéndice II

Elementos traza de pirita

Tabla II.1. Contenido de elementos traza en pirita del *"Nivel Superior"*

Nivel superior

Muestra	TH-3-4	TH-3-3	TH-3-2	TH-3-5-1
Ti^{47}	4,797	6,130	7,014	6,765
V^{51}	0,187	0,230	0,924	0,043
Mn^{55}	39,138	26,254	20,970	4,356
Fe^{57}	461000	461000	461000	461000
Co^{59}	58,931	95,559	2,166	42,007
Ni^{60}	0,617	0,924	0,423	0,728
Cu^{65}	1447,322	337,689	160,166	1047,023
Zn^{66}	87,076	19,395	227,278	29,480
As^{75}	485,230	474,720	1003,026	104,972
Zr^{90}	0,010	0,007	0,011	0,002
Mo^{95}	0,227	0,288	1,871	1,000
Ag^{107}	9,651	11,398	6,081	35,587
Cd^{111}	0,295	*<LD*	0,456	0,484
Sn^{118}	23,762	22,151	0,483	6,600
Sb^{121}	192,081	188,293	314,966	182,629
La^{139}	0,002	0,002	0,010	0,001
Au^{197}	0,471	0,542	0,758	0,591
Tl^{205}	5,465	3,857	512,170	72,364
Pb^{208}	2273,407	1682,974	2080,478	13744,238
Bi^{209}	63,881	86,326	45,691	179,463

<LD: menor del límite de detección

Tabla II.2. Contenido de elementos traza en pirita del *"Sulfuros de grano fino".*

Sulfuros masivos de grano fino							
Muestra	TH-74-2	TH-74-1	TH-74-4	TH-74-3	TH-73-1	TH-73-3	TH-73-2
Ti^{47}	6,349	7,601	8,170	9,638	6,232	9,057	12,683
V^{51}	0,023	0,020	0,013	0,039	0,023	0,416	0,480
Mn^{55}	4,277	4,326	10,943	14,661	5,606	4,554	5,236
Fe^{57}	461000	461000	461000	461000	461000	461000	461000
Co^{59}	52,972	69,217	42,150	124,244	0,205	0,740	0,719
Ni^{60}	9,390	10,807	5,499	17,189	0,260	1,830	1,523
Cu^{65}	84,827	63,005	2293,628	1123,456	2647,004	55,131	85,594
Zn^{66}	1,378	1,912	13,030	118,565	4644,860	437,909	629,555
As^{75}	16,375	6,484	39,904	435,202	45,591	497,080	459,938
Zr^{90}	*<LD*	*<LD*	*<LD*	0,005	*<LD*	*<LD*	*<LD*
Mo^{95}	0,182	*<LD*	0,176	0,138	*<LD*	0,336	0,413
Ag^{107}	0,486	0,061	6,411	78,578	116,030	6,169	5,186
Cd^{111}	0,313	0,326	*<LD*	0,925	10,139	1,132	1,602
Sn^{118}	0,241	0,171	5,563	11,376	94,606	2,293	14,088
Sb^{121}	12,854	1,770	56,537	213,275	192,429	1975,626	1250,450
La^{139}	*<LD*	*<LD*	0,006	0,021	0,001	0,001	0,001
Au^{197}	0,905	*0,005*	1,093	6,312	0,289	3,350	2,570
Tl^{205}	0,016	0,012	0,130	0,885	106,956	98,954	70,665
Pb^{208}	69,739	4,088	2111,622	7274,437	12846,313	5980,720	2268,463
Bi^{209}	32,521	0,460	106,877	1453,084	186,950	6,891	5,534

<LD: menor del límite de detección

Sulfuros masivos de grano fino

Muestra	FP-EL-298-3	FP-EL-298-2	FP-EL-298-1
Ti^{47}	7,926	7,972	8,557
V^{51}	0,938	0,449	0,261
Mn^{55}	160,293	10,406	16,387
Fe^{57}	461000	461000	461000
Co^{59}	110,778	158,833	56,969
Ni^{60}	1,730	0,559	0,319
Cu^{65}	911,109	1981,130	1461,819
Zn^{66}	64,283	43,335	90,583
As^{75}	863,684	2258,271	605,467
Zr^{90}	0,009	0,005	*<LD*
Mo^{95}	0,472	0,539	0,731
Ag^{107}	3,495	4,978	3,662
Cd^{111}	*<LD*	0,754	0,880
Sn^{118}	5,147	7,835	8,320
Sb^{121}	289,745	367,321	300,435
La^{139}	0,005	0,001	0,001
Au^{197}	0,281	0,359	0,252
Tl^{205}	0,808	0,908	0,818
Pb^{208}	725,311	1262,676	1673,651
Bi^{209}	34,583	46,582	37,671

<LD: menor del límite de detección

Tabla II.3. Contenido de elementos traza en pirita del *"brecha".*

Brecha o conglomerado				
Muestra	TH-44-1	TH-44-2	TH-44-4	TH-44-3
Ti^{47}	7,480	8,402	9,680	8,737
V^{51}	0,017	0,907	4,852	0,714
Mn^{55}	4,403	829,844	423,780	190,365
Fe^{57}	461000	461000	461000	461000
Co^{59}	434,173	258,748	734,285	157,372
Ni^{60}	1,659	1,301	3,134	2,128
Cu^{65}	1,633	2873,193	6570,510	3443,293
Zn^{66}	1,053	942,588	1441,706	1022,931
As^{75}	278,976	221,932	4811,515	422,557
Zr^{90}	*<LD*	0,009	0,017	0,006
Mo^{95}	0,104	0,501	0,339	0,329
Ag^{107}	0,058	10,025	16,526	13,276
Cd^{111}	0,170	2,013	2,732	2,417
Sn^{118}	0,169	8,290	10,088	5,328
Sb^{121}	3,123	225,543	308,648	300,808
La^{139}	*<LD*	0,048	0,011	0,010
Au^{197}	0,019	3,492	6,452	3,883
Tl^{205}	0,007	0,277	0,335	0,754
Pb^{208}	6,858	4033,027	1094,337	4409,405
Bi^{209}	0,213	99,396	158,120	108,799

<LD: menor del límite de detección

Tabla II.4. Contenido de elementos traza en pirita del *"carbonatado".*

Mineralización carbonatada

Muestra	TH-40-1	TH-40-2	TH-40-3	TH-77-1	TH-77-2	TH-77-3	TH-77-4
Ti^{47}	7,493	8,670	8,073	6,631	7,888	7,851	7,992
V^{51}	0,207	1,159	1,929	0,096	0,065	0,025	0,221
Mn^{55}	220,144	104,428	301,936	4,480	27,675	4,597	96,499
Fe^{57}	461000	461000	461000	461000	461000	461000	461000
Co^{59}	20,983	3,280	35,259	72,377	14,525	260,523	11,716
Ni^{60}	0,532	1,083	2,362	0,780	3,548	0,883	2,225
Cu^{65}	236,959	192,921	611,818	1799,634	4279,705	1472,746	4888,793
Zn^{66}	834,784	377,627	6677,570	14,710	161,011	7,235	110,481
As^{75}	407,117	413,594	3131,010	452,198	1222,207	380,640	881,382
Zr^{90}	0,060	1,430	0,133	*<LD*	0,004	*<LD*	0,003
Mo^{95}	*<DL*	*<DL*	3,261	0,318	0,806	0,294	0,998
Ag^{107}	3,943	113,544	13,750	5,355	29,948	5,503	32,854
Cd^{111}	1,627	1,148	12,179	*<LD*	0,817	*<LD*	0,475
Sn^{118}	74,411	14,330	104,470	13,288	134,208	20,236	53,892
Sb^{121}	71,542	158,313	413,235	300,402	458,451	450,092	692,267
La^{139}	0,003	0,003	0,021	*<LD*	*<LD*	0,004	0,005
Au^{197}	0,653	0,743	8,160	2,112	4,299	2,149	5,247
Tl^{205}	0,660	4,814	376,800	13,372	2,964	9,788	5,689
Pb^{208}	710,496	25215,543	3431,986	403,985	686,756	133,855	2504,032
Bi^{209}	21,795	282,530	41,491	36,175	50,503	28,267	87,355

<LD: menor del límite de detección

Mineralización carbonatada

Muestra	FT-EL-258-5	FT-EL-258-1	FT-EL-258-4	FT-EL-258-2	FT-EL-258-3	TH-47-2
Ti^{47}	7,519	10,181	9,767	8,964	8,683	43,700
V^{51}	2,905	6,321	4,610	2,441	1,388	11,917
Mn^{55}	548,426	424,119	62,993	518,536	342,585	1348,395
Fe^{57}	461000	461000	461000	461000	461000	461000
Co^{59}	116,483	72,784	57,703	207,095	102,087	240,896
Ni^{60}	12,010	40,162	12,918	9,466	10,655	4,433
Cu^{65}	2422,133	1938,689	603,225	858,173	2522,909	1048,349
Zn^{66}	18297,016	8874,519	61,067	3824,379	1089,397	8883,625
As^{75}	411,316	426,980	510,566	438,846	277,363	768,654
Zr^{90}	0,001	0,005	0,004	0,009	*<DL*	0,179
Mo^{95}	0,621	19,193	1,980	0,302	0,222	0,280
Ag^{107}	7,484	14,237	7,646	14,633	4,776	13,368
Cd^{111}	39,313	24,685	0,377	6,928	2,067	17,623
Sn^{118}	16,580	24,681	1,791	7,980	3,729	33,880
Sb^{121}	192,481	753,283	540,657	438,383	334,754	199,067
La^{139}	0,005	0,009	0,004	0,020	0,014	0,041
Au^{197}	0,250	0,751	0,556	0,542	0,322	3,021
Tl^{205}	0,431	1,131	0,551	0,716	0,327	1,873
Pb^{208}	1300,669	2348,887	1127,516	1606,537	1772,152	3832,536
Bi^{209}	24,964	48,466	24,971	45,378	19,359	52,868

<LD: menor del límite de detección

Tabla II.5. Contenido de elementos traza en pirita del *"stockwork".*

Stockwork							
Muestra	TH-76-3	TH-76-2	TH-76-1	FP-FT-343-1	FP-FT-343-2	FP-FT-343-4	FP-FT-343-3
Ti^{47}	5,186	6,365	7,574	173,171	9,784	10,346	10,027
V^{51}	0,285	0,578	0,426	35,404	0,014	0,149	0,044
Mn^{55}	8,088	13,528	17,706	423,767	2,063	4,099	2,462
Fe^{57}	461000	461000	461000	461000	461000	461000	461000
Co^{59}	18,240	33,605	8,423	243,514	26,996	337,107	180,009
Ni^{60}	1,279	0,721	1,397	83,738	86,815	43,972	25,196
Cu^{65}	1620,114	2142,979	1644,713	225,620	362,030	406,195	185,697
Zn^{66}	138,349	698,484	119,980	19,682	3,465	7,560	7,846
As^{75}	1656,551	4732,271	1707,004	2180,920	1990,723	1683,870	3781,258
Zr^{90}	0,003	0,002	0,007	3,408	*<LD*	*<LD*	*<DD*
Mo^{95}	0,213	1,202	0,147	0,137	0,204	0,206	0,132
Ag^{107}	7,783	6,788	6,231	7,343	0,326	3,745	2,277
Cd^{111}	0,421	1,027	0,454	0,197	*<LD*	0,204	*<LD*
Sn^{118}	48,051	36,121	6,668	3,484	0,240	0,777	0,388
Sb^{121}	263,586	261,394	234,968	179,436	5,288	111,430	71,196
La^{139}	*<LD*	*<LD*	0,003	2,554	*<LD*	*<LD*	*<LD*
Au^{197}	2,906	1,420	2,048	8,043	1,245	4,210	4,577
Tl^{205}	175,552	17,569	165,419	2,783	0,043	0,153	0,293
Pb^{208}	5351,570	1244,194	2200,959	218,265	5,414	77,340	51,793
Bi^{209}	34,580	25,896	26,105	257,263	6,772	158,880	82,933

<LD: menor del límite de detección

Apéndice III

Referencia de las publicaciones del autor de la tesis

Publicaciones

Tornos, F., Peter, J.M., Allen, R., **Conde, C**., 2015. Controls on the sitting and style of volcanogenic massive sulphide deposits. Ore Geology Reviews 68, 142-163.

Tornos, F., Solomon, M., **Conde, C**., Spiro, B.F., 2008. Formation of the Tharsis massive sulfide deposit, Iberian Pyrite Belt: geological, lithogeochemical, and stable isotope evidence for deposition in a brine pool. Economic Geology 103, 185-214.

Mellado, D., González Clavijo, E., Tornos, F., **Conde. C**., 2006. Geología y estructura de la Mina de Río Tinto (Faja Pirítica Ibérica, España). Geogaceta 40, 231-234.

Tornos, F., **Conde, C**., 2002. La influencia biogénica en la formación de los yacimientos de sulfuros masivos de la Faja Pirítica Ibérica. Geogaceta 32, 235-238.

Comunicaciones y poster

Tornos, F., **Conde, C**., Chiaradia, M., Velasco, F., 2015. Evolving subduction-related basins control de formation of VMS deposits in the Iberian Pyrite Belt.

Conde, C., Tornos F., 2014. Volcanic stratigraphy and geochemistry of the VS complex in the northern Iberian Pyrite Belt. Macla 19.

Conde, C., Tornos, F., Large, R., Danyushevsky, L.V., Solomon, M., 2009 Laser Ablation-ICPMS Analysis of Trace Elements in Pyrite from the Tharsis Massive Sulphide Deposit. Biennial SGA Meeting, Townsville 2009. Australia.

Conde, C., Lentz, D., Walker, J., Tornos, F., 2008. Petrology and geochemistry of the Cu-rich zone at the Brunswick No.6 Zn-Pb-Cu-Ag VMS deposit, Bathurst Mining Camp, New Brunswick (Canada). 33 International Geological Congress, Oslo 2008. Norway.

Conde, C., Tornos F., 2007. Using the geochemistry of volcanic rocks for understanding VMS deposits, Northern Iberian Pyrite Belt .Meeting of the IGCP Project 502,Tokio (Japón), November 2007.

Conde, C., Tornos, F., Doyle, M., 2007. Geology and lithogeochemistry of the unique Las Cruces VMS deposit, Iberian Pyrite Belt. Biennial SGA Meeting, Dublin 2007. Ireland.

Conde, C., Tornos, F., Mellado, D., González Clavijo, E., Martín Rubí, J.A., 2007. Lithogeochemistry of the volcanic sequence hosting the Río Tinto ore deposit (Iberian Pyrite Belt, Spain). 3rd International Applied Geochemistry Symposium (IAGS), Oviedo, España. pp. 187.

Conde, C., Tornos, F., Matthäi, S.K., Geiger, S., 2006. Modelización del transporte de calor y fluido en los sulfuros masivos encajados en pizarras de la Faja Pirítica Ibérica, España. SEM-SEA 2006, Oviedo, España. Macla 6, 137-139.

Tornos, F., **Conde, C**., 2006. Estilos de sulfuros masivos volcanogénicos: Donde y porqué se forman las mineralizaciones en fondos marinos. XIII Congreso Peruano de Geología, 17-20 Oct, Lima, Peru.

Tornos, F., **Conde, C**., Velasco, F., 2005. Are magmatic fluids necessary to form the giant massive sulphide deposits of the Iberian Pyrite Belt? GAC-MAC-CSPG-CSSS, Halifax 2005, Canada. Abstracts Volume pp. 195.

Conde, C., Matthäi, S.K., Geiger, S., Tornos, F., Herrington, R., 2005. Heat and fluid modeling of the shale-hosted massive sulphides in the Iberian Pyrite Belt, Spain. GAC-MAC-CSPG-CSSS, Halifax 2005, Canada. Abstracts Volume pp. 31.

Crespo, J.L., Rodriguez, P., Moro, M.C., Cabrera, R., **Conde, C.,** Fernandez, A., Rodriguez, I., 2000. El yacimiento de scheelita de Los Santos (Salamanca). Geotemas 1, 25-28.

La influencia biogénica en la formación de los yacimientos de sulfuros masivos de la Faja Pirítica Ibérica

The biogenic influence in the formation of massive sulphide deposits of the Iberian Pyrite Belt

F. Tornos [1] y C.Conde [1]

[1] Instituto Geológico y Minero de España. C/Azafranal, 48-50. 37002 Salamanca. E-mail: f.tornos@igme.es

ABSTRACT

The Tharsis supergiant massive sulphide deposits shows evidence of being formed by exhalative processes on the seafloor. The carbonate-siderite ore is interpreted as a bacterial mound while the bulk of the orebody seems to be formed in a brine pool by mixing of sulphur-depleted deep brines with H_2S generated by hyperthermophile (archeo-)bacteria in the chemoclyne. This mechanism is significantly slower but geochemically much more effective that mound accretion on the seafloor and is interpreted as being the reason of the presence of supergiant massive sulphide deposits in the Iberian Pyrite Belt.

Key words: *Massive sulphides, Iberian Pyrite Belt, termophile bacteria*

Geogaceta, 32 (2002), 235-238
ISSN:0213683X

Introducción

Uno de los aspectos más relevantes en los sistemas hidrotermales submarinos actuales es la presencia de una cadena trófica relacionada con el calor y presencia de H_2S (Rona, 1988; Herzig y Hannington, 1995). Las chimeneas y montículos hidrotermales asociados son rápidamente colonizados por (arqueo-) bacterias y otras especias más evolucionadas que basan su existencia en procesos de oxidación/reducción de H_2S/SO_4 y CH_4/CO_2. A pesar de ser fenómenos ampliamente descritos en sistemas submarinos actuales, pocos son los sulfuros masivos fósiles que muestran evidencias claras de actividad biológica (Russell, 1996; Little *et al.*, 1997; Little *et al.*, 1999). Esto es posiblemente debido a que la mayor parte de los sulfuros masivos que se forman actualmente no son propiamente exhalativos, sino que forman estructuras de remplazamiento infrayacentes a los montículos hidrotermales, que sólo ocupan una pequeña proporción del sistema (e.g., Herzig y Hannington, 1995). Salvo en condiciones de preservación excepcionales, los montículos son oxidados y erosionados en pocas decenas de años.

La Faja Pirítica Ibérica es una de las provincias metalogenéticas más importantes del mundo, con más de 1800 Mt de sulfuros masivos y stockworks infrayacentes

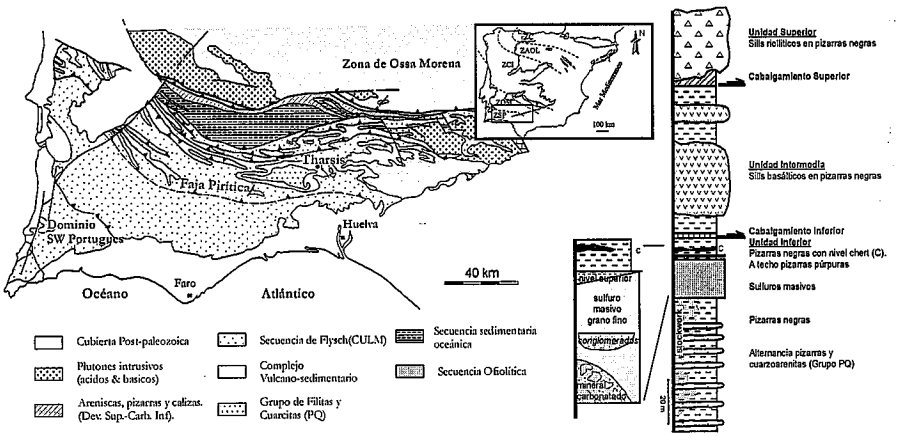

Fig. 1.- Mapa geológico de situación y columna litológica del yacimiento de Filon Norte (Tharsis).

Fig. 1.- Geological map and lithologic column of the Filon Norte (Tharsis) orebody.

(e.g., Leistel *et al.*, 1998). Tiene una serie de características que hacen de ella un distrito único, tales como la elevada proporción de pizarras, la poca potencia de rocas volcánicas y su situación en una zona de extensión intracontinental (Quesada, 1998). A diferencia de en otras provincias equivalentes, muchos de los depósitos se han formado sobre el fondo marino (Tornos, 2000). Esto es especialmente evidente en los yacimientos gigantes de la zona sur, en la que las mineralizaciones están encajadas en pizarras y tienen abundantes estructuras sedimentarias, pueden ser ricas en sideri-ta y tienen valores de $\delta^{34}S$ significativamente bajos.

El depósito de Filón Norte (Tharsis)

El depósito de Filón Norte se encuentra situado en el borde este de la estructura de Puebla de Guzmán (Fig. 1). Los sulfuros masivos se localizan en los primeros metros de pizarras oscuras del Complejo Volcano Sedimentario (Fig. 1) directamente sobre la alternancia de pizarras y cuarcitas del Grupo PQ. Si se exceptúan esporádicos niveles epiclásticos, no hay rocas volcánicas ligadas a los sul-

Fig. 2.- Estructuras sedimentarias del nivel superior de los sulfuros masivos. Ancho de la fotografía: 6 mm.

Fig. 2.- Sedimentary structures in the uppermost massive sulphides. Width of photo: 6 mm

furos masivos. Sobre éstos se disponen unos m de pizarras negras ricas en pirita con un nivel característico de chert gris. Esta unidad (Unidad Inferior de Tornos et al., 1998) está cabalgada por pizarras con sills máficos intensamente ankeritizados y por pizarras con sills riodacíticos.

Bajo los sulfuros masivos se dispone una potente zona de stockwork de más de 400 m de potencia que se desarrolla sobre la parte más inferior del Complejo Volcano Sedimentario y en el Grupo PQ. Este stockwork no parece estar directamente ligado a una falla, sino que forma masas estratoides irregulares. En las zonas más superiores hay pequeños cuerpos irregulares de sulfuros semimasivos remplazando a las pizarras pero siempre cortando al stockwork. El contacto del stockwork con los sulfuros masivos exhalativos es neto, sugiriendo que la exhalación hidrotermal fue difusa a través de los sedimentos alterados y no canalizada a través de chimeneas.

Los sulfuros masivos propiamente dichos forman un lentejón de unos 1500 m de longitud, 400-600 m de anchura y 80 m de potencia media, que probablemente sea fruto del apilamiento tectónico de una lámina poco potente con una extensión original aproximada de 2-4 km^2 (Tornos *et al.*, 1998). En general, son rocas monótonas formadas mayoritariamente por pirita de grano muy fino (<30 μm) en la que se suelen reconocer estructuras framboidales residuales. Esta piritita tiene frecuentes intercalaciones de conglomerados formados por corrientes de turbidez. Son niveles métricos con base no erosiva y sin granoselección con fragmentos heterométricos de pirita y pizarra soportados por pirita de grano más fino. En la zona inferior (S) del yacimiento hay una facies característica con fragmentos cm consistentes en una alternancia submm de sulfuros y siderita de grano muy fino que están soportados por pirita y siderita de grano más grueso (mineral carbonatado). Esta facies forma una estructura lenticular de dimensiones hectométricas y unos 40 m de potencia (Strauss y Beck, 1990). En su zona más interna se han reconocido estructuras métricas formadas por pirita con estructura botroidal que podrían corresponder a las zonas más proximales.

Finalmente, y definiendo el contacto de los sulfuros masivos con las pizarras negras suprayacentes hay un nivel de potencia métrica con abundantes estructuras sedimentarias. En él alternan niveles cm de brechas con pirita y siderita (equivalentes al mineral carbonatado) con niveles de pizarras y capas de pirita con granoselección negativa y estructuras de tipo *slump* o *scour and fill* en la que abundan los cantos blandos de pizarra (Figura 2) y que se interpretan como producto de la erosión de los sulfuros en relación con fallas sinsedimentarias.

Los niveles más inferiores de los sulfuros masivos muestran abundantes evidencias de que el sistema estaba oxidado cuando se depositaron los primeros sulfuros. Hay restos de marcasita, abundantes fantasmas de hematites remplazada por magnetita y de sulfatos remplazados por pirita. Igualmente, las relaciones Ni-Mn-V de las pizarras suprayacentes indica que las condiciones sub-(óxicas) se restauraron muy pronto tras la finalización de la actividad hidrotermal (Tornos y Spiro, 1999). Sólo las pizarras con pirita que se superponen directamente a los sulfuros masivos muestran evidencias de formación en condiciones anóxicas.

La temperatura de precipitación de

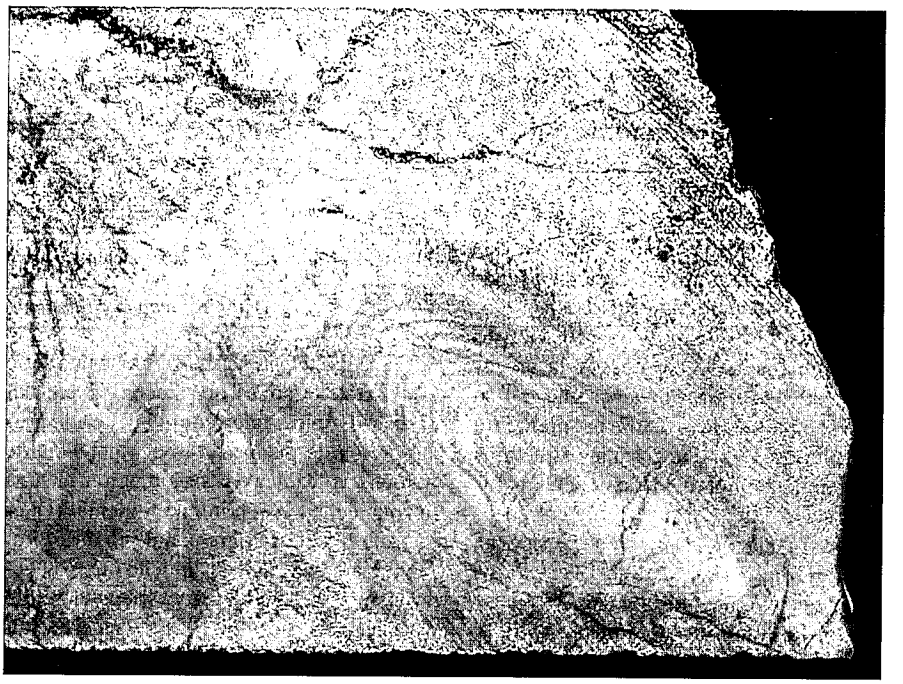

Fig. 3.- Estructura de escape biogénica en el contacto basal de los sulfuros masivos. Ancho de la fotografía: 8 cm.

Fig. 3.- Escape biogenic structure in the footwall of the massive sulphides. Width of photo: 8 cm

Geología y estructura de la Mina de Río Tinto (Faja Pirítica Ibérica, España)

Geology and structure of Rio Tinto Mine (Iberian Pyrite Belt, Spain)

D. Mellado [(1)], E. González Clavijo [(1,2)], F. Tornos [(1)] y C. Conde [(1)].

[(1)] Instituto Geológico y Minero de España. Oficina de Proyectos de Salamanca. C/ Azafranal 48. 37001 Salamanca.
[(2)] Dirección actual: INETI, Departamento de Geologia, Ap. 7586, 2720-866, Amadora, Portugal.
d.mellado@igme.es; emilio.clavijo@ineti.pt; f.tornos@igme.es; c.conde@igme.es.

ABSTRACT:

The Rio Tinto mining district is regarded as the largest volcanogenic massive sulphide district worldwide, but its geologic and structural setting remains poorly disclosed. The mineralized sequence includes a lower unit of interbedded mafic volcanics, shale and conglomerate overlain by a felsic dome-sill complex. The massive sulphides occur within the felsic rocks, either as exhalative deposits on the top or as replacive masses within the volcaniclastic rocks.

The present review has a special aim on structural geology bearing up a genetic model update for the ore. Regional thin-skinned tectonic was clearly identified as the leading Variscan structural style in the district. Several stocked units bounded by thrust-faults display normal polarity on structural and sedimentary criteria basis. Reconstruction of the palaeogeography prior to the tectonic stacking reveals a very extensive mineralizing system.

Key words: Río Tinto, Massive Sulphide, Iberian Pyrite Belt, South-Portuguese Zone.

Geogaceta, 40 (2006), 231-234
ISSN: 0213683X

Introducción

El distrito minero de Río Tinto es uno de los ocho depósitos gigantes de sulfuros masivos de la Faja Pirítica Ibérica y quizás la mayor concentración de sulfuros masivos en la corteza terrestre, con más de 400 Mt de sulfuros masivos y unos 2000 Mt de stockwork de baja ley. Se ha explotado interrumpidamente desde siglo VIII a.c. hasta la actualidad, marcando un importante hito en la historia de la minería mundial.

A pesar de su importancia histórica y minera, existen pocos trabajos recientes dedicados a la interpretación de su geología, estructura y metalogenia (e.g., Williams, 1934; Rambaud, 1969; García Palomero, 1980; Boulter, 1993; Tornos, 2005). En este trabajo se presentan los primeros resultados de un estudio geológico y estructural del distrito minero, comparando los resultados con otros trabajos de carácter más regional (e.g., Silva *et al.,* 1990; Quesada, 1998; Onézime *et al.*, 2002).

Encuadre geológico

La Zona Sud-Portuguesa (ZSP) es la unidad más meridional, en las coordenadas actuales, del segmento Ibérico del Macizo Varisco (Fig. 1). Se trata de un terreno exótico acrecionado al autóctono ibérico como un cinturón de pliegues y cabalgamientos de vergencia suroeste (Silva *et al.*, 1990; Quesada, 1998) y con un grado metamórfico bajo. La Faja Pirítica Ibérica, su unidad más septentrional, es una banda de más de 250 Km de largo y 75 Km de anchura máxima, donde se han localizado más de 80 yacimientos de sulfuros masivos y más de 300 de manganeso.

Desde un punto de vista estratigráfico, la Faja Pirítica presenta rocas sedimentarias e ígneas de edad Devónico Superior–Carbonífero. Se pueden diferenciar tres unidades litoestratigráficas, que de muro a techo, son el Grupo de Filitas y Cuarcitas (Grupo PQ), el Complejo Volcano-Sedimentario (CVS) y el Grupo Culm (Schermerhorn, 1971). En este periodo los ambientes evolucionan desde una plataforma estable (Grupo PQ) hasta una cuenca antepaís sinorogénica, con la deposición del flysch (Grupo Culm) en un surco que se desplaza hacia el sur siguiendo el avance de la orogenia Varisca (Silva *et al*., 1990; Quesada, 1998). El desarrollo de cuencas de tipo *pull-apart* durante las etapas más tempranas de la colisión oblicua facilitó el ascenso de un vulcanismo predominantemente dacítico con proporciones más accesorias de basalto, riolita y andesita a unas subcuencas, con depósitos pizarrosos y de rocas químicas, como jaspe y sulfuros masivos.

Las estructuras de deformación presentes en la Faja Pirítica tradicionalmente se han agrupado en tres fases principales de deformación (Quesada, 1998; Onezime *et al.*, 2002; Soriano *et al.*, 2002). En una primera fase, se generan pliegues vergentes al sur asociados a cabalgamientos, que son sincrónicos con el metamorfismo. Las estructuras de segunda fase son las predominantes en la Faja Pirítica y consisten en pliegues y cabalgamientos vergentes al sur, subparalelos a los de primera fase. La interferencia con los pliegues D_1 homoaxiales, produce lineaciones de intersección de dirección E-O. La tercera fase se caracteriza por la presencia de un despegue que desplaza los materiales sinorogénicos hacia el sur, disponiéndolos sobre la unidad de cabalgamientos que imbrican al Grupo PQ y al CVS.

Litoestratigrafía del área de Río Tinto

Las unidades estratigráficas definidas en el área de Río Tinto corresponden a materiales del Complejo Vulcano-Sedimentario y Grupo Culm, no habiéndose observado los materiales del grupo PQ. La secuencia litológica simplificada se muestra en la figura 2. Los criterios tectónicos y sedimentarios observados en las distintas unidades indican siempre una polaridad normal de las mismas.

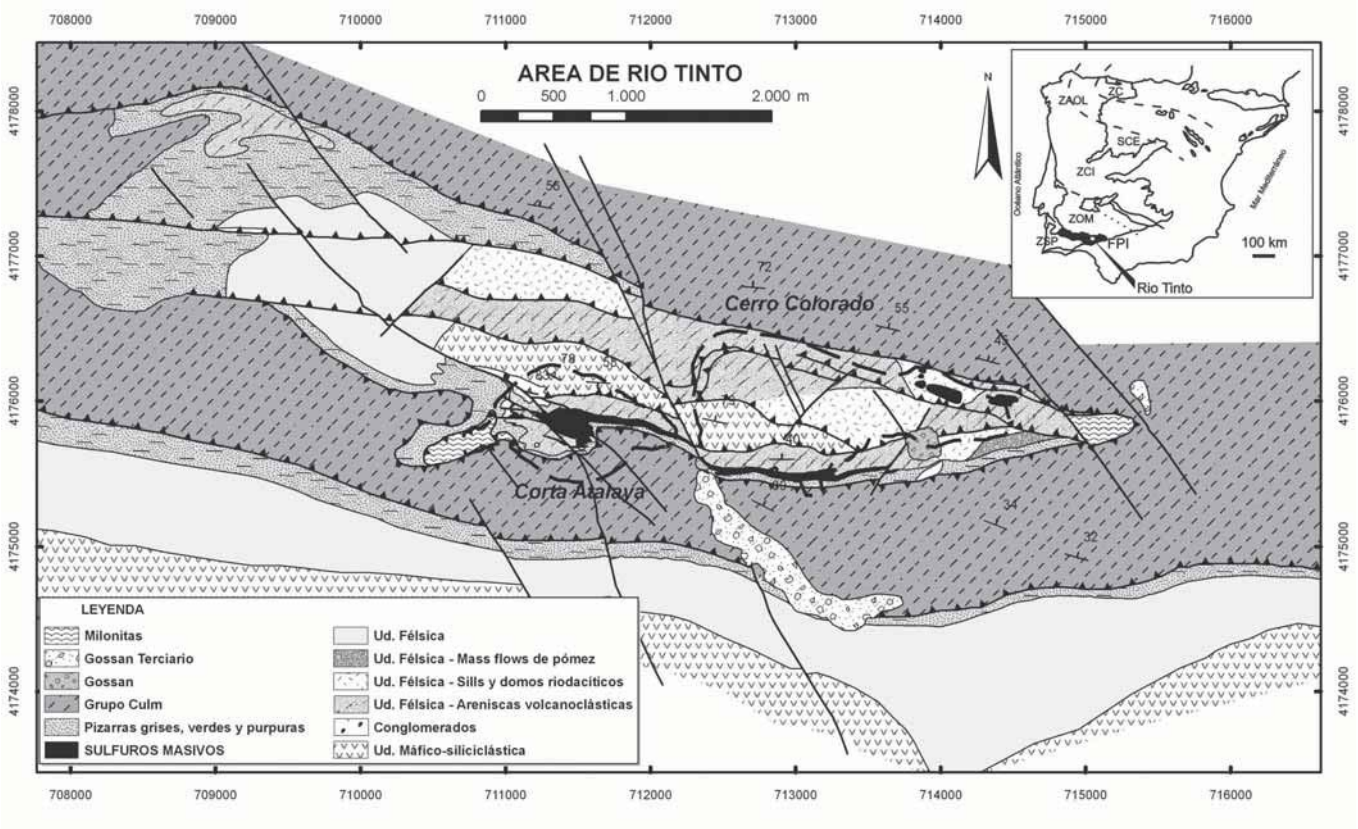

Fig. 1.- Mapa geológico del área de Río Tinto.

Fig. 1.- Geologic map of Río Tinto area.

En la base de la columna estratigráfica aparece una Unidad Máfico-siliciclástica, formada por intercalaciones de pizarra y basalto, éste último constituido por coladas con *pillow lavas* locales. También se distinguen dos tipos de rocas intrusivas, diques y *sills* subvolcánicos máficos, con desarrollo de estructuras peperíticas en sus contactos (Boulter, 1993) y en algunos casos, metamorfismo de contacto. En la parte superior de esta unidad dominan las areniscas volcanoclásticas de derivación básica. Esta unidad aflora en una banda continua de dirección este-oeste en el Antiforme de Cerro Colorado (Fig. 1) (García Palomero, 1980) y es similar a la que se encuentra en la parte sur del gran Sinforme de Rio Tinto, concordante sobre el Grupo PQ. Geoquímicamente las rocas volcánicas tienen composiciones basalto-andesíticas. Boulter *et al*. (2004) encuentran una diferencia geoquímica entre las rocas volcanoclásticas máficas y los cuerpos masivos, basándose en los análisis de los elementos traza (Ti/Nb). Hacia el techo de esta unidad, aumenta la proporción de rocas sedimentarias, apareciendo en Corta Atalaya un nivel de conglomerado pizarroso (García Palomero, 1980) matriz-soportado, con cantos dominantes de pizarra y, en menor medida, de rocas volcánicas félsicas y máficas. Dentro de él hay concentraciones locales de sulfuros que reemplazan preferentemente a algunos clastos de naturaleza variable. La granulometría, forma y disposición de los cantos del conglomerado parece indicar un transporte mínimo.

Sobre la unidad descrita aparece una Unidad Félsica, generalmente separada de la anterior por estructuras tectónicas, aunque localmente se han observado contactos intrusivos de las facies masivas. Está formada por una sucesión muy homogénea de rocas volcánicas de composición dacítica a riodacítica. Aunque suelen mostrar una intensa alteración hidrotermal que ha borrado muchas de las estructuras, es posible diferenciar rocas volcanoclásticas poco estructuradas acumuladas probablemente por procesos de *mass flow* y equivalentes a hialoclastitas transportadas. Tienen cristales y fragmentos de cuarzo y plagioclasa en una matriz de grano fino. También se han reconocido (cripto-) domos de rocas masivas e hialoclastitas y diques subvolcánicos de la misma composición; en conjunto, la Unidad Félsica parece corresponder a un complejo de domos submarinos intruidos o interestratificados en depósitos pizarrosos. Los contactos de las rocas masivas con las rocas sedimentarias suelen mostrar un borde vítreo y contactos peperíticos. Esta Unidad es químicamente muy homogénea, con una distribución similar de elementos traza (TiO_2/Al_2O_3 o Zr/Al_2O_3, entre otros) indicando un origen volcánico común.

Sobre el techo de la Unidad Félsica aparece de manera concordante la mineralización. Los sulfuros masivos aparecen como un lentejón (Filón Sur) formado por pirita con cantidades accesorias de calcopirita, esfalerita, galena y trazas de otros sulfuros. La mayor parte de los sulfuros están recristalizados y no se reconocen estructuras primarias. Sólo localmente es posible observar un bandeado sedimentario y venas zonadas relacionadas con las zonas de alimentación. Estos sulfuros masivos se han interpretado como exhalativos y acumulados en una subcuenca anóxica sobre una zona de exhalación de carácter difuso (Solomon *et al*., 2002; Tornos, 2005).

La unidad sedimentaria superior, denominada Serie de Transición por García Palomero (1980) está formada por pizarras grises con intercalaciones de cinerita félsica y algunas intercalaciones de sedimentos químicos (jaspe). Se sitúa en el mismo nivel estratigráfico que los sulfuros masivos pudiéndose observar las interdigitaciones entre ambas unidades litológicas. En varias zonas de Cerro Colorado y Corta Atalaya las pizarras presentan zonas irregulares de color morado y verde intenso y en las que la coloración no sigue la estratificación.

Economic Geology, v. 103, pp. 185–214

Formation of the Tharsis Massive Sulfide Deposit, Iberian Pyrite Belt: Geological, Lithogeochemical, and Stable Isotope Evidence for Deposition in a Brine Pool

Fernando Tornos,†

Instituto Geológico y Minero de España, Azafranal 48, 37001 Salamanca, Spain

Michael Solomon,

Centre for Ore Deposit Research, University of Tasmania, Private Bag 79, Hobart, Tasmania, Australia 7001

Carmen Conde,

Instituto Geológico y Minero de España, Azafranal 48, 37001 Salamanca, Spain

and Baruch F. Spiro

Natural History Museum, Cromwell Road, London SW7 5BD, United Kingdom

Abstract

The giant Tharsis massive sulfide deposit is one of the largest shale-hosted orebodies in the Iberian Pyrite Belt. It consists of several ore lenses located in the lowermost VSC and overlying a thick siliciclastic sequence Phyllite-Quartzite Group. The ore lenses are up to 1,500 m long, 130 m thick, and tectonically stacked within shale with rare sandstone layers that have been dated as late Strunian. Most of the massive sulfides are monotonous fine-grained pyrite. In the footwall of the orebody there are some siderite-rich facies (carbonate ore) consisting of laminated and brecciated sulfides and siderite that form mounds. We interpret these to be biogenic mounds formed proximal to the vents, probably by accumulation of *thermophila archea* (bacterial mats) and the products of their erosion. Stockwork veins occur in shale beneath most of the massive sulfide lenses. At the base of the ore lenses there are relics of laminated iron oxides, sulfates, and marcasite, which are partially replaced by pyrite. Seven kilometers west is the San Jorge mine, where small pyrite lenses occur in shale probably at the same stratigraphic position as Tharsis.

The shale stratigraphically below the massive sulfides has a chemical composition mainly consistent with its formation in oxic to suboxic conditions and is characterized by low Mo contents (<50 ppm), low V/Cr ratios (<2), and high Fe but variable Mn contents. Shale directly related to the massive sulfide formation is characterized by high V/Cr ratios (>4) and low Mn contents indicative of deposition in an anoxic setting. A few meters above the massive sulfides the shale again shows evidence of deposition under oxic to suboxic conditions. The deposition of the massive sulfides was synchronous with a major geochemical change at the basin scale, involving a major increase in the Ca and base metal contents, S/total organic carbon, V/Cr, and K_2O/Na_2O ratios of the shale, probably related to the onset of the volcanism and hydrothermal activity. Shale that hosts the massive sulfides is also characterized by an over maturation of the organic, plankton-derived compounds that are not observed in the shale away from the orebodies. The destruction of this organic matter having $\delta^{13}C$ values between –31 and –25 per mil is probably the source of ^{13}C-depleted carbonate. The siderite in the carbonate ore and the ankerite within the alteration zone have isotopic signatures that can be interpreted as the product of mixing of fluids having $\delta^{18}O$ and $\delta^{13}C$ compositions of +8 to +10 and –6 per mil, respectively (i.e., hydrothermal fluid and cooler seawater) but having isotopically light carbon ($\delta^{18}O$ = –1 to 0‰ and $\delta^{13}C$ = –20‰). The massive sulfides have $\delta^{34}S$ values between –33 and +4 per mil, similar to those of pyrite in the footwall and hanging-wall shale (–29 to +5‰). Stockwork vein sulfides, however, range from –4.5 to +1.9 per mil.

Sedimentary textures in sulfides, the stratiform morphology, asymmetric distribution of wall-rock alteration, an indication of widespread biogenic activity and lack of evidence of major replacement in the hanging wall or laterally, show that the massive sulfides were deposited on the sea floor. The lack of evidence for the rubble mounds that characterize modern black smoker systems and the lack of barite and of oxidized facies suggest sulfide deposition occurred in an anoxic basin from a diffuse venting system.

Fluid inclusions in stockworks of other massive sulfide deposits in the Iberian Pyrite Belt have salinities ranging from 3 to 12 wt percent NaCl equiv and homogenization temperatures up to 350°C. A high proportion of these fluids would have reversed buoyancy, collecting in depressions to form brine pools. The $\delta^{34}S$ values of the massive sulfides at Tharsis are consistent with the mixing of vent sulfur with sulfur depleted in ^{34}S and probably derived from the biogenic reduction of seawater sulfate. Biogenically reduced sulfur may have been supplied by H_2S leached from the footwall shale, biologic activity within the mounds, and biological reduction of sulfate diffusing downward from overlying oxic seawater. Sulfate is interpreted to have been reduced at temperatures in the range of 60° to 100°C, leading to the immediate precipitation of sulfide muds from the metal-rich fluids that would have filled the proposed brine pool. Early venting and mixing with oxic seawater proba-

† Corresponding author: e-mail, f.tornos@igme.es

bly formed the oxidized mineral assemblages at the base of the massive sulfides and led to the formation of the biogenic mounds. In this model, progressive venting led to the gradual displacement of seawater from the bottom of the basin and formation of a reduced brine layer. The existence of biogenic mounds and other indicators of biological activity such as the low $\delta^{34}S$ compositions of the sulfides and the presence of burrows, suggest that biological activity was widespread and probably critical to the formation of the massive sulfide deposit at Tharsis.

The proposed genetic model may apply to the other shale-hosted, giant, massive sulfide deposits of the southern Iberian Pyrite Belt, such as Las Cruces, Aznalcollar-Los Frailes, Valverde, Lousal, Neves Corvo, and particularly Sotiel-Migollas.

Introduction

The Iberian Pyrite Belt, located in southern Iberia, contains over 80 massive sulfide deposits and several tens of small prospects (Routhier et al., 1980; Sáez et al., 1996; Leistel et al., 1998b; Carvalho et al., 1999; Tornos, 2006). Most of the giant deposits with more than 100 million metric tons (Mt) of ore are located in the southern Iberian Pyrite Belt and spatially associated with shale (Las Cruces, Aznalcóllar-Los Frailes, Sotiel-Migollas, Valverde, Tharsis, Lousal, Neves Corvo and Filón Sur of Rio Tinto). Only Aljustrel and La Zarza are volcanic-hosted orebodies, and they are situated in the northern Iberian Pyrite Belt.

The depositional processes of the shale-hosted massive sulfide deposits remain controversial. Whereas several authors have suggested that they formed by subsea-floor replacement of the host mudstone (e.g., Aznalcóllar: Almodóvar et al., 1998), or by infilling beneath a chert cap (e.g., Tharsis: Barriga and Fyfe, 1988), others consider the ores to be of exhalative origin (e.g., Rio Tinto: Solomon et al., 1980; Badham, 1982; Boulter, 1993; Neves Corvo: Gaspar, 1996) or a combination of both processes (Relvas, 2000). Tornos et al. (1998) suggested that the Tharsis orebody was deposited in a brine pool or a restricted anoxic basin, and Tornos and Spiro (1999), Tornos et al. (2003), and Tornos (2006) extended the concept to other shale-hosted deposits. For Aznalcóllar, Valverde, and Rio Tinto, Solomon et al. (2002) showed from fluid inclusion data that the fluids in stockwork quartz would not have been buoyant on mixing with seawater and would have ponded on the sea floor if basins existed.

In this paper we describe the geology and nature of the orebodies within the Tharsis deposit and test and develop the exhalative, basin-filling or brine-pool model by considering geological and geochemical data from the massive sulfides and the host shale.

Regional Geology of The Iberian Pyrite Belt

The Iberian Pyrite Belt comprises a series of marine basins developed during sinistral transcurrent faulting generated by the oblique subduction and collision of Laurentia with Gondwana during the Variscan (Late Devonian-Carboniferous; Silva et al., 1990; Quesada et al., 1991; Leistel et al., 1998b; Oliveira and Quesada, 1998; Matte, 2001). These basins formed within the passive margin of Laurentia, now represented by the South Portuguese zone but adjacent to the continent-continent suture (Fig. 1).

The oldest rocks in the Iberian Pyrite Belt are a sequence of quartz-rich sandstone and shale (Phyllite-Quartzite Group, Late Devonian) that were deposited on a stable epicontinental shelf. The Phyllite-Quartzite Group is several thousand meters thick (Moreno et al., 1996). In the uppermost Phyllite-Quartzite Group there is an increase in the proportion of sandstone and the presence of very heterogeneous facies, including shallow to subaerial reef limestone, delta-related deposits, and mass flows (Moreno et al., 1996) that probably were deposited during early Variscan orogenesis. The overlying Volcanic Sedimentary Complex (VSC) is a highly variable unit up to 1,300 m thick. It is characterized by the presence of dacitic-rhyolitic dome complexes and sills, basaltic lava flows and sills, and thick pumice- and crystal-rich felsic volcaniclastic units interbedded with detrital sedimentary rocks, mostly mudstone with some graywacke and sandstone (e.g., Routhier et al., 1980; Boulter, 1993; Soriano and Martí, 1999; Rosa et al., 2004; Tornos, 2006). The felsic volcanic rocks have low Al and high Nb calc-alkaline compositions, whereas the mafic rocks belong to the alkaline to continental tholeiitic suites (Munhá, 1983; Mitjavila et al., 1997; Thieblemont et al., 1998). Andesite is less common, and only predominates locally in the northern part of the belt. Stratigraphically high in the volcano-sedimentary sequence there is a locally developed horizon, up to 30 m thick, of hematitic radiolaria-rich, purple-colored shale with Mn-bearing jasper lenses. The formation of the VSC and coeval sulfide deposits occurred between the uppermost Devonian and the middle-late Visean (ca. 360–330 Ma: Silva et al., 1990).

The VSC is capped by the Flysch Group (Culm), consisting of synorogenic turbidites that filled the foreland basin of the orogen. It is highly diachronous, with southwestern progradation and ranges in age from late Visean to middle-late Pennsylvanian (Oliveira, 1990). The Variscan deformation was initiated by the oblique collision between the two continental terranes and obduction of the South Portuguese zone on the Ossa Morena zone (Fig. 1) in a transpressional setting. Younger southward thrusting was responsible for thin-skinned deformation dominated by thrust and fold tectonics (Quesada, 1998). The metamorphic grade is mostly very low, in the prehnite-pumpellyite facies. However, in the northern part of the Iberian Pyrite Belt and near the thrusts, where the metamorphic grade is within the greenschist facies (Munhá, 1990), the original textures are commonly masked by an intense deformation and recrystallization.

Geology of the Tharsis Deposit

The Tharsis deposit is located in the northeast zone of the large, east-west–trending Puebla de Guzmán antiform (Fig. 2), where the lowermost VSC conformably overlies the Phyllite-Quartzite Group and is exposed in the core of the structure. Here, the VSC is characterized by the presence of a 100- to 150-m-thick, monotonous, shale-rich sequence (Tharsis Formation) that is overthrust by felsic volcanic rocks (Fig. 2). The Tharsis Formation crops out discontinuously for more

Ore Geology Reviews 68 (2015) 142–163

Contents lists available at ScienceDirect

Ore Geology Reviews

journal homepage: www.elsevier.com/locate/oregeorev

Review

Controls on the siting and style of volcanogenic massive sulphide deposits

Fernando Tornos [a,*], Jan M. Peter [b], Rodney Allen [c,d], Carmen Conde [e]

[a] Centro de Astrobiología — Consejo Superior de Investigaciones Científicas, Ctra Ajalvir km. 4.5., 28850 Torrejón de Ardoz, Spain
[b] Geological Survey of Canada, 601 Booth Street, Ottawa, Ontario K1A 0E8, Canada
[c] Boliden Group, Exploration Department, SE-776 98 Garpenberg, Sweden
[d] Luleå University of Technology, SE-971 87 Luleå, Sweden
[e] c/Vilar Formoso 66, 37008 Salamanca, Spain

ARTICLE INFO

Article history:
Received 19 December 2013
Received in revised form 29 December 2014
Accepted 5 January 2015
Available online 10 January 2015

Keywords:
Volcanogenic massive sulphide deposits
Copper
Zinc
Gold
Silver
Lead
Hydrothermal
Seafloor

ABSTRACT

Volcanogenic massive sulphide (VMS) deposits form in subaqueous environments from circulating hydrothermal fluids heated by volcanic activity. These deposits form as sulphide mounds, stratiform exhalative and/or replacive bodies and commonly have stockwork/vein mineralization in their immediate footwall. These various "styles" are essentially facies of mineralization, each one being the product of a particular set of conditions that control the ore-forming processes and the consequent geometry and architecture (style) of the deposits. These controls include the physical and/or chemical nature of the host rocks, the temperature and composition of the hydrothermal fluids and the redox state of the depositional environment.

The style of exhalative deposits is controlled by the salinity of the vented fluids and the redox state at the seafloor. Hydrothermal fluids with salinities less than twice that of seawater that vented into open, oxic oceanic environments, typically formed small mound and chimney complexes, unless they were rapidly covered by sediments or volcanic rocks. The massive sulphides were rapidly oxidized and partly dissolved by seawater. In contrast, stratiform sheet-like deposits are typically formed in anoxic bottom waters. Anoxic marine conditions were periodically of global extent – particularly prior to 2.4 Ga – or of a regional nature. Local anoxic conditions can also be self-induced by the exhalation of saline and reducing hydrothermal fluids that ponded in bathymetric depressions such as second- or third-order basins to form a brine pool. These exhalative systems may have been initiated as chimney vent complexes and subsequently overlain by stratiform sulphides formed under the self-induced anoxic conditions. Deposits formed in anoxic environments can be significantly larger than those in oxic settings, and this is attributed to several factors that include longer-lived hydrothermal circulation, more efficient sulphide precipitation and reduced or inhibited oxidation thereof.

Replacement of volcanic and sedimentary strata by sulphide typically occurs within the feeder zones beneath the exhalative mineralization. However, successions with abundant porous, permeable and/or reactive rocks such as glassy and/or pumiceous volcaniclastic rocks, and in some cases limestone, favoured the development of large replacive deposits, that may have had little surficial expression on the sea floor.

VMS deposits at spreading centres within oceanic crust formed almost exclusively as mounds. Most of them have not been preserved, likely due to oxidation of the sulphides in the prevailing oxic environment and/or destruction of oceanic crust during subsequent subduction. Intra-continental rifts, arc rifts and back-arc rifts commonly have more complexity in their structure, and facies architecture and environments and can host all styles of VMS mineralization. In these settings, early extension favoured the formation of restricted basins with ideal conditions for the onset of hydrothermal activity and development of anoxic bottom waters, whereas in mature rifts the conditions were less conducive for the formation of regionally extensive anoxic environments. Formation of replacive deposits was permissible in all settings with porous or reactive subsea-floor strata. Replacive mineralization is the most likely to be preserved in the geological record due to the sulphides being physically shielded from oxidative weathering and mechanical erosion at the seafloor.

The various styles of VMS mineralization can rarely be distinguished using a single criterion; in most cases multiple criteria are required.

Mound style mineralization is distinguished by: (a) mound- or lens-shaped morphology; (b) presence of chimney fragments; (c) presence of abundant sedimented sulphide breccias; (d) location on a stratigraphic boundary

* Corresponding author.
E-mail addresses: f.tornos@csic.es (F. Tornos), jpeter@nrcan.gc.ca (J.M. Peter), Rodney.Allen@boliden.com (R. Allen), carconri@gmail.com (C. Conde).

http://dx.doi.org/10.1016/j.oregeorev.2015.01.003

(ore horizon); and (e) association with a thin horizon or thicker stratigraphic interval of fine-grained clastic rocks (e.g., shale, mudstone) that accumulated at slow sedimentation rates.
Stratiform exhalative mineralization is distinguished by: (a) sheet-like morphology prior to deformation; (b) presence of fine-grained clastic host rocks that accumulated at relatively slow rates (e.g., mudstone); (c) presence of local or extensive planar stratification.
Replacive mineralization is characterized by: (a) irregular geometry and distribution of sulphide bodies; (b) gradation from massive sulphides to semi-massive sulphides and disseminated mineralization with relict textures of the host rock; and (c) originally pumiceous, glassy or reactive host rocks emplaced at high depositional rates (mass flow deposits, lavas, carbonate-altered mass flow deposits) or limestone.
One deposit or district may comprise two or more of these main styles of mineralization. In many cases the main styles of VMS mineralization present in a particular region can be predicted from examination of the facies architecture and depositional environments of the host succession. Recognition of the style(s) of mineralization that occur in a particular basin or mineral belt enables exploration models to be improved and should influence the strategy of exploration for VMS deposits.

Contents

1. Introduction

Volcanogenic massive sulphide (VMS) deposits are one of the best known and well-studied ore deposit types (e.g., Franklin et al., 1981, 2005; Lydon, 1988a). Their occurrence in marine volcanic and volcanosedimentary sequences of almost all ages (from ca. 3.5 Ga to present) on all continents, together with their economic importance as a source of base (Cu, Pb, Zn), precious (Ag, Au) and other metals (e.g., Co, Sn, In, Cd, Tl, Ga, Se, Sb, Bi) and their direct comparison with present-day analogues have made them the focus of numerous studies. Most of these studies concern the determination of geodynamic setting (Sawkins, 1990; Ludden and Peloquin, 1996; Piercey et al., 2001), the physical volcanology of the deposits (Allen, 1992), host rock compositions (Barrie et al., 1993; Lentz, 1999), "ore" mineralogy (Marcoux et al., 1996), the nature and extent of hydrothermal alteration (Barrett et al., 2001; Large et al., 2001b), the geochemistry of the mineralizing fluids (Peter and Scott, 1993; Zaw et al., 1996) and the superimposed metamorphism and deformation (Marshall and Spry, 2000). However, of the several hundreds of papers dealing with VMS deposits, only a few provide a detailed description of the setting/environment of massive sulphide precipitation, accumulation and preservation.

Here, we compile and discuss existing information to show that VMS deposits formed in a restricted number of styles ("facies") of mineralization, including sulphide mounds and related chimneys, stratiform exhalative bodies and/or replacive mineralization. The aim of this study is to present an overview of VMS formation mechanisms and the influences that the site of formation can have on the style of mineralization, and present criteria for distinguishing between the different ore forming environments. These interpreted modes of emplacement can have profound implications for the formulation of effective mineral exploration programmes and the refinement of genetic models.

2. Evolution of thought regarding styles of VMS mineralization

Solomon and Walshe (1979) commented that there is "considerable uncertainty regarding the way that the sulphide bodies accumulate at/or near the seafloor and the reasons for their varying shape and composition". However, similarities among many VMS deposits suggest that only a few mechanisms can be responsible for their formation. Ohashi (1919, 1920) was probably the first to document the evidence that the formation of massive sulphide ores on the sea floor is linked to volcanism. His landmark papers on the Kosaka deposits in the Hokuroku district of Japan caused debate in Japan for decades and went largely unnoticed in the "western world". In fact, the later pioneer studies of the Rio Tinto deposits suggested that these deposits were formed by replacement of igneous rocks by interaction with magmatic fluids (Williams, 1934). Only in the late 1950s to early 1960s did some authors, working in Canada, Sweden and Australia, argue that massive